Study on corrosion protection of organic coatings using electrochemical techniques: Developing electrochemical noise method, effect of surface preparation and inhomogeneity of organic coatings

Submitted for the Degree of Doctor of Philosophy
At the University of Northampton

2013

Seyed Sina Jamali

DEDICATION

To my amazing wife, Neda, who has been my strength, serenity and encouragement to face all the challenges life has thrown at us and always had faith in me even when I couldn't find a way through.

Declaration of originality

This thesis is submitted in fulfilment of the requirement for the award of Doctor of Philosophy, in the faculty of Science and Technology, University of Northampton and the work is wholly performed by me unless otherwise referenced and acknowledged. The document has not been submitted for any qualification at any other academic institution.

Seyed Sina Jamali

June 2013

TABLE OF CONTENTS

ACKNOWLEDGEMENTS

I wish to express my sincerest gratitude to Dr. Douglas J. Mills, my supervisor and friend, for his patience and guidance. From the first days of me struggling with the new environment, language and culture, through to all those days of working with me in the lab, helping me through the hardships and teaching me the language of science, you have always been an outstanding support. Thanks for trusting me and believing in me. Thanks for opening the doors of a whole new world to me and thanks for treating me like a colleague all the way through. Your passion for science, commitment and humour made it an honour and a pleasure to work with you.

I would like to gratefully thank my director of studies, Prof. Phil Picton, for his invaluable assistance throughout all steps of the work and particularly with the financial support.

I also wish to thank Prof. John Sykes, my advisor at Oxford University, Dr Steve Mabbutt, my second supervisor and Prof. Dennis Tallman from North Dakota State University for their invaluable input through the sessions of theoretical discussion and experimental work, particularly in regards to the development of electrochemical noise technique.

I would like to thank Payam Mokhtarian at the Centre for Statistical and Survey Methodology (CSSM), University of Wollongong for his invaluable input towards the statistical modelling of inhomogeneity in organic coatings, which added a great deal of value to this work.

I also wish to thank Dr. Chris Weirman and Dr. James Sullivan from the Department of Material Science, University of Swansea, for their assistance with SVET experiments and characterization of bare steel surface.

I would like to thank my friend Kasia (Katarzyna) Schaefer for her advice and help throughout the initial steps of this project. It was her interesting work which triggered the story written in this thesis.

Thanks are also due to Jeremy Twigg and RGL Ltd for provision of the hydroblasted and wet abrasive blasted steel panels and also to Pronto paints, AKZO Nobel/international paints, Nuplex, Perstorp, BYK for provision of materials.

Institute for Creative Leather Technologies (ICLT) at the University of Northampton, Park Campus was my second home for the first two years of my studies, 2009-2010, for which I am very grateful. The work described in this thesis has been mostly performed using the facilities provided at the ICLT's laboratories. Its friendly environment made it a joyful and memorable time during the two years of my stay in the UK. I'd also like to thank the staff and friends at ICLT especially Dr. Paula Antunes, Sarah Lee, Mandy Taylor, Dr. Mark Wilkinson, Addis Duki and Cherry Wang who were always there to help when I needed. I also wish to thank my dear friend Matthew Lee who helped me from the first days in UK through to the end of this PhD with his big heart. I'm very thankful for this friendship which I wish to last forever.

Thanks are also due to David Watson, postgraduate research manager at the University of Northampton, for his valuable assistance in every step of my PhD, especially since my move to Australia.

Certain (financial) circumstances towards the end of the second year of studies resulted in a mandatory move to Australia, where the 3rd and 4th years of work (mainly in the form of data analysis and writing) was conducted. Since the move, Wollongong and in particular the University of Wollongong in Australia has become my second and beloved home. I wish to gratefully thank my directors Prof. Gordon G. Wallace and A/Prof. Simon E. Moulton and all my friends at Intelligent Polymer Research Institute, University of Wollongong, in particular Dr. Javad Foroughi, Willo Grosse, Joseph Giorgio, Leo Stevens and Jared Barnes for helping me through this big change.

There is an acknowledgement to Dr. J E O (Jack) Mayne and Prof. David Scantlebury whose works have been a great inspiration. Their discoveries have no doubt extended the borders of science in the field of corrosion and protection, but also facilitated this amazing chain of the science from Jack Mayne through David Scantlebury to his students (Dr M Attar and Dr M Mirabedini), and finally to me, that I am grateful for.

Finally I would like to thank the love, inspiration and support of those close to me. This work would never have happened without the support of my amazing wife, Neda. Mum, I really appreciate your love and encouragement and the effort and commitment you put into my education. Reza, you are the definition of the support and love of a brother in my vocab. Safa, thanks for being an awesome brother and wish you the very best of luck with your PhD. And Dad, thanks for your love and encouragement. Your loving memory will continue to illuminate my way till the last day I live and I hope I have made you proud. I also wish to thank Mohammad and Nahid, my parents in law for their valuable support.

Last but not least, I wish to thank my beautiful niece and nephew, Rastin and Niki, who cheered me up every time I spoke to them or even thought of them. I wish them the very best of life and prosperity in the long journey ahead of them.

ABSTRACT

This study looks into two important aspects of corrosion protection of steel by organic coatings, steel surface preparation and ionic conduction through the coating, as well as development of the electrochemical noise method as an effective assessment method. Surprising and somehow controversial previous findings at the University of Northampton showed an inverse relationship between the roughness of metal substrate and performance of paint coating. So this study was initially launched to further study the effect of metal surface preparation. Four conventional surface preparation methods including ultra high pressure (UHP) hydroblasting, wet abrasive blasting, acid pickling and emery abrasion were studied and compared to an as received control surface. A particular interest of this work was the high demand for an environmentally friendly surface preparation method, e.g. as afforded by UHP hydroblasting, to replace the traditional wet abrasive blasting method. Results of this study revealed the important role of the innate native oxide film and the deleterious effect of contaminants on the protective performance of organic coating. Also it was shown that a highly active surface and large surface profile can be deleterious if an appropriate interaction between paint and metal is not achieved. Results of this study confirmed the earlier findings and suggested the UHP hydroblasting is a successful, cost effective and environmentally friendly surface preparation method and a modern replacement for wet abrasive blasting method.

In addition to the effectiveness of metal surface preparation, the ability of organic coating in preventing ions access to metal plays an equally important role in defining the anti-corrosion performance of a coated metal. Hence the mechanism of ionic conduction through organic coatings and their inhomogeneity which are normally formed in crosslinking systems was extensively studied with the aim of finding the cause of formation of the more permeable areas and the ways by which they can be prevented. Several structural and environmental parameters were examined including the coating thickness, multi-layer paint application, curing temperature, partially non-functional resin, pigmentation and solvent. Experimental results showed that the solvent degree to which can escape, the non-

functional polymer parts and inherently hydrophilic functional groups of organic coatings are the main parameters causing inhomogeneity and highly ion permeable areas. A statistical model was also developed that can be used to estimate number of permeable areas or corrosion initiation sites in a large area of coating.

A particular concern of this work throughout the entire study was development of the electrochemical noise measurement (ENM) in the sense of a good assessing technique for protection efficiency of a coating system. Previous studies have shown great potential of ENM as a practical technique in the field. However, the technique always involved measuring the electrochemical noise between two or three isolated electrodes which cannot be easily provided in certain applications such as submerged structures or inside storage tanks. Also involvement of two or three electrodes in the measurement induces an ambiguity in regards to which electrode dominates the result. Here an attempt was made to perform the noise measurement on a single working electrode so that it can be used in more practical situations. Preliminary results indicate this approach holds promise.

LIST OF FIGURES

LIST OF TABLES

Chapter 1

Principles of Corrosion

1.1 Corrosion basics

Corrosion as a general term can be defined as the spontaneous interactions between a substance and its environment which leads to a change in properties resulting in lower levels of thermodynamic free energy. Corrosion term in metallurgical concept embodies transferring electrons from the oxidized species to reduced species as the outcome of electron affinities of metals [1]. In anodic reaction the metal loses electron and becomes oxidized. The produced electron is being consumed by an electroactive species at the metal surface in cathodic reaction. In Aqueous corrosion the aqueous phase or electrolyte conveys electroactive species and the charge which has been produced due to the anodic and cathodic reactions. The schematic corrosion process for a divalent metal, M, is shown in Figure 1.1. In this example cathodic reaction is reduction of oxygen which is the dominating cathodic reaction in neutral environments like seawater, fresh water, soil and the atmosphere [2]. In the case of steel corrosion, primary product of anodic reaction, $Fe(OH)_2$, may be deposited on the anodic sites but in presence of oxygen can be oxidized further to Fe_2O_3 or FeOOH and form the red-brownish rust. If the access of oxygen is strongly limited, Fe_3O_4 (black Magnetite) is formed which is one part Wüstite (FeO) and one part Hematite (Fe_2O_3). Figure 1.2 illustrates this sequence as a function of distance from metal surface. Also the Figure 1.3 details cathodic reactions in corrosion of steel.

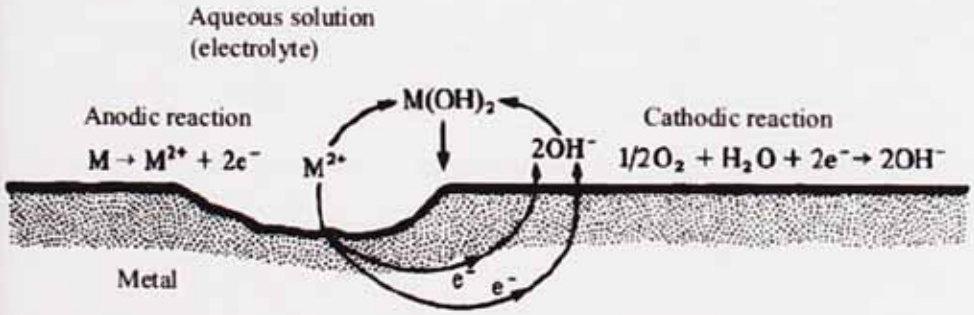

Figure 1.1 Aqueous corrosion of a divalent metal M in an electrolyte containing oxygen showing reduction of oxygen as cathodic reaction and dissolution of metal as anodic reaction [2].

Any fundamental approach to the phenomena of corrosion must involve consideration of the structural features of the metal, the nature of the environment and the reactions that occur at the metal/electrolyte interface. The more important factors involved may be summarized as follows [3]:

1. Metal- composition, detailed atomic structure, microscopic and macroscopic heterogeneities or imperfection, stress (tensile, compressive, cyclic), etc.

2. Environment - chemical nature, concentrations of reactive species and deleterious impurities, pressure, temperature, velocity, etc.

3. Metal/environment interface - kinetics of metal oxidation and dissolution, kinetics of reduction of species in solution; nature and location of corrosion products; film growth and film dissolution, etc.

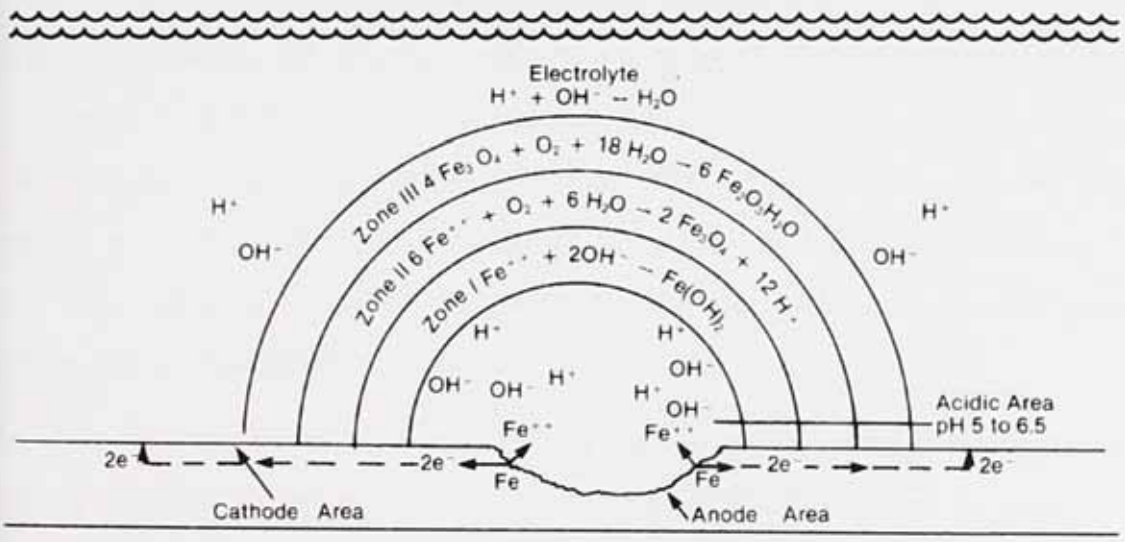

Figure 1.2 Anodic reactions in aqueous corrosion of steel showing oxidation of Fe to Fe^{2+} and Fe^{3+} with increasing the oxidation state as cation gains more access to oxygen [4].

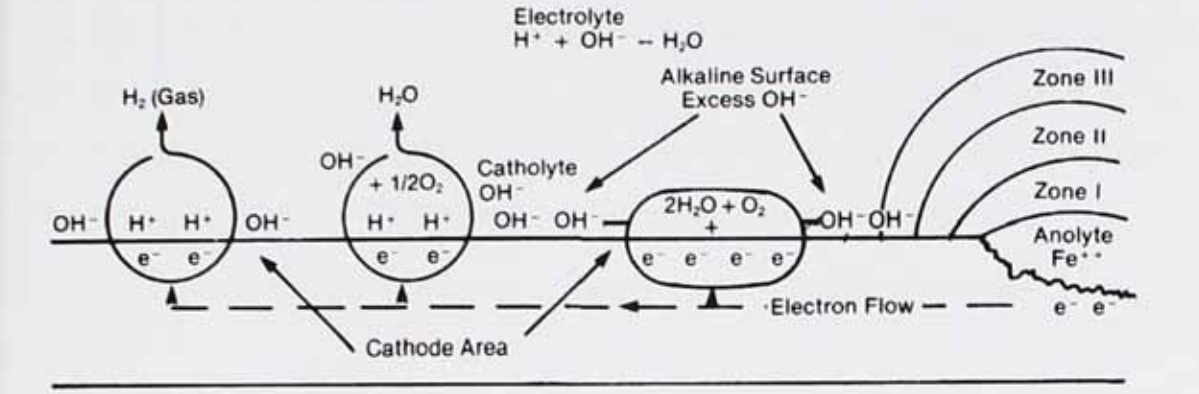

Figure 1.3 Consumption of electron in cathodic reactions in corrosion of steel resulting in reduction of oxygen and water [4]

1.2 Driving force of corrosion (thermodynamic)

In spontaneous processes the thermodynamic potential energy (e.g. mechanical, electrical, chemical) decreases [3]. The American scientist Josiah Willard Gibbs (1839–1903) was the first to suggest in 1876 the use of chemical potential for the identification of the direction of the chemical (among them corrosion) processes. Today this chemical potential is called Gibbs energy, and is designated as "G" for pure substances [5]. Therefore reduction in Gibbs energy, $\Delta G < 0$, indicates that the reaction (including electrochemical reactions and corrosion processes) can happen spontaneously.

The production of almost all metals (and engineering components made of metals) involves adding energy to the system. As a result of this uphill thermodynamic struggle, the metal has a strong driving force to return to its native, low energy oxide state. This return to the native oxide state is called metallic corrosion. Below, values for some of known oxidation reactions during corrosion of steel are shown.

Table 1.1 Gibbs energy changes for some spontaneous corrosion reactions

Reaction	ΔG°_{298}, *kJ/mol*
$4Fe_{(s)} + 3O_{2(g)} \rightarrow 2Fe_2O_{3(s)}$	-742.2
$Fe_{(s)} + 2H_2O_{(l)} \rightarrow Fe(OH)_{2(s)} + H_{2(g)}$	-15.7
$4Fe_{(s)} + 6H_2O_{(l)} + 3O_{2(g)} \rightarrow 4Fe(OH)_{3(s)}$	-1397.2

The data of ΔG for the above-mentioned corrosion reactions show that iron (Fe) may corrode in air, in water with and without dissolved oxygen. Note that the value of the Gibbs energy change (ΔG) does not show the reaction rate. The negative value of the Gibbs energy change just indicates whether the reaction can happen spontaneously or not.

The change in Gibbs energy in a chemical reaction can be calculated according to the equation (1).

$$\Delta G = \Delta G^{\circ} + RT.\ln\frac{[P]}{[R]} \quad (1)$$

Where ΔG is the change in Gibbs energy for the given reaction, ΔG^0 is the standard Gibbs energy difference, R is the universal gas constant, T is temperature in Kelvin and [P] and [R] are activity of products and reactants respectively. ΔG can also be written as:

$$\Delta G = n.F.E \quad (2)$$

where n is the number of electrons involved in the reaction, F, the Faraday constant (96,485 C/mol) and E, electrolytic potential produced by reaction. Substitution of ΔG from equation (2) in equation (1) at 25 °C derives equation (3) which is known as *Nernst* equation and represents the relationship between concentrations of electroactive species with the electrolytic potential provided at the metal surface [6].

$$E = E^{\circ} - \frac{0.059}{n}\log\frac{a_{red}}{a_{ox}} \quad (3)$$

(E. observed potential, E^0. potential of standard equilibrium corresponding to the electrode potential when the activity of ions in the solution is 1 M, n. number of electrons involved in reaction, a_{red}. ionic activity of reduced species, a_{ox}. ionic activity of oxidized species)

A Pourbaix diagram is a graphical representation of Nernst equation for the various possible reactions taking place during corrosion of a metal in a given environment. Using the Nernst equation the relationship between pH, concentration of electroactive species and the corrosion potential can be extracted. Figureure 1.4 shows a simplified Pourbaix diagram (also known as

equilibrium or E-pH diagram) for corrosion of iron in water at 25 °C with reactions 5-13 participating with $a_{Fe^{2+}} = 10^{-6}$.

$Fe^{2+} + 2e \leftrightarrow Fe$ (5)

$Fe^{3+} + e \leftrightarrow Fe^{2+}$ (6)

$Fe^{2+} + 2H_2O \leftrightarrow Fe(OH)_2 + 2H^+$ (7)

$Fe^{3+} + 3H_2O \leftrightarrow Fe(OH)_3 + 3H^+$ (8)

$Fe_2O_3 + 6H^+ + 2e \leftrightarrow 2Fe^{2+} + 3H_2O$ (9)

$Fe_3O_4 + 8H^+ + 2e \leftrightarrow 3Fe^{2+} + 4H_2O$ (10)

$3Fe_2O_3 + 2H^+ + 2e \leftrightarrow 2Fe_3O_4 + H_2O$ (11)

$H^+ + e \leftrightarrow \frac{1}{2} H_2$ or $H_2O + e \leftrightarrow \frac{1}{2} H_2 + OH^-$ (12)

$2H_2O \leftrightarrow O_2 + 4H^+ + OH^-$ or $4OH^- \leftrightarrow O_2 + 2H_2O + 4e$ (13)

In practice numerous reactions may participate in the corrosion process of steel. The presence of other electroactive species and non-standard conditions will change the regions of corrosion and immunity to some extent [8]. Pourbaix diagram can be used to predict corrosion behavior of metal and composition of corrosion product in a given environment and design an appropriate protection plan [2].

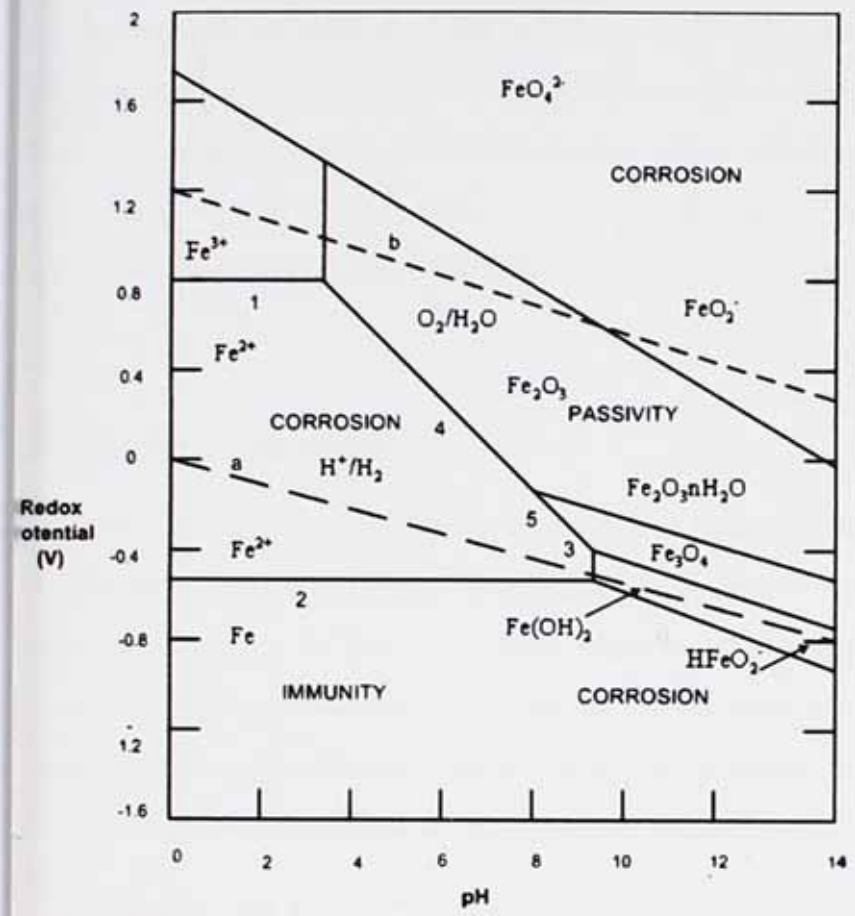

Figure 1.4 Potential-pH diagram for iron/water system at 25°C and $a_{Fe^{2+}} = 10^{-6}$ [7]

At the metal-electrolyte interface due to the polar character of water molecules, and the charge centers in ions that induce electric charges on the metal surface, an *electrical double layer* (EDL) establishes. Electrical double layer (also called Helmholtz layer) is a term first suggested by the German physical chemist Hermann Ludwig Ferdinand von Helmholtz in 1879. EDL comprises electrically charged parallel planes separated by distances of the order of magnitude of a few water molecules and forms a capacitor. This electrical interface produces electric energy/potential which is the driving force for movement of electrons and the corrosion process. Equation (14) represents relationship between electric potential at the metal surface and the amount of charge provided at the metal surface.

$$Q = C.E_a \quad (14)$$

(C is the proportionality coefficient of capacity of the capacitor)

The type and amount of charge at EDL depends on the surface characteristics and type and concentration of electroactive species at the electrolyte-metal interface. As a result of surface and environment heterogeneities the metal surface acquires different local potentials across the surface. Flow of electron from lower potential areas (anodic sites) to higher potential areas (cathodic sites) completes the electrochemical circuit and hence is conducive to corrosion.

1.3 Corrosion kinetics

Corrosion kinetics is a discipline dealing with the definition of corrosion rate, influence of various factors on corrosion rate and determination of the corrosion mechanism. Corrosion rate depends on variety of factors including the type of metal and its properties (e.g. crystalline structure, heterogeneity etc), presence of surface film, mechanical properties (presence of stresses), thermal treatment, type of environment (water, acid, alkali, salt, soil, atmosphere, etc.), temperature, flow rate and the corrosion mechanism.

When cathodic and anodic reactions happen at the same time on a surface, individual potentials corresponding to each reaction cannot be measured. In this situation a polyelectrode or mixed electrode forms with an electrolytic potential between cathodic and anodic reversible potentials. This mixed potential is so called *open circuit potential* (OCP) or rest corrosion potential at which the total rate of oxidation is equal to the total rate of reduction. The Figureure 1.5 graphically expresses the anodic and cathodic currents and their relationship with the corrosion potential. The interception of Tafel lines at which the sum of anodic oxidation current is equal to the sum of cathodic reduction currents defines corrosion potential and corrosion rate [6,9]. The mixed potential theory was derived originally to explain experimental electrochemical laboratory measurement. The usefulness of E-log I diagrams is that they combine thermodynamics and kinetics to form a whole picture: the potential axis is the thermodynamic factor and the current axis is the kinetic factor [10].

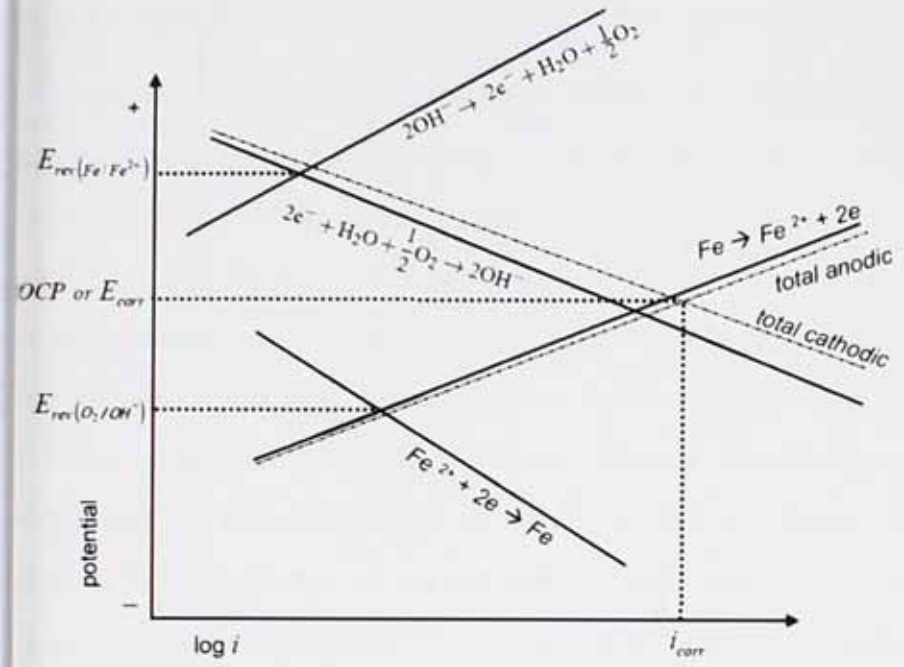

Figure 1.5 Anodic and cathodic half-cell reactions present simultaneously on a corroding steel surface [6].

If the Tafel line equation ($E = a + b\ Log\ I$, a and b are Tafel constants) be written separately for anodic and cathodic reactions, from solving them together equation (15) will be resulted which represents the relation between OCP with anodic/cathodic area ratio [11].

$$E_{corr} = E_{0.5} - \left[\frac{1}{b_a} + \frac{1}{|b_c|}\right] \log \frac{f_a}{f_c} \qquad (15)$$

Where f_a and f_c are anodic and cathodic area fractions respectively so that $f_a+f_c=1$, b_a and b_c are Tafel constants and $E_{0.5}$ is the corrosion potential when anodic area is equal to cathodic area ($f_a=f_c=0.5$). From the equation (15) it can be concluded that increasing the cathode/anode area ratio increases the OCP.

1.4 Oxide film

A relatively protective oxide film forms rapidly on clean surface of steel in the air. Gilroy and Mayne have measured the thickness of oxide film on carbon steel and shown that it increases from 1.6 nm at one day to 3.5 nm after one year [12]. The air formed passivating film on iron is determined to be Fe_3O_4, γ-Fe_2O_3 (cubic form of Fe_2O_3 crystal) or FeOOH (depending on the conditions under which it is formed), at the very early stages of exposure to air. Surface analysis of passive films on iron, as well as other metals such as aluminum and stainless steel, shows that the outer surfaces are usually more hydrated. This of course, only can be expected from film growth in aqueous solution or highly humid environment. The inner regions of the films tend to be less hydrated or not hydrated at all. In near neutral solutions the passive film on Fe (2-6 nm thick) has been characterized as the so-called cubic oxide γ-Fe_2O_3 overlying a thin film of Fe_3O_4 on the metal surface [3,13]. Studies have reported that α-, β-, γ-FeOOH, γ-Fe_2O_3, Fe_3O_4, and amorphous oxyhydroxides are of the main species that form the rust layer on steel [14–16].

Corrosion products in certain conditions may deposit on the metal surface and form a dense, continuous and intact layer which lowers conduction of ions from oxide-metal interface to electrolyte. Such oxide layer passivates the metal surface and reduces the corrosion rate by hindering anodic reactions. In practice, some of the highly reactive metals like aluminum, magnesium, tantalum, niobium, etc. are relatively stable in oxygen whereas other reactive metals such as the alkali and alkaline-earth metals oxidize rapidly and completely. In these examples, the kinetics of the reaction is controlled by the nature of the oxide film formed on the metal surface, which forms a protective barrier in the former group of metals and a non-protective one in the latter.

The properties characterizing a typical passivating oxide film are low ionic conductivity and low solubility. Table 1.2 lists electrical and solubility properties of different forms of iron oxide. Due to these properties the oxide prevents to a large extent the transport of metal cations from sites in the crystal structure of the metal to the liquid, i.e. it prevents the anodic dissolution. Such oxide films on steel are typically formed in dry air and not by deposition of corrosion

products from the electrolyte, as the latter usually gives more or less porous surface layers. It has been suggested that oxygen concentration and rapid oxidation of iron(II) to iron(III) hydroxide and precipitation of insoluble oxide/hydroxides play an important role in formation of an adherent and dense rust film [17,18]. The pore-plugging mechanism by these insolating oxide/hydroxides in a defective rust layer was suggested as a natural mechanism of corrosion inhibition. Also it has been shown that such rust layer is perm-selective in a way that allows permeation of cations but prevents diffusion of anions through the oxide film [17]. Although the oxide layer resulted by precipitation of corrosion products in electrolyte reduces both anodic and cathodic reactions to some extent, but it is not sufficiently barrier against flow of corrosion reactants to give efficient passivity. The passivating oxide layer that forms in a strong oxidizing environment, e.g. chromate solutions, is characterized as iron(III) form of oxides in close connection with the crystal structure of the metal [2].

Pilling and Bedworth [19] made the earliest attempt to correlate the oxide layer physical characteristics to its protective properties. They defined the Pilling-Bedworth ratio (P-B ratio) as the ratio of the volume of the elementary cell of a metal oxide to the volume of the elementary cell of the corresponding metal (from which the oxide is created). Therefore a P-B ratio close to 1 corresponds with a consistent and dense oxide layer which can efficiently protect metal from further corrosion as long as it is not chemically attacked and broken down by aggressive species, e.g. chloride. Also P-B ratios <1 or >2 represent discontinuous and porous oxide characteristics, respectively, that do not provide an effective protection against corrosion. P-B ratio of 1.69 for FeO:Fe indicates a relatively protective oxide, however FeO tends to convert to hydrated forms and Fe_2O_3 and Fe_3O_4 oxide forms in aqueous environment with P-B ratios of 2.14 and 2.10, respectively, which represent a porous oxide layer under compressive stress [20].

The passivating oxide film on steel in the air is extremely thin and in essence fragile, chemically, electrochemically and mechanically, but the fragility depends on the metal and the environment. It has been shown that the presence of chloride ion in the electrolyte enhances dissolution of oxide layer and breaks down the passivity which is typically followed by pitting corrosion [21–23]. In fact passive film formation is a dynamic process competing with active

metal dissolution and thickening of the passive oxide film that results in corrosion current reduction [6]. Due to the insulating properties (dielectric constant) of most of the oxide forms of steel being higher than the electrolyte, growth of oxide layer increases the value of capacitance formed at the electrical double layer. Also a thickened oxide film, constituted from corrosion products precipitation, hinders the flow of oxygen toward the cathodic reaction sites and the corrosion process is retarded by the low diffusion rate i.e. corrosion becomes diffusion controlled [24].

Table 1.2 Physico-chemical properties of corrosion products of iron [5]

Chemical formula	Name	Density, g/cm^3	Color	Electro-conductive properties	Thermal behavior
FeO	Wüstite	5.4–5.7	Gray-black	Very low electro-conductivity, 10 Ohm^{-1}·m^{-1}, Semiconductor	Decomposes to Fe and Fe_3O_4 below 570°C. Melts at 1371–1424°C
α-Fe_2O_3	Haematite	5.25	Brick-red to black	Insulator	Decomposes to Fe_3O_4 at 1457°C
γ-Fe_2O_3	Maghemite	4.88	Brown	Semiconductor to insulator	Transforms to α-Fe_2O_3 above 250°C
Fe_3O_4	Magnetite	5.20	Black-grayish	Good electro-conductivity, 10^4–10^5 Ohm^{-1}·m^{-1}, Conductor	Melts at 1597°C
$Fe(OH)_2$	Ferrous Hydroxide	3.40	White-blue	Insulator	Decomposes* to Fe_3O_4 and H_2 at ~100°C
α-FeOOH	Goethite	4.20	Yellow, reddish-brown	Insulator	Dehydrates to α-Fe_2O_3 at ~200°C**
γ-FeOOH	Lepidokrokite	3.97	Orange	Insulator	Dehydrates to γ-Fe_2O_3 at ~200°C**

*$Fe(OH)_2$ is unstable in contact with traces of O_2 at ~20°C and transforms into α-FeOOH, γ-FeOOH or Fe_3O_4 depending on the conditions.
**The presence of water causes conversion to α-Fe_2O_3 at lower temperature.

1.5 Heterogeneity

The idea of electrochemical heterogeneity belongs to the Swiss scientist De la Rive (1837) who investigated dissolution of zinc and its alloys in hydrochloric acid, and observed that the more contaminates in zinc alloy results is the greater dissolution rate of zinc in the acid. De la Rive suggested that such contaminants formed micro-galvanic cells and probably resulted in acceleration of corrosion of zinc in the acid. Electrochemical heterogeneity influences the corrosion rate through providing larger number of anodic dissolution sites. It also encourages the localized forms of corrosion (e.g. pitting corrosion) which are by far more dangerous and costly compared to uniform corrosion pattern [25,26]. An early study by Enos at 1925 showed that corrosion properties of carbon steel does not change significantly by varying the carbon content of steel while environmental factors such as temperature can remarkably alter the corrosion rate [27]. In fact, in corrosion of steel heterogeneity of primarily formed oxide film plays a key role. A highly defective or heterogeneous oxide film provides larger number of pathways for electroactive species to flow from anodic sites and enhances the corrosion process [28]. Because of semi-conductive behaviour of typical oxide layers on steel, reduction reactions in neutral solutions take place on the surface of oxide layer which provides a large cathodic area.

Heterogeneities associated with the metal structure have been classified in Table 1.3 as atomic (also see Figure 1.6), microscopic (visible under an optical microscope), and macroscopic scale heterogeneities. Detailed mechanism of all aspects of corrosion (e.g. the passage of a metallic cation from the lattice to the solution, specific effects of ions and species in solution in accelerating or inhibiting corrosion or causing stress-corrosion cracking, etc.) involves consideration of the detailed atomic structure of the metal or alloy.

Table 1.3 Structural heterogeneities in metals important to corrosion resistance properties [3]

1. Atomic (Figure 1.1). (a) Sites within a given surface layer (b) Sites at edges of partially complete layers. (c) Point defects in the surface layer: vacancies (molecules missing in surface layer), kink sites (molecules missing at edge of layer), molecules adsorbed on top of complete layer. (d) Disordered molecules at point of emergence of dislocations (screw or edge) in metal surface.
2. Microscopic (a) Grain boundaries-usually, but not invariably, more reactive than grain interior. (b) Phases-metallic (single metals, solid solutions. intermetallic compounds), nonmetallic, metal compounds, impurities, etc. - heterogeneities due to thermal or mechanical causes.
3. Macroscopic (a) Discontinuities on metal surface-cut edges, scratches, discontinuities in oxide films (or other chemical films) or in applied metallic or non-metallic coatings. (b) Bimetallic couples of dissimilar metals. (c) Geometrical factors-general design, crevices, contact with non-metallic materials. etc.

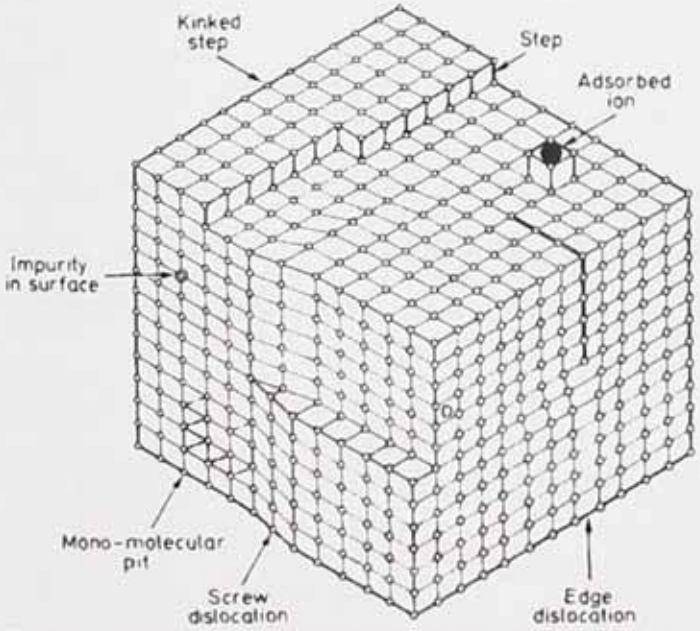

Figure 1.6 Surface imperfections in metallic lattice responsible for electrochemical heterogeneity and formation of micro-galvanic cells as an initiating factor for aqueous corrosion [3].

Macroscopic heterogeneities, e.g. crevices, discontinuities in surface films, bimetallic contacts etc. will have a pronounced effect on the location and the kinetics of the corrosion reaction. Etching the metal surface for metallographic identification is an example of the effect of discontinuity on localized corrosion which takes advantage of the different corrosion rates of phases (the grain boundaries are usually etched more rapidly than the rest of the grain due to the greater reactivity of the disarrayed metal). It has been also shown that the geometrical depth of the surface roughness or irregularities plays a key role in providing potential sites for pit formation and active localized corrosion. Anodic sites tend to form at the bottom of dents where the surface has lowest access to oxygen and gives highest value of local current density [29].

Apart from the metallurgical heterogeneities, the heterogeneity of the environment (for example, differences in concentrations of dissolved oxygen, pH, and temperature gradient on the metal's surface) may also result in the formation of anodic and cathodic zones on the metal surface (electrochemical heterogeneity), resulting in corrosion. According to the Nernst equation (Eq. 16), if two sites on a carbon steel surface differ in dissolved oxygen concentrations, $[O_2]_1$ and $[O_2]_2$, these sites acquire different electrolytic potentials

$$E = E_1 - E_2 = \frac{RT}{nF}.\ln\frac{[O_2]_1}{[O_2]_2} \qquad (16)$$

This difference in potentials makes a local galvanic cell called *differential aeration cell* with higher potential parts being cathodic sites and lower potential parts becoming anodic sites (dissolution of metal and corrosion) resulting in localized corrosion [3].

1.6 Methods of corrosion monitoring

1.6.1 Open circuit potential

When cathodic and anodic reactions happen at the same time on a surface, individual potentials corresponding to each reaction cannot be measured. In this situation a polyelectrode

or mixed electrode forms with an electrolytic potential between cathodic and anodic reversible potentials. This mixed potential is so called *open circuit potential* (OCP) or rest corrosion potential at which the total rate of oxidation is equal to the total rate of reduction [6,9]. The corrosion potential measured at an open electric circuit (OCP) can be used as a qualitative characteristic of the corrosion process on a metal surface. The corrosion potential is measured in comparison with reference electrodes such as calomel, silver/silver chloride, or copper/copper sulphate electrodes. As discussed earlier, according to the equation (5) if the ratio of anodic/cathodic area increases, the OCP value drops and an increase in fraction of cathodic area causes a rise in the OCP. In practice, since cathodic reactions happen on oxide layer or passivated areas and anodic areas are the sites at which active dissolution of metal or corrosion happens, rise of corrosion potential is considered as passivation and lowering the corrosion rate. Also if the corrosion potential of a metal decreases with time, the corrosion process intensifies. Breakdown of oxide layer in neutral solutions, as it provides larger number anodic sites, reduces the OCP value. However these general rules are not always correct as many factors can shift the potential values towards more positive or negative values, but these shifts may not necessarily be related to the corrosion status of metals. For example, a decrease of oxygen concentration at the steel surface causes more negative corrosion potential values (Nernst equation. It should be noted that while OCP is a reliable measure of corrosion thermodynamic it may not correspond with corrosion kinetic on the metal surface [5,30].

1.6.2 Polarisation technique

Potentiodynamic polarization technique is the only practical technique for measuring the instantaneous corrosion rate. Other methods of measuring corrosion rate such as weight loss may be used to measure the corrosion rate only in the long term. It must be kept in mind that polarization is a destructive electrochemical technique since it intensifies the driving force for corrosion reactions by providing extra electrons for anodic reaction (anodic polarization) or accelerating cathodic reactions by demanding more electrons (cathodic polarization). By studying the change of corrosion rate at potentials higher and lower than OCP, rate of corrosion

at rest potential can be extrapolated. Also active-passive behavior, corrosion resistance and anodic-cathodic reactions can be analysed [30].

Linear polarization (LPR) method uses a very small potential spectrum, ±20 mV with respect to OCP, where the corrosion rate has linear or Ohmic correlation with potential. Then the polarisation resistance can be obtained in a reasonably less destructive manner using equation 17:

$$R_p = \frac{\Delta E}{\Delta I} \quad (17)$$

Stern and Geary (1957) [31] showed that the corrosion current i_{corr} can be calculated if we know the polarization resistance R_p:

$$i_{corr} = \frac{B}{R_p} \quad (18)$$

where B is the Stern–Geary constant (mV) depending on the type of the metal and environment. Knowing anodic and cathodic Tafel constants, β_a and β_c, B can be calculated according to equation 19:

$$B = \frac{1}{2.3R_p}\left(\frac{\beta_a.\beta_c}{\beta_a + \beta_c}\right) \quad (19)$$

Evans diagrams are produced by expanding the polarization range to higher extents (app ±100 mV with respect to OCP). Using linear parts of Evans diagram at anodic and cathodic branches, Tafel curve is reproducible. Corrosion rate is calculated as the current density at which cathodic and anodic branches intercept. Also anodic and cathodic reactions and the rate controlling mechanism of corrosion (diffusion or activation) can be studied using anodic and cathodic Tafel constants [2,5,30,32]. It has been shown by Mansfield and Oldham that Stern-Geary equation for measuring corrosion rate is valid only when corrosion potential lies far from the reversible potentials of either of oxidation or reduction reactions [33].

1.6.3 Electrochemical impedance spectroscopy

EIS studies the system response to the application of a periodic small amplitude AC signal. These measurements are carried out in a range of ac frequencies with small magnitude of polarizing potential (e.g. ±10 mV) around the OCP. Analysis of the system response provides information about the phenomena which can impede the current flow. This applies to electrochemical processes at the metal-electrolyte interface, oxide layer and corrosion products, barrier layers (e.g. organic coatings) and electrolyte resistance. Each of these elements affects the alternating current at different frequencies and so can be characterized separately. The corroding system can be then simulated with an electrical equivalent circuit (EEC) where each element of circuit represents a phenomenon in actual electrochemical process. For example capacitive aspect of an organic coating introduces time lag and a measureable phase angle to the applied electric signal in discrete frequencies different from frequencies affected by double layer capacitive. Change in capacitance value of organic coating is typically connected with water-uptake which increases its dielectric constant, while change in capacitance value of electrical double layer is normally a result of chemical change in composition of EDL at metal-electrolyte interface and/or change in thickness of diffusion layer [6,34]. Finding a proper EEC to match the experimental spectrum could be in many cases challenging. So special attention should be given to selection of EEC to comply with the physical model of corroding system and yet produce an acceptable fit with the experimental data; addition of circuit elements simply to improve the fit is unacceptable [35].

1.6.4 Electrochemical noise measurement

Electrochemical noise consists of low-frequency, low-amplitude fluctuations of current and potential due to electrochemical activity associated with corrosion processes. Potential noise is measured by collecting the potential versus time record between a noisy corroding electrode and a noiseless reference electrode using a high-impedance digital voltmeter. This is essentially a measurement of the open circuit potential. Measurement of current noise is made using a zero resistance ammeter (ZRA) connecting two identical working electrodes immersed in the

same electrolyte [36]. ENM is one of the very few entirely non-destructive techniques (NDT) for electrochemical characterization as it does not perturb current or potential of the corroding system. Several developments have been made in the last decade to increase the versatility and effectiveness of ENM using one, two or three working electrodes [37].

Electrochemical noise data can be analysed either statistically or by examining the noise spectrum. Figureure 1.7 illustrates how pit formation produces current and potential transients. In most cases current is the controlling parameter and the potential is response of the rest of surface to the local corrosion current. The current from the pit is largely drawn from the capacitance of the passive film, causing the potential to fall over the period of the current transient and then rise more slowly as the passive film recharges as a result of cathodic reaction [36]. If clear isolated transients are observed, it is possible to derive considerable information about the pitting process. The area under a transient in a current noise time record indicates the charge involved in the transient and hence the volume of pit formed. In general, localized corrosion processes are facilitated by rough, heterogeneous surfaces, as roughness and imperfections help to support the local changes in chemical conditions that are responsible for the localization of the corrosion [38].

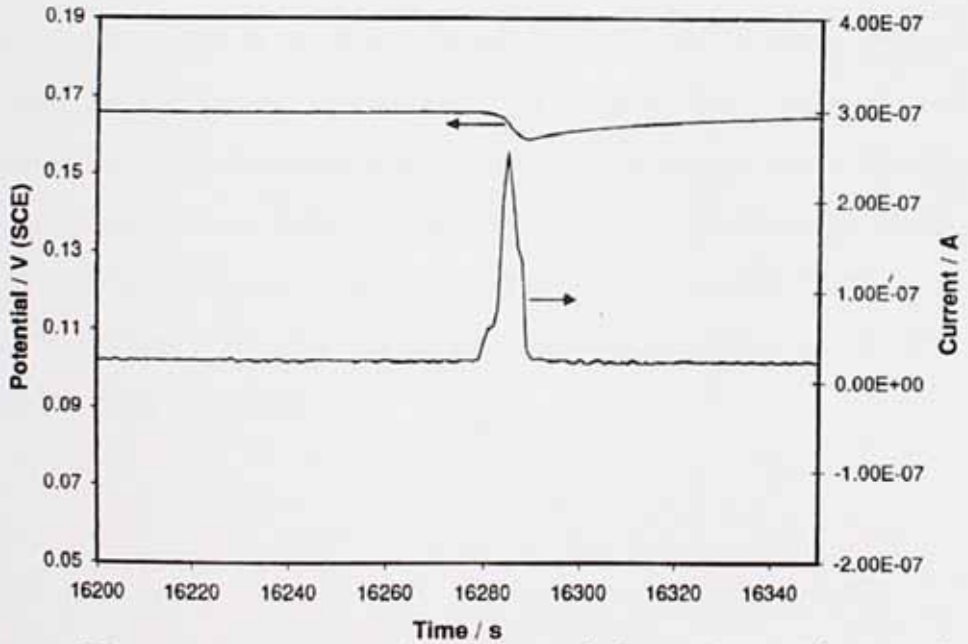

Figure 1.7 current and potential time records for a 304 stainless steel in 3.5% NaCl solution, showing pitting events [36].

Electrochemical noise can be characterized by some common statistical parameters including the mean, the variance, and the standard deviation. In particular, the standard deviation, σ, is used as a measure of the amplitude of the variation in the noise signal. Skew and kurtosis sometimes give indications of the form of corrosion (e.g. localized or uniform) occurring [39]. The electrical resistance noise can be calculated as a derivative of a potential and a current noise according to Ohm's law (Eq. 20), and these values are usually in accord with the linear polarization resistance [40] value and the impedance value from EIS [41].

$$R_n = \frac{\sigma_V}{\sigma_I} \qquad (20)$$

where R_n is the noise resistance in ohms, and σ_V and σ_I are the standard deviation in the potential and current noise signals, respectively.

1.6.5 Scanning vibrating electrode technique (SVET)

The scanning vibrating electrode technique (SVET) is a well-established electrochemical technique that allows the spatial distribution of the often highly localised electrochemical reactions of corrosion to be investigated. A single pseudoreference electrode is scanned across the corroding surface to identify anode and cathode locations, the current density, and the current density vectors in solution. This enables direct measurement of the progress and intensity of local corrosion processes on a site-by-site basis. The SVET utilizes a movable microtip electrode to detect the potential gradients produced by localised ionic current fluxes within the solution above a corroding surface at a small fixed distance. Consequently the current density in the direction of the electrode oscillation can be calculated using calibrated potential data [32,42,43].

1.7 Methods of corrosion inhibition

As discussed earlier in this chapter, electrochemical corrosion consists of three processes:

1. Anodic, or oxidizing, process – passing of metal cations into solution and releasing of electrons on the metal surface:

$M(s) \rightarrow Mn^{+}_{(aq)} + ne^{-}$ (M – metal; $Mn^{+}_{(aq)}$ – metallic cations in solution)

2. Flow of the electrons released from the anode (low electric potential site) to the cathode (high electric potential site).

3. Cathodic, or reduction, process – any process that receives electrons by neutral or charged species D:

$D_{(aq)} + ne- \rightarrow D^{n-}{}_{(aq)}$

Elimination of one of these processes will decelerate corrosion of metal and that process becomes rate determining step or controlling mechanism of corrosion.

All corrosion prevention methods aim at removing or reducing the effect of one or more of the conditions leading to corrosion using the following strategies:

1. Selecting a material that does not corrode in the given environment.

2. Changing the environment, e.g. removing the oxygen or adding anticorrosion chemicals (inhibitors).

3. Using a design that will avoid corrosion, e.g. preventing the accumulation of water so that the metal surface can be kept dry.

4. Changing the potential, most often by making the metal more negative and thus counteracting the natural tendency of the positive metal ions to be transferred from the metal to the environment, e.g. cathodic protection

5. Applying coatings on the metal surface, these operate by a variety of mechanisms e.g. metallic and most inorganic coatings isolate the metal from the environment, organic coatings interfere with conduction between anodes or cathodes and/or create chemical conditions at the interface which encourage passivation.

The use of paint coatings is the most common method for corrosion prevention. Protective coatings are unique specialty products which represent the most widely used method of corrosion control. They are used to give long-term protection under a broad range of corrosive conditions, extending from atmospheric exposure to full immersion in strongly corrosive solutions. The following chapter reviews the mechanisms by which the organic coatings protect metal against corrosion with an emphasis on the role of surface preparation of metal and presence of structural inhomogeneity in organic coatings.

References

[1] U.R. Evans, The Mechanism of Oxidation and Tarnishing, Transactions of The Electrochemical Society. 91 (1947) 547–572.

[2] E. Bardal, Corrosion and protection, Springer, London, 2004.

[3] L.L. Sheir, R.A. Jarman, G.T. Burstein, eds., Corrosion. Volume 1: Metal/Environment Reactions, 3rd ed., Butterworth-Heinemann, Oxford, UK, 1994.

[4] C.G. Munger, L.D. Vincent, Coating fundamentals, in: Corrosion Prevention by Protective Coatings, 2nd ed., NACE International, Houston, TX, 1999: pp. 61–85.

[5] A. Groysman, Corrosion for Everybody, Springer, Dordrecht, 2010.

[6] D.A. Jones, Principles and prevention of corrosion, 2nd ed., Prentice-Hall, NJ, USA, 1996.

[7] Z. Ahmed, Principles of corrosion engineering and corrosion control, 1st editio, Butterworth-Heinemann, Oxford, UK, 2006.

[8] E.D.J. Verink, Simplified procedure for constructing Pourbaix diagram, in: R.W. Revie (Ed.), Uhlig's Corrosion Handbook, 2nd editio, John Wiley & Sons, Inc, NY, USA, 2000: pp. 116–124.

[9] D.L. Piron, The electrochemistry of corrosion, NACE International, Houston, TX, 1991.

[10] I. Andijani, S. Turgoose, Studies on corrosion of carbon steel in deaerated saline solutions in presence of scale inhibitor, in: WSTA IV Gulf Conference, Bahrain, 1999: pp. 223–231.

[11] S. Barnartt, Electrochemical nature of corrosion, in: R. Baboian (Ed.), Electrochemial Techniques for Corrosion Engineering, NACE International, Houston, TX, 1986: pp. 1–11.

[12] D. Gilroy, J.E.O. Mayne, The oxidation of iron at room temperature, Corrosion Science. 5 (1965) 55–58.

[13] P.R. Roberge, Handbook of Corrosion Engineering,, 1st ed., McGraw-Hill, NY, USA, 2000.

[14] M. Yamashita, H. Miyuki, Y. Matsuda, T. Nagano, T. Misawa, The long term growth of the protective rust layer formed on weathering steel by atmospheric corrosion during a quarter of a century, Corrosion Science. 36 (1994) 283–299.

[15] U. Evans, The corrosion and oxidation of metals Vol. 2, Arnold, London, 1976.

[16] C. Leigraf, T.E. Graedel, Atmospheric corrosion, Electrochem. Soc. Ser., John Wiley & Sons, Inc, New York, 2000.

[17] H. Tamura, The role of rusts in corrosion and corrosion protection of iron and steel, Corrosion Science. 50 (2008) 1872–1883.

[18] C.F. Dong, H.B. Xue, X.G. Li, H.B. Qi, Y.F. Cheng, Electrochemical corrosion behavior of hot-rolled steel under oxide scale in chloride solution, Electrochimica Acta. 54 (2009) 4223–4228.

[19] N.B. Pilling, R.E. Bedworth, The Oxidation of Metals at High Temperature, Journal of the Institute of Metals. 29 (1923) 529–582.

[20] E. McCafferty, Introduction to corrosion science, 1st editio, Springer, New York, 2010.

[21] U. Bertocci, An Examination of Current Fluctuations during Pit Initiation in Fe-Cr Alloys, Journal of The Electrochemical Society. 131 (1984) 1011–1017.

[22] Y.F. Cheng, M. Wilmott, J.L. Luo, The role of chloride ions in pitting of carbon steel studied by the statistical analysis of electrochemical noise, Applied Surface Science. 152 (1999) 161–168.

[23] H.E.H. Bird, B.R. Pearson, P. a. Brook, The breakdown of passive films on iron, Corrosion Science. 28 (1988) 81–86.

[24] Y. Waseda, S. Suzuki, eds., Characterization of Corrosion Products on Steel Surfaces, Springer, Berlin Heidelberg, Germany, 2006.

[25] C.H. Hare, Corrosion Phenomena: specific forms, Journal of Protective Coatings & Linings. (1998) 63–77.

[26] J.R. Scully, The fundamentals of corrosion, 2nd editio, Persamon Press, Oxford, UK, 1975.

[27] G.M. Enos, Fundamental Factors in Corrosion, Industrial & Engineering Chemistry. 17 (1925) 793–797.

[28] D. Talbot, J. Talbot, Corrosion Science and Technology, CRC Press, Boca Raton, USA, 1998.

[29] X. Tang, Y.F. Cheng, Localized dissolution electrochemistry at surface irregularities of pipeline steel, Applied Surface Science. 254 (2008) 5199–5205.

[30] S.W. Tait, An introduction to electrochemical corrosion testing for practicing engineering and scientists, Pair o Docs publications, Racine, Wisconsin, 1994.

[31] M. Stern, A.L. Geary, Electrochemical Polarization: I. A theoretical analysis of the shape of polarization curves, Journal of The Electrochemical Society. 104 (1957) 56.

[32] R.G. Kelly, J.R. Scully, D.W. Shoesmith, R.G. Buchheit, Electrochemical Techniques in Corrosion Science and Engineering, , Marcel Dekker, USA 2003, NY, USA, 2003.

[33] F. Mansfeld, K. Oldham, A modification of the Stern—Geary linear polarization equation, Corrosion Science. 11 (1971) 787–796.

[34] A. Lasia, Electrochemical Impedance Spectroscopy and its Applications, in: B.E. Conway, J.O.M. Bockris, R.E. White (Eds.), Modern Aspects of Electrochemistry, Springer US, 2002: pp. 143–248.

[35] G.S. Frankel, Electrochemical Techniques in Corrosion: Status, Limitations, and Needs, Journal of ASTM International. 5 (2008) 101241.

[36] R.A. Cottis, S. Turgoose, Electrochemical impedance and noise, NACE International, Houston, TX, 1999.

[37] D.J. Mills, S.S. Jamali, M.T. Tobiszewski, Developing electrochemical measurements in order to assess anti-corrosive coatings more effectively, Progress in Organic Coatings. 74 (2012) 385–390.

[38] H.A.A. Al-Mazeedi, R.A. Cottis, A practical evaluation of electrochemical noise parameters as indicators of corrosion type, Electrochimica Acta. 49 (2004) 2787–2793.

[39] R.A. Cottis, M.A.A. Al-Awadhi, H. Al-Mazeedi, S. Turgoose, Measures for the detection of localized corrosion with electrochemical noise, Electrochimica Acta. 46 (2001) 3665–3674.

[40] G. Gusmano, G. Montesperelli, S. Pacetti, A. Petitti, Resistance electrochemical noise as a tool for corrosion rate prediction, in: Corrosion 96, NACE International, Denver, Co, 1996: p. paper No. 336.

[41] S.S. Jamali, D.J. Mills, C.P. Woodcock, Ways of increasing the effectiveness of the electrochemical noise method for assessment of organic coatings on metal, ECS Transactions. 24 (2010) 115–125.

[42] H.N. McMurray, J. Searle, B. Wilson, The use of SVET for investigating changes in the corrosion mechanism induced by forming galvanised steel samples, in: EuroCorr 2000, Maney publishing, London, 2000.

[43] H.N. McMurray, D. Williams, D.A. Worsley, Perturbation of diffusion controlled oxygen reduction kinetics by the scanning vibrating electrode in the corrosion of galvanized steel, in: 204th ECS Metting, Electrochemical society, 2003: p. Abs. 471.

Chapter 2

Corrosion control by means of organic coatings

2.1 Paint structure and generic coatings types

Organic coatings are complex mixtures of chemical substances that can be grouped into four broad categories: (1) binders, (2) volatile compounds, (3) pigments, and (4) additives [1]. The binder or resin is the polymeric part of the coating which binds together the other substances in the coating and forms a continuous film that adheres to the substrate. Many of the coating's physical and mechanical properties including flexibility, hardness, chemical resistance, UV-vulnerability, and water and oxygen transport are determined wholly or in part by the particular resin or blend of resins used [2]. Polymeric coatings are most often categorized based on the chemical structure of the binder as this defines to a large extent the suitability of the coating for a particular application. Important classes of polymeric binders are amino resins, polyurethanes, epoxies, acrylics, polyesters, drying oils, alkyds, vinyl and silicon resins. Although general properties are attributed to each generic type of resins (e.g. UV vulnerability of epoxies or good flexibility of polyurethanes), literally hundreds of resins are now commercially manufactured and available within each group, all with chemically unique structure. A paint formulator may purposely blend several resins to take advantage of the characteristics of each.

The complete polymeric structure of the binder could form either by pre-polymerization or on-site polymerization when applied on the substrate [3]. In the former case polymers are prepared before the application and polymeric structure does not change during the film formation process. Binders of this group generally have the highest initial molecular weight and formation of film takes place by the evaporation of solvent only (thermo-plastic). The on-site polymerization refers to active binders that complete the polymerization process after application by reacting with oxygen, secondary reactive resin or radical polymerization by a photoinitiator. Binders of this group produce the highest final molecular weight and in most cases a polymeric network that cannot be dissolved in solvents or melted (thermo-set) after formation.

2.2 Protective organic coatings

Protection afforded by an organic coating could be regarded as protection against UV, colour fading, abrasion and scratch, micro-organisms (anti-fouling coatings), dirt pick-up (anti-graffiti coatings) or corrosion. Throughout this book protective properties will be regarded as the ability of organic coatings in protecting metal substrate against electrochemical corrosion. However degradation induced by other environmental factors, e.g. UV or abrasion, can significantly affect the anti-corrosive properties as well [4,5]. Any discussion which considers the prevention of aqueous metallic corrosion, usually takes as its starting point the electrochemical model of the corrosion of mild steel in a neutral electrolyte with the four important processes involved linked in series namely; the anodic reaction, the cathodic reaction and the conductive pathways for ions and electrons [6]. Inhibition of the anodic or cathodic reactions or an interruption of the ionic flow are the three key elements that cause a significant reduction of the corrosion rate [7]. Thus, all corrosion prevention measures are aimed at removing or suppressing one of these three. One of the most convenient, and certainly the oldest method of protecting a substrate from the detrimental effects of the environment, is to coat it with a polymeric paint to isolate it from its surroundings [8]. At first it was thought that effective paints isolate their substrate from all potentially corrosive species, i.e. oxygen, water and ions. However this is now clarified that polymeric coatings are relatively permeable to water and oxygen and corrosion protection is normally afforded by isolation from ions. An effective protection by barrier mechanism requires that coatings impede the ionic conduction and remain adherent in the presence of water and the products of metallic corrosion [9,10].

Development, selection and qualification of new coatings for a specific application/environment require a thorough characterization of the coating and prediction of the performance in the given environment [11]. The most reliable way of studying the suitability of a coating for a specific substrate and environment is to actually expose coated substrate to the environment in which the coating will ultimately be applied [3,12]. In practice, outdoor exposure tests require a very long evaluation time, e.g. up to 10-20 years, before a reliable conclusion can be drawn. Consequently, results are not provided in a commercially acceptable time period [13,14]. Many studies have been devoted to prediction of the

performance and durability of the protective coatings in the past few decades, however the overall performance and durability is very difficult to assess because it is affected by several internal and external factors [15]. The natural rate of coating degradation and corrosion can be accelerated by altering the temperature, humidity, pH, salt concentration and intensity of UV radiation in so-called accelerated corrosion testing [16–19]. Ideally, the stresses only cause the system to fail faster than it normally would, while the mechanism of failure remains the same as in the non-accelerated condition. In many cases, the correlation between accelerated test methods and natural outdoor exposure concerns a progression of corrosion or disbondment from mechanical damage, which cannot necessarily be translated into lifetime predictions of intact coatings [20]. Also the diversity of paint types applied to different substrates exposed to a variety of environments results in more than one degradation mechanism and many factors are likely to be involved to varying degrees [21].

2.3 Protection mechanisms

In order to improve durability and performance of protective coatings it is essential to achieve an in-depth understanding of the mechanisms by which organic coatings afford corrosion protection. The major protection mechanism of a coating is determined by the type of pigment used in the paint formulation. Pigments come in three major types: inhibitive, sacrificial and barrier [22]. Consequently the main protection mechanisms are known as surface passivation by corrosion inhibitor, cathodic protection by electrochemically active coatings and ion deprivation.

2.3.1 Corrosion inhibitors

Corrosion inhibitors have been widely used to yield a uniform corrosion in aqueous solutions and avoid early failures due to highly localized corrosion [23]. The anticorrosive mechanism of inhibitive coatings relies on passivation of the substrate and build-up of a protective layer consisting of insoluble metallic complexes, which impede transport of aggressive species by acting as a barrier [24]. Inhibitive pigments are classified according to their effect on the anodic and cathodic reactions. Cathodic inhibitors, such as inorganic salts of zinc, magnesium and

manganese, suppress corrosion at the cathode by forming insoluble deposits with hydroxyl ions in neutral environments [25]. These pigments increase the cathodic resistance against polarization, forming visible films on metallic surfaces. Anodic inhibitors, such as inorganic salts of phosphate [26,27], borate [28,29], molybdate [30] and silicate compounds , form a protective oxide film on the metal surface. Anodic inhibitors are adsorbed onto the surface of the substrate and reduce the rate of corrosion by increasing the anodic polarization. A more recent development of corrosion inhibitors are rare-earth compounds that have gained increasing attraction in the last decade as a replacement for the toxic inhibitors such as chromate salts [31,32]. The inhibitive properties of rare earth compounds were first introduced by Hinton *et al.* on corrosion protection of aluminium in saline media [33]. Effectiveness of rare earth compounds as green corrosion inhibitors has been demonstrated for ferrous metals [34–36], zinc [37,38] and aluminium [39–41].

Defects formed during installation and service life of a painted metal could initiate the corrosion which spreads underneath the paint coating and reduce the performance and service life of protective system. Corrosion inhibitive pigments are introduced in organic coatings mainly to control the corrosion and its consequences, e.g. cathodic delamination and anodic undermining [42]. Cathodic delamination and anodic undermining are the two main mechanisms of corrosion induced coating disbondment from a metal substrate. The highly alkaline electrolyte present in cathodic regions under the paint film weakens the coating-metal bonds resulting in cathodic delamination, while in anodic undermining dissolution of underlying metal results in anodic disbondment. Corrosion inhibitors, depending on their inhibition mechanism, i.e. cathodic, anodic or both, passivate the metal surface and prevent the paint disbondment. The addition of inhibitors provides protection to the damage zones through the so-called "self-healing" effect by formation of another protective layer [43]. Self-healing effect is generally defined as the ability of coating to recover after a mechanical damage and effectively continue to protect the underlying substrate. In most cases this is achieved by replenishing the damaged area with reactive chemicals being stored in the coating layer [44]. The solubility of inhibitive pigment and permeability of binder to provide a consistent release of

inhibitor over a long period of protection play key roles in effectiveness of an inhibitive coating [45].

2.3.2 Electrochemically active coatings

Two main groups of electrochemically active protective coatings are conductive polymers and sacrificial coatings. The latter group is the polymer coatings filled with a sacrificial metal pigment, e.g. zinc or magnesium, which are galvanically coupled with the substrate to provide cathodic protection. Due to the need for electrical contact to the substrate, sacrificial coatings are only applied as a primer coat. The protection mechanism remains cathodic protection as long as there is conductive network of zinc powders inside the coating through to substrate. In the long term, corrosion of zinc interrupts the conductive network by turning zinc into non-conductive zinc corrosion products which changes the protection mechanism to barrier effect [46,47]. The inorganic zinc-rich coatings are considered relatively porous to ingress of electrolyte with primary valency bond of the polymer to zinc atoms on the particles of zinc dust pigment. This affords good film strength, adhesion, electrical conductivity, and cathodic protection [10,48].

Conducting polymers are a unique group of organic polymer with capability of electronic, chemical and/or electrochemical interaction with active metals. The mechanism by which the conducting polymers protect active metal from corrosion is not fully understood, however a number of mechanisms have been proposed [49]. Altering the corrosion potential, creating a diffusion limiting electro-magnetic field, barrier protection and gradual release of dopant to act as corrosion inhibitor are the main suggested mechanisms [50,51]. Efficiency of a conducting polymer as a corrosion inhibitor greatly depends on the nature of metal surface and electrochemical potential at the interface, physico-chemical properties of the polymer such as functional groups, steric factors, aromaticity and the electronic structure of the molecules [52].

2.3.3 Barrier coatings

Historically, a number of different theories regarding the role of the barrier function in corrosion protection have emerged [53,54]. For many years, it was believed that barrier coatings might function by excluding water and oxygen from the metal [8]. Crennell observed a general cathodic behaviour of painted steel when coupled with bare steel in saline solutions. Therefore he suggested that protection properties of paint coatings are attributed to encapsulation of Fe^{2+} and OH^- as primary corrosion product which thus results in their accumulation at steel surface and subsequent passivation [55]. This belief was soundly disputed when, in the early 1950s, JEO Mayne measured the amount of water and oxygen passing through a normal 100 um paint film [56]. He found water and oxygen permeability levels to be much higher than the levels needed to initiate and sustain the average rate of corrosion on unprotected steel. Therefore the protection was attributed to the high electrical resistance and low ionic permeability of coatings that impeded anodic/cathodic reactions. This was in line with findings of Smith, Bacon and Rugg [57] which showed direct relationship between electrolytic resistance and the corrosion protection afforded by paint coatings. Theoretical studies by Pearson and Brook [58] revealed that increased resistance between anode and cathode above 10^6 $\Omega.cm^2$ drives the steel potential into passivity region, therefore they suggested that paint coatings mitigate corrosion by passivation of substrate.

The cathodic characteristic of painted steel when coupled by bare steel in salt solution was also explained by Mayne as ohmic potential drop caused by the ionic resistance. Figure 2.1 illustrates the effect of ohmic drop on corrosion potential on Evans diagram. The measured potential of bare steel in a conducting electrolyte would be given by point B, the corrosion potential, where the cathodic polarization curve CB and the anodic curve AB intersect. Mayne considered that on painted steel the high electrolyte resistance of the paint would introduce an ohmic potential drop between the anodic and cathodic areas by impeding the current passing through cathode/liquid/anode circuit. If the cathode/liquid and anode/liquid resistances are equal the measured potential would be equal to E which lies half-way between D and D. Mayne suggested that anodic areas are situated at small weak points on steel so that the resistance of the approach to the smaller anodes would be greater. This would move the potential E nearer

to D than F and therefore E, representing the corrosion potential of painted steel, would be cathodic to the potential B for unpainted steel. More recently Evans diagrams for Zn/Fe [59] and Fe/Cu [60] coupled electrodes were constructed by Sykes and Xu using potentiostatic current measurements at different over-potentials. Their results indicated that in addition to the ohmic drop, caused by the resistive paint, the polarization of electrodes beneath the coating also makes an important contribution to the corrosion protection afforded by paint coating particularly when the coating's resistance is relatively low.

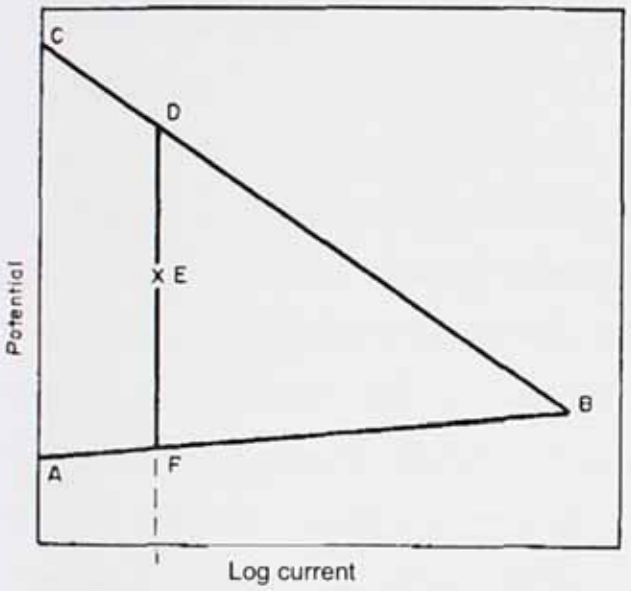

Figure 2.1 Evans diagram for a metal corroding in a high resistance electrolyte [55].

More than two decades after the early observations of Mayne, Hageen and Funke [61] measured the permeability to water and oxygen for a number of paint coatings and showed that water permeation is far beyond the requirement to sustain normal rate of corrosion for bare steel. However their results showed that oxygen permeation in many cases are lower than that of required for normal rate of bare steel corrosion. They concluded that in absence of ionic contamination and negligible rate of ionic conduction, oxygen permeation is the corrosion rate determining steps. Funke [62] explains the importance of oxygen in depolarizing the cathodic sites as well as keeping the charge balanced at anodic sites by oxidation of soluble Fe(II) to insoluble Fe(III). This explanation is consistent with findings of Buttrey *et al.* [63] who studied

corrosion behaviour in food can. They found an inverse relationship between oxygen concentration in the can and the charge transfer resistance while the coating resistance found to be independent of oxygen concentration.

Funke [62] also showed that water plays a key role in loss of adhesion but may not be rate determining step for corrosion. Funke also suggests that some of the factors that contribute to low permeability may interfere with adhesion; in particular, polar functional groups appear to be essential to achieving good adhesion, but are likely to increase permeability and contribute to water sensitivity [64]. Guruviah measured the permeability to water and oxygen of alkyd, epoxy and chlorinated rubber paint films and worked out its relationship with the corrosion rate of painted steel achieved in salt fog exposure test [60]. His results showed much less oxygen permeability than was measured by Mayne and a good correlation between the corrosion rate and oxygen permeation suggesting that the oxygen permeation could be the rate controlling step. Water permeation although not directly controlling but is very important to the protective properties of coatings. Aqueous channels are the pathways from which corrosive ions get to the metal substrate and corrosion products are transported away [66,67]. Improvement of corrosion resistance of epoxy coating by increasing the hydrophobicity and lowering the water uptake was reported by Zhang *et al.* [68]. Water accumulation at the interface is also the factor responsible for blistering and loss of adhesion [69,70]. It was also determined as the main cause of interlayer adhesion loss in multi-coat paint systems [71]. Water and oxygen permeability is mainly controlled by chemical structure of polymer film. It is believed that higher polarity of a polymer encourages water permeation while reduces the oxygen penetration [72,73]. Modification of coating systems with hydrophobic non-polar coal-tar has been a traditional solution to lower the inherent water absorption of coatings [74]. A number of other factors also play a part in water absorption including pigmentation level and pigment type [75], glass transition temperature and polymer free volume [76] and solvent selection [77]. Li *et al.* studied the effect of thermal cycling and glass transition temperature on the water taken up by epoxy coatings. They observed irreversible increase of water absorption with increasing solution temperature which drastically reduced the ionic resistance [78]. No molecular mechanism was advanced to explain the increased water absorption.

It appears that water, oxygen and ions each play a part in corrosion of a painted metal. There have been evidence that show even very high resistance coating do not perfectly prevent corrosion [79]. It is proposed that corrosion of such systems is initiated by water uptake of coating causing its resistance to fall. The slight corrosion at this stage is due to presence of water and oxygen and not the presence of aggressive ions unless they have been present at the interface in the form of contamination. Corrosion would continue as the local break down of paint film makes it more permeable to ions. The type of ion that can diffuse through the coating is greatly dominated by the chemical structure of film and size of conduction pathways [73]. Today, electrochemical techniques have became the main method of protective coatings evaluation used in scientific research [80–83]. This indicates the general acceptance of charge conduction behaviour as the main criterion for protectiveness of a paint coating as electrochemical techniques are mainly responsive to charge movements and fairly insensitive to oxygen permeation.

It has been shown that coatings with inherent negative charge tend to permeate cations more whereas positively charged polymer films are more permeable to anions [7,84,85]. This characteristic is referred as "permselectivity" which to a large extent governs the mechanism of blistering and its consequent adhesion loss [69,86,87]. Sharer and Sykes [88] measured a much larger activation energy required for charge transfer at the interface than that required for ionic conduction through the paint film suggesting that ionic conduction through the weak points of film is not the corrosion rate determining step. However, they proposed that separation of anodic and cathodic sites underneath the paint film and the need for ionic conduction at both areas may lead to good protection where the coating is not significantly degraded at one of the regions.

2.4 Failure mechanisms

2.4.1 Adhesion failure and role of surface preparation

The ultimate stage of coating failure is often considered as its detachment from the metal surface. Corrosion induced adhesion loss from steel is firmly established as a cathodic phenomenon in either the form of cathodic blistering or cathodic disbondment from coating defects [15,89]. Figure 2.2 shows the model, proposed by Dickie and Hammond, by for the initial stages of corrosion induced paint adhesion loss. In this simple phenomenological model, the initial oxidation of iron and reduction of oxygen occur locally at a break in the paint film (or at some other site of electrolyte penetration). As the process proceeds, a rust deposit forms, and the anodic and cathodic sites tend to separate and become localized. At a more advanced stage of the process, the cathodic reaction continues under the paint film resulting in progressive adhesion loss [89,90]. This model was further verified by Jorcin *et al.* [91] who looked at the delamination process around a scribed epoxy primer on steel using LEIS technique. The development of the corrosion products in the scratch and diffusion of oxygen through the coating were determined as key factors.

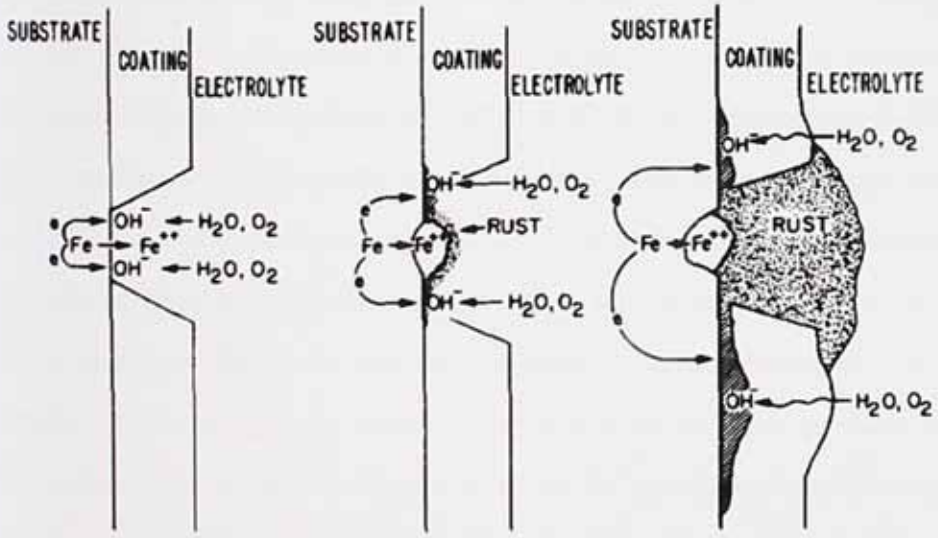

Figure 2.2 Simplified model of the initial stages of paint delamination by corrosion [89]

Upon exposure of painted metal to humidity/aqueous environment water molecules penetrate the coating relatively easily and form a thin layer of water at coating/metal interface. Water molecules can effectively compete with functional groups of the polymer film to establish boding with the metal [62,92]. Typical value for the binding energy of secondary metal/polymer interaction is in the range of about 25 kJ/mol or lower, while metal-water interaction have binding energies in the range of 40-65 kJ/mol [93]. This brings about randomly distributed anodic and cathodic regions underneath the paint which are separated by polymer phase. The alkalinity of the cathodic reaction products is one of the main reasons of cathodic disbondment due to hydrolysis of polymer bonds and osmotic pressure underneath the paint film. At anodic sites metal surface is dissolved resulting in anodic disbondment. Studies also revealed that in many cases the lateral diffusion of cations along the metal/polymer interface (Figure 2.3) is the rate determining step for disbondment [94–96]. However, degradation of polymer in the long term may impact the disbondment rate of coating by changing transport pathways of ions [97]. An earlier study by Parks and Leidheiser [84] showed that lateral diffusion is the predominant mechanism of ionic conduction at free corrosion potential (OCP) while diffusion through coating become the major pathway for ionic motion under cathodic polarization. Pommersheim *et al.* [98] employed this principal to develop a mathematical model for predicting coating degradation and adhesion loss. They concluded that blistering and coating failure is a function of cation transport, osmotic pressure, cathodic delamination and mechanical stress. Yang *et al.* [99,100] demonstrated that blistering is initiated by formation of micro-osmotic cells at locally low resistance areas of the coating. According to Stratman *et al.* [101] electrochemical reactions that lead to a degradation of the metal/polymer interface are influenced by the electron-transfer properties at the interface, the redox properties of the oxide between the metal and the polymer, and the chemical stability of the interface with respect to those species, which are formed during the electron transfer reaction. A direct connection was found by Wielant *et al.* [102] between oxide surface energies, adhesion of the polymer film after sample exposure in humid atmosphere and the delamination rate of the polyurethane coating on steel substrates with different interfacial iron oxide structure and morphology. An increasing polar oxide surface energy component was correlated with

increasing polymer/iron oxide peel-off forces and deceleration of delamination. Surface preparation is an effective tool to produce an optimal substrate with desired electrochemical and geometrical characteristics and establishment of good bonding with the paint film.

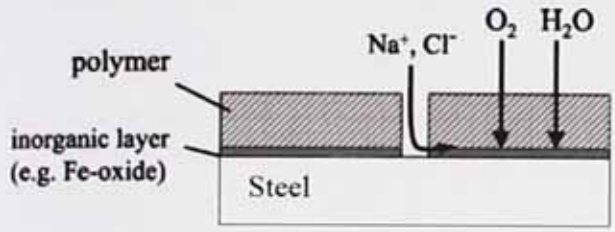

Figure 2.3 Diffusion pathways for water, oxygen and ions [101]

Surface preparation of metal prior to painting may be defined as modification of the surface, either by modifying the material to a small depth (e.g. by phase transition, interdiffusion or ion implantation) or by modifying the surface itself (e.g. morphology, structure, chemistry etc) in order to improve corrosion resistance and interfacial bonding. This is generally done by thermal treatment, diffusion treatment, ion bombardment, mechanical treatment, chemical and physical-chemical treatments [103]. Removal of contaminant from the metal surface prior to painting is vital to avoid early blistering and loss of adhesion [104]. Thermodynamically, an appropriate bonding between metal and paint is achieved only when the free surface energy, surface tension, of the substrate is higher than, or equal to, the surface tension of paint [105]. Surface preparation assists adhesion through providing potentially active sites on the substrate for both primary and secondary bonding, removal of contaminants and increasing the number of reaction sites and mechanical entanglement. Surface treatment may also passivate the surface to form an additional barrier layer (conversion oxide layer) or activate the surface to improve the substrate/paint interaction. Number of studies have indicated the beneficial effect of surface pretreatment by formation of a conversion film, organic compounds and electrochemical modification on the adhesion strength and corrosion resistance of organic coatings [106–111]. However, the interaction between organic coupling agents, e.g. silane groups, and polymer film in aqueous environment should be considered carefully as

incompatibility between coupling agent and coating or hydrolysable interfacial bonds may result in early failure of the coating [112]. Superior performance of silane treated substrate has been reported where silane is covalently adhered to the substrate [113]. Naderi *et al.* [114] looked at the effect of mill scale removal by comparing the solvent degreasing and acid pickling methods and its impact on performance of polyester-epoxy powder coating. They observed higher resistance to corrosion and disbondment of the substrate without mill scale. Detrimental effect of mill scale was attributed to its faster breakdown and dissolution in chloride containing media.

Activation of surface by mechanical means, e.g. manual, pneumatic or electric tools or blast cleaning, has been most often investigated with regards to the paint/metal bonding. In a study by Roper *et al* different surface profiles were produced by controlling the abrasive velocity in grit blasting and resulted surfaces were coated by 6 different types of organic coatings. Adhesion measurement after salt spray exposure revealed better performance of high profile surfaces in maintaining good interfacial adhesion [115]. In contrast with this result, Jin *et al.* found better adhesion of chlorinated rubber to smoother steel substrate [116]. They produced different surface roughness on steel by using different grades of emery. The surprising result was explained based on formation of interfacial microcracks between paint and substrate suggesting that rougher surface contains larger cracks.

In a recent study by Khun and Frankel [117], the effect of surface roughness at nano scale and profile texture on cathodic disbondment was studied. They observed decreased disbondment as a result of increased roughness which they attributed to the increased interactions between the coatings and the substrates associated with larger surface area. Their results also showed faster disbondment in the direction of parallel abrasion lines than perpendicular to the lines due to the barrier effect of groove side walls compared to groove valleys. This was also pointed out earlier by Jin *et al.* [116] who studied the effect of abrasion direction on disbanded area of chlorinated rubber coated steel. They observed that disbonding front shape changes to elliptical (instead of the usual circular shape) when surface roughness was oriented parallel by abrasion in one direction.

Mills and Schaefer [118] used water-jetting, wet garnet blasting and abrasion methods to prepare steel surface prior to painting with alkyd and compared the corrosion resistance of coated surfaces. Their results showed detrimental impact of garnet blasting even in comparison with non-treated control sample. They suggested that oxide layer characteristic varies by the preparation method and is responsible for changes in corrosion resistance. Studies of Schaefer and Mills made the baseline and triggered the current research scribed in this book. Lin *et al.* [119] also found inverse correlation between substrate roughness and corrosion resistance of painted steel. The early failure of sand blasted substrate compared to untreated surface was attributed to insufficient thickness of epoxy coating at the peaks of surface profile and non-uniform distribution of coating by the spin-coating technique. Santagata *et al.* [120] studied the performance of chlorinated rubber coating on steel surface differently prepared by sandblasting, pickling, pickling+phosphating and pickling+wash primer. Best performance was observed on pickled+phosphate surface followed by pickled surface with sandblasted surface exhibiting the lowest performance. The corrosion behaviour correlated well with the water absorption percentage, the delaminated area and the membrane ionic resistance performance. Vesga *et al.* [121] compared the effect of water-jetting and sand blasting on corrosion resistance of painted steel. They reported higher efficiency of sand blasting than normal water-jetting and water-jetting with inhibitor containing solution. No explanation was given for this outcome.

The influence of surface reactivity on protective properties of paint coatings was studied by Walter [21]. His results indicated that paint films deteriorate faster on more reactive substrates. A direct relationship between the performance of painted metals with the corrosion resistance of unpainted substrates is reported. Similar result was obtained by Mills *et al.* [122] who studied the corrosion resistance of epoxy primer on surfaces with differing reactivity including aluminum, steel, zinc and phosphated steel and zinc. Their results showed better performance of primer on aluminum which was attributed to the inertness of the substrate. They suggested that the corrosion inhibition depends highly on reactivity of the metal substrate where the coating resistance falls within the uncertain protection region (10^6-10^8 ohms.cm^2). This results was also in-line with earlier studies by Mayne and Mills [123] in which they examined coatings

resistance on steel and platinum. Their results showed higher resistance of coating on inert substrates (i.e. platinum or passivated steel) than the resistance on an active substrate (i.e. plain steel). The lower resistance on the active substrate was explained by the provision of ions from both sides of coating while in the case of inert substrate the ionic diffusion could occur only from one side.

2.4.2 Ionic conduction and role of electrochemical inhomogeneity

It has been firmly acknowledged that as soon as the coating bond with the metal substrate is lost, corrosion proceeds with no need for ion transfer through paint film [62]. This is because the electrical resistance between cathodic and anodic areas is much lower along the weakened interface than through the paint film. However, it is believed that as long as a certain level of adhesion exists, ionic resistance of coating controls the corrosion rate. Early studies of Bacon, Smith and Rugg [57] revealed the significance of ionic conduction for corrosion resistance properties of organic coating. It was observed that a coating that maintained a resistance of 10^8 Ohm.cm^2 provided good corrosion protection while one whose resistance fell below 10^6 Ohm.cm^2 did not. A subsequent sharp drop in resistance was determined as pre-cursor to coating failure.

Two contradictory hypothesis proposed by Mayne [56] and Corti [124] explain possible mechanisms for ionic conduction through paint films. According to Corti, the rate of permeation across the film is affected by the presence of small imperfections or pores, which extend through the film and have cross sections distinctly larger than the free areas normally present between the atomic groups in the membrane matrix. Mayne's model, on the other hand, infers that the passage of ions is through the bulk matrix of the film but there are regional differences within a single coating with regards to ion selectivity [6]. Latter studies of Mayne and Scantlebury [125] however, revealed that highly permeable areas form only a small fraction of the coating. Moongkhamklang and Taylor [126] utilized fluorescence microscopy with an ion-specific chromophore to identify the mode of ion entry through an epoxy coating. Their results indicated that following exposure to NaCl, chloride ions are clustered in discrete sites on the

surface of epoxy resins which corroborates the discrete pore concept proposed by Corti. In a different study, they also observed a relation between water activity and the number of discrete sites of chloride accumulation, with the number of sites increasing as the water activity increases [127]. They concluded that initial water uptake in epoxy coatings occurs at discrete sites on the surface of the coatings. White *et al.* [128] showed that the failure mode of painted steel mainly depends on the type and rate of the ions diffusing through the paint film. It was found that if the generation of corrosion products occurs faster than its removal by diffusion through the coating or into the steel, a blister forms. But if the rate of generation is less than its removal rate, the can be a complete disbonding of the coating with no visible blister. Worsley *et al.* [129] studied the effect of coating porosity on failure mechanism of polyester coated galvanized steel by SVET. Coatings of different porosity were produced by differing the curing time. It was shown that the level of porosity in the organic coating plays a major role in the mechanism of corrosion by altering the permeability and barrier properties.

Modes of ion transport through paint film was first studied Kinsella and Mayne [130]. Two distinct forms of conduction were identified. The first was I, or inverse type conduction, where the resistance of the film coincided with that of the solution. The second mode of through-film transport that was identified was named D, or direct type conduction where the film's resistance follows that of the external solution. They suggested that water content of film is the controlling factor of ion transport. They also observed a significant effect of ventilation during the curing process of paint film on its conduction mode. Presence of both modes of ionic conduction in most polymeric coatings renders them electrochemically heterogeneous surfaces. A typical dependence of coating resistance to the electrolyte concentration for D and I type coatings is given in Figure 2.4.

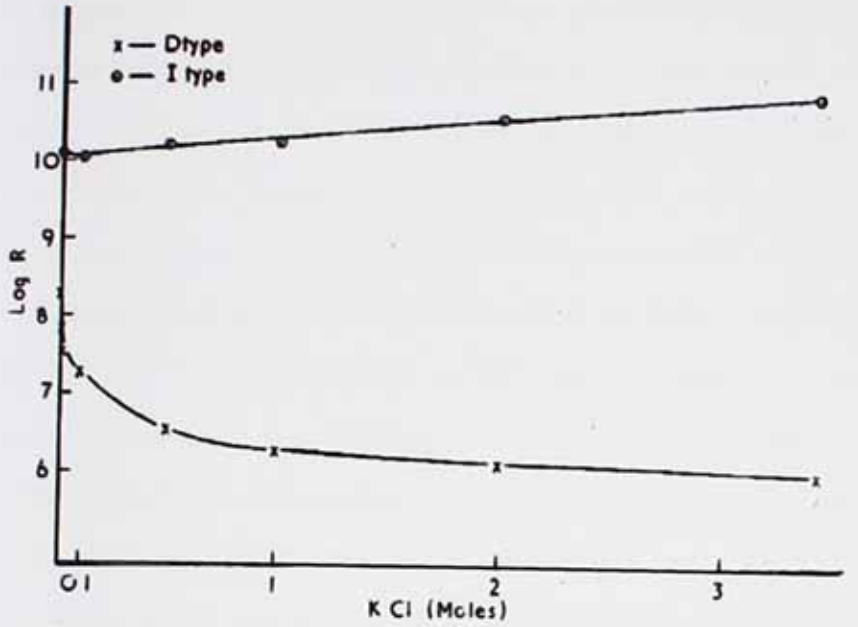

Figure 2.4 Typical dependence of coatings resistance to solution concentration for D and I type coating showing the direct relationship between ionic strength and coating conductivity for D type coatings and inverse relationship for I types [131].

A series of systematic studies were made by Mayne and his co-workers on the factors that play a part in the D/I type behaviour of organic coatings. It was determined by Mayne and Scantlebury that D type conduction cannot be attributed to macro capillaries unless these are of molecular dimension. A typical value of 10^8 ohm.cm^2 for a D type coating in 1 N potassium chloride yields in about 1,000 Å radii for the pore [125]. Their results also showed higher water uptake and lower hardness of D type area. The effect of D/I type behaviour on protection afforded by paint coatings was studied by Mills and Mayne [132] who showed a direct relationship between the presence of D type areas in the film and the occurrence of under-film corrosion. Effect of solvent on coating homogeneity was studied later by Mayne [133]. Solvent free epoxy coatings exhibited a homogeneous structure suggesting that solvents may interfere with the process of cross-linking and that films of improved protective value may be obtained by elimination of solvent from system. Several studies have revealed the great influence of polymer type on its D/I type behaviour [132,134,135]. White *et al.* [134] found highly D type behaviour of fluoropolymer coating while epoxy coatings exhibited hardener dependant behaviour.

Wu *et al.* [136] studied the effect of coating thickness and multi-layered systems on electrochemical inhomogeneity of alkyd and polyurethane coatings using a wire-beam multi-electrode. Their results confirmed previous findings in relation to the effect of thickness on film electrochemical homogeneity. They reported an overall increase of coating resistance accompanied by improved homogeneity as a result of higher film thickness. The effect of heterogeneously distributed pores on local resistance exhibition and blistering was also studied by Zou and Thierry using LEIS ad SKP [137]. Locally higher water absorbent areas of coating were determined as blistering and delamination initiation sites. Van Westing *et al.* [138] showed that the water-uptake by coating can also introduce inhomogeneity that in the long term results in heterogeneous condensation of water at coating/substrate interface and loss of adhesion. Earlier degradation of acrylic coating at locally lower resistance areas of film has been demonstrated by Szocinski, Darowicki and Schaefer [139] using contact mode imaging of AFM.

In addition to the inherent properties of coating that encourage corrosion, such as hydrophilicity, a coating system may contain inhomogeneities such as air bubbles, cracks, microvoids, contaminants, trapped solvents, nonbonded and weak areas, pigment-resin and coating-substrate interfacial defects [140]. Each of these factors will influence the transport of aggressive species through the coating and along the coating-substrate interface and subsequently influence the protective properties. Some of these factors are discussed on more detailed in the next section.

2.5 Factors affecting coating's permeability

2.5.1 Physico-chemical structure of polymer

Oxygen transport through coating films depends on the solubility of the gas in the polymer and its ability to diffuse through the polymeric matrix [73]. Permeability of coatings to gases decreases with increasing polarity while highly polar polymers are highly permeable to water because of the high levels of water solubility in the matrix. Kamimura and Kishikawa [141] found that in cathodic disbondment of polyethylene (highly non-polar polymer) from steel, diffusion of oxygen takes place at a high rate through the coating while migration of ions to the disbondment front is limited to interfacial conduction. In addition to the polarity level of polymer, other structural elements such as cross-linking density, hydrogen bonding, glass transition temperature, molecular orientation and crystallinity affect the permeability of polymer films [142]. Kinsella *et al.* [143] studied the effect of temperature on water absorption and observed a minimum water absorption of an epoxy and an alkyd coating at their Tg. Permeability of polymers changes significantly at the glass transition temperature (Figure 2.5). Polymers having higher Tg than service temperature give comparatively better barrier properties. This is because above Tg, the free volume increases due to cooperative movements of the segments. Humidity can also plasticize the polymer resulting in lower Tg and higher permeability [16,66,144]. Bierwagen *et al.* [145] reported irreversible decrease of Tg as a result of water plasticization effect during immersion of epoxy coating in 3% NaCl solution. Despite the usual drop of coating resistance due to exposure to corrosive media, an increase in resistance of a free standing alkyd film was reported by Macedo *et al.* [146]. Comparison between aerated and de-aerated solution showed that the unusual increase of resistance could be attributed to the structural change in alkyd by the oxygen.

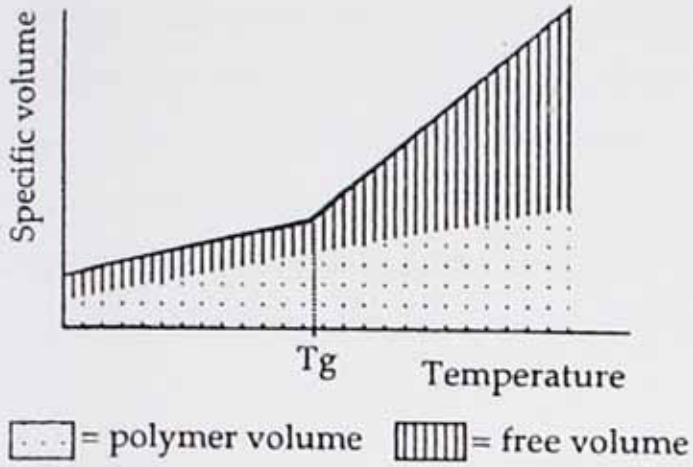

Figure 2.5 Changes of apparent and free volume of polymers as a function of temperature and Tg [66].

2.5.2 Pigmentation

Mayne and Scantlebury studied the effect of pigmentation with iron oxide on conduction mode of alkyd and epoxy [135]. An initial increase of D characteristic followed by decrease of D type behaviour was observed by increasing the level of pigmentation. The initial increase of D characteristic was attributed to the segregation of low molecular weight polymers around pigment particles and its contribution to easier ion transverse via the adsorbed layer on the surface of pigment particles rather than through the cross-linked polymer network. Mills and Mayne further studied the effect of pigmentation by including zinc oxide and making comparison with red lead and iron oxide pigments [147]. Their results showed increase of D characteristic by increasing the pigmentation level which, in some cases, fell slightly before rising to 100 per cent as the CPVC was approached. Pigmentation of paints above the critical pigment volume concentration (CPVC) results in a very high permeability to water, oxygen and ions through the porosity and void formation between the pigment particles [75]. However, it has been revealed that voids may form at PVC values under CPVC as a result of inhomogeneous dispersion [148]. Because the polymer space-filling is disrupted by the fluctuations in the pigment density, the polymer may not completely fill the interstitial volume in the densely-packed islands of the coating. Hence, voids may form in the densely-packed islands even when PVC<CPVC. As a result, the physical properties of the coating affected by void formation will

change gradually below the CPVC, rather than a sharp change at CPVC. Figure 2.6 schematically represents the void formation in pigment clusters of an inhomogeneous dispersion. Lamellar shape pigments such as aluminium flake, stainless steel flake and glass flakes have long been used successfully to prolong the conduction pathways and decrease the coatings permeability when well oriented within the paint film [8,149]. Figure 2.7 schematically shows the proposed mechanism for impeded diffusion by lamellar pigments.

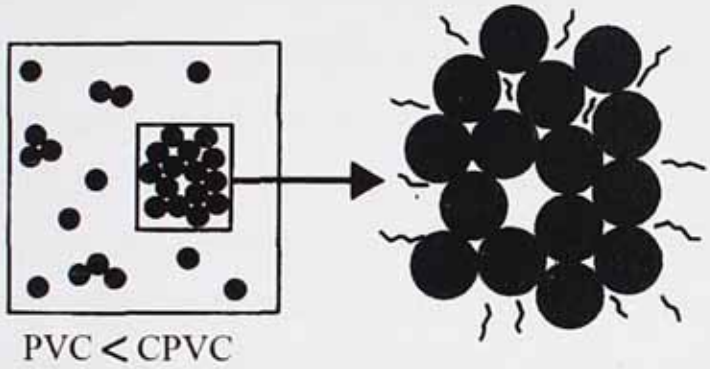

Figure 2.6 The proposed model for void formation due to heterogeneous pigment dispersion at PVC<CPVC in the densely packed. The polymer molecules are represented by squiggly lines [148].

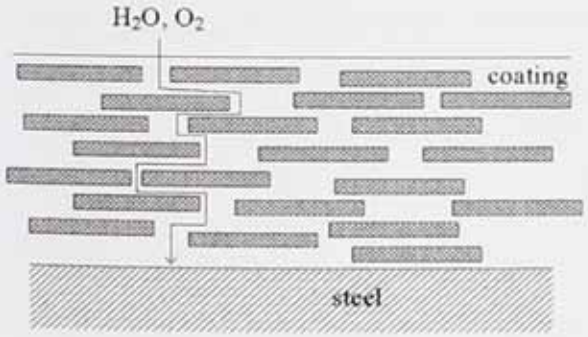

Figure 2.7 Schematic representation of the diffusion hindered by flake-like pigments [15].

Effective pigmentation can significantly lower the water transport in coatings. However, factors like incomplete dispersion, flocculation and poor binding between pigment and resin

may diminish this effect substantially and may even lead to an overall rise in water transport [150]. Also it was shown recently that hydrophilic pigments may increase the water permeability by transport of water through the interface between polymer and pigment particles [151].

2.5.3 Solution composition

Type of the ions present in the environment plays an important role as smaller size ions (particularly cations) with higher mobility in solution penetrate the coating more easily. Several studies have revealed that the mobility of cations and hence their corrosive properties are inversely proportional to their size [95,152–154]. It was shown that the ion exists within the polymer in the hydrated state which decreases as cation size increase resulting in faster permeation and subsequent adhesion loss (table 2.1) [155]. The mobility of hydrated ions of alkali metals increases in the order of $Cs^+ > K^+ > Na^+ > Li^+$ with the Li^+ being the least mobile. In contrast, the hydrated ion size and thus diffusion rate of halides are proportional to their anion size (e.g. $Cl^- > Br^-$). It was also shown that rate of both water and cationic migration through coating films is increased when a cathodic potential is applied to the coated metal.

Table 2.1 Dimensions of the alkali metals ions in non-hydrated and hydrated form [154].

Ion	Ion radius (Å)	Hydrated ion radius (Å)
Li^+	0.68	3.40
Na^+	0.98	2.76
K^+	1.33	2.32
Cs^+	1.67	2.28

2.5.4 Thickness

Several studies have considered the effect of coating thickness on protective properties of organic coating all generally agreeing that increasing the thickness of coating improves the barrier properties and corrosive resistance [95,116,156,157]. However, a number of studies

have obtained dissimilar results suggesting that higher thickness of paint film may not necessarily result in better protection. Raja *et al.* [158] studied the effect of thickness and pigmentation on water uptake and electrochemical impedance of alkyd coatings. They found that coating resistance is fairly independent of thickness for high water absorbent coating (TiO_2 pigmented alkyd) while for alkyd varnish with far less water uptake, increasing the thickness increased the coating resistance. It has been shown that increasing the coating thickness has almost no effect on the amount of water up taken by the coating [70,159]. It appears that there is a possible critical minimum film thickness above which coating protective performance was greatly enhanced and that there was also a maximum limiting film thickness above which increasing film thickness made little contribution to corrosion protection [160,161].

An special care must be taken in applying thicker coatings as they are more prone to solvent entrapment and consequent micro defects and blistering [162]. Also a significant increase of coating's internal stress by increasing the thickness has been shown by Islam [163]. The stored internal stress may result in early delamination of coating upon exposure to aqueous media. The general trends in the protection of metal structures by coatings go towards the use of thicker systems with several different layers resulting in very high barrier properties with newly developed coatings. For such systems, the critical parameter for the protection is related to the ability to maintain good interfacial properties.

2.5.5 Chemical consistency

Monetta *et al.* [164] also examined the effect of molecular inhomogeneity of coating on protective properties by altering the crosslinking agent/epoxy ratio and curing temperature. It was found that performance of the coating improves by approaching the stoichiometric ratio of curing agent and epoxy and by increasing the curing temperature which was attributed to lowering the uptake of water and ingress of chloride. The role of cross-link density on resistance behaviour of UV light curable paint was studied by Rais-Ali and Richardson [165]. Different cross-link densities were obtained by varying the UV light intensity. Changing D type behaviour to I type was found by increasing the cross-link density. Leidheiser *et al.* [166] studied the effect

of curing condition on temperature dependence of electrolytic resistance for eleven different coatings. Their results showed better heat stability of the coatings which were cured at elevated temperature. Temperature dependence of the coatings which were cured at lower temperature was attributed to the presence of unreacted hydrophilic components or residual solvents in the cured coating.

In waterborne coatings residues of surfactants, used to emulsify the polymer in aqueous solution, remain in the dried film which increases the hydrophobicity and the film water uptake when exposed to aqueous media [167,168]. The lower level of protection afforded by waterborne paint has been shown elsewhere [169]. Polymeric materials are present in form of particles/micelles, which are separated by the continuous aqueous phase. Heterogeneity in such systems is additionally affected by particle size distribution, hydrophobicity, glass transition temperature (Tg) and molecular weight distribution [170].

2.6 Surface preparation methods

Selection of preparation method depends particularly on the substrate specification, type and thickness of coating, final exposure environment and economic considerations [103]. The efficiency of surface preparation depends on the type of contaminant and the surface preparation method. Various cleaning techniques may be used but none is truly universal. to achieve an optimum surface will depend on the cleaning methodology. Simply washing the surface with water, for example, will have a nominal effect on removing low energy organic contaminants such as oil films and grease deposits. Solvent washing and solvent vapor degreasing, which may effectively remove oils and greases, will have little effect on inorganic salts. These contaminants may be removed more easily with water. Heat and mechanical energy will improve the efficiency of the cleaning operation when applied with water, solvent or detergent solution. Wiping, rubbing, scrubbing, sanding and water and abrasive blasting represent increasing levels of force that can be used to remove surface contaminants.

Techniques that provide sufficient energy to remove the contamination and scarify the surface may be particularly useful because they will simultaneously clean the surface and

increase the true surface area of the substrate compared to its apparent planar area. The surface profile which is resulted by these methods can be controlled precisely by careful selection of abrasive type, velocity, size and application method [171,172]. Chemical cleaning techniques such as acid etching and alkaline passivation accomplish the same thing as blasting for metal, although alkaline cleaning gives no profile. Abrasive blasting and acid pickling will also chemically remove tightly bonded oxides and other scales that cannot be removed by other techniques. These techniques strip away oxide films that chemically saturate metal surfaces and free up reactive groups on the surface for subsequent reaction with potentially complementary groups on the paint binder [173].

2.7 Methods of coating characterization and assessing protectiveness

2.7.1 Visual assessment

Visual observation is the primary assessment method which deals with macro defects such as pitting, blistering, and flaking. Optical devices are often helpful to describe the observations in detail. Ratings based on pure visual and subjective assessment of appearance involve a high personal factor. Subjective assessments are made of the evaluation of each type of defect by comparison with standard charts, and a percentage area of specimen surface affected is estimated in each case [174]. Visual assessment gives a quick measure of the extent of corrosion, however in some cases results might be misleading and cannot be reported and analyzed as easy as the quantitative data [175]. Also visual assessments are incapable of predicting the paint performance since they can evaluate failure only after they have happened at a reasonable level.

2.7.2 Ionic resistance by DC measurement

The simplest and quickest quantitative method of measuring the protection properties of organic coatings is by measuring the current flow through the film as in indicator of the ionic conduction, thereby the effectiveness of barrier properties of the film [176]. Figure 2.8 illustrates the simple classification for coatings protectiveness made by Bacon, Smith and Rugg [57].

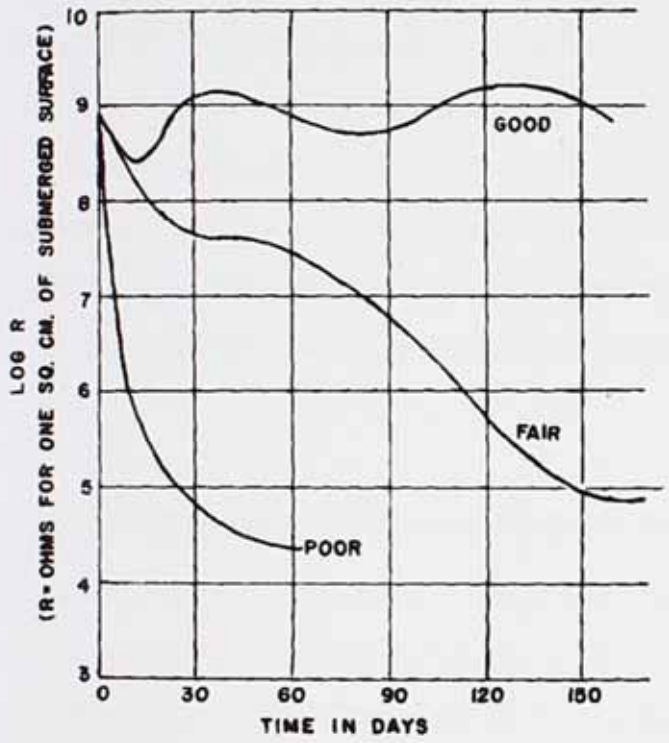

Figure 2.8 Schematic representation of behaviour of resistance for "good', "fair" and "poor" coatings after exposure to electrolyte [57]

2.7.3 Electrochemical Impedance Spectroscopy

The application of DC electrical resistance measurements for evaluation of protective properties of paint coatings was questioned by Mikhailovskii *et al.* [177,178] by observation of some disagreement between DC resistance and anti-corrosive ability of paint. They pointed out that in some cases the DC resistance may not necessarily be a true measure of the anti-

corrosive ability of paint and that many coatings are found whose DC resistance is low but which have a good anti-corrosive ability. They suggested that a more meaningful term was that of a resistance related to a retardation of the electrochemical process occurring at the coating metal interface. With aid of new EIS analysis programs and sensitive AC response analyzers detailed information on the permeability of coatings, delaminated areas and delamination rate, the formation and density of the oxide scale beneath the coating and diffusion mechanism can be studied [66,179]. Precise selection of equivalent electrical circuit to simulate the actual elements of electrochemical system and fit the collected data is the essential key to data analysis [180]. The amount of water up-taken by coating has also been an important parameter determined by EIS and extensively studied using the capacitance element of coating extracted from EIS data [181–184]. Amirudin and Thierry [185] reviewed the usefulness of EIS for studying the polymer coated metals with the ultimate emphasis on unique capabilities of the technique on determining the parameter which no other simple technique could yield, e.g. very minute areas of disbondment, water uptake and the prediction ability.

2.7.4 Electrochemical Noise Measurement (ENM)

Use of ENM for assessment of corrosion resistance was first introduced to the field of organic protective coatings by Skerry and Eden in the late 90s [186]. Since then it has found extensive use in examining coatings performance [81,187–190]. Bierwagen and his co-workers have made a major contribution to establishment and validation of the technique by applying it to a range of polymeric coatings to study the performance of technique for a large range of organic coatings as well as studying thermal and water plasticization effects [145,191–195]. Several studies have gone on in the past decade by Mills and his co-workers [196–199] to overcome the field limitations ENM for assessment of protective organic coatings. Development of new practically useable cell configuration and field testing protocol render the ENM a promising electrochemical technique for laboratory and on-site coating testing. The next chapter of this thesis continues the previous works in this field with the aim to unify the ENM

protocol and overcome the difficulty of measurement in the awkward shape immersed surfaces.

2.7.5 Adhesion measurement

As discussed earlier, strong interfacial bonding between coating and metal substrate is essential for a high level of corrosion protection. Therefore, it is important to utilize a reliable and reproducible method of adhesion testing in order to examine the coating performance and understand the failure mechanism. The ASTM D4541-02: Standard test method for pull-off strength of coatings using portable adhesion testers, defines the testing criteria for adhesion measurement using pull-off method. ASTM 4541 is also equivalent to ISO 4624 and EN 24624. Several studied utilized pull-off test method to examine the effect of surface preparation on anticorrosion performance of organic coatings [108,113,115,200–202]. Pull-off adhesion testers measure the force required to pull a specified diameter of coating away from its substrate. The measured pull-off force provides a direct indication of the bond strength between the coating and the substrate. During operation, the flat face of a pull stub (dolly), shown in Figure 2.9, is adhered to the coating to be evaluated. The main advantages of pull-off method over the more traditional cross-hatch method are the provision of quantitative result, improved reproducibility and recognition of different failure modes [203,204]. Apart from the inherent inconsistency of bonding across the coating/metal interface, several other parameters may introduce variation of result and must be eliminated including: pull rate, coating thickness, curing time, dolly preparation and adhesive used for attaching the dolly to coating [205].

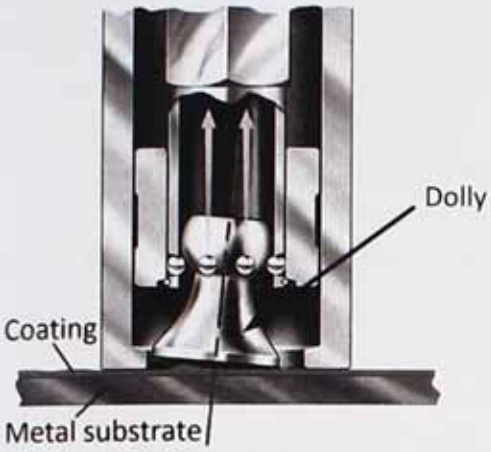

Figure 2.9 Cross-sectional view of pull-off adhesion measurement mechanism [206].

2.7.6 Physico-mechanical properties

Physico-mechanical test methods such as dynamical mechanical analysis (DMA) and differential scanning calorimetry (DSC) have extensive use in the paint industry to evaluate the paint performance in certain environmental conditions as well as studying the morphology of coating [207,208]. In the context of anticorrosion coatings, physico-mechanical testing is mainly used to study the relevance of structural and morphological changes of paint film to the protection afforded by coating [209]. Mechanical properties may be analysed by DMA in a range of temperatures (DMTA) or a range of stress-strains. DMTA and DSC have been widely applied to organic coatings to study their cure mechanism [210], UV aging [211], and the relationship between permeability of coatings, morphology and temperature [145,212–214].

References

[1] Z.W.J. Wicks, F.N. Jones, S.P. Pappas, What are coatings?, in: Organic Coatings, Science and Technology, 2nd ed., John Wiley & Sons, Inc, New York, USA, 1999: pp. 1–5.

[2] A. Forsgren, Composition of the anticorrosion coating, in: Corrosion Control through Organic Coatings, CRC Press, Boca Raton, FL, USA, 2006: pp. 11–55.

[3] C.G. Munger, L.D. Vincent, Coating fundamentals, in: Corrosion Prevention by Protective Coatings, 2nd ed., NACE International, Houston, TX, 1999: pp. 61–85.

[4] R. Zhang, H. Chen, H. Cao, H. Huang, C.M. Mallon, L.P. E, et al., Degradation of polymer coating systems studied by positron annihilation spectroscopy. IV. Oxygen effect of UV irradiation, Journal of Polymer Science. 39 (2001) 2035.

[5] J. Pospisil, S. Nespurek, Photostabilization of coatings. mechanisms and performance, Progress in Polymer Science. 25 (2000) 1261.

[6] D. Greenfield, J.D. Scantlebury, The protective action of organic coatings on steel: a review, The Journal of Corrosion Science and Engineering. 3 (2000) paper 5.

[7] J.E.O. Mayne, Paints for the protection of steel—A review of research into their modes of action, British Corrosion Journal. 5 (1970) 106–111.

[8] C.H. Hare, Barrier coatings, Journal of Protective Coatings and Linings. (1998) 17–37.

[9] R.A. Dickie, F.L. Floyd, Polymeric materials for corrosion control: An overview, in: R.A. Dickie, F.L. Floyd (Eds.), Polymeric Material for Corrosion Control, American Chemical Society, Washington, DC, 1986: pp. 1–16.

[10] C.H. Hare, Corrosion control of steel by organic coatings, in: R.W. Revie (Ed.), Uhlig's Corrosion Handbook, Third, John Wiley & Sons, Inc, Hoboken, NJ, USA, 2011: pp. 1023–1039.

[11] W.M. Bos, Prediction of coating durability: early detection using electrochemical methods, PhD thesis, Dept. Materials Science and Engineering, Delft University of technology, 2008.

[12] É. Fekete, B. Lengyel, Accelerated testing of waterborne coatings, Progress in Organic Coatings. 54 (2005) 211–215.

[13] M. Zapponi, T. Pérez, C. Ramos, C. Saragovi, Prohesion and outdoors tests on corrosion products developed over painted galvanized steel sheets with and without Cr (VI) species, Corrosion Science. 47 (2005) 923–936.

[14] J. Pospíšil, J. Pilar, N. Billingham, M. A, Z. Horak, S. Nespurek, Factors affecting accelerated testing of polymer photostability, Polymer Degradation and Stability. 91 (2006) 417–422.

[15] P. a. Sørensen, S. Kiil, K. Dam-Johansen, C.E. Weinell, Anticorrosive coatings: a review, Journal of Coatings Technology and Research. 6 (2009) 135–176.

[16] G.P. Bierwagen, D.E. Tallman, J. Li, L. He, C. Jeffcoate, EIS studies of coated metals in accelerated exposure, Progress in Organic Coatings. 46 (2003) 149–158.

[17] B.R. Appleman, Survey of accelerated test methods for anti-corrosive coating performance, Journal of Coatings Technology. 62 (1990) 57–67.

[18] G.P. Bierwagen, L. He, J. Li, L. Ellingson, D.E. Tallman, Studies of a new accelerated evaluation method for coating corrosion resistance — thermal cycling testing, Progress in Organic Coatings. 39 (2000) 67–78.

[19] S. Chong, A comparison of accelerated tests for steel bridge coatings in marine environments, Journal of Protective Coatings & Linings. (1997) 20–33.

[20] B. Appleman, Predicting exterior marine performance of coatings from salt fog-two types of errors, Journal of Protective Coatings & Linings. 9 (1992) 134–143.

[21] G.W. Walter, A critical review of dc electrochemical tests for painted metals, Corrosion Science. 26 (1986) 39–47.

[22] C.H. Hare, Corrosion and its control by coatings, in: A.A. Tracton (Ed.), Coatings Technology Handbook, 3rd ed., CRC Press, Boca Raton, FL, USA, 2006: pp. 102.1–102.9.

[23] C.H. Hare, Corrosion Phenomena: specific forms, Journal of Protective Coatings & Linings. (1998) 63–77.

[24] E. McCafferty, chapter 12: corrosion inhibitors, in: Introduction to Corrosion Science, Springer, New York, NY, 2010: pp. 357–402.

[25] I.. Zin, R.. Howard, S.. Badger, J.D. Scantlebury, S.B. Lyon, The mode of action of chromate inhibitor in epoxy primer on galvanized steel, Progress in Organic Coatings. 33 (1998) 203–210.

[26] R. Romagnoli, V. Vetere, Heterogeneous reaction between steel and zinc phosphate, Corrosion. 51 (1995) 116.

[27] T. Narayanan, Surface pretreatment by phosphate conversion coatings–a review, Rev. Adv. Mater. Sci. 9 (2005) 130–177.

[28] M. Buchler, P. Schmucki, P. Bohni, Iron passivity in borate buffer, Journal of Electrochemical Society. 145 (1998) 609–614.

[29] P. Mosner, A. Kalendova, L. Koudelka, Anticorrosion properties of SrO–ZnO–B2O3–P2O5 pigments, Dyes and Pigments. 45 (2000) 29–34.

[30] M. Sakashita, N. Sato, The effect of molybdate anion on the ion-selectivity of hydous ferric oxide films in chloride solutions, Corrosion Science. 17 (1977) 473.

[31] V.S. Sastri, Environmentally friendly corrosion inhibitors, in: Green Corrosion Inhibitors: Theory and Practice, 1st ed., Wiley-VCH, Hoboken, NJ, USA, 2011: pp. 257–303.

[32] T. Peng, R. Man, Rare earth and silane as chromate replacers for corrosion protection on galvanized steel, Journal of Rare Earths. 27 (2009) 159–163.

[33] B. Hinton, D. Arnott, N. Ryan, The inhibition of aluminum alloy corrosion by cerous cations, Metals Forum. 7 (1984) 211–217.

[34] M. Forsyth, K. Wilson, T. Behrsing, C. Forsyth, G.B. Deacon, A. Phanasgoankar, Effectiveness of rare-earth metal compounds as corrosion inhibitors for steel, Corrosion. 58 (2002) 953–960.

[35] M. Forsyth, M. Seter, B. Hinton, G.B. Deacon, P. Junk, New "green" corrosion inhibitors based on rare earth compounds, Australian Journal of Chemistry. 64 (2011) 812–819.

[36] A. Amadeh, S.R. Allahkaram, S.R. Hosseini, H. Moradi, A. Abdolhosseini, The use of rare earth cations as corrosion inhibitors for carbon steel in aerated NaCl solution, Anti-Corrosion Methods and Materials. 55 (2008) 135–143.

[37] B. Hinton, L. Wilson, The corrosion inhibition of zinc with cerous chloride, Corrosion Science. 29 (1989) 967–985.

[38] S.M. Powell, H.N. McMurray, D.A. Worsley, Use of the Scanning reference electrode technique for the evaluation of environmentally friendly, nonchromate corrosion inhibitors, Corrosion. 55 (1999) 1040–1051.

[39] T.H. Muster, D. Lau, H. Wrubel, N. Sherman, a. E. Hughes, T.G. Harvey, et al., An investigation of rare earth chloride mixtures: combinatorial optimisation for AA2024-t3 corrosion inhibition, Surface and Interface Analysis. 42 (2010) 170–174.

[40] T.H. Muster, H. Sullivan, D. Lau, D.L.J. Alexander, N. Sherman, S.J. Garcia, et al., A combinatorial matrix of rare earth chloride mixtures as corrosion inhibitors of AA2024-T3: Optimisation using potentiodynamic polarisation and EIS, Electrochimica Acta. 67 (2012) 95–103.

[41] D. Arnott, B. Hinton, N. Ryan, Cationic film-forming inhibitors for the corrosion protection of AA 7075 aluminum alloy in chloride solutions, Materials Performance. 26 (1987) 42–47.

[42] M. Mahdavian, M.M. Attar, Investigation on zinc phosphate effectiveness at different pigment volume concentrations via electrochemical impedance spectroscopy, Electrochimica Acta. 50 (2005) 4645–4648.

[43] M. Zaharescu, L. Predoana, a. Barau, D. Raps, F. Gammel, N.C. Rosero-Navarro, et al., SiO2 based hybrid inorganic–organic films doped with TiO2–CeO2 nanoparticles for corrosion protection of AA2024 and Mg-AZ31B alloys, Corrosion Science. 51 (2009) 1998–2005.

[44] M.L. Zheludkevich, Self-healing anticorrosion coatings, in: S.K. Chosh (Ed.), Self-healing Materials: Fundamentals, Design Strategies, and Applications, Wiley-VCH, Weinheim, 2008: pp. 101–140.

[45] C.H. Hare, Inhibitive Primers for Metal : Fundamental consideration, Journal of Protective Coatings & Linings. (1998) 48–62.

[46] S. Feliu, R. Barajas, J. Bastidas, M. Morcillo, Mechanism of cathodic protection of zinc-rich paints by electrochemical impedance spectroscopy. 1. galvanic stage, Journal of Protective Coatings & Linings. 61 (1989) 63.

[47] S. Feliu, R. Barajas, J. Bastidas, M. Morcillo, Mechanism of cathodic protection of zinc-rich paints by electrochemical impedance spectroscopy. 2. barrier stage, Journal of Protective Coatings & Linings. 61 (1989) 71.

[48] C.H. Hare, Zinc-rich primers I: design principles, Journal of Protective Coatings & Linings. (1998) 17–38.

[49] D.E. Tallman, G. Spinks, A. Dominis, G.G. Wallace, Electroactive conducting polymers for corrosion control. Part 1. General introduction and a review of non-ferrous metals, Journal of Solid State Electrochemistry. 6 (2002) 73–84.

[50] R.-G. Hu, S. Zhang, J.-F. Bu, C.-J. Lin, G.-L. Song, Recent progress in corrosion protection of magnesium alloys by organic coatings, Progress in Organic Coatings. 73 (2012) 129–141.

[51] G. Spinks, A. Dominis, G.G. Wallace, D.E. Tallman, Electroactive conducting polymers for corrosion control. Part 2. Ferrous metals, Journal of Solid State Electrochemistry. 6 (2002) 85–100.

[52] S.A. Umoren, Polymers as corrosion inhibitors for metals in different media - a review, The Open Corrosion Journal. 2 (2009) 175–188.

[53] N.H. Frick, H.L. Gerhart, H.E. Gilbert, E.E. Parker, Polymer coatings. annual review, Industrial & Engineering Chemistry. 61 (1969) 60–75.

[54] V.J. Buttignol, R.E. Cutforth, D.E. Eskra, N.H. Frick, H.L. Gerhart, Protective coatings. annual review, Industrial & Engineering Chemistry. 58 (1966) 44–56.

[55] J. Wolstenholme, Electrochemical methods of assessing the corrosion of painted metals-areview, Corrosion Science. 13 (1973) 521–530.

[56] J.E.O. Mayne, The mechanism of inhibition of the corrosion of iron and steel by means of paint, Official Digest. 24 (1952) 127.

[57] R.C. Bacon, J.J. Smith, F.M. Rugg, Electrolytic Resistance in Evaluating Protective Merit of Coatings on Metals, Industrial and Engineering Chemistry. 40 (1948) 161–167.

[58] B. Pearson, P. Brook, The synthesis of electrode polarisation curves, Corrosion Science. 32 (1991) 387–398.

[59] J.M. Sykes, Y. Xu, Investigation of electrochemical reactions beneath paint using a combination of methods, ECS Transactions. 24 (2010) 137–146.

[60] J.M. Sykes, Y. Xu, Electrochemical studies of galvanic action beneath organic coatings, Progress in Organic Coatings. 74 (2012) 320–325.

[61] H. Haagen, W. Funke, Prediction of the corrosion protective properties of paint films by permeability data, J. Oil Col. Chem. Assoc. 58 (1975) 359–364.

[62] W. Funke, Toward a unified view of the mechanism responsible for paint defects by metallic corrosion, Industrial & Engineering Chemistry Product Research and Development. 24 (1985) 343–347.

[63] F.E. Buttrey, J.A. McAlister, H.N. McMurray, Advanced electrochemical methods for food can evaluation, Ironmaking & Steelmaking. 26 (1999) 291–296.

[64] W. Funke, How organic coating systems protect against corrosion?, in: R. Dickie, F.L. Floyd (Eds.), Polymeric Material for Corrosion Control, American Chemical Society, Washington, DC, 1986: p. 222.

[65] S. Guruviah, The relationship between the permeation of oxygen and water through paint films and corrosion of painted mild steel, Journal of the Oil and Colour Chemists Association. 53 (1970) 669–679.

[66] F.M. Geenen, Characterization of organic coatings with impedance measurement, PhD thesis, Dept. Materials Science and Engineering, Delft University of Technology, 1991.

[67] H.J. Leidheiser, R.D. Granata, Ion transport through protective polymeric coatings exposed to an aqueous phase, IBM Journal of Research and Development. 32 (1988) 582–590.

[68] S. Zhang, S. Li, X. Luo, W. Zhou, Mechanism of the significant improvement in corrosion protection by lowering water sorption of the coating, Corrosion Science. 42 (2000) 2037–2041.

[69] D. Greenfield, J.D. Scantlebury, Blistering and delamination processes on coated steel, The Journal of Corrosion Science and Engineering. 2 (2000) paper 26.

[70] E. Van Westing, G. Ferrari, J.H.W. de Wit, The determination of coating performance with impedance measurements—II. Water uptake of coatings, Corrosion Science. 36 (1994) 957–977.

[71] a. Miszczyk, T. Schauer, Electrochemical approach to evaluate the interlayer adhesion of organic coatings, Progress in Organic Coatings. 52 (2005) 298–305.

[72] C.H. Hare, Water Permeability in unpigmented films, Journal of Protective Coatings and Linings. (1997) 67–86.

[73] C.H. Hare, The permeability of coatings to oxygen, gases, and ionic solutions, Journal of Protective Coatings & Linings. (1997) 66–80.

[74] C.H. Hare, A review of polyurethanes: Formulation variables and their effects on performance, Journal of Protective Coatings & Linings. (2000) 34–44.

[75] D.Y. Perera, Effect of pigmentation on organic coating characteristics, Progress in Organic Coatings. 50 (2004) 247–262.

[76] C.H. Hare, Free volume, Journal of Protective Coatings & Linings. (1996) 67–80.

[77] C.H. Hare, Effects of solvents on coating films, Journal of Protective Coatings & Linings. (1997) 69–81.

[78] J. Li, C.S. Jeffcoate, G.P. Bierwagen, D.J. Mills, D.E. Tallman, Thermal transition effects and electrochemical properties in organic coatings: Part 1 - initial studies on corrosion protective organic coatings, Corrosion. 54 (1998) 763–771.

[79] G.W. Walter, A critical review of the protection of metals by paints, Corrosion Science. 26 (1986) 27–38.

[80] G.P. Bierwagen, Reflections on corrosion control by organic coatings, Progress in Organic Coatings. 28 (1996) 43–48.

[81] J.N. Murray, Electrochemical test methods for evaluating organic coatings on metals: an update. Part II: single test parameter measurements, Progress in Organic Coatings. 31 (1997) 255–264.

[82] J.N. Murray, Electrochemical test methods for evaluating organic coatings on metals: an update. Part III: Multiple test parameter measurements, Progress in Organic Coatings. 31 (1997) 375–391.

[83] J.N. Murray, Electrochemical test methods for evaluating organic coatings on metals: an update. Part I. Introduction and generalities regarding electrochemical testing of organic coatings, Progress in Organic Coatings. 30 (1997) 225–233.

[84] P. Jeffrey, H.J. Leidheiser, Ionic migration through organic coatings and its consequences to corrosion, Industrial & Engineering Chemistry Product Research and Development. 25 (1986) 1–6.

[85] H.J. Leidheiser, W. Wang, L. Igetoft, The mechanism for the cathodic delamination of organic coatings from a metal surface, Progress in Organic Coatings. 11 (1983) 19–40.

[86] B.W. Cherry, Corrosion and the role of blistering at the coating/substrate interface, Corrosion and Materials. 36 (2011) 37–41.

[87] D.H. Van Der Weijde, E.P.M. van Westing, J.H.W. de Wit, EIS measurements on artificial blisters in organic coatings, Electrochimica Acta. 41 (1996) 1103–1107.

[88] Z. Sharer, J.M. Sykes, Insights into protection mechanisms of organic coatings from thermal testing with EIS, Progress in Organic Coatings. 74 (2012) 405–409.

[89] R. a. Dickie, Paint adhesion, corrosion protection, and interfacial chemistry, Progress in Organic Coatings. 25 (1994) 3–22.

[90] R.A. Dickie, J.S. Hammond, J.W. Holubka, Interfacial chemistry of the corrosion of polybutadiene-coated steel, Industrial & Engineering Chemistry. 20 (1981) 339–343.

[91] J.-B. Jorcin, E. Aragon, C. Merlatti, N. Pébère, Delaminated areas beneath organic coating: A local electrochemical impedance approach, Corrosion Science. 48 (2006) 1779–1790.

[92] T. Nguyen, E. Byrd, D. Bentz, Quantifying water at the organic film/hydroxylated substrate interface, The Journal of Adhesion. 48 (1995) 169–194.

[93] I. Linossier, F. Gaillard, M. Romand, A spectroscopic technique for studies of water transport along the interface and hydrolytic stability of polymer/substrate systems, The Journal of Adhesion. 70 (1999) 221.

[94] J. Pommersheim, T. Nguyen, Z. Zhang, C. Lin, Cation diffusion at the polymer coating/metal interface, Journal of Adhesion Science and Technology. 9 (1995) 935–951.

[95] F. Deflorian, S. Rossi, The role of ions diffusion in the cathodic delamination rate of polyester coated phosphatized steel, Journal of Adhesion Science and Technology. 17 (2003) 291–306.

[96] H. Bi, J.M. Sykes, Cathodic disbonding of an unpigmented epoxy coating on mild steel under semi-and full-immersion conditions, Corrosion Science. 53 (2011) 3416–25.

[97] J. Wielant, R. Posner, R. Hausbrand, G. Grundmeier, H. Terryn, Cathodic delamination of polyurethane films on oxide covered steel – combined adhesion and interface electrochemical studies, Corrosion Science. 51 (2009) 1664–1670.

[98] J.M. Pommersheim, T. Nguyen, Z. Zhang, J.B. Hubbard, Degradation of organic coatings on steel: Mathematical models and predictions, Progress in Organic Coatings. 25 (1994) 23–41.

[99] X.F. Yang, D.E. Tallman, S.G. Croll, G.P. Bierwagen, Morphological changes in polyurethane coatings on exposure to water, Polymer Degradation and Stability. 77 (2002) 391–396.

[100] X.F. Yang, D.E. Tallman, G.P. Bierwagen, S.G. Croll, S. Rohlik, Blistering and degradation of polyurethane coatings under different accelerated weathering tests, Polymer Degradation and Stability. 77 (2002) 103–109.

[101] G. Grundmeier, M. Stratmann, Adhesion and de-adhesion mechanisms at polymer/metal interfaces: mechanistic understanding based on in situ studies of buried interfaces, Annual Review of Materials Research. 35 (2005) 571–615.

[102] J. Wielant, R. Posner, R. Hausbrand, G. Grundmeier, H. Terryn, Cathodic delamination of polyurethane films on oxide covered steel–Combined adhesion and interface electrochemical studies, Corrosion Science. 51 (2009) 1664–70.

[103] E. Almeida, Surface treatments and coatings for metals. A general overview. 1. surface treatments, surface preparation, and the nature of coatings, Industrial & Engineering Chemistry Research. 40 (2001) 3–14.

[104] K. Gowers, J.D. Scantlebury, Blistering phenomena on lacquered mild steel, Corrosion Science. 23 (1983) 935–942.

[105] C.H. Hare, Adhesion I, Journal of Protective Coatings & Linings. (1996) 77–87.

[106] S. Bistac, M.F. Vallat, J. Schultz, Durability of steel/polymer adhesion in an aqueous environment, International Journal of Adhesion & Adhesives. 18 (1998) 365–369.

[107] M. Mahdavian, M.M. Attar, Evaluation of zinc phosphate and zinc chromate effectiveness via AC and DC methods, Progress in Organic Coatings. 53 (2005) 191–194.

[108] B.N. Zand, M. Mahdavian, Evaluation of the effect of vinyltrimethoxysilane on corrosion resistance and adhesion strength of epoxy coated AA1050, Electrochimica Acta. 52 (2007) 6438–6442.

[109] M. Mahdavian, Investigation of corrosion inhibitive effect of imidazole derivatives as replacement of chromate compounds, PhD thesis, Department of Polymer and Coating, Tehran Polytechnic, 2009.

[110] L. Fedrizzi, F. Deflorian, S. Rossi, L. Fambri, P.L.L. Bonora, Study of the corrosion behaviour of phosphatized and painted industrial water heaters, Progress in Organic Coatings. 42 (2001) 65–74.

[111] N. Baute, C. Jerome, L. Martinot, M. Mertens, V.M. Geskin, R. Lazzaroni, et al., Electrochemical Strategies for the Strengthening of Polymer-Metal Interfaces, Eur. J. Inorg. Chem. (2001) 1097–1107.

[112] M.K. Harun, S.N.A.S. Ismail, S.B. Lyon, Effect of surface pretreatment on water absorption and wet adhesion of organic coatings, Corrosion Engineering, Science and Technology. 41 (2006) 255–258.

[113] J.B. Bajat, J.P. Popić, V.B. Mišković-Stanković, The influence of aluminium surface pretreatment on the corrosion stability and adhesion of powder polyester coating, Progress in Organic Coatings. 69 (2010) 316–321.

[114] R. Naderi, M.M. Attar, M.. Moayed, EIS examination of mill scale on mild steel with polyester–epoxy powder coating, Progress in Organic Coatings. 50 (2004) 162–165.

[115] H. Roper, R. Weaver, J. Brandon, The effect of peak count of surface roughness on coating performance, Journal of Protective Coatings & Linings. (2005) 52–64.

[116] X. Jin, K. Tsay, A. Elbasir, J.D. Scantlebury, The adhesion and disbonding of chlorinated rubber on mild steel, in: M.W. Kendig, H.J. Leidheiser (Eds.), Symposium on Corrosion Protection by Organic Coatings, Electrochemical society, Pennington, USA, 1987: pp. 37–47.

[117] N.W. Khun, G.S. Frankel, Effects of surface roughness, texture and polymer degradation on cathodic delamination of epoxy coated steel samples, Corrosion Science. 67 (2012) 152–160.

[118] D.J. Mills, K. Schaefer, Use of electrochemical methods to examine different surface preparation methods for organic coatings on steel, Progress in Organic Coatings. 69 (2010) 193–198.

[119] C. Lin, T. Nguyen, M. McKnight, Relation between AC impedance data and degradation of coated steel: 1. Effects of surface roughness and contamination on the corrosion behavior of epoxy-coated, Progress in Organic Coatings. 20 (1992) 169–186.

[120] D.M. Santágata, P.R. Seré, C.I. Elsner, A.R. Di Sarli, Evaluation of the surface treatment effect on the corrosion performance of paint coated carbon steel, Progress in Organic Coatings. 33 (1998) 44–54.

[121] L.F. Vesga, E. Vera, J.H. Panqueva, Use of the electrochemical impedance spectroscopy to evaluate the performance of a primer applied under different surface preparation methods, Progress in Organic Coatings. 39 (2000) 61–65.

[122] D.J. Mills, S.J. Mabbutt, G.P. Bierwagen, Y. Pae, S. Berg, The effect of the substrate on the electrochemical response of protective coatings, in: 13th International Corrosion Congress Proceedings: Towards Corrosion Prevention, Melbourne, 1996: p. paper no. 432.

[123] J.E.O. Mayne, D.J. Mills, The effect of the substrate on the electrical resistance of polymer films, Journal of Oil and Colour Chemists Association. 58 (1975) 155–159.

[124] H. Corti, F.-P. R, D. Gomez, Protective organic coatings: membrane properties and performance, Progress in Organic Coatings. 10 (1982) 5–33.

[125] J.E.O. Mayne, J.D. Scantlebury, Ionic conduction in polymer films II. inhomogeneus structure of varnish films, British Polymer Journal. 2 (1970) 240–243.

[126] P. Moongkhamklang, S.. Taylor, The delineation of ionic pathways in organic coatings using a molecular probe technique, Progress in Organic Coatings. 46 (2003) 259–265.

[127] P. Moongkhamklang, S. Taylor, The delineation of ionic pathways in epoxy coatings using molecular probes, in: V. Agarwala (Ed.), Tri-service Corrosion Conference, Las Vegas, Nevada, 2003: p. paper no. AM025715.

[128] M.L. White, H. Vedage, R.D. Granata, H.J. Leidheiser, Failure mechanisms for organic coatings subjected to 0.1M sulfuric acid, Industrial & Engineering Chemistry Product Research and Development. 25 (1986) 129–132.

[129] D.. Worsley, D. Williams, J.S.. Ling, Mechanistic changes in cut-edge corrosion induced by variation of organic coating porosity, Corrosion Science. 43 (2001) 2335–2348.

[130] E.M. Kinsella, J.E.O. Mayne, Ionic conduction in polymer films I. influence of electrolyte on resistance, British Polymer Journal. 1 (1969) 173–176.

[131] D.J. Mills, The function of basic pigments in protection by organic coatings, PhD thesis, Dept. of Materials Science and Metallurgy, University of Cambridge, 1973.

[132] D.J. Mills, J.E.O. Mayne, The inhomogeneous nature of polymer films and its effect on resistance inhibition, in: H.J. Leidheiser (Ed.), Corrosion Control by Organic Coatings, NACE International, Bethelehem, PA, USA, 1981: pp. 12–17.

[133] J.E.O. Mayne, The crosslinking and adhesion to mild steel of epoxypolyamine films, in: J.D. Scantlebury, M.W. Kendig (Eds.), Advance in Corrosion Protection by Organic Coatings III, Electrochemical society, Cambridge, UK, 1989: pp. 1–7.

[134] M.L. White, D.J. Mills, H.J. Leidheiser, Resistance measurements of organic coatings as a means for evaluating corrosion protection in acid solutions, in: M.W. Kendig, H.J. Leidheiser (Eds.), Corrosion Protection by Organic Coatings, Electrochemical society, San Diego, Calif., 1986: pp. 208–216.

[135] J.E.O. Mayne, J.D. Scantlebury, Ionic conduction in polymer films IV. the effect of pigmentation with iron oxide, British Corrosion Journal. 3 (1971) 237–239.

[136] C.-I. Wu, X. Zhou, Y. Tan, A study on the electrochemical inhomogeneity of organic coatings, Progress in Organic Coatings. 25 (1995) 379–389.

[137] F. Zou, D. Thierry, Localized electrochemical impedance spectroscopy for studying the degradation of organic coatings, Electrochimica Acta. 42 (1997) 3293–3301.

[138] E.P.M. van Westing, G.M. Ferrari, F.M. Geenen, J.H.W. de Wit, In situ determination of the loss of adhesion of barrier epoxy coatings using electrochemical impedance spectroscopy, Progress in Organic Coatings. 23 (1993) 89–103.

[139] M. Szociński, K. Darowicki, K. Schaefer, Application of impedance imaging to evaluation of organic coating degradation at a local scale, Journal of Coatings Technology and Research. (2012) 1–8.

[140] T.N. Nguyen, J.B. Hubbard, G.B. McFadden, A mathematical model for the cathodic blistering of organic coatings on steel immersed in electrolytes, Journal of Coatings Technology. 63 (1991) 43–52.

[141] T. Kamimura, H. Kishikawa, Mechanism of cathodic disbonding of three-layer polyethylene-coated steel pipe, Corrosion. 54 (1998) 979–987.

[142] N.S. Sangaj, V.C. Malshe, Permeability of polymers in protective organic coatings, Progress in Organic Coatings. 50 (2004) 28–39.

[143] E.M. Kinsella, J.E.O. Mayne, J.D. Scantlebury, Ionic conduction in polymer films III. influence of temperature on water absorption, British Polymer Journal. 3 (1971) 41–43.

[144] C. Le Pen, C. Lacabanne, N. Pébère, Structure of waterborne coatings by electrochemical impedance spectroscopy and a thermostimulated current method: influence of fillers, Progress in Organic Coatings. 39 (2000) 167–175.

[145] G.P. Bierwagen, C.S. Jeffcoate, J. Li, S. Balbyshev, D.E. Tallman, D.J. Mills, The use of electrochemical noise methods (ENM) to study thick, high impedance coatings, Progress in Organic Coatings. 29 (1996) 21–29.

[146] M.C.S.S. Macedo, I.C.P. Margarit-Mattos, F.L. Fragata, J.-B. Jorcin, N. Pébère, O.R. Mattos, Contribution to a better understanding of different behaviour patterns observed with organic coatings evaluated by electrochemical impedance spectroscopy, Corrosion Science. 51 (2009) 1322–1327.

[147] D.J. Mills, J.E.O. Mayne, Structural changes in polymer films. part 2: the effect of the pigment zinc oxide on the electrolytic resistance and transition temperature; some

comparisons with the pigments iron oxide and red lead, Journal of Oil and Colour Chemists Association. 66 (1983) 88–93.

[148] R.S. Fishman, D.A. Kurtze, G.P. Bierwagen, Pigment inhomogeneity and void formation in organic coatings, Progress in Organic Coatings. 21 (1993) 387–403.

[149] O.Ø. Knudsen, E. Bardal, U. Steinsmo, Effect of barrier pigments on cathodic disbonding Part 1: aluminium and glass pigmets, Journal of Corrosion Science & Engineering. 2 (1999) paper 13.

[150] G.K. Van Der Wel, O.C.G. Adan, Moisture in organic coatings—a review, Progress in Organic Coatings. 37 (1999) 1–14.

[151] P. Donkers, H. Huinink, S.J.F. Erich, N. Reuvers, O.C.G. Adan, Water permeability of pigmented waterborne coatings, Progress in Organic Coatings. 76 (2013) 60–69.

[152] H.J. Leidheiser, Mechanism of deadhesion of organic coatings from metal surfaces, in: R.A. Dickie, F.L. Floyd (Eds.), Polymeric Material for Corrosion Control, American Chemical Society, Washington, DC, 1986: p. 124.

[153] M. Mcleod, J.M. Sykes, Blistering of paint coatings on steel in sea water, in: K.N. Stafford (Ed.), Coatings and Surface Treatment for Corrosion and Wear Resistance, Ellis Horwood, Chichester, England, 1984: p. paper no. 21.

[154] F. Deflorian, S. Rossi, An EIS study of ion diffusion through organic coatings, Electrochimica Acta. 51 (2006) 1736–1744.

[155] H.J. Leidheiser, A. Vertes, J.E. Roberts, Polymer/metal and polymer/ion interactions in proective coatings, Hyperfine Interactions. 57 (1990) 1955–1962.

[156] H.J. Leidheiser, M.W. Kendig, Conjecture on delamination of organic coatings by corrosion, Industrial & Engineering Chemistry Product Research and Development. 17 (1978) 54–55.

[157] S. Skale, V. Doleček, M. Slemnik, Electrochemical impedance studies of corrosion protected surfaces covered by epoxy polyamide coating systems, Progress in Organic Coatings. 62 (2008) 387–392.

[158] V.S. Raja, R. Gayathiri Devi, A. Venugopal, N.C. Debnath, J. Giridhar, Evaluation of blistering performance of pigmented and unpigmented alkyd coatings using electrochemical impedance spectroscopy, Surface and Coatings Technology. 107 (1998) 1–11.

[159] N. Hirose, S. Tanaka, T. Tanaki, I. Sekine, Effect of film thickness on coated film degradation by scanning acoustic microscope and nanoindentation tester, Journal of Electrochemical Society. 150 (2003) B282–B287.

[160] J. Li, Study on corrosion protection of organic coatings using electrochemical techniques: Thermal property characterization, film thickness investigation, and coating performance evaluation, PhD thesis, North Dakota State University, 2002.

[161] K. Schaefer, MSc thesis: Investigation into influence of different surface preparation methods on performance of anti-corrosive organic coatings on steel, University of Northampton, 2008.

[162] M. Schilling, Solvent entrapment and osmotic blistering, Journal of Protective Coatings & Linings. (2004) 24–26.

[163] M. Islam, In-situ measurement and monitoring of internal stress in organic coatings, in: Corrosion Protection by Organic Coatings, Cambridge, UK, 2004.

[164] T. Monetta, F. Belluccei, L. Nicodemo, L. Nicolais, Protective properties of epoxy-based organic coatings on mild steel, Progress in Organic Coatings. 21 (1993) 353–369.

[165] A. Rais-Ali, M. Richardson, The role of crosslink density in influencing the electrical resistance behaviour of polymeric coatings, British Polymer Journal. (1980) 57–60.

[166] H.J. Leidheiser, R.D. Granata, K. Kovaleski, Corrosion control through a better understanding of the metallic substrate/organic coating interface; Annual report. Part 3: Temperature dependence of the low frequency impedance of polymeric coatings, Zettlemoyer Center for Surface Studies, Lehigh University, Bethelehem, PA, USA, 1990.

[167] A. Hellgren, P. Weissenborn, K. Holmberg, Surfactants in water-borne paints, Progress in Organic Coatings. 35 (1999) 79–87.

[168] L.N. Butler, C.M. Fellows, R.G. Gilbert, Effect of surfactants used for binder synthesis on the properties of latex paints, Progress in Organic Coatings. 53 (2005) 112–118.

[169] D.J. Mills, S.J. Mabbutt, Inhomogeneities in organic coatings. a look at their importance to protection and at ways of detecting them, in: I. Sekine, M.W. Kendig, D. Scantlebury, D.J. Mills (Eds.), Advances in Corrosion Protection by Organic Coatings III, Electrochemical society, Noda, Japan, 1997: pp. 89–100.

[170] A. Overbeek, Polymer heterogeneity in waterborne coatings, Journal of Coatings Technology and Research. 7 (2009) 1–21.

[171] A. Howl, Surface preparation as applied in the process of refurbishing containers:: the Selection and Use of Abrasive blast cleaning equipment, Anti-Corrosion Methods and Materials. 23 (1976) 7–16.

[172] E. Almeida, Surface treatments and coatings for metals. A general overview. 2. coatings: application processes, environmental conditions during painting and drying, and new tendencies, Industrial & Engineering Chemistry Research. 40 (2001) 15–20.

[173] C.H. Hare, Adhesion: Part 2, Journal of Protective Coatings & Linings. (1996) 79–95.

[174] S. El-Sawy, Guidelines for corrosion testing of coated and uncoated metals, Anti-Corrosion Methods and Materials. 32 (1985) 16–18.

[175] J. Kittel, N. Celati, M. Keddam, H. Takenouti, Influence of the coating–substrate interactions on the corrosion protection: characterisation by impedance spectroscopy of the inner and outer parts of a coating, Progress in Organic Coatings. 46 (2003) 135–147.

[176] H.J. Leidheiser, Electrical and electrochemical measurements as predictors of corrosion at the metal-organic coating interface, Progress in Organic Coatings. 7 (1979) 79–104.

[177] J.D. Scantlebury, K.N. Ho, D.A. Eden, Impedance measurements on organic coatings on mild steel in sodium chloride solution, in: F. Mansfeld, U. Bertocci (Eds.), Electrochemical Corrosion Testing, American socienty for testing and materials, Baltimore, 1981: pp. 187–197.

[178] Y.N. Mikhailovskii, V. V Leonov, N.D. Tomashov, Measuring the resistance of insulating protective coatings on metals immersed in electrolytes, in: N.D. Tomashov, E.N. Mirolyubov (Eds.), Corrosion of Metals and Alloys, Israel programme for scientific translation, Jerusalem, 1966: pp. 202–209.

[179] F.M. Geenen, J.H.W. de Wit, E.P.M. van Westing, An impedance spectroscopy study of the degradation mechanism for a model epoxy coating on mild steel, Progress in Organic Coatings. 18 (1990) 299–312.

[180] P. Bonora, F. Deflorian, L. Fedrizzi, Electrochemical impedance spectroscopy as a tool for investigating underpaint corrosion, Electrochimica Acta. 41 (1996) 1073–1082.

[181] D. Brasher, A. Kingsbury, Electrical measurements in the study of immersed paint coatings on metal. I. Comparison between capacitance and gravimetric methods of estimating water-uptake, Journal of Applied Chemistry. 4 (1954) 62–72.

[182] J.M. Sykes, A variant of the Brasher–Kingsbury equation, Corrosion Science. 46 (2004) 515–517.

[183] O.A. Stafford, B.R. Hinderliter, S.G. Croll, Electrochemical impedance spectroscopy response of water uptake in organic coatings by finite element methods, Electrochimica Acta. 52 (2006) 1339–1348.

[184] F. Deflorian, L. Fedrizzi, S. Rossi, P.L. Bonora, Organic coating capacitance measurement by EIS: ideal and actual trends, Electrochimica Acta. 44 (1999) 4243–4249.

[185] A. Amirudin, D. Thierry, Application of electrochemical impedance spectroscopy to study the degradation of polymer-coated metals, Progress in Organic Coatings. 26 (1995) 1–28.

[186] B. Skerry, D. Eden, Electrochemical testing to assess corrosion protective coatings, Progress in Organic Coatings. 15 (1987) 269–285.

[187] A. Aballe, A. Bautista, U. Bertocci, F. Huet, The measurement of the noise resistance for corrosion applications, in: Corrosion 2000, NACE International, 2000: p. paper no. 00424.

[188] E. Garcia, J. Mojica, F.J. Rodriguez, J. Genescá, J.J. Carpio, Assessing of three industrial paint coatings by electrochemical noise, in: CORROSION 98, NACE International, 1998: p. paper No. 379.

[189] F. Mansfeld, C. Lee, The frequency dependence of the noise resistance for polymer-coated metals, Journal of the Electrochemical Society. 144 (1997) 2068–2071.

[190] F. Mansfeld, L.T. Han, C.C. Lee, G. Zhang, Evaluation of corrosion protection by polymer coatings using electrochemical impedance spectroscopy and noise analysis, Electrochimica Acta. 43 (1998) 2933–2945.

[191] G.P. Bierwagen, X. Wang, D.E. Tallman, In situ study of coatings using embedded electrodes for ENM measurements, Progress in Organic Coatings. 46 (2003) 163–175.

[192] G.P. Bierwagen, D.J. Mills, D.E. Tallman, B.S. Skerry, Reproducibility of electrochemical noise data from coated metal systems, in: J. Kearns, J.R. Scully, P.R. Roberge, D.L. Reichert, J.L. Dawson (Eds.), First International Symposium on Electrochemical Noise Measurement for Corrosion Applications, ASTM, Montreal, Quebec, 1994: pp. 427–445.

[193] Q. Le Thu, G.P. Bierwagen, S. Touzain, EIS and ENM measurements for three different organic coatings on aluminum, Progress in Organic Coatings. 42 (2001) 179–187.

[194] R.. De Rosa, D.. Earl, G.P. Bierwagen, Statistical evaluation of EIS and ENM data collected for monitoring corrosion barrier properties of organic coatings on Al-2024-T3, Corrosion Science. 44 (2002) 1607–1620.

[195] G.P. Bierwagen, D.E. Tallman, J. Li, S. Balbyshev, M. Zidoune, Electrochemical noise studies of aircraft coatings over Al 2024 T-3 in accelerated exposure testing, in: Corrosion 2000, NACE International, 2000: p. paper no. 00427.

[196] D.J. Mills, M. Broster, I. Razaq, Continuing work to enable electrochemical methods to be used to monitor the performance of organic coatings in the field, Progress in Organic Coatings. 63 (2008) 267–271.

[197] S.J. Mabbutt, D.J. Mills, Novel configuration for electrochemical noise measurements, British Corrosion Journal. 33 (1998) 158–160.

[198] S.J. Mabbutt, G.P. Bierwagen, D.J. Mills, New experimental arrangement for the acquisition of electrochemical noise data from high resistance organic anti-corrosive coatings, Anti-Corrosion Methods and Materials. 49 (2002) 264–269.

[199] S.J. Mabbutt, D.J. Mills, C.P. Woodcock, Developments of the electrochemical noise method (ENM) for more practical assessment of anti-corrosion coatings, Progress in Organic Coatings. 59 (2007) 192–196.

[200] A. Momber, S. Koller, H. Dittmers, Effects of surface preparation methods on adhesion of organic coatings to steel substrates, Journal of Protective Coatings and Linings. (2004) 44–50.

[201] B. Tepe, B. Gunay, Evaluation of pre-treatment processes for HRS (hot rolled steel) in powder coating, Progress in Organic Coatings. 62 (2008) 134–144.

[202] B. Ramezanzadeh, M.M. Attar, Evaluation of the effects of surface treatments on the cathodic delamination and anticorrosion performance of an epoxy-nanocomposite on steel substrate, Journal of Coatings Technology and Research. 10 (2012) 47–55.

[203] Z. Sun, K.-T. Wan, D.A. Dillard, A theoretical and numerical study of thin film delamination using the pull-off test, International Journal of Solids and Structures. 41 (2004) 717–730.

[204] G. Rogers, Test instruments for coating adhesion, Materials Performance. 42 (2003) 40–44.

[205] Y.H. Baek, M.K. Chung, S.M. Son, E.H. Song, C.S. Shin, K.K. Baek, Reliability on coating pull-off adhesion strength test, in: CORROSION 2009, NACE International, Atlanta, GA, 2009: p. paper no. 09007.

[206] DeFelsko Webpage accessed 29 April 2013, Dolly preparation for pull-off adhesion testing, <http://www.defelsko.com/technotes/DollyPreparation.htm>. (n.d.).

[207] J. V Koleske, Mechanical Properties of Solid Coatings, in: R.A. Meyers (Ed.), Encyclopedia of Analytical Chemistry, John Wiley & Sons, Inc, Charleston, USA, 2006: pp. 1–15.

[208] W. Schlesing, M. Buhk, M. Osterhold, Dynamic mechanical analysis in coatings industry, Progress in Organic Coatings. 49 (2004) 197–208.

[209] C.H. Hare, The mechanical properties of coating films and their characterisation, Protect. Coat. Europe. 1 (1996) 42–57.

[210] R. Mafi, S.M. Mirabedini, M.M. Attar, S. Moradian, Cure characterization of epoxy and polyester clear powder coatings using Differential Scanning Calorimetry (DSC) and Dynamic Mechanical Thermal Analysis (DMTA), Progress in Organic Coatings. 54 (2005) 164–169.

[211] L. Fedrizzi, A. Bergo, M. Fanicchia, Evaluation of accelerated aging procedures of painted galvanised steels by EIS, Electrochimica Acta. 51 (2006) 1864–1872.

[212] M. Delucchi, S. Turri, a. Barbucci, S. Novelli, G. Cerisola, Investigation on physico-chemical and electrochemical properties of fluoropolyether coatings, Progress in Organic Coatings. 44 (2002) 227–232.

[213] N. Tahmassebi, S. Moradian, S.M. Mirabedini, Evaluation of the weathering performance of basecoat/clearcoat automotive paint systems by electrochemical properties measurements, Progress in Organic Coatings. 54 (2005) 384–389.

[214] L.H. Yang, F.C. Liu, E.H. Han, Effects of P/B on the properties of anticorrosive coatings with different particle size, Progress in Organic Coatings. 53 (2005) 91–98.

Chapter 3

Development of Electrochemical Noise Technique: towards a practical method for assessing performance of organically coated metal on-site

3.1 Introduction

3.1.1 History of noise technique

Electrochemical noise measurement comprises simultaneous measurement of potential and current fluctuations caused by spontaneous electrochemical reactions. It is a non-destructive/non-intrusive technique capable of monitoring basic changes in an electrochemically active system. The technique has been used to calculate R_n as a measure of corrosion resistance [1,2] and also statistical methods have been applied to evaluate the corrosion regime [3–5]. ENM provides mechanistic information about the corrosion uniformity/localization of uncoated systems which may not be acquired by the techniques such as EIS and DC measurements. The sensitivity of electrochemical noise to the local electrochemical activity on steel surface has been shown by Wharton *et al.* [6].

Since first introduced to the field of organic coatings in 1986 [7] the Electrochemical Noise Method (ENM) has found increasing use as an effective way of assessing the protection afforded by organic coatings on metals [8–11]. It has been shown frequently that the noise resistance conforms with the protection level afforded as measured by other well-established techniques such as EIS [12–16] and linear polarization resistance (LPR) [14]. Noise resistance has been also used as equal to polarization resistance, both practically [17] and theoretically [18], to calculate the corrosion rate. Sanchez-Amaya *et al.* [19] successfully utilized electrochemical noise to distinguish between the different stages of degradation of an epoxy coating. High sensitivity of ENM to the changes at coating/metal interface and its ability to measure very high resistances, e.g. E+12-E+14 $\Omega.cm^2$, has been recently reported by Deya *et al.* [20]. Conner *et al.* [21] used ENM for assessing the effectiveness of plasma surface pre-treatment prior to coating. The high sensitivity of ENM to the ionic composition of electrolyte, its ability to distinguish the onset of corrosion and good correlation with EIS result was reported.

The usefulness and simplicity of the ENM technique plus the relatively quick measurement and inexpensive instrumentation makes the method potentially ideal for in-situ corrosion assessments. It has been successfully implemented as a fast electrochemical technique in conjunction with wire-beam multi-electrodes where a quick examination of a large number of electrodes is required [4,22,23]. It also offers the advantage of being a non-

interfering measurement compared to DC techniques (e.g. DC measurement of resistance using electrometers) where the applied potential alters the system from the steady state. The DC measurements by means of an external potential/current, and its consequent interference, will not ideally represent system characteristics in a self-corroding and uninterrupted condition and also more time will be required to reach the steady state [12].

3.1.2 Methods of data analysis

- Graphical data analysis for un-coated metal

The simplest approach to data analysis is the visual assessment of the noise data to acquire mechanistic information about corrosion pattern. The shape and the occurrence frequency of current and potential transients may be considered as an indication of corrosion pit formation and its repassivation/propagation [5,24]. This approach has been solely used for analysis of ENM data collected from uncoated (bare) metal surfaces and gives qualitative results for comparative corrosion studies. Therefore this method will not be further discussed in here as this chapter aims at the application of ENM on organically coated metals. Figure 3.1 shows potential/current transients caused by meta-stable pitting of steel in 0.05M $Ca(OH_2)$+0.025M NaCl solution [24].

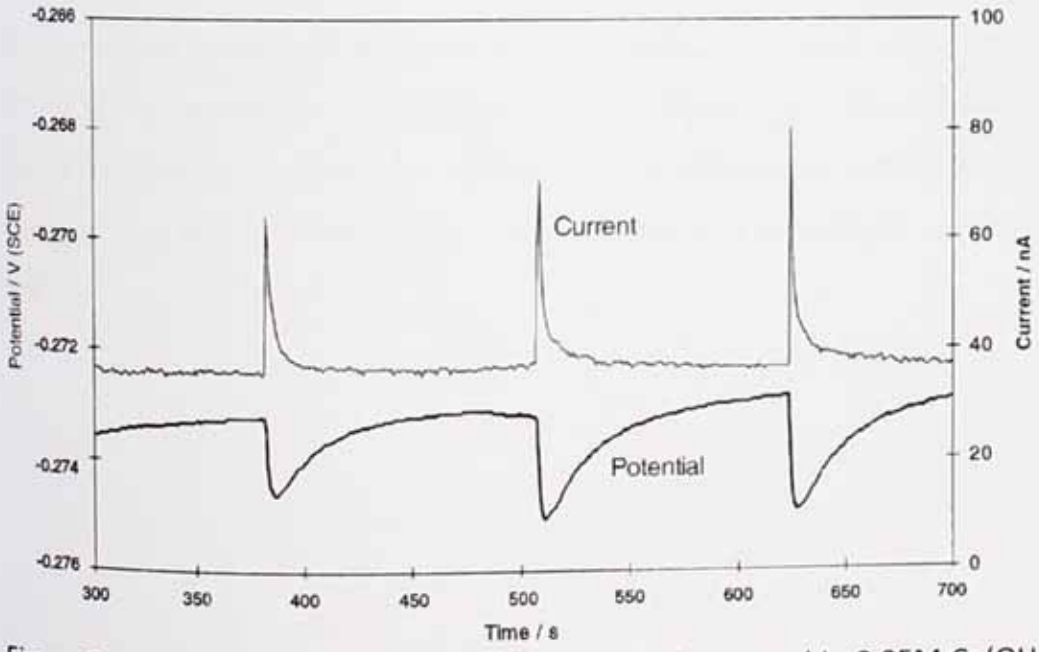

Figure 3.1 Current and potential time records for bare steel in 0.05M $Ca(OH_2)$+0.025M NaCl solution showing the pitting event [24].

- Statistical data analysis for coated metal

The transients of potential and current are not normally found in noise data obtained from coated metal. Figure 3.2 shows a typical noise data collected from polymer coated steel with relatively high performance.

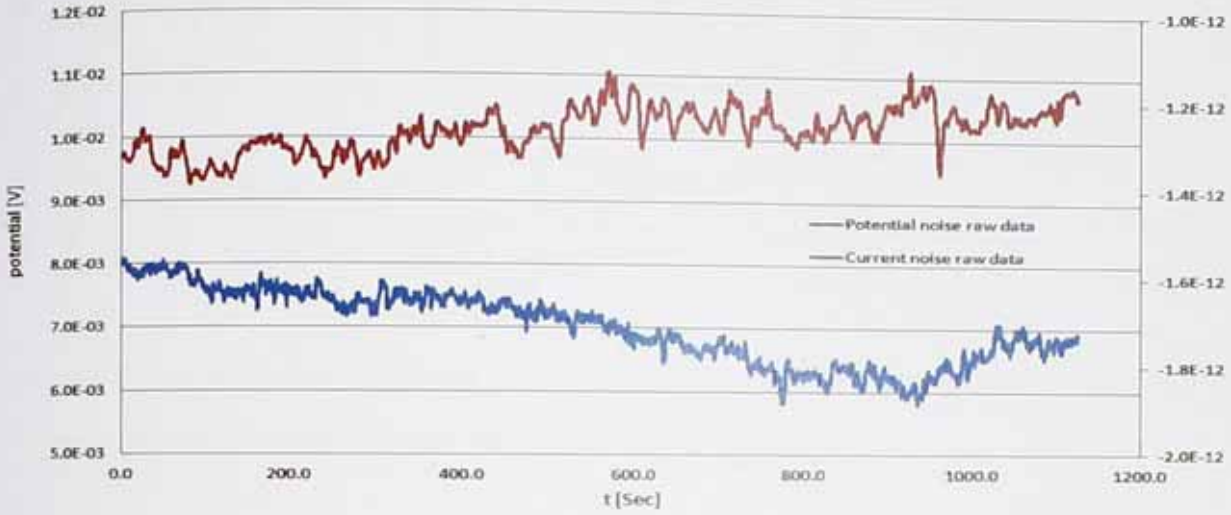

Figure 3.2 Typical current and potential noise data of a polymer coated steel.

In addition to the high frequency fluctuation, in many cases, the data set contains a general drift that deviate the signal from the stationary state. The drift is usually in one direction and caused by a DC source, such as the potential shift of sample during measurement or the small external potential/current from the instrumentation. It is important to remove the DC drift from the noise signal when applying the statistical analysis to the noise data [25]. Drift removal is normally performed by subtracting a linear regression line from the raw data resulting in a smaller variation around the mean value zero (Figure 3.3).

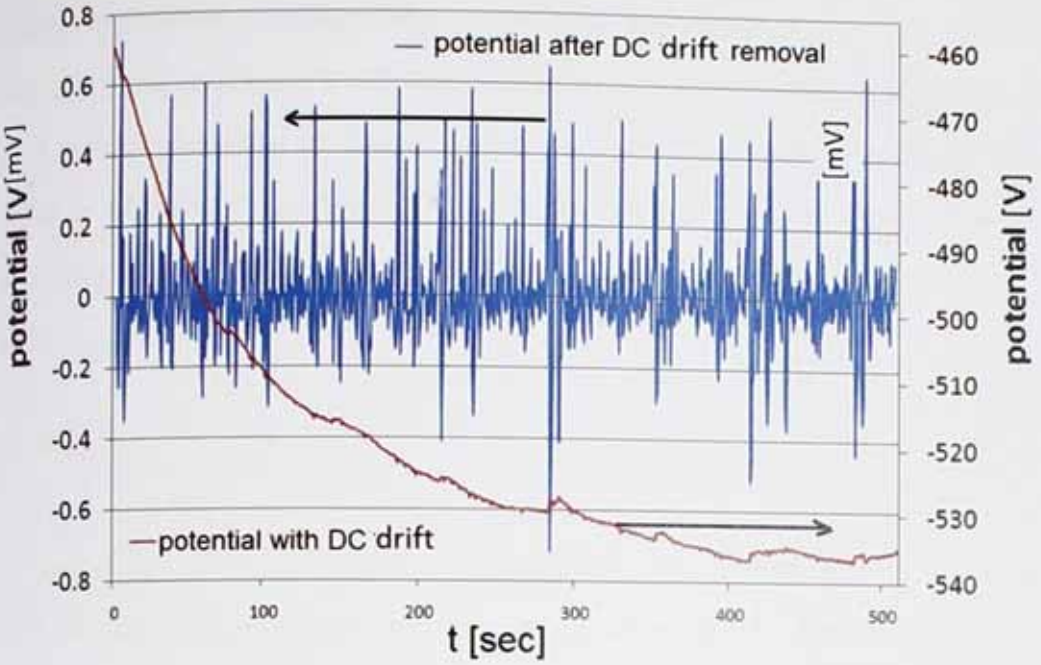

Figure 3.3 Effect of treating a drifting data set to eliminate the DC part of signal and prevent erroneous statistical analysis of electrochemical noise data.

The basic quantitative derivative of noise date is the noise resistance in the time domain, R_n, which is calculated in accordance with Ohm's law, equation (1).

$$R_n = \frac{\sigma(V)}{\sigma(I)} \quad (1)$$

where σ(V) and σ(I) are the standard deviations of potential and current fluctuations. In order to derive a valid R_n, potential and current noise data should have a Gaussian (normal) distribution. The equation 1 implies that σ(V) decreases and σ(I) increases as the coating degrades [26,27]. However, increase of both σ(V) and σ(I) as a result of coating degradation has been also reported elsewhere [28]. The usefulness of R_n for basic assessment of organic coatings and ranking their performance has been extensively demonstrated elsewhere [29–32].

Mansfeld and co-workers have performed electrochemical noise (ECN) measurements for a number of coating systems and have emphasized the need for analysis of ECN data not only in the time domain, but also in the frequency domain in order to extract mechanistic information [27,33]. It has been suggested that R_n is equal to R_{sn} and DC limit of impedance spectrum in bode plot only when diffusion process dominates the corrosion process. For

highly protective coatings with capacitive behaviour R_n is frequency dependant and therefore may not have a definite relationship to a particular coating property [34–36]. The time domain data can be transferred to frequency domain using the fast Fourier transform (FFT) or Maximum Entropy Method (MEM) algorithms. The Power Spectral Density (PSD) plot may be used to calculate the spectral noise resistance, R_{sn}, according to the equation (2):

$$R_{sn}(f) = \sqrt{\frac{\psi_V(f)}{\psi_I(f)}} \quad (2)$$

where Ψ_V and Ψ_I are the PSD's of potential and current noise respectively. The minimum and maximum frequencies that can be resolved in the frequency domain are given by equation (3):

$$f_{min} = \frac{1}{N \cdot \Delta t}, \quad f_{max} = \frac{1}{2 \cdot \Delta t} \quad (3)$$

with N the total number of samples and Δt the time increment between samples. Typical sampling times of 1024 s and sampling rates of 2 points/s applied in the present studies lead to a frequency range from 1 Hz to 1 mHz. The degradation process of a paint coating may be analysed by contributions from charge transfer reactions at high frequencies and mass transport reactions at low frequencies.

Other analytical approaches such as statistical modelling [37], wavelet analysis [38–40], fractal analysis [41], artificial neural network [42,43] and Cluster and discriminant analysis [44,45] have been implemented mainly in order to acquire mechanistic information about the active/passive state and the corrosion pattern of bare metals. Statistical analysis have been also applied to determine the corrosion localization underneath the paint films with limited success [46–48].

3.1.3 Alternative arrangements with a view to develop an on-site method

The ENM technique with the original arrangement, for instance with a salt bridge (Figure 3.4), is well established and is commonly applied for studying electrochemical behaviour of

corroding systems in the laboratory. This method uses two nominally identical but separate working electrodes and works effectively for both bare metals and coated metals. The current between the two working electrodes is measured by a zero resistance ammeter (ZRA) simultaneously with the potential of these electrodes (now in effect coupled together by the potentiometer) with respect to a noiseless standard electrode (normally a Saturated Calomel Electrode (SCE)). However, it will usually be impractical to find two nominally identical but separate working electrodes in the real/site environment, e.g. a bridge or a ship. A first step towards making the technique more practically useable for organically coated metal on site was taken by Mills and Mabbutt in 1998 [49]. The so-called "Single Substrate" (S.S.) (Figure 3.5) arrangement is a re-arrangement of the original salt bridge arrangement. It replaces the working electrodes (the two substrates) by SCEs and uses the substrate as the pseudo reference. Noiseless SCE's make electrolytic contact with the corroding surface and the current perturbation measured by ZRA originates from the electrochemical activity of the two coupled areas of the specimen. This arrangement was also successfully utilized for *in-situ* monitoring of corrosion behaviour and degradation rate of coated substrates using embedded Pt electrodes by Bierwagen et al. [46]. There has been further work carried out on the validation of the technique, mainly by Mabbutt [12,50–52].

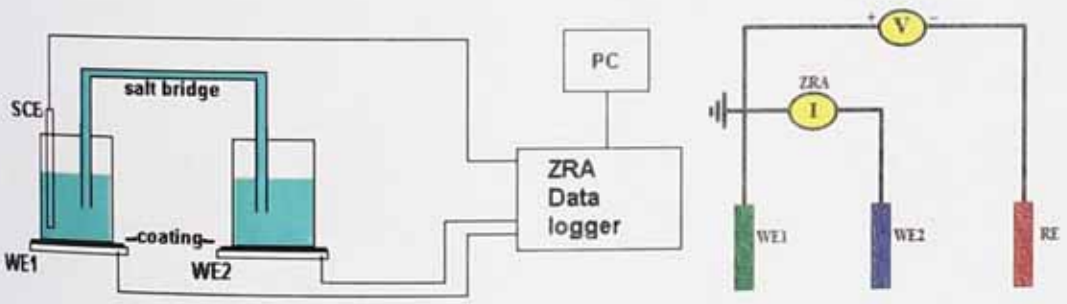

Figure 3.4 Standard "Salt-Bridge" electrochemical noise configuration in which the current is measured by a zero resistance ammeter (ZRA) between two nominally identical working electrodes (WE1 and WE2) simultaneously with potential using a saturated calomel reference electrode (SCE) (left) and a schematic representation of the electrical circuit utilised for the measurement (right).

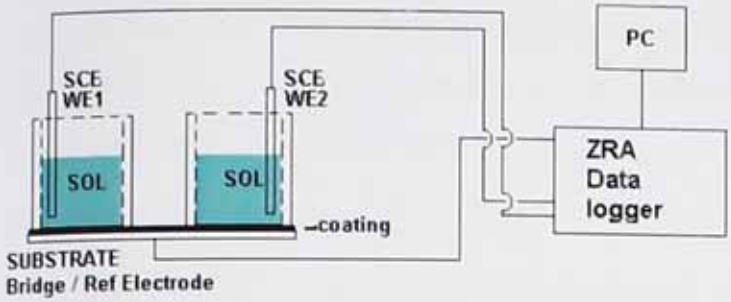

Figure 3.5 Schematic laboratory arrangement for Single Substrate (SS) measurement [12].

A further development was made by Woodcock *et al.* mainly to eliminate the need for electrical connection to substrate and to make the technique more practically useable [53,54]. In this new, so-called "NO Connection to Substrate" (NOCS) arrangement, potential noise is measured against the third SCE which, similar to the working electrodes, is in electrolytic contact with the specimen. The NOCS arrangement is shown is Figure 3.6. Main advantages of this configuration are elimination of wired electrical contact to substrate (no need for paint removal when the sample is fully coated) and the use of a highly stable reference electrode. The usefulness of the NOCS arrangement has been also reported elsewhere [43].

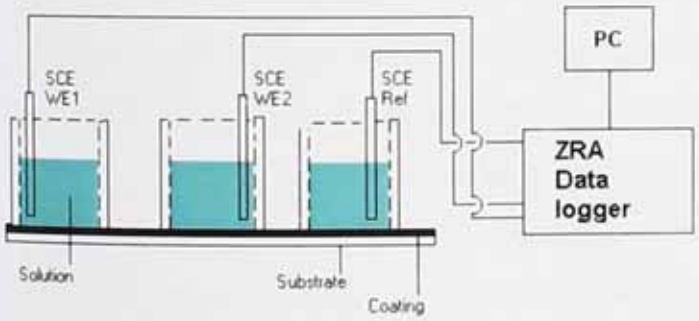

Figure 3.6 Schematic laboratory arrangement for NOCS measurement [12].

An overview of the newly developed ENM arrangements and practical approach to implement these for *in-situ* measurement has been discussed by Mills in Ref. [55]. Despite all the efforts to make ENM a practical on-site method, field evaluation offers a significant challenge, particularly in the case of submerged structures and awkwardly shaped substrates, where providing and isolating the two or three working electrodes (for SS and

NOCS arrangements respectively) may be impractical. Also in contrast with most laboratory experiments, field measurements are usually performed on random surfaces with unknown resistance values. So, practically all the proposed noise data collection arrangements introduce a significant uncertainty in regards to *which area has dominated the measured* R_n.

In this chapter a summary of work associated with asymmetry of electrodes in NOCS arrangement is presented. The main part of the chapter deals with a new arrangement for ENM with the intention to make noise measurement on a single working electrode. The so-called "Single Cell" (SC) arrangement is introduced to provide the capability of measuring noise resistance for immersed objects or inside storage tanks without the need for two isolated working electrodes. Also since only one area (WE) is involved in the measurement, it eliminates the uncertainty introduced by multiple working electrodes. Also efforts have been made to develop a testing protocol for on-site noise measurement.

3.2 Experimental

Sample Preparation

A range of coating systems from low to high protection properties were selected to achieve relatively low, medium and high resistance. The low resistance coating was a maintenance alkyd paint (supplied by Pronto Paint Co., Derbyshire, UK) based on a long oil alkyd resin pigmented with zinc phosphate at thickness of about 90µm on steel Q panel. A single coat epoxy and a two coat epoxy primer/polyurethane topcoat systems (both supplied on Q panel by Liquid Plastics Ltd) at overall thicknesses of 290µm and 320µm respectively, were chosen to represent medium and high resistances. The very high resistance coating was a double coat system consisting of a glass-flake pigmented polyurea topcoat on an iron oxide primer with overall thickness of about 380µm on a garnet blasted steel panel supplied by Akzo-Nobel. These four coating systems were each used as representive of typical coatings with low, medium, high and very high resistances as measured using a high impedance DC instrument (solid state Keithley Electrometer model 610C). They all had at least 3 weeks exposure to 0.5M NaCl in cells attached with silicone adhesive to expose 11.4 cm^2 of the coated metal to the solution.

DC resistance measurement

A solid state Keithley Electrometer model 610C, made by Keithley Instruments, Inc., Cleveland, USA, was used to measure the DC resistance of samples against a SCE in a two electrode arrangement.

AC impedance measurement

AC impedance measurements were performed using an automated CH instrument electrochemical 660D workstation with a SCE as the reference electrode. A standard 3 electrode arrangement was used for EIS measurements using a platinum electrode as auxiliary electrode within ±10 mV around OCP within 10kHz-10mHz range of frequency. All the results presented have been corrected for area (i.e. per cm^2).

Noise data acquisition

The two ZRA/potentiometer electrochemical workstations used for noise measurement were an ACM Gill AC and a CH instrument 660D. The instrumental noise was checked by measuring the noise without samples being connected. Noise signal was collected at 2 Hz sampling rate for 1024 data points unless otherwise mentioned. SCE was used as reference electrode in all experiments. The DC drift in the time domain was removed by "ENANALIZ" programme developed by Prof. R Cottis, School of Materials, The University of Manchester. DC drift is the superimposed DC voltage/current on noise signal generated by instrument, electrode's asymmetry or other sources of over potential. In addition to the noise resistance, R_n, the spectral noise resistance, R_{sn}, was also computed using two mathematical transformation methods to frequency domain, fast fourier transform (FFT) and maximum entropy method (MEM). The R_{sn} at 0.002Hz was taken as the DC limit and was compared to the coating resistance given by other techniques. Spectral noise resistance was also plotted as a function of frequency and compared to the Z(f) given by EIS.

3.3 Asymmetric electrode measurement with NOCS arrangement

As briefly described above (section 3.1.3), NOCS arrangement engages three areas of paint surface for measuring electrochemical potential noise (EPN) and electrochemical current noise (ECN) simultaneously. The noise resistance measured using NOCS arrangement on samples with "known" similar resistances has shown a good agreement between R_n obtained by NOCS and the actual resistance of individual samples [12,32,54]. Accuracy and reproducibility of the ENM measurements made by NOCS configuration is studied [56] (data not presented here) and it has been shown that NOCS arrangement produces satisfactory results, in-line with other well-established electrochemical techniques, when all three engaged paint samples have similar resistances. However, in practice a fairly common situation is a distribution of resistances across the paint surface, e.g. bimodal D and I type resistance inhibition of most paint films. Therefore, in order to extend the NOCS usefulness as a stand-alone assessment technique, it is crucial to determine the influence of individual samples on the R_n when dissimilar resistances are involved.

NOCS arrangement has been extensively studied in the early stages of this work in order to determine the effect of asymmetric electrodes [56]. ENM was performed with NOCS arrangement on three samples where one of the three resistances forming a group in the NOCS measurement differed significantly from the other two. The aim was to find out which electrode dominates the R_n in NOCS arrangement. Some important remarks of this study were that:

- In most cases the noise resistance is, to a large extent, governed by the potential noise rather than by the current flowing between the two working electrodes.

- The RE does not seem to entirely dominate when the cells connected to both WEs are high resistance and the cell connected to the RE is lower. Here R_n takes a value in between the WEs and the RE.

- It was shown that the NOCS arrangement is insensitive to the changes of current noise. Consequently it was suggested that SCE might not be an ideal tool for measuring the current noise between asymmetric electrodes. SCE reference electrode is a non-polarisable

electrode by definition, and produces a very low level of potential noise [57]. However, similar to other noisy reference electrodes, it is not immune against current noise and may evolve high levels of current perturbation when coupled with a noisy electrode (this hypothesis is further investigated in the section 3.4.6 of this chapter). It is suggested that in combination of one low and one high resistance WEs, the SCEs used for data collection adapt to the noisiest signal, thereby reflecting the noise level of the noisier electrode (low resistance). An alternative explanation is that the ZRA connection between a low resistance sample (high level of potential noise) and a high resistance sample (low level of potential noise) results in one low resistance sample that in overall exhibits high level of potential noise. Therefore the potential of the low resistance sample dominates the potential noise and to a large extent the resultant R_n.

- Maximum entropy method (MEM) was compared with fast Fourier transformation (FFT) for production of PSD plots. It was shown that MEM produces smoother plots which are easier to analyse and compare with Bode plots from EIS measurement.

The work was continued by Mills, Jamali and Tobiszewski [58] to further investigate the reproducibility and the frequency dependence of R_n when measured by NOCS arrangement. The R_{sn}(f=0.1Hz) was found in good agreement with |Z| at f=0.1Hz from the Bode plot which suggests a reasonable frequency dependence of the ENM. In most cases the R_{sn} did not change much in the frequency range 0.1Hz to f_{min} which can be attributed to the dominance of resistive behaviour rather than a capacitive behaviour in this range of frequency. It was also shown that NOCS arrangement may result in erroneous R_n when used on very low resistance coatings, e.g. R≈4E+4 $\Omega.cm^2$. It was also shown that in an asymmetric configuration with one low resistance sample and two high resistance samples, the effect of the low resistance sample is more pronounced when connected to either of the WEs rather than when it is connected to the RE. This is consistent with the second hypothesis advanced earlier to explain the insensitivity of NOCS arrangement to the one "good" WE when the other has low resistance.

In a more recent work by Mularczyk, Mills and Picton [59] NOCS was utilized to identify the "odd" electrode among the three, when the other two had similar resistance. An asymmetry within the ZRA/potentiometer was found advantageous for measuring individual resistances of electrodes by exchanging samples between WE1, WE2 and RE. The

asymmetry within ZRA/potentiometer was also proposed in the previous study [58] as a possible mean of differentiation between non-identical electrodes.

As a conclusion to all the above studies in regards to the NOCS arrangement, special care must be taken when measuring unknown resistances in practice. Repeating the ENM by exchanging samples between the WEs and RE seems a necessity in order to distinguish the level of performance of each electrode.

3.4 Measuring electrochemical noise resistance on a single electrode

3.4.1 The Single Cell arrangement and data acquisition

The SC set-up suggested here comprises one working electrode and a noiseless reference electrode as shown in Figure 3.7. Unlike previous experimental procedures, the electrochemical current noise (ECN) and electrochemical potential noise (EPN) are not (and cannot be) measured simultaneously, so it is essential to be sure that the corroding sample remains in an unchanged condition throughout the time of experiment. Since the noise data collection is relatively quick (e.g. 512 data point at 2 Hz takes about 4 min) and the process of data collection imposes no external stimulus this is a reasonable assumption. In most cases under field conditions the coated structure was well equilibrated by the time the measurements are made.

The EPN was carried out by recording the sample potential against a SCE. This was performed (similar to a conventional three-electrode ENM) under open-circuit conditions where now only the electrochemical potential noise is measured. Then the SCE was attached to the auxiliary electrode as well as the RE and ECN was performed by holding the sample at its mean free corrosion potential under potentiostatic control. ECN cannot be made directly using a ZRA due to the potential difference between the substrate and the SCE that would generate a DC current flow. Accordingly the substrate potential was determined as the mean value of electrochemical potential noise data set. This was then implemented electronically by the potentiostatic technique, with the SCE serving as both

reference and auxiliary electrodes. This is permissible for high resistance coatings where the current is too small to perturb the reference electrode. A separate auxiliary electrode can be added where necessary. The ECN was carried out by taking 512 current measurements at 2 Hz at the free corrosion potential.

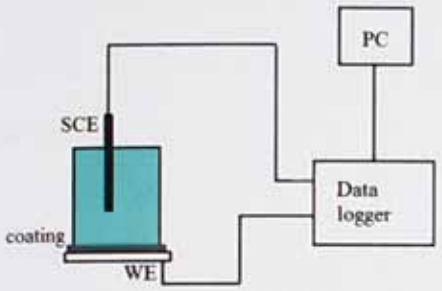

Figure 3.7 Single cell (SC) electrochemical noise arrangement [60].

The concept of sequential measurement of electrochemical potential noise and electrochemical current noise may also be applied to a two working electrode arrangement without electrical connection to substrate. Similar to NOCS arrangement (Figure 3.6), EPN may be measured between two SCEs in electrolytic contact with areas of interest. Subsequently, current noise can be measured between the same two electrodes. One advantage of this could be the less ambiguous result due to using fewer numbers of cells. It should be noted that the previous ENM arrangements have all used more than one working electrode which leaves an uncertainty with *which electrode dominates the result*. The first intention of this new arrangement is to obtain noise data from a single working electrode. However same concept is applicable to two working electrodes configuration when no electrical connection to substrate can be made.

3.4.2 Validity of R_n measured by SC arrangement

The accuracy and validity of the method was examined by comparing the R_n obtained by SC arrangement with the AC impedance at 0.01 Hz and the DC resistance all taken at the same time. Figure 3.8 reveals a very good agreement between $R_{n(SC)}$, $|Z|_{0.01Hz}$ and R_{DC} values across the whole range of coating resistances. It is clear that for the purpose of monitoring the coating performance this new method agrees with the others within normal tolerances.

S.C. arrangement is capable of differentiating the coatings with different levels of protective properties, i.e. low, fair, good and excellent, which is associated with their level of ionic resistance. The coatings used for this study were quoted earlier in section 3.2. It should be noted that some differences could originate from difference in the electrochemical signals used for measurements. The external potential applied to the sample in DC measurement and sinusoidal potential perturbation applied in EIS measurement may alter the mechanism of ionic conduction inside the polymer film which results in slightly different resistance values.

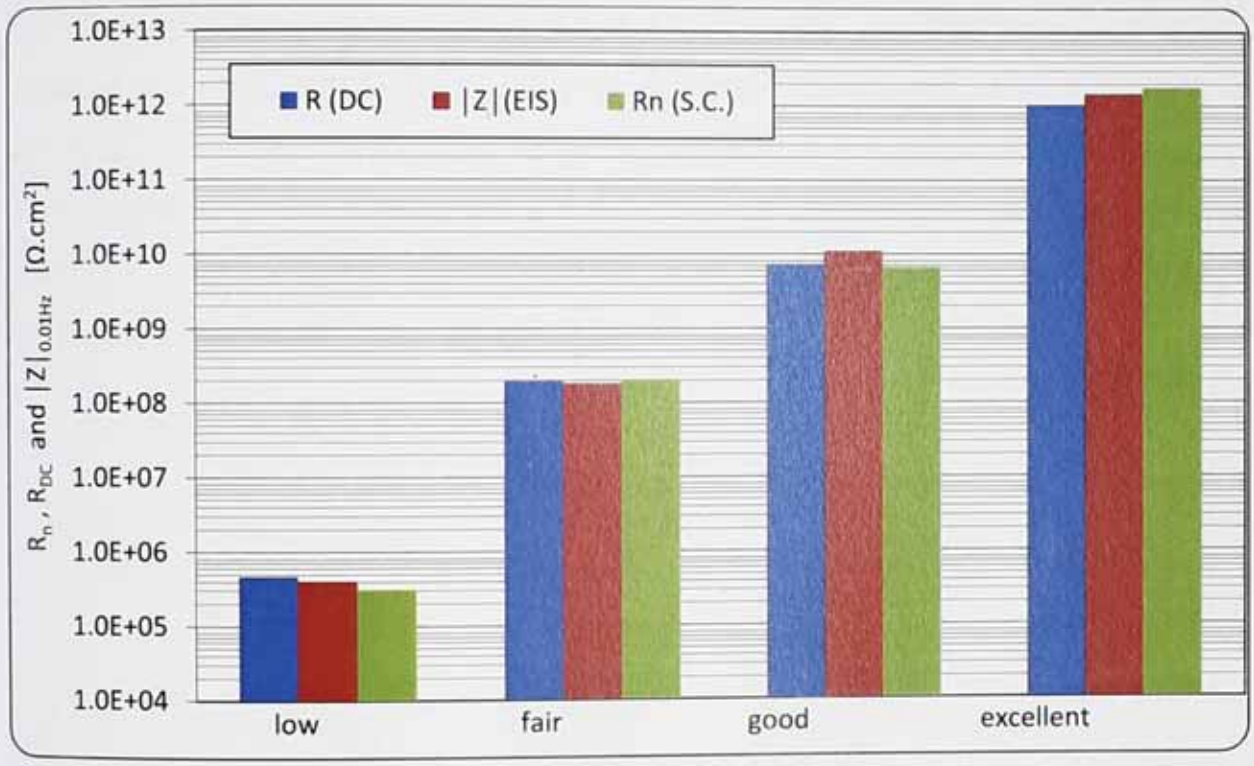

Figure 3.8 Comparison between values obtained from DC measurement, EIS and ENM (S.C. arrangement) for a range of coating protection abilities from poor to very high.

3.4.3 Examining the reproducibility of SC on similar coatings

Assessing the performance of a paint coating in practice involves testing different areas of the paint to obtain an average value of protection properties. Therefore, it is crucial for an electrochemical method to reliably and reproducibly examine different areas of the paint with slightly different properties and obtain results within an acceptable tolerance. Here SC arrangement is used to examine three different areas of coated steel with an alkyd paint

with 80±5 µm thickness. EPN and ECN were independently performed using SCE at 2 Hz sampling rate to collect 2048 data sets. DC resistance and AC impedance were also used as complementary tests of accuracy. Figure 3.9 compares the resistance values acquired by the three techniques for each cell. None of the techniques ranks the coatings similar to one another. This could be due to the experimental error or different nature of each test. For instance DC method only measures the resistance of coating against ionic transport provoked by an external DC potential while ENM also considers the passivation state and stability of potential underneath the paint. Consequently under-film passivation, e.g. at the cathodic sites, may have a significant influence on the resistance measured by ENM while it may be ignored by the DC resistance. Table 3.1 shows the statistical analysis of results obtained by three measurements using each method. Coefficient of variation (Cv) is calculated by dividing the standard deviation by mean value as a normalized measure of dispersion. By definition Distributions with CV < 1 are considered low-variance, while those with CV > 1 are considered high-variance. All three methods show low variance in their ability to examine similar paint coatings.

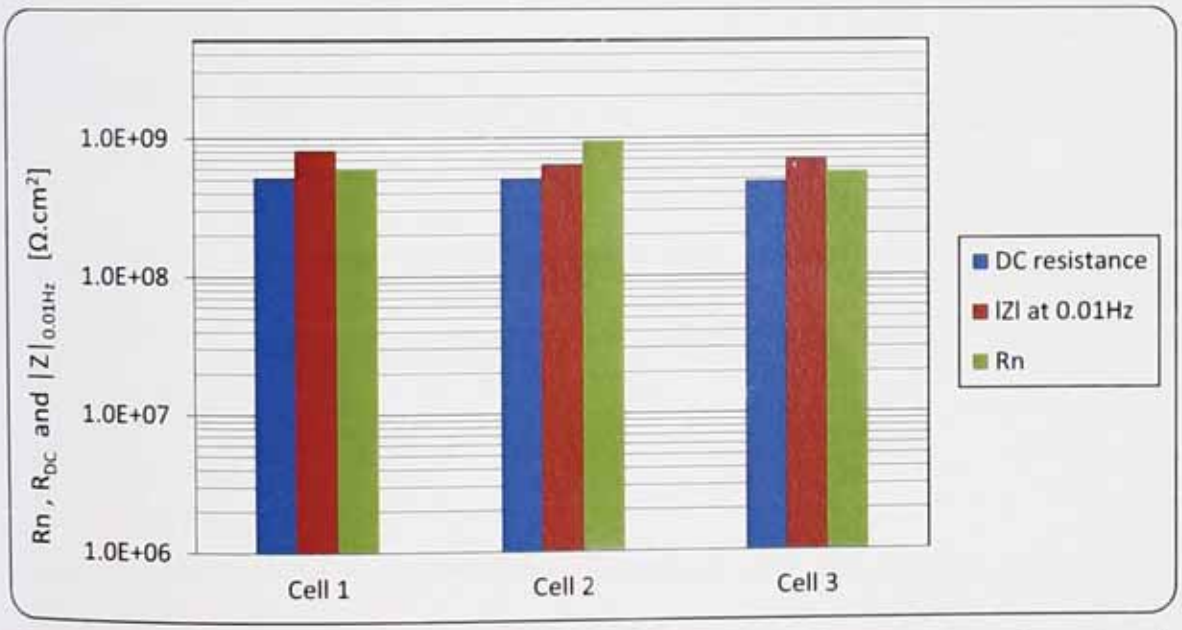

Figure 3.9 Reproducibility of SC arrangement for testing different areas of a painted metal with relatively close resistances.

Table 3.1 Statistical analysis of reproducibility and comparison between DC measurement, AC impedance and ENM with SC arrangement based on three measurements on an alkyd coating.

	Cell 1	Cell 2	Cell 3	ST. DeV	mean	Cv
DC resistance	5.20E+08	5.10E+08	4.80E+08	2.08E+07	5.03E+08	0.04
$\|Z\|$ at $_{0.01Hz}$	8.15E+08	6.40E+08	6.97E+08	8.93E+07	7.17E+08	0.12
R_n	5.90E+08	9.41E+08	5.60E+08	2.12E+08	6.97E+08	0.30

Figures 3.10, 3.11, and 3.12 provide further information on the conformance of the EIS and R_{sn} in the frequency domain as well as DC method and R_n. Reasonable coherence between EIS and R_{sn}, within the overlapped area, indicates the promising potential of ENM by SC arrangement as an alternative to EIS for practical assessments of a single area of interest in the field.

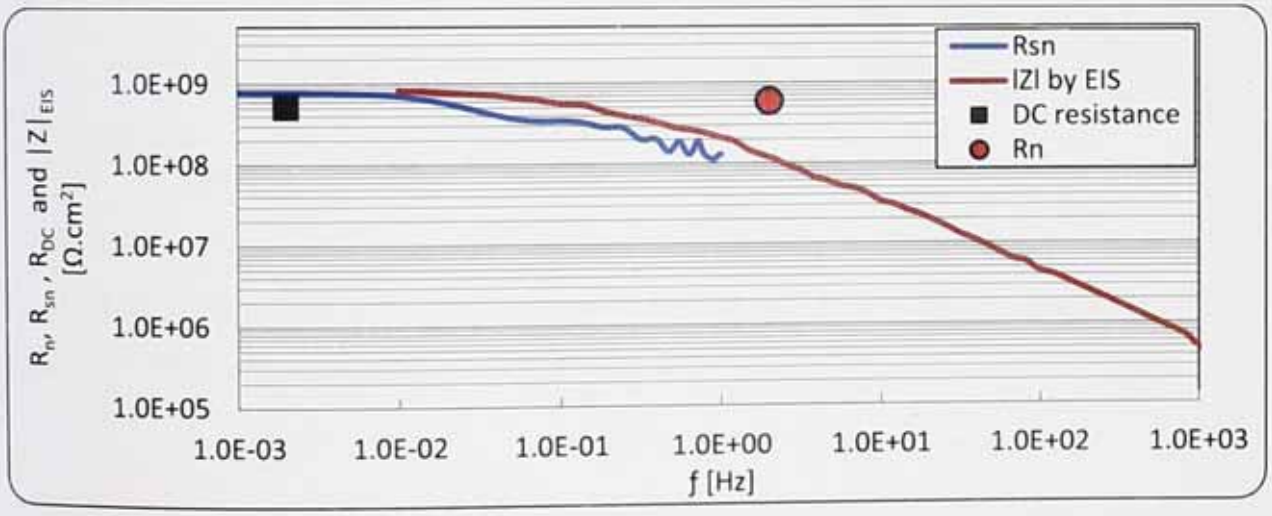

Figure 3.10 Comparison between different methods and data analysis approaches for an alkyd paint film with moderate resistance sample 1.

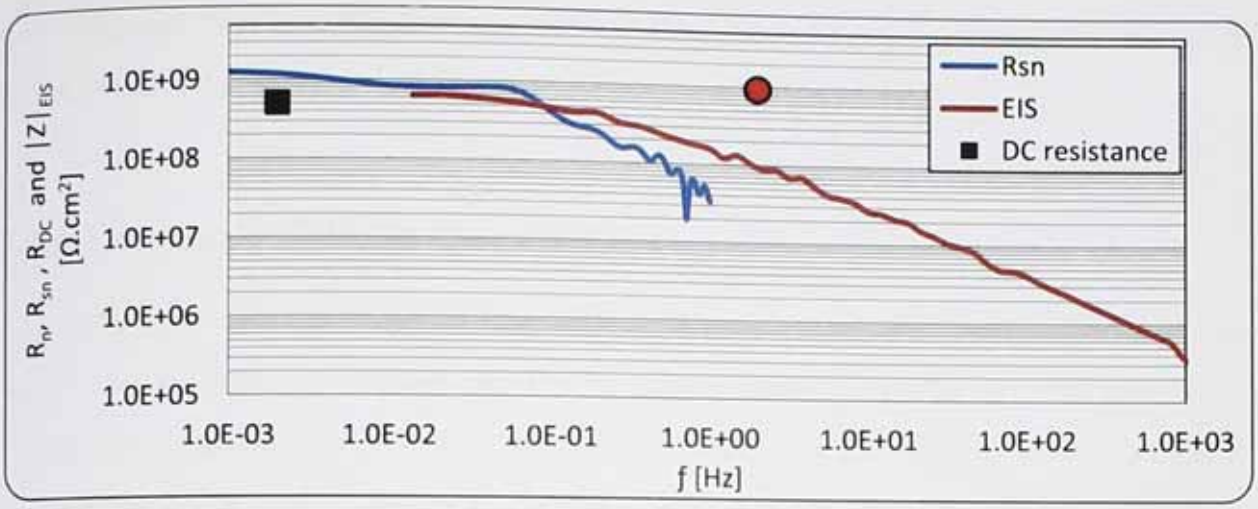

Figure 3.11 Comparison between different methods and data analysis approaches for an alkyd paint film with moderate resistance sample 2.

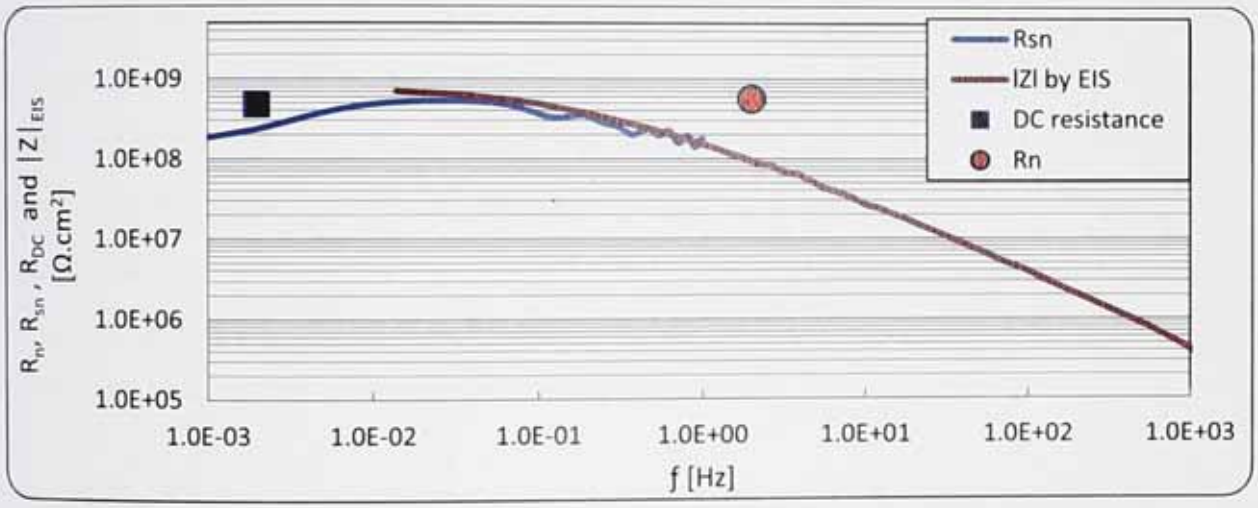

Figure 3.12 Comparison between different methods and data analysis approaches for an alkyd paint film with moderate resistance sample 3.

It should be remembered that the $|Z|_{fmin}$ parameter from EIS may include the impedance of two or more individual electrochemical processes that are distinguishable as separate semi-circles in a Nyquist plot. However, R_n typically represents the sum of the coating resistance and the charge transfer resistance. As it happens in these particular samples no evidence of two time constants was apparent from the Bode plots. The overall conformance of the R_n with $R_{sn}(f_{min})$ implies the resistive behaviour (frequency independent) of coating rather than capacitive behaviour over the frequency at which the noise resistance

was measured. This may suggest that, in most cases, ions have penetrated into the paint film at the time of measurement and the system was in a steady state.

3.4.4 Frequency domain data analysis

A 2048 point data set acquired from independent ECN and EPN measurements of the "good" coating were transferred into the frequency domain and PSD of noise resistance ($R_{SN}(f)$) was produced. The Bode plot from the AC impedance experiments is superimposed on the same graph to compare the $R_{SN}(f)$ to the $|Z(f)|$ plot obtained from EIS and check how closely the Bode plot can be reproduced mathematically from a single cell noise measurement. Although the value from the noise method falls off at the lowest range of frequencies, Figure 3.13 reveals close agreement between $R_{SN}(f)$ and $|Z(f)|$ plots. This observation has an important implication which is that it indicates the possibility of using noise measurement technique to monitor corrosion behaviour in a single cell and get the same result as one would get using the more complicated and time-consuming AC impedance technique. The similar slopes of PSD plots of current and potential (Figure 3.14) indicate that R_n is a frequency independent measure of the corroding system [36,61]. This is also confirmed by equality of R_n and R_{sn} that implies the resistive behaviour of the paint film rather than a capacitive behaviour (frequency dependant).

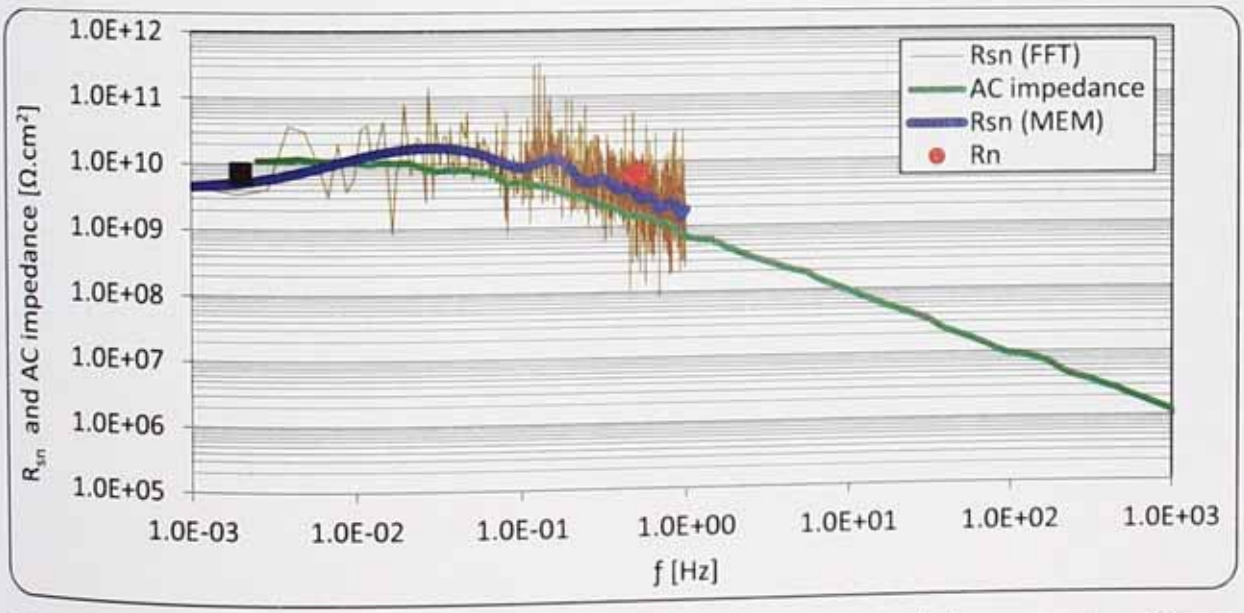

Figure 3.13 Comparison between different methods and data analysis approaches for an alkyd varnish film with relatively high resistance.

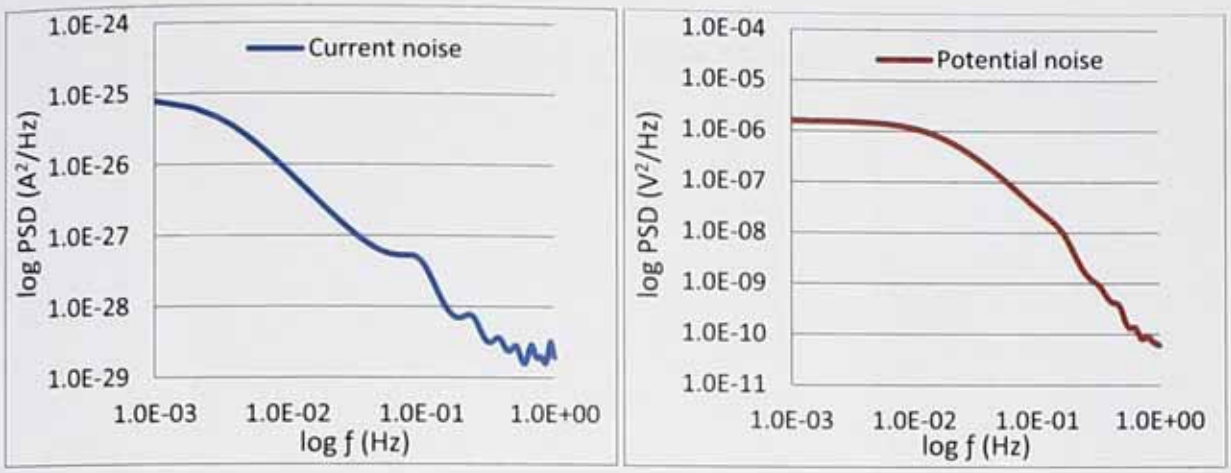

Figure 3.14 PSD plots of current (left) and potential (right) data obtained by MEM for an alkyd varnish film with relatively high resistance.

3.4.5 Noise data repeatability/consistency

Since the EPN and ECN data collections are not simultaneous it is crucial to ensure that corroding system has reached an acceptable steady state. To assess this the set of the 2048 noise data points, used for the frequency domain data analysis, was divided into 8 separate groups of 256 data "sets" and the Rn was calculated for each set individually. Figure 3.15 compares the Rn computed for 2048 data points (the whole set) to the Rn calculated for smaller sets of data extracted from the whole range. Although the shorter data sets imply a cut-off at a slightly higher (e.g. in this case 8x) low frequency limit, good agreement between the overall Rn and the Rn of each sub-group without any significant trend shows that system is in steady state and noise resistance does not change significantly over time.

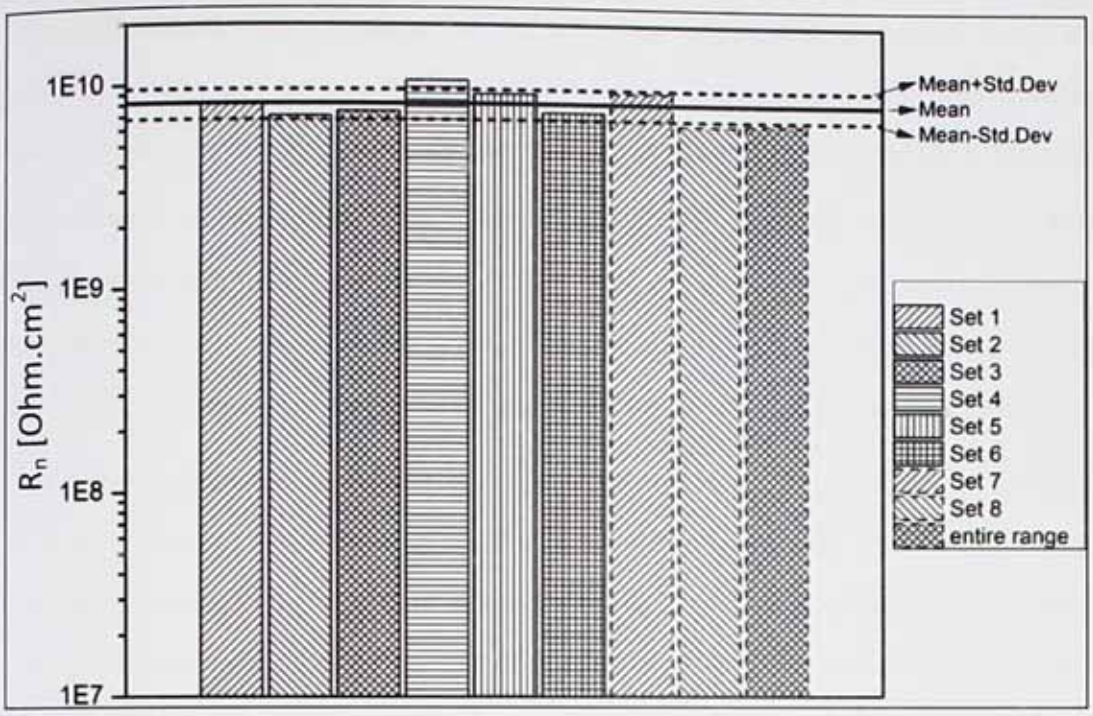

Figure 3.15 R_n values showing Repeatability of 2048 point data set when divided into eight sequential sections.

R_n values of 6 sets of data are within 1xσ (standard deviation) around the mean value which shows a normal distribution of data. This method may be considered an efficient way to assess the state of corroding cell in the laboratory. In a practical situation on site, several measurements may also be made and compare the Rn to ensure that steady state has been reached.

3.4.6 Role of the reference electrode

When a reference electrode is being used in noise measurements, a minimal contribution of RE in the noise signal is desirable. The Ag/AgCl reference is well known to be light sensitive and may generate reasonable level of noise, thus it is suggested that is be avoided for electrochemical noise measurement [61]. It should be noted that, similar to single substrate [49] and NOCS [53] arrangements, the contribution of RE in the current noise signal is as important as potential noise when the single cell arrangement is used. This is unlike the traditional salt-bridge arrangements where RE is only involved in measuring the noise potential. Cottis and Turgoose [24] explain that high resistance electrode confines the current passing through the circuit, therefore the electrode with higher resistance will

dominate the current noise within an asymmetric couple. In simple terms the reference electrode noise will be applied across the cell by the action of the potentiometer. This will cause a current to flow through the cell. Consequently the reference electrode potential noise power will generate a current power given by $\overline{E_{n,ref}^2}/Z_s^2$, where $\overline{E_{n,ref}^2}$ is the potential noise power of the reference electrode (defined as variance of noise signal) and Z_s is the impedance of the cell generating the current noise [57]. Therefore a larger impedance of the corroding sample will reduce the influence of the RE on the current noise signal.

Concerning the noise potential, as little as possible standard deviation of RE is desirable so that the measured potential noise signal reflects only the sample perturbation. Figures 3.6 and 3.17 show the standard deviation of current and potential noise generated by SCE, Ag/AgCl reference electrodes and the samples used for this study. The relatively large current noise generated by SCE is very close to the noise generated by low resistant painted sample. This reveals the practical limit of the SCE used for this study and suggests that the use of SCE for measuring the electrochemical current noise of very low resistance, e.g. R<1E+5 $\Omega.cm^2$, and highly noisy samples should be avoided. In practice, in the case of high impedance, less noisy, electrodes the noisiness of current will be confined with the barrier effect of coating thus SCE will have minimal influence on the measured current noise. Further studies on other REs, such as $Cu/CuSO_4$, may be undertaken to find a better RE which does not impede the current noise generated by the very low resistance specimen. Figure 3.23 indicates 7 to 10 orders of magnitude lower potential noise generated by SCE compared to painted samples. It also shows the relatively noisy characteristic of Ag/AgCl reference electrode which explains why Ag/AgCl REs are not recommended for electrochemical noise measurement.

Figure 3.16 Standard deviation of the current noise generated by SCE and Ag/AgCl reference electrode and painted samples.

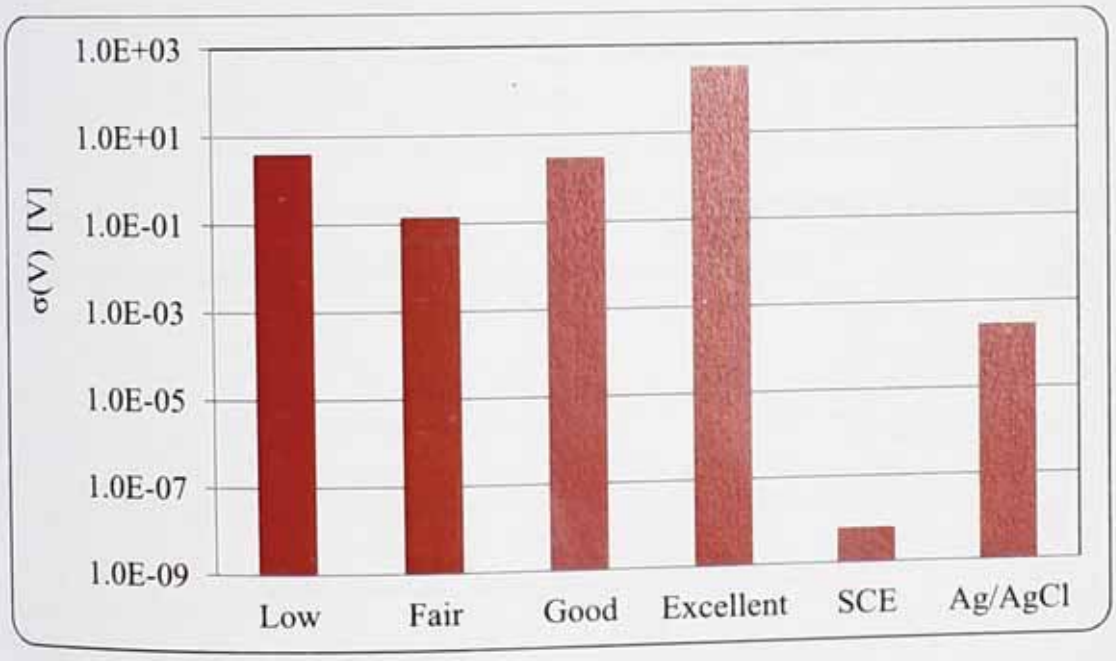

Figure 3.17 Standard deviation of the potential noise generated by SCE and Ag/AgCl reference electrode and painted samples.

Instrumental noise was also checked by measuring the electrical current noise and potential simultaneously without any electrochemical noise source being connected. The standard deviation of the instrumental noise was measured 1.09E-11 for the current noise

and zero for the noise potential. The actual current and potential noise data are shown in Figures 3.18 and 3.19 respectively. No evidence of systematic noise was observed which indicates acceptable filtering of the systematic noise generated by power source. Therefore the current noise cannot be interfered by the instrument and/or the computer. It should be noted that the electrical current noise also indicates the limitation of instrument in measuring electrochemical noise of the extremely low currents.

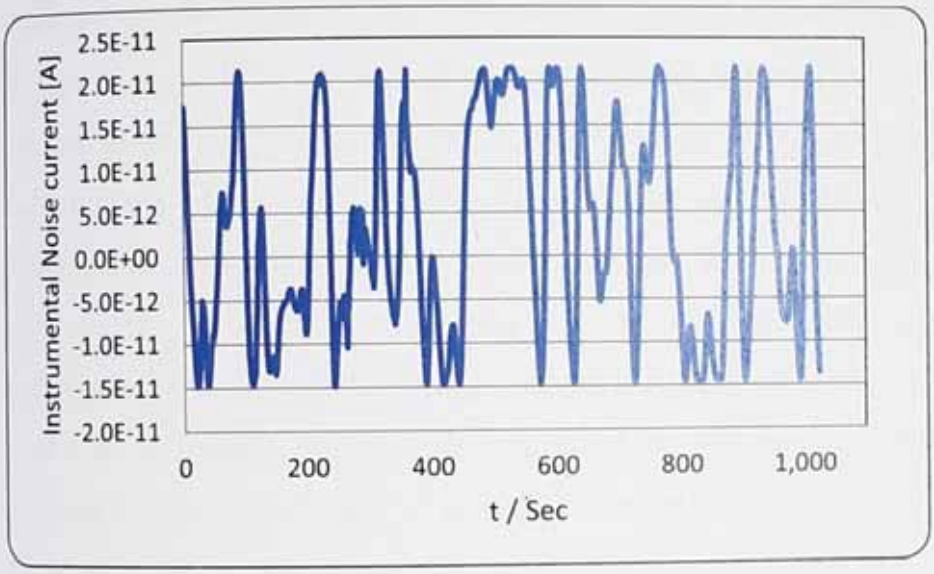

Figure 3.18 Instrumental current noise of the CH instruments Potentiostat/Galvanostat model 660D measured in an open circuit without electrodes.

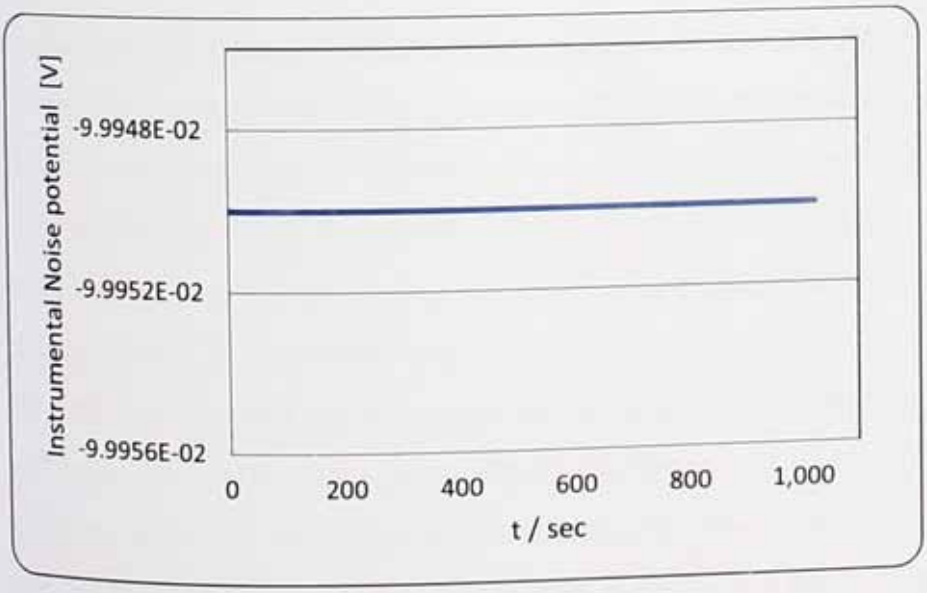

Figure 3.19 Instrumental potential noise of the CH instruments Potentiostat/Galvanostat model 660D measured in an open circuit without electrodes.

Use of a noisy reference electrode was investigated and compared to standard noiseless RE set up in a 3 or 4 electrode configurations by Bertocci *et al.* [62–65] both theoretically and experimentally. Their model revealed the necessity of symmetry between RE and WEs when a noisy RE was used in order to avoid systematic error. The experimental work was performed on bare metal where the impedance values are necessarily much lower than coated substrates and the current flow is not impeded by a barrier coating. It was also assumed that the corrosion process takes place under the activation control which is highly unlikely in the case of polymer coated metal. It was shown that the validity of R_{sn} depends on the assumption that both working electrodes have the same impedance and that the corrosion process takes place under the activation control. However, the assumption about the identical impedance of both test electrodes is hard to fulfil in practice. Cottis has discussed the possibility of the use of a Pt probe as an asymmetric second working electrode for measuring R_n on bare corroding metal and considered it impractical [66]. It was shown that a small (thereby high resistance) Pt probe will dominate the current noise flowing through the ZRA while a large Pt probe will render the working electrode a large anode thus largely affecting the potential noise. This makes the accurate and independent measurement of both elements of noise, the current and the potential, impossible. The importance of electrode symmetry when measuring electrochemical noise on bare metal has been also shown elsewhere [67].

Bautista and Huet [68] discussed the theoretical aspects of ENM on asymmetric coated electrodes when one has higher impedance than the other. It was shown that the current tends to be dominated by the electrode with higher impedance while the other electrode controls the potential fluctuation. Mansfeld *et al.* [69] studied noise measurement on asymmetric electrodes consisting of a highly protective coating and a defective coating by the salt bridge arrangement. They observed slightly lower $\sigma(V)$ and significantly higher $\sigma(I)$ on defective coatings when coupled together. On the other hand, R_n measured for one defective and one undamaged coatings was almost identical to that of two undamaged coatings. They concluded that R_n is dominated by the current flow which is hindered when one electrode is a good barrier and renders the defective coating insignificant. They made a suggestion as a future work about the usefulness of measuring current noise data for one

polymer coated electrode coupled with bare metal of the same type or a small Pt wire by a ZRA as a measure of its performance. In the SC arrangement, introduced here, it is believed that the high impedance of the coating governs the current noise (similar to that of proposed by Bautista and Huet [68], Mansfeld *et al.* [69] and Cottis [66]) while the non-noisy SCE does not contribute to the potential noise leading to a relatively independent noise signal mainly reflecting characteristics of the sole working electrode. This brings about the possibility of accurate measurement of current and potential noise and a valid calculation of R_n in reasonable agreement with other electrochemical techniques (e.g. EIS, DC).

Also as a final remark on the S.C. arrangement, it should be noted that although the potential drifts over time in open circuit, using potentiostatic current noise measurements results in an extremely small superimposed DC current (typically 1-2 pA for the high-performance coating). This is a result of superimposed potential in the second step of measurement when measuring the noise current. The DC current drifts over time, but as suggested earlier by good agreement between S.C. results and other methods, i.e. DC and EIS, this does not appear to affect the R_n measurement significantly if data is treated appropriately and DC trend is removed from the raw noise data. This is also evident from the good repeatability of the noise data using S.C arrangement.

3.5 Practical electrodes and measurement criteria for on-site applications

3.5.1 Practical reference electrodes for on-site use

The noise level of Pt, Cu and printed Carbon (C) electrodes was investigated. The aim was to select the best practical electrode as Reference electrode in SS, SC or NOCS configurations for on-site measurements. It is very important that the RE contributes as little as possible to the measured noise signal. SCE is generally accepted as a reference electrode with negligible level of potential noise and hence the three other pseudo references were compared against that SCE to measure the potential noise. Current noise was measured directly between two identical Pt, Cu, C electrodes. Each of the above electrodes was immersed as nominally identical pairs in a glass beaker containing 0.5M NaCl solution and the current noise was measured. The Figure 3.20 shows the actual set-up for measuring the potential noise and current. The factor of noisiness has been calculated for the above electrodes as a criterion of their effectiveness as reference electrodes for noise measurement. Coefficient of variation, the standard deviation divided by the mean, was calculated as a measure of the noisiness of the signal [24]. The factor of noisiness for current noise and potential noise is plotted in Figures 3.21a and 3.21b respectively. The noise level of Pt, Cu and C electrodes (for both current and potential) is in the order of C > Cu > Pt indicating that Pt is the most *practically* stable RE while the C is the least stable.

Figure 3.20 Experimental set-up for measuring electrochemical noise produced by Cu and C electrodes.

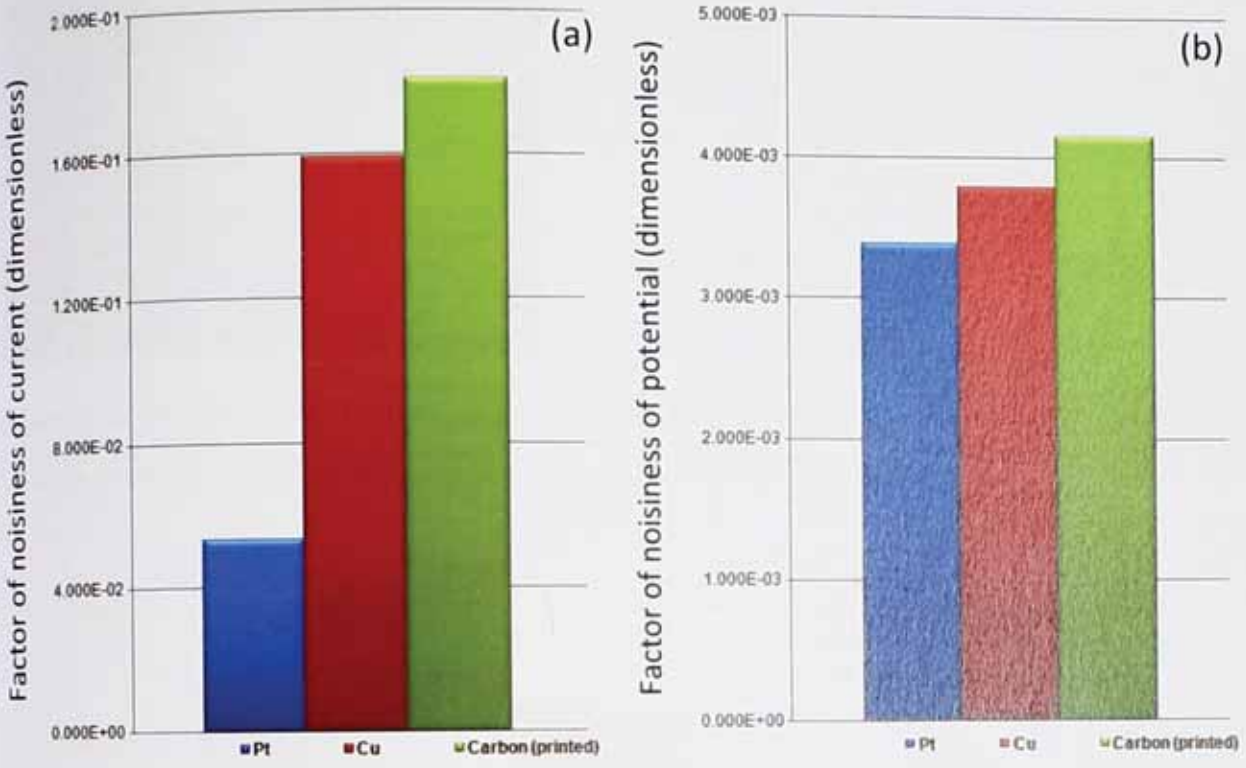

Figure 3.21 Noisiness of current (a) and potential (b) generated by two nominally identical Pt, Cu and C electrodes.

3.5.2 Actual measurements with Pt, Cu and carbon reference electrodes

Pt, Cu and C electrodes were used in a SC arrangement to reveal which electrode can more accurately be used for electrochemical noise measurement. In order to provide electrolytic connection between the electrode and coated panel, a conductive pad was made by cutting a filter paper into 3×3 cm pieces and soaking in 0.5 M NaCl [70]. Figure 3.22 shows the actual experimental set-up for noise data collection. The DC resistance value has been used as the validity criterion. The result presented in Figure 3.23 confirms that Pt is the more accurate electrode for electrochemical noise measurement with the least deviation from DC value compared to Cu and C. However all of the electrodes have shown an acceptable performance and can be used for ENM in the field.

Figure 3.22 Experimental set-up for electrochemical noise measurement with Single Cell arrangement using Carbon, Cupper and Platinum as reference electrode.

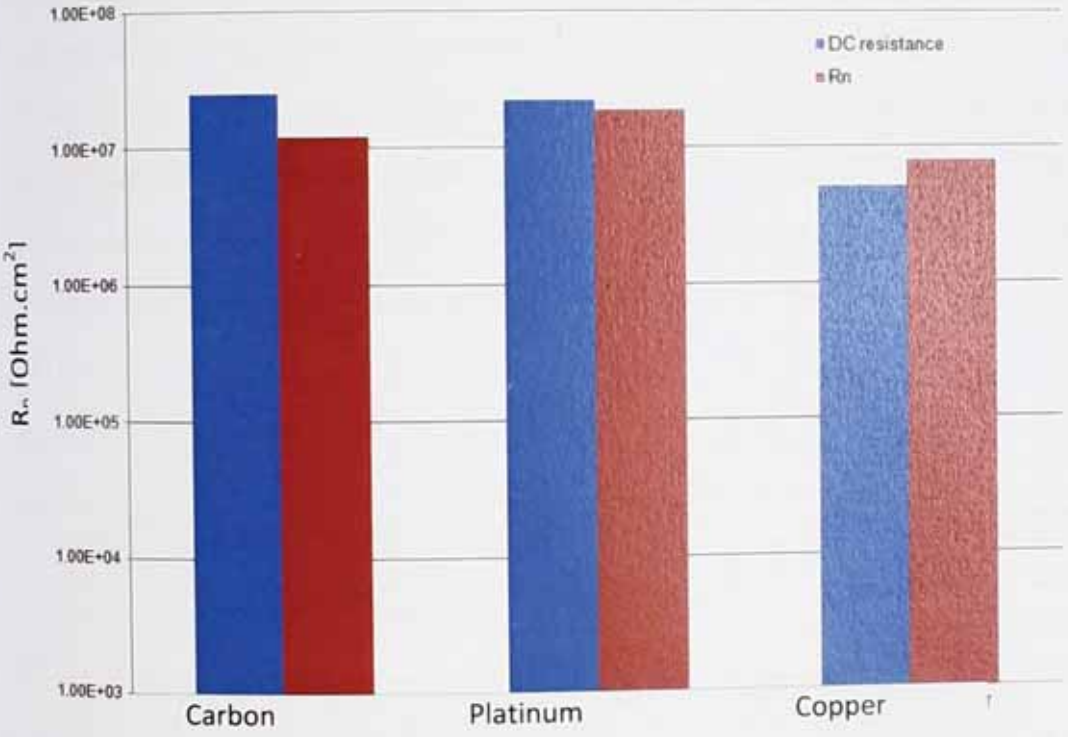

Figure 3.23 Validity of the noise resistance measured by carbon, Pt and Cu electrodes in single cell arrangement.

3.5.3 Sampling rate

In order to investigate the effect of sampling rate and number of data points on the accuracy of R_n, the noise data was collected at 1 Hz, 2 Hz and 10 Hz with 512 data points being recorded. The time needed for data collection was 8.5 min, 4.3 min and 51 sec respectively. Also the noise at 10 Hz was measured with 215 data points in a fairly quick, 25

Sec, measurement. All of the noise measurements were performed with single substrate (SS) arrangement. The DC resistance and AC impedance were also measured. These values were compared with the noise resistance to define at which sampling rate the R_n is still reliable and gives a consistent result. A range of coating resistances were studied in contact with 0.5M NaCl solution. All of the measurements were repeated twice to make sure that the result was reproducible and the average of two measurements is reported. Figures 3.24, 3.25, and 3.26 show the effect of signal sampling rate on the R_n compared to $|Z|_{0.01Hz}$ and DC resistance for low, medium and high resistant coatings respectively. Figure 3.30 reveals that the noise measurement on relatively low resistance coatings ($<10^8 \Omega.cm^2$) is quite sensitive to sampling rate and gives higher values at high frequencies. Thereby it is suggested that making noise measurement at frequencies higher than 2 Hz is avoided. It appears that using shorter times and higher frequencies tend to generally overestimate the low resistances. It has been also suggested that at high frequency noise sampling, other sources of noise, e.g. instrumentation and electronic devices, become significant and therefore data collection at high frequencies should be avoided [27]. The poor correlation of R_n and DC results with EIS is attributed to the instrument limitation and the need for EIS scan at lower frequencies, e.g. 0.001 Hz.

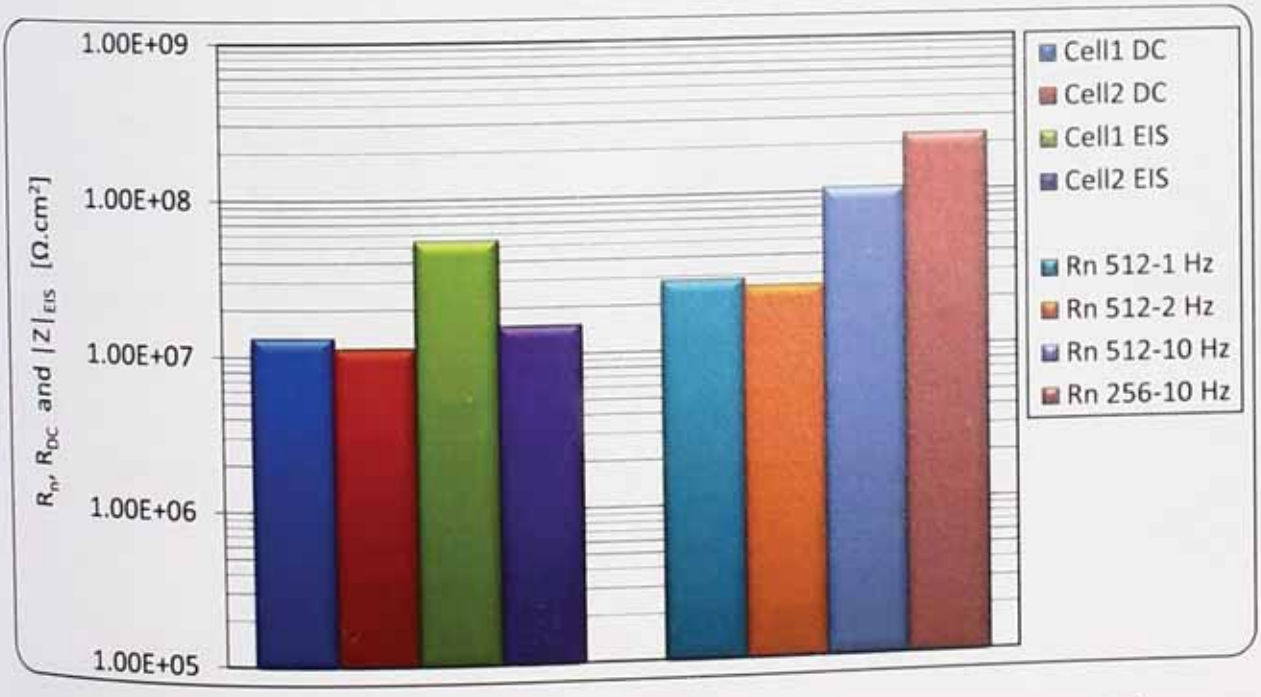

Figure 3.24 Influence of sampling rate on $R_{n(SS)}$ examined by DC resistance and $|Z|_{0.01Hz}$ on identical working electrodes with relatively low resistances (~1×10^7 $\Omega.cm^2$).

Figure 3.25 Influence of sampling rate on $R_{n(SS)}$ examined by DC resistance and $|Z|_{0.01Hz}$ on identical working electrodes with medium resistances (~2.5×10^8 $\Omega.cm^2$).

Figure 3.26 Influence of sampling rate on $R_{n(SS)}$ examined by DC resistance and $|Z|_{0.01Hz}$ on identical working electrodes with relatively high resistances (~1×10^{11} $\Omega.cm^2$).

3.5.4 Equilibrium time required to reach a steady state for ENM on thick/high resistance coatings

In order to study the effect of coating thickness and high resistances on the minimum time required for coating to be in contact with solution, electrochemical noise measurement has been performed on three different thicknesses of coating within 5-10 min intervals. 100 µm Epoxy primer, 300 µm Polyurea topcoat and 800 µm Epoxy primer were exposed to 0.5 M NaCl solution and electrochemical noise data was collected using single substrate set-up with 2 Hz sampling rate and 512 data points. As it is shown in the Figure 3.27, the first two systems (100 µm Epoxy, 300 µm Polyurea) have gained a consistent Noise value after about 20 min contact with electrolyte. The gradual drop of Rn after 20 min is connected with the natural process of corrosion and opening up of micro-pores within the coating.

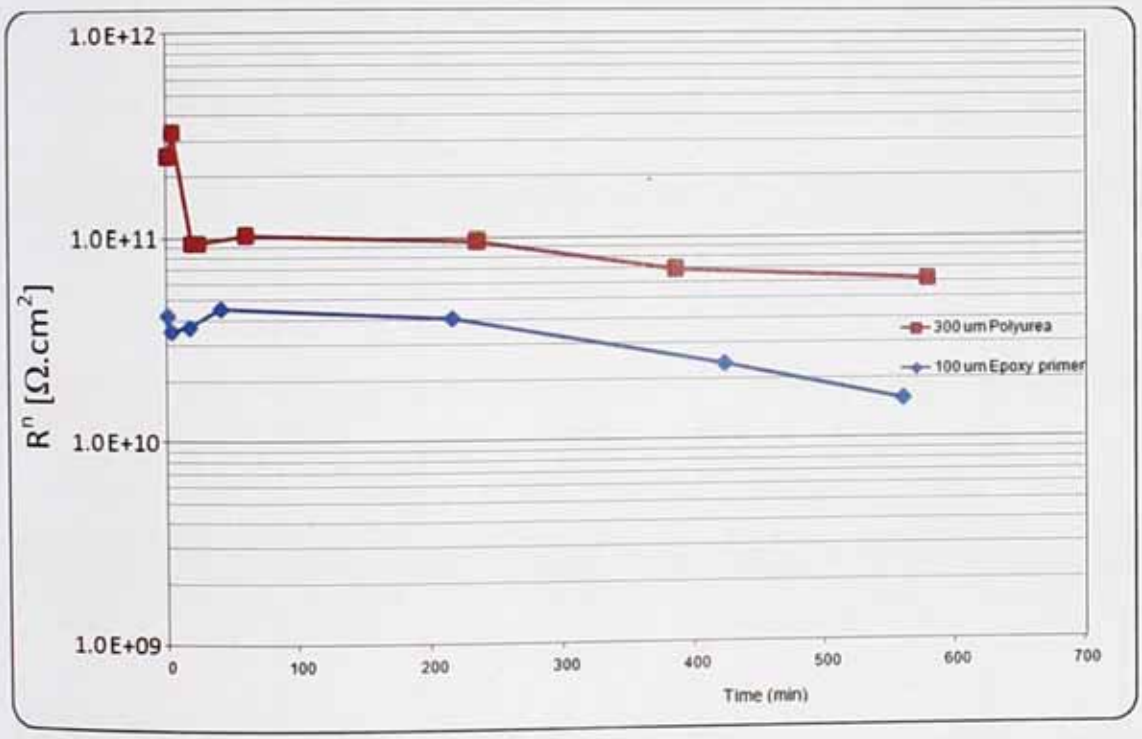

Figure 3.27 R_n value as a function of time of contact with 0.5 M NaCl solution for a typical corrosion resistance epoxy paint coating (with 100µm thickness) and a polyurea coating (with 300µm thickness).

Unlike the first two paint systems shown in Figure 3.27, no "meaningful" potential noise signal could be detected on the 800 µm Epoxy primer system (Figure 3.28) before 10 hrs contact with electrolyte. It must be noted that all above coatings were fresh and dry prior to the experiment. In the case of noise measurement on the organic coatings which have been

under service condition for a while, the electrochemical system is anticipated to be already stabilized and the electrochemical noise can be measured more quickly. However, for dry and non-degraded paint film a relationship between the resistance of the paint, Rn, and equilibrium time seem to exist as suggested previously by Mills *et al.* [70]. It was suggested to leave the sample for 30-45 min to reach the equilibrium state. However, for very high thickness coating, e.g. 800 µm epoxy system, the results obtained here suggest a longer time is required. For high resistance thick coating systems, repetitive ENM is recommended until similar results are obtained to indicate the system has reached equilibrium.

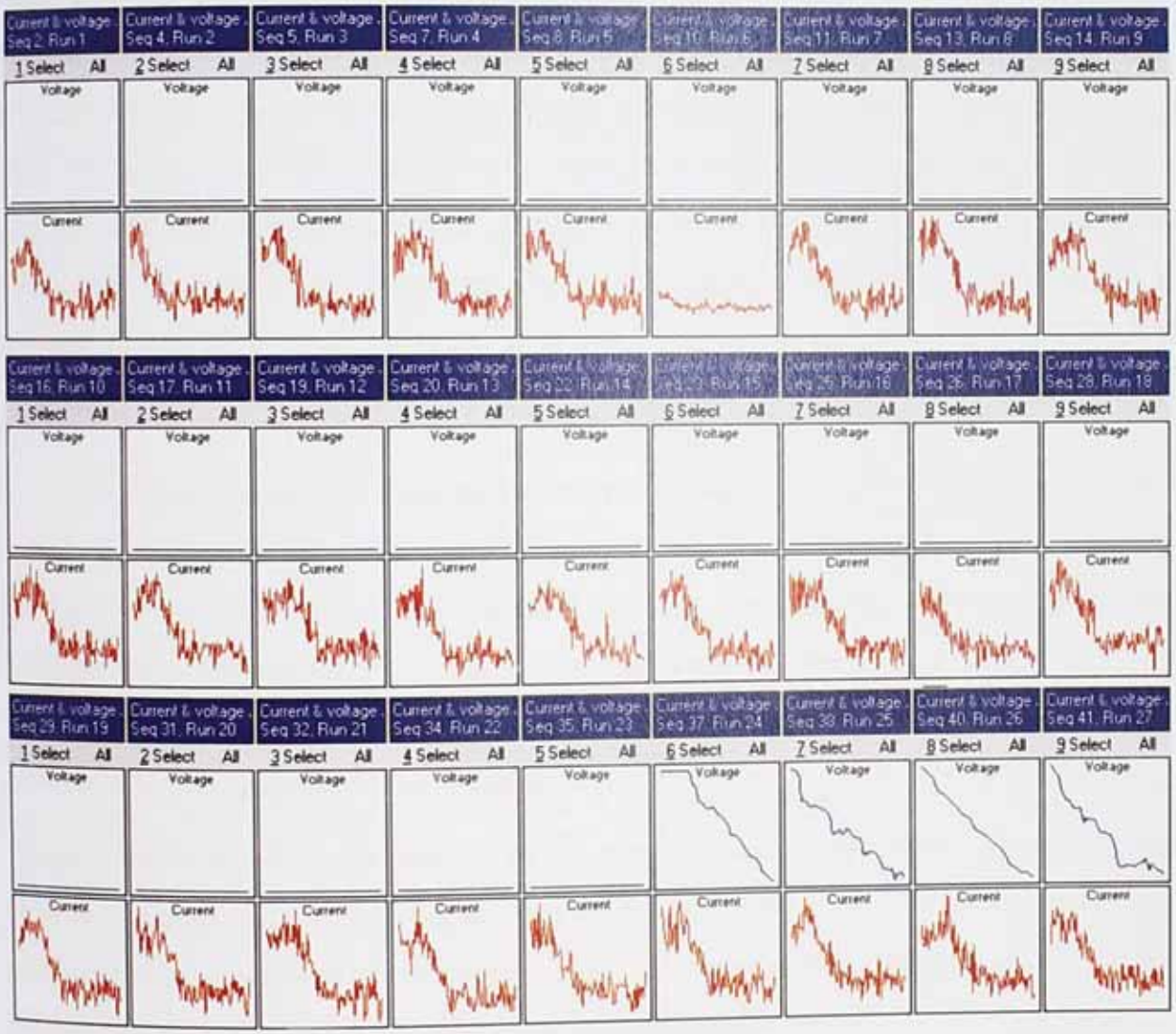

Figure 3.28 Sequential ENM with 24 min interval between each two measurement on 800 µm Epoxy primer system after contact with 0.5 M NaCl solution.

3.6 Summary

A new arrangement, single cell (SC), for electrochemical noise data collection has been proposed and utilized to examine the protective properties of a set of organic coatings. The reliability of the method was checked with complementary DC and EIS measurements. The noise resistance (R_n) calculated with single cell arrangement was in line with the impedance |Z| measured by EIS at 0.01Hz and with the DC resistance. Repeatability of the measurement was examined by dividing a large set of data into several small data sets. Noise resistance was measured for each group separately and compared to the overall noise resistance. Good agreement was observed between the R_n from each segment and the overall R_n. Further verification was given by transferring time domain data into the frequency domain and comparison between spectral noise resistance plot (R_{SN}) and the Bode plot obtained from EIS. Spectral noise plot has revealed a very good compliance with $|Z_f|$. Also the current and potential PSD plots were compared to examine the independency of R_n from sampling frequency. Similarity of the slopes of current and potential PSD plots reveals that R_n is frequency-independent and therefore it is a representative parameter of the corroding system.

It is clear that this method does not replicate the measurements that would be obtained using two identical samples and a ZRA where the shifts in potential of the isolated sample are free from any polarization by the second electrode. Therefore the shifts in potential will be larger here. Meanwhile the current shifts will also be larger because the potential is constrained at a fixed free-corrosion potential. It appears that these two factors balance out giving results that agree with other methods.

This new arrangement shows promise to solve the problem of measuring electrochemical noise where preparing two isolated working electrode is difficult, or characterization of one particular area is required. It has shown great potential to be a functional method for electrochemical noise data collection on a single working electrode.

Further steps were taken towards making ENM a practically useable assessment technique in the field by studying use of a pseudo-reference electrode as data collection terminals. The noisiness of Pt, Cu and printed Carbon (C) electrodes was ranked in the order: C > Cu > Pt. This result was confirmed by the actual Rn measurement with SS arrangement on painted

steel. More accurate result was obtained by Pt reference electrode followed by Cu, with C being the least accurate. However all of the electrodes have shown relatively acceptable performance when compared with EIS and DC resistance measurements and may be used for ENM in the field.

Effect of data collection rate on accuracy of ENM was studied by measuring noise resistance at 1, 2, 5 and 10 sampling frequency on a range of coating resistances. The most reliable, yet relatively fast, sampling frequency was determined as 2 Hz. Inaccurate result was obtained by ENM at 5 and 10 Hz on relatively low resistance coatings ($<10^8$ $\Omega.cm^2$). Also the time required to reach the steady state for ENM was studied for a range of thick paint films with relatively high resistance ($>10^{10}$ $\Omega.cm^2$). Different equilibrium times observed for different systems indicate the necessity of repetitive measurements until a steady result is obtained.

Publications

- D.J. Mills, S.S. Jamali, M.T. Tobiszewski, Developing electrochemical measurements in order to assess anti-corrosive coatings more effectively, Progress in Organic Coatings. 74 (2012) 385–390.
- S.S. Jamali, D.J. Mills, C.P. Woodcock, Ways of Increasing the Effectiveness of the Electrochemical Noise Method for Assessment of Organic Coatings on Metal, ECS Transactions. 24 (2010) 115–125.
- D.J. Mills, S.S. Jamali, Novel Set-up for application of Electrochemical Noise Measurement (ENM) on Protective Coatings, 2nd International Conference Corrosion and Material Protection, Prague, Czech Republic, 19-22 April 2010.
- S.S. Jamali, D.J. Mills, To Develop a Working Prototype of an Instrument for Determining the Integrity of Anti-corrosion Paint Coatings, Final report of the consultancy project for Midland Corrosion Services (MCS) Ltd., Rowsley, Derbyshire, England, 2011.
- S.S. Jamali, D.J. Mills, J.M. Sykes, Measuring electrochemical noise resistance on a single electrode, *under preparation*

References

[1] J. Mojica, E. Garcia, F.J. Rodriguez, J. Genescá, Evaluation of the protection against corrosion of a thick polyurethane film by electrochemical noise, Progress in Organic Coatings. 42 (2001) 218-225.

[2] D.J. Mills, S.J. Mabbutt, G.P. Bierwagen, Investigation into mechanism of protection of pigmented alkyd coatings using electrochemical and other methods, Progress in Organic Coatings. 46 (2003) 176-181.

[3] H.A.A. Al-Mazeedi, R.A. Cottis, A practical evaluation of electrochemical noise parameters as indicators of corrosion type, Electrochimica Acta. 49 (2004) 2787-2793.

[4] Y. Tan, Sensing localised corrosion by means of electrochemical noise detection and analysis, Sensors and Actuators B: Chemical. 139 (2009) 688-698.

[5] Y.F. Cheng, M. Wilmott, J.L. Luo, The role of chloride ions in pitting of carbon steel studied by the statistical analysis of electrochemical noise, Applied Surface Science. 152 (1999) 161-168.

[6] J.A. Wharton, B.G. Mellor, R.J.K. Wood, C.J.E. Smith, Crevice corrosion studies using electrochemical potential noise measurements, in: Corrosion 2000, NACE International, Houston, TX, USA, 2000: p. paper no. 00417.

[7] D. Eden, M. Hoffman, B. Skerry, Application of electrochemical noise measurements to coated systems, in: R.A. Dickie, F.L. Floyd (Eds.), Polymeric Material for Corrosion Control, American Chemical Society, 1986: pp. 36-47.

[8] B. Skerry, D. Eden, Electrochemical testing to assess corrosion protective coatings, Progress in Organic Coatings. 15 (1987) 269-285.

[9] B.S. Skerry, A. Alavi, K.I. Lindgren, Environmental and electrochemical test methods for the evaluation of protective organic coatings, Journal of Coatings Technology. 765 (1988) 97-106.

[10] G.P. Bierwagen, D.E. Tallman, J. Li, S. Balbyshev, M. Zidoune, Electrochemical noise studies of aircraft coatings over Al 2024 T-3 in accelerated exposure testing, in: Corrosion 2000, NACE International, 2000: p. paper no. 00427.

[11] H. Ashassi-Sorkhabi, D. Seifzadeh, M. Raghibi-Boroujeni, Analysis of electrochemical noise data in both time and frequency domains to evaluate the effect of ZnO nanopowder addition on the corrosion protection performance of epoxy coatings, Arabian Journal of Chemistry. (2012).

[12] S.J. Mabbutt, D.J. Mills, C.P. Woodcock, Developments of the electrochemical noise method (ENM) for more practical assessment of anti-corrosion coatings, Progress in Organic Coatings. 59 (2007) 192-196.

[13] Q. Le Thu, G.P. Bierwagen, S. Touzain, EIS and ENM measurements for three different organic coatings on aluminum, Progress in Organic Coatings. 42 (2001) 179-187.

[14] G. Gusmano, G. Montesperelli, S. Pacetti, A. Petitti, Resistance electrochemical noise as a tool for corrosion rate prediction, in: Corrosion 96, NACE International, Denver, Co, 1996: p. paper No. 336.

[15] M. Behzadnasab, S.M. Mirabedini, K. Kabiri, S.S. Jamali, Corrosion performance of epoxy coatings containing silane treated ZrO2 nanoparticles on mild steel in 3.5% NaCl solution, Corrosion Science. 53 (2011) 89-98.

[16] C. Valentini, J. Fiora, G. Ybarra, A comparison between electrochemical noise and electrochemical impedance measurements performed on a coal tar epoxy coated steel in 3% NaCl, Progress in Organic Coatings. 73 (2012) 173-177.

[17] B. Lengyel, L. Mészáros, G. Mészáros, E. Fekete, F. Janaszik, I. Szenes, Electrochemical methods to determine the corrosion rate of a metal protected by a paint film, Progress in Organic Coatings. 36 (1999) 11-14.

[18] J.E. Chen, W.F. Bogaerts, The physical meaning of noise resistance, Corrosion Science. 37 (1995) 1839-1842.

[19] J.M. Sanchez-Amaya, R.M. Osuna, M. Bethencourt, F.J. Botana, Monitoring the degradation of a high solids epoxy coating by means of EIS and EN, Progress in Organic Coatings. 60 (2007) 248-254.

[20] M.C. Deyá, B. del Amo, The assessment of a smart anticorrosive coating by the electrochemical noise technique, Progress in Organic Coatings. 76 (2013) 525-532.

[21] K.D. Conners, W.J. van Ooij, D.J. Mills, G.P. Bierwagen, Comparison of electrochemical impedance spectroscopy and electrochemical noise measurement of plasma polymerised films as pretreatment for cold rolled steel, British Corrosion Journal. 35 (2000) 141-144.

[22] Y.-J. Tan, T. Wang, T. Liu, N.-N. Aung, Studying and evaluating anti-corrosion coatings and inhibitors using the wire beam electrode method in conjunction with electrochemical noise analysis, Anti-Corrosion Methods and Materials. 53 (2006) 30-42.

[23] Y.-J. Tan, N.N. Aung, T. Liu, Novel corrosion experiments using the wire beam electrode. (I) Studying electrochemical noise signatures from localised corrosion processes, Corrosion Science. 48 (2006) 23-38.

[24] R.A. Cottis, S. Turgoose, Analysis of electrochemical noise, in: Electrochemical Impedance and Noise, NACE International, Houston, TX, USA, 1999: p. 90.

[25] F. Mansfeld, Z. Sun, C.H. Hsu, A. Nagiub, Concerning trend removal in electrochemical noise measurements, Corrosion Science. 43 (2001) 341-352.

[26] H. Xiao, F. Mansfeld, Evaluation of coating degradation with electrochemical impedance spectroscopy and electrochemical noise analysis, Journal of The Electrochemical Society. 141 (1994) 2332.

[27] F. Mansfeld, L.T. Han, C.C. Lee, C. Chen, G. Zhang, H. Xiao, Analysis of electrochemical impedance and noise data for polymer coated metals, Corrosion Science. 39 (1997) 255-279.

[28] a Conde, J. de Damborenea, Monitoring of vitreous enamel degradation by electrochemical noise, Surface and Coatings Technology. 150 (2002) 212-217.

[29] D.E. Tallman, G.P. Bierwagen, S. Touzain, Electrochemical noise methods applied to the study of organic coating and pretreatments, in: CORROSION 98, NACE International, Houston, TX, USA, 1998: p. paper no. 380.

[30] F. Mansfeld, H. Xiao, Y. Wang, Evaluation of localized corrosion phenomena with electrochemical impedance spectroscopy (EIS) and electrochemical noise analysis (ENA), Materials and Corrosion. 46 (1995) 3-12.

[31] G.P. Bierwagen, C.S. Jeffcoate, J. Li, S. Balbyshev, D.E. Tallman, D.J. Mills, The use of electrochemical noise methods (ENM) to study thick, high impedance coatings, Progress in Organic Coatings. 29 (1996) 21-29.

[32] D.J. Mills, C.P. Woodcock, Use of electrochemical noise method and electrochemical impedance spectroscopy for investigation of a set of organic coatings on steel, in: "Managing Corrosion for Sustainability" EuroCorr 2008, Dechema, Edinburgh, 2008.

[33] C. Lee, F. Mansfeld, Analysis of electrochemical noise data for a passive system in the frequency domain, Corrosion Science. 40 (1998) 959-962.

[34] F. Mansfeld, L.T. Han, C.C. Lee, G. Zhang, Evaluation of corrosion protection by polymer coatings using electrochemical impedance spectroscopy and noise analysis, Electrochimica Acta. 43 (1998) 2933-2945.

[35] M. Hernández, J. Genescá, J. Uruchurtu, a. Barba, Correlation between electrochemical impedance and noise measurements of waterborne coatings, Corrosion Science. 51 (2009) 499-510.

[36] F. Mansfeld, C. Lee, The frequency dependence of the noise resistance for polymer-coated metals, Journal of the Electrochemical Society. 144 (1997) 2068-2071.

[37] T. Zhang, X. Liu, Y. Shao, G. Meng, F. Wang, Electrochemical noise analysis on the pit corrosion susceptibility of Mg–10Gd–2Y–0.5Zr, AZ91D alloy and pure magnesium using stochastic model, Corrosion Science. 50 (2008) 3500-3507.

[38] J.J. Kim, Wavelet analysis of potentiostatic electrochemical noise, Materials Letters. 61 (2007) 4000-4002.

[39] a. Aballe, M. Bethencourt, F.J. Botana, M. Marcos, Using wavelets transform in the analysis of electrochemical noise data, Electrochimica Acta. 44 (1999) 4805-4816.

[40] Z. Dong, X. Guo, J. Zheng, L. Xu, Calculation of noise resistance by use of the discrete wavelets transform, Electrochemistry Communications. 3 (2001) 561-565.

[41] X.F. Liu, H.G. Wang, H.C. Gu, Fractal characteristic analysis of electrochemical noise with wavelet transform, Corrosion Science. 48 (2006) 1337-1367.

[42] S. Reid, G.E.C. Bell, G.L. Edgemon, The use of skewness, kurtosis and neural networks for determining corrosion mechanism from electrochemical noise data, in: Corrosion/98, NACE International, 1998: p. paper no. 176.

[43] M. Halama, D. Jerolitsch, P. Linhardt, G. Fafilek, Active corrosion management in automotive industry: Hyphenation of electrochemical noise analysis with artificial neural networks – feasibility study . Part I, in: "Corrosion: From the Nanoscale to the Plant" Eurocorr 2009, Dechema, Nice, France, 2009.

[44] J.Y. Huang, X.P. Guo, Y.B. Qiu, Z.Y. Chen, Cluster and discriminant analysis of electrochemical noise data, Electrochimica Acta. 53 (2007) 680-687.

[45] J.Y. Huang, Y.B. Qiu, X.P. Guo, Analysis of electrochemical noise of X70 steel in Ku'erle soil by cluster analysis, Materials and Corrosion. 60 (2009) 527-535.

[46] Q. Su, K. Allahar, G.P. Bierwagen, Embedded electrode electrochemical noise monitoring of the corrosion beneath organic coatings induced by ac–dc–ac conditions, Electrochimica Acta. 53 (2008) 2825-2830.

[47] M. Metikos-Hukovic, M. Loncar, C. Zevnik, Monitoring the electrochemical potential noise produced by coated metal electrodes, Materials and Corrosion. 40 (1989) 494-499.

[48] H. Greisiger, T. Schauer, On the interpretation of the electrochemical noise data for coatings, Progress in Organic Coatings. 39 (2000) 31-36.

[49] S.J. Mabbutt, D.J. Mills, Novel configuration for electrochemical noise measurements, British Corrosion Journal. 33 (1998) 158-160.

[50] D.J. Mills, S.J. Mabbutt, Developments in the electrochemical noise method to assess anti-corrosive coatings and inhibitors, in: 7th International Symposium on Electrochemical Methods in Corrosion Research, Budapest, Hungary, 2000: p. paper no. 145.

[51] S.J. Mabbutt, G.P. Bierwagen, D.J. Mills, New experimental arrangement for the acquisition of electrochemical noise data from high resistance organic anti-corrosive coatings, Anti-Corrosion Methods and Materials. 49 (2002) 264-269.

[52] S.J. Mabbutt, D.J. Mills, Recent UK work investigating anti-corrosive organic coatings using the electrochemical noise method (ENM), Surface Coatings International Part B: Coatings Transactions. 84 (2001) 277.

[53] C.P. Woodcock, D.J. Mills, H.T. Singh, Using novel electrochemical test methods to aid in the development of low volatile organic compound (VOC) coatings, Journal of Corrosion Science and Engineering. 8 (2004) 1-10.

[54] C.P. Woodcock, D.J. Mills, H.T. Singh, Use of electrochemical noise method to investigate the anti-corrosive properties of a set of compliant coatings, Progress in Organic Coatings. 52 (2005) 257-262.

[55] D.J. Mills, Comparison of ENM , EIS and DC resistance for assessing and monitoring anti-corrosive coatings, Journal of Corrosion Science and Engineering. 8 (2004) paper 12.

[56] S.S. Jamali, D.J. Mills, C.P. Woodcock, Ways of increasing the effectiveness of the electrochemical noise method for assessment of organic coatings on metal, ECS Transactions. 24 (2010) 115-125.

[57] R.A. Cottis, S. Turgoose, Measurement of electrochemical noise, in: Electrochemical Impedance and Noise, NACE International, Houston, TX, USA, 1999: p. 58.

[58] D.J. Mills, S.S. Jamali, M.T. Tobiszewski, Developing electrochemical measurements in order to assess anti-corrosive coatings more effectively, Progress in Organic Coatings. 74 (2012) 385-390.

[59] L. Mularczyk, D.J. Mills, P. Picton, Developments in the Electrochemical Noise Method to make it more practical for assessment of anti-corrosive coatings, in: I.V. Aoki, H.G. De Melo (Eds.), 10th Symposium on Electrochemical Methods in Corrosion Research, Maragogi, Brazil, 2012.

[60] D.J. Mills, S.S. Jamali, Novel set-up for application of electrochemical noise measurement (ENM) on protective coatings, in: 2nd International Conference Corrosion and Material Protection, Prague, Czech Republic, 2010.

[61] R.A. Cottis, S. Turgoose, Electrochemical impedance and noise, NACE International, Houston, TX, 1999.

[62] U. Bertocci, C. Gabrielli, F. Huet, M. Keddam, Noise resistance applied to corrosion measurements. I. Theoretical analysis, Journal of The Electrochemical Society. 144 (1997) 31-37.

[63] U. Bertocci, C. Gabrielli, F. Huet, M. Keddam, P. Rousseau, Noise resistance applied to corrosion measurements II. Experimental tests, Journal of The Electrochemical Society. 144 (1997) 31-37.

[64] U. Bertocci, F. Huet, Noise resistance applied to corrosion measurements. III. Influence of the instrumental noise on the measurements, Journal of Electrochemical Society. 144 (1997) 2786-2793.

[65] A. Bautista, U. Bertocci, F. Huet, Noise Resistance Applied to Corrosion Measurements: V. Influence of Electrode Asymmetry, Journal of The Electrochemical Society. 148 (2001) B412.

[66] R.A. Cottis, The significance of electrochemical noise measurements on asymmetric electrodes, Electrochimica Acta. 52 (2007) 7585-7589.

[67] A.M. Lowe, H. Eren, S.I. Bailey, Electrochemical noise analysis: detection of electrode asymmetry, Corrosion Science. 45 (2003) 941-955.

[68] A. Bautista, F. Huet, Noise Resistance Applied to Corrosion Measurements IV. Asymmetric coated electrodes, Journal of Electrochemical Society. 146 (1999) 1730-1736.

[69] F. Mansfeld, C. Chen, C. Lee, H. Xiao, The effect of asymmetric electrodes on the analysis of electrochemical impedance and noise data, Corrosion Science. 38 (1996) 497-513.

[70] D.J. Mills, M. Broster, I. Razaq, Continuing work to enable electrochemical methods to be used to monitor the performance of organic coatings in the field, Progress in Organic Coatings. 63 (2008) 267-271.

Chapter 4

Effect of surface preparation on the protection afforded by an organic coating

4.1 Introduction

A well-prepared surface is the foundation on which the paint system is built. It is generally accepted that inadequate surface pretreatment is the major cause of protection failure of organically coated metals in the early stages [1]. The primary purpose of metal pretreatment is to remove loose scales and dirt and roughen the surface for the subsequent paint application [2]. Dense oxide layers, e.g. mill scale, can to some extent protect steel from atmospheric corrosion [3]. However they are quite unstable in contact with aqueous corrosive media and can lead to early delamination of coating and therefore they have to be removed prior to painting [4,5]. Surface pretreatment improves the interfacial bonding by strengthening the electrostatic bonds (Van der Waals) and the mechanical interlocking between the coating and substrate irregularities [6]. Almost all generic types of industrial anti-corrosive coatings possess highly polar chemical structure and the electrostatic bond between the coating and metal substrate plays an important role in the interfacial adhesion. Oils, greases, and other organics may reduce the surface energy of normally high-energy metal surfaces from values near 400 dyne/cm to values < 20 dyne/cm, thereby reducing wetting and impeding or even eliminating adhesion of the film [7]. So theoretically metal surface pretreatment activates the surface and promotes adhesion. Also an increased surface profile enhances the chance of entanglement of polymeric chains into the surface irregularities. As surface roughness increases the specific surface area, it provides more electrical and mechanical sites to improve the coating bond with substrate. Most adhesion theories consider a rough surface to be favourable for achieving a high adhesive strength with a given organic coating [8]. In spite of this, some investigations have shown no relationship [9,10] or inverse relationship [11,12] between corrosion protection properties of the organic coating and the surface roughness.

Mills and Schaefer used water-jetting, wet garnet blasting and abrasion methods to prepare steel surface prior to painting with alkyd and examined the performance of coating [12]. Immersion in 3% NaCl solution and accelerated condition, salt fog, tests were used with somewhat limited correlation. However in most cases hydroblasted substrate produced the second best performance after non-treated, control, sample. There was a slight difference between the samples prepared by hydroblasting at two different pressures (20 K(psi) and40K(psi)) that was considered insignificant. Their results, as illustrated in

Figure 4.1, showed detrimental impact of garnet blasting. They suggested that oxide layer characteristic varies by the preparation method and is responsible for changes in corrosion resistance. *This study made the baseline and triggered the current research described in this chapter.* In the present study, surfaces produced by five common surface preparation methods have been characterized and the anti-corrosive performance of coated substrates have been examined both electrochemical and mechanically. The Mills and Schaefer work gave a clear indication of poor performance of abrasive blasted surface and good performance of hydroblasted surface, however it was felt necessary to repeat that work with different set of coatings along with in-depth characterization of the bare metal surface to understand how surface preparation alters the coating performance.

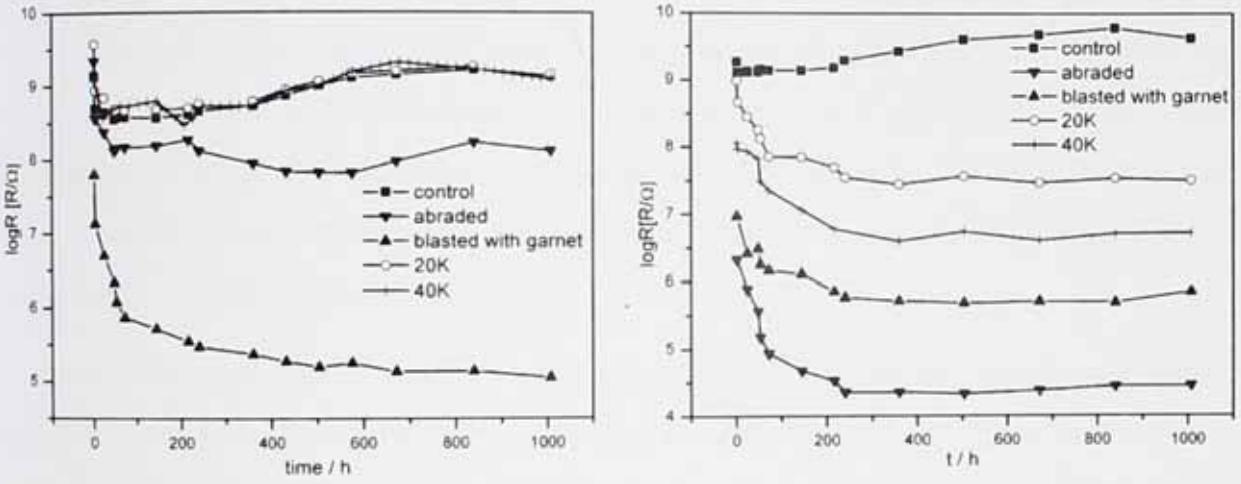

Figure 4.1 DC resistance as a function of time for (a) alkyd and (b) vinyl coated steel in 3% NaCl previously prepared with five different surface preparation methods (Figure reproduced from Ref. [12])

4.1.1 Background on the effect of surface preparation

In neutral conditions in air, a thin layer of protective oxide layer instantaneously forms on the clean steel surface. The initial corrodibility of steel when exposed to aqueous solution depends both on the species present in the solution and on the resistance of this oxide layer against breaking down [13]. The corrosion resistance of mild steel in, say, a neutral NaCl solution has been shown to depend highly on the formation of a passivating iron oxide layer

and the extent to which this layer is partially destroyed by pitting [14]. It has been shown that break down of the protective oxide layer and formation of the meta-stable and stable pits is, to a large extent, governed by the presence and concentration of chloride ions [3,15,16]. Geometrical depth of the surface irregularities plays a part in providing potential sites for pit formation and active localized corrosion. Deeper surface irregularities encourage the formation of stable anodic sites where the surface has the lowest access to oxygen and gives the highest value of local current density [17]. Also it has been revealed that the steel surface with a deeper surface profile, when coated with a thin layer of organic coating, exhibits lower corrosion resistance [18]. Apart from the geometry of the surface profile, the characteristics of the oxide film produced by each surface preparation method play a key role on the corrosion resistance. Atmani et al. [15,19] showed that on steel prepared by acid etching the oxide layer was more sensitive to chloride than the oxide on as-received cold-rolled and abraded steel. The surface characterization results revealed that a pre-existing thicker oxide layer mainly composed of Fe_2O_3 and FeOOH was removed after surface preparation and was substituted by a thin layer of Fe_2O_3. Higher stability of as-received surface was attributed to the structural difference and higher thickness of the oxide layer.

There have been several studies on the effect of poorly prepared surface on corrosion resistance of organically protected steel [20–22]. The results generally implied that the poor surface preparation accelerates corrosion and blistering due to the osmotic effect and the presence of contaminant underneath the paint film. In another study Vesga *et al.* [23] reported a better performance of protective coating on sand blasted steel compared to wet-blasted surface. Their results showed an early failure of the wet-blasted surface due to the presence of water in the preparation method and its influence on the surface characteristics. Elsner *et al* [24] achieved the same result comparing wet and dry sand-blasted steel. Their results also showed the detrimental effect of millscale or a thick and deadherant oxide layer which may form on the surface after preparation. Knapp and Taylor [25] compared the adhesion of a thermal sprayed metallic coating on waterjet and grit blasted steel surface. Their result showed better adhesion on waterjetted surface. Poor performance of grit blasted surface was attributed to the contamination and inclusion of embedded grit particles into the surface resulting in a weakened interface. In contrast, the

surface structure of waterjet roughened samples showed a high degree of microroughness and a high negative skewness of the surface height distribution that was considered favourable for mechanical bonding. Patel *et al.* [26] studied adhesion of a powder coating of degreased, acid etched and grit blasted stainless steel surface. They showed that despite the cleanness and activity of the acid etched surface, it had a poor adhesion to the coating while the high profile of grit blasted surface produces good bonding with the coating, regardless of the reasonable oxide layer.

4.2 Experimental

4.2.1 Materials and sample preparation

The five surface pretreatment methods used were : degreasing the as-received Q-panel with iso-propanol; abrasion with 180 grit emery; acid etching (in 20%W hydrochloric acid for 100 sec followed by rinsing with distilled water); UHP (ultra high pressure) water-jetting at 40K psi; wet abrasive (garnet) blasting at 10K psi (garnet entrained in water). The latter four preparation methods remove the existing oxide layer and/or introduce surface roughness. Degreasing, abrasion and acid etching methods were performed on steel Q-Panels and wet abrasive blasting and hydroblasting were applied on the low carbon steel panels provided by Rentajet Group Ltd. All samples were placed in a desiccator immediately after preparation. Figure 4.2 shows ultra high pressure (UHP) hydroblasting process in practice.

Figure 4.2 Preparation of steel panels using UHP hydroblasting method at 40K psi pressure.

The alkyd varnish was based on a short oil soya based alkyd resin with 40% v/v solid content. The solvent was Xylene. The alkyd paint was based on the same resin pigmented with calcium diphosphate, (also known as calcium pyrophosphate with the chemical structure of $Ca_2O_7P_2$). Both alkyd varnish and alkyd paint were supplied by Pronto industrial paints Ltd.

Two coats were applied on steel panels by spray to obtain a final DFT of about 120 µm. Air spray application was particularly chosen with the intention to minimize the chance of air pockets entrapment within the irregularities of rough surfaces.

Solvent base and waterborne polyurethane coatings were acrylic polyol (OH functional) resins crosslinked with polyisocyanate. The solvent based acrylic was SETALUX 1196 XX-60 polyol with 60%v/v solid content and Xylene as solvent. Waterborne acrylic was SETAQUA 6515 which was a polyol emulsion in DI water/butylglycol/solvesso 100 (85.8/7.6/6.6). Both poly-acrylic resins were supplied by Nuplex. Both poly-acrylic resins were crosslinked with Tolonate HDT-LV2 which was a solvent free, low viscosity aliphatic polyisocyanate based on Hexamethylene Diisocyanate trimer (HDI homopolymer) supplied by Perstorp. Stoichiometric mixing ratio of 1:1 of NCO:OH was used for solvent base PU. Mixing ratio of 1.25:1 (excessive polyisocyanate) was used for waterborne PU to compensate for NCO-water reaction. The waterborne and solvent based polyurethanes were applied with thickness of 95 µm and 75 µm, respectively.

The epoxy coating was an epoxy/polyamine coating with 100 µm film thickness. Epoxy resin was EPIKOTE 1001 (supplied by Hexion) which is a solid epoxy resin produced from bisphenol A and epichlorohydrin with epoxy equivalent group (EEW), or epoxy molar mass, of 450-500 g/eq. Polyamine was diethylenetriamine (DETA) supplied by Dow with MW of 103.17 and H active index of 20.6.

Bearing in mind the high surface profile of wet abrasive blasted and hydroblasted surfaces, special attention was given to ensure that the 120 µm thickness of paint had covered all the peaks and irregularities of the surface.

4.2.2 Testing methods

-Surface characterization

(i) SEM-EDXS

A Hitachi S-3000N SEM equipped with Energy dispersive X-ray spectroscopy (EDXS), Princeton Gamma-Tech Inc., was used for morphological examination and elemental analysis. SEM creates a magnified image of the surface by scanning it with a focused beam of electrons. The electrons interact with electrons in the sample, producing various signals that can be detected and that contain information about the sample's surface topography and composition. EDXS is an analytical technique used for the elemental analysis or chemical characterization of a sample. This spectroscopy technique relies on the energy of the electron beam to excite the electrons in the sample. These excited electrons change orbitals and give off x-rays with characteristic energies. These x-rays are collected and allow for both characterization and quantification of the elements in a sample.

(ii) Profilometry

The contact surface profile was measured for wet abrasive blasted and hydroblasted surfaces using Taylor Hobson equipment, model Talysurf Series 2, provided at Department of Materials Engineering, University of Swansea, UK. Optical profilometry was performed using a wyko NT9100 optical profilometer (Veeco instruments Inc.) provided at Intelligent Polymer Research Institute (IPRI) at University of Wollongong, Australia. The increase in actual surface area and the missing volume which resulted by roughening the surface were calculated.

(iii) Surface free energy measurement

Contact angle was measured as an indicator of the surface free energy and its wettability. The sessile drop method was measured by a contact angle goniometer to capture the profile of pure water on steel substrate. The angle formed between the liquid/solid interface and the liquid/vapour interface is the contact angle as shown in the Figure 4.3.

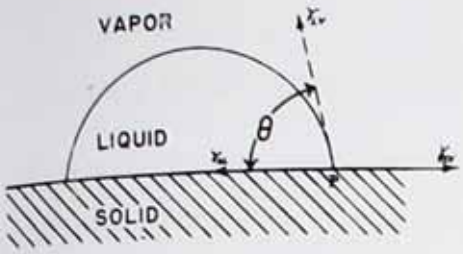

Figure 4.3 Contact angle of a sessile drop.

Contact angle may be used to quantify the wettability of a solid surface by a liquid via the Young equation, equation 4.1. A given system of solid, liquid, and vapour at a given temperature and pressure has a unique equilibrium contact angle.

$$\gamma_{SL} = \gamma_{SV} - \gamma_{LV}(\cos\theta) \qquad \text{(Eq. 4.1)}$$

where solid–vapour interfacial energy is denoted by γ_{SV}, the solid–liquid interfacial energy by γ_{SL}, the liquid–vapour interfacial energy (i.e. the surface tension) by γ_{LV}, and the equilibrium contact angle is θ. If the liquid molecules are strongly attracted to the solid molecules then the liquid drop spreads out on the solid surface, corresponding to a small contact angle.

- Bulk electrochemical testing methods

Open circuit potential (OCP), EIS and potentiodynamic polarization measurements were performed using an automated ACM GillAC potentiostat/galvanostat/FRA. Exposed area of sample was 3.8 cm^2 and SCE (Standard Calomel Electrode) was used in all cases as reference electrode. EIS was performed within 10kHz-10mHz range with 10mV voltage perturbation around OCP. Potentiodynamic polarization was performed within ±250 mV around OCP at the scan rate of 120mV/min. β_a and β_c were calculated by fitting anodic and cathodic reaction lines on anodic and cathodic branch of Evans curve at 100mV-150mV overpotentials.

- Scanning Vibrating Electrode Technique (SVET)

SVET experiments were performed using an in-house built SVET facility provided at Department of Materials Engineering, University of Swansea, UK. The micro-positioning XYZ stage and the microelectrode tip are shown in Figure 4.4. The exposed area was approx. 10×10 mm and the rest of surface was masked using an adhesive tape to avoid interference. All surfaces were assumed flat and so the 4 point height scan method was employed to adjust the 150 µm distance between the vibrating probe and the metal surface. Measurement resolution was 100 µm between each pair of consecutive points. A map of current density was obtained using the integrated program. Repetitive scans were conducted to track changes in surface activity.

Figure 4.4 SVET XYZ stage (left) and the rastering microelectrode tip (right) over degreased Q-panel specimen in 0.001 M NaCl solution.

- DC resistance

The DC resistance of coated samples was measured by a solid-state Keithley electrometer model 610C in a two electrode configuration against the SCE. This instrument can make accurate measurements on samples with impedances up to 1E+12 ohms.

All the electrochemical experiments on the bare metal surfaces were conducted in 0.001 M NaCl solution at RT (18-22°C). The electrochemical experiments on coated metal were performed using PVC cells affixed to the coating by epoxy glue. The PVC cells were filled

with 0.5M NaCl exposing 11.4cm^2 of surface to electrolyte. For each coating on a given substrate, 5 cells were measured and the average is reported.

-Adhesion

The adhesion strength of coated surfaces was measured using an automatic Defelsko PosiTest Pull-off adhesion tester model AT-A at pull rate of 100 psi/s with 20mm size of dollies. To measure wet adhesion, samples were masked on the back and edges of the panels and then they were placed in a water bath containing 0.5 M NaCl solution at 55 °C. To make the adhesion measurements the samples were removed from the water bath, the surface was swabbed dry and then they were left for a few minutes before aluminium dollies were attached to the coating by means of cyanoacrylate super-glue.

4.3 Results and discussion. Part 1

Bare metal characterization

4.3.1 Elemental analysis

SEM micrographs of surfaces produced by different techniques are given in Figures 4.5-4.9. Degreased as-received Q-panel (Figure 4.5) shows minimal surface irregularity with a number of defects across the relatively dense oxide film. Abrasion with emery appears to remove the pre-existing oxide film leaving a surface with shallow, well oriented grooves (Figure 4.6). The acid-etching as shown in Figure 4.7 has effectively attacked the grain boundaries without generating a reasonable surface profile. EDXS elemental mapping of the acid etched sample (data not presented here) showed a highly homogeneous surface. Hydro-blasting has remarkably changed the surface structure and generated a porously patterned oxide film with submicron sized irregularities (Figures 4.8a and 4.8b). EDXS elemental analysis and mapping showed heterogeneous distribution of oxygen (Figure 4.8c) with higher concentration of oxygen at areas of high carbon content, supposedly grain boundaries. Grain boundaries are regions of atomic mismatch and less dense atomic packing [27]. Thus grain boundary oxidizes more rapidly compared to the crystalline lattice [28,29]. This is usually referred to as "grain-boundary penetration" where oxygen diffuses

along the grain boundaries, reacts with the steel, and forms iron oxide preferentially at the grain boundaries. SEM micrographs of the wet abrasive blasting are shown in Figures 4.9a and 4.9b. Abrasive blasting produces a very coarse structure with a number of foreign particles embedded into the steel. EDXS mapping micrographs, Figures 4.9c-4.9e, show elemental distribution of Si, O and Al, respectively. Further EDXS analysis, Figure 4.10, identified these particles as Al_2O_3, MgO and SiO_2 which is similar to the chemical composition of garnet particles used in the blasting process suggesting that the particles are fragments from crushed garnet originated from the preparation material. Oxide form on all surfaces was identified Wustite (FeO).

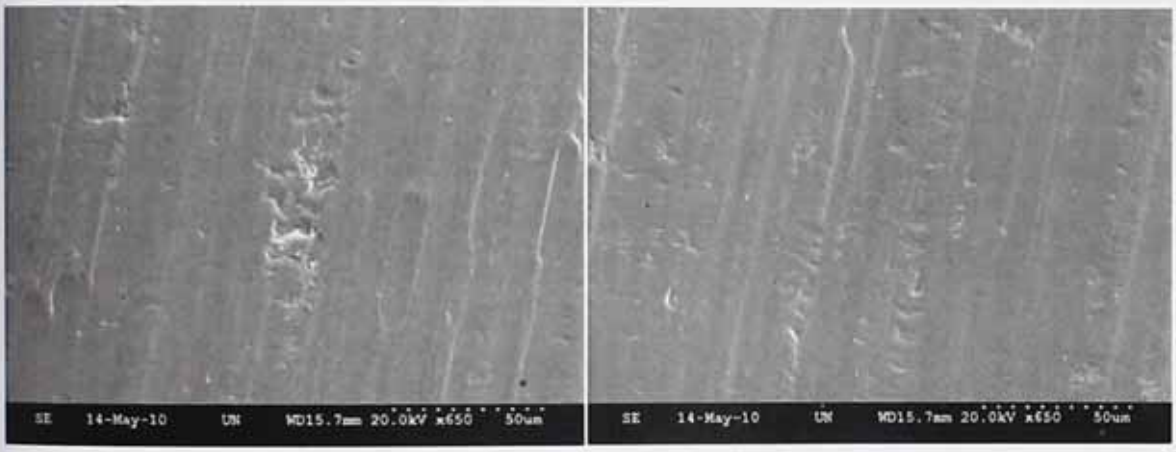

Figure 4.5 SEM micrographs of as-received (steel) Q-panel from different locations with 650 magnification, accelerating voltage of 20kV.

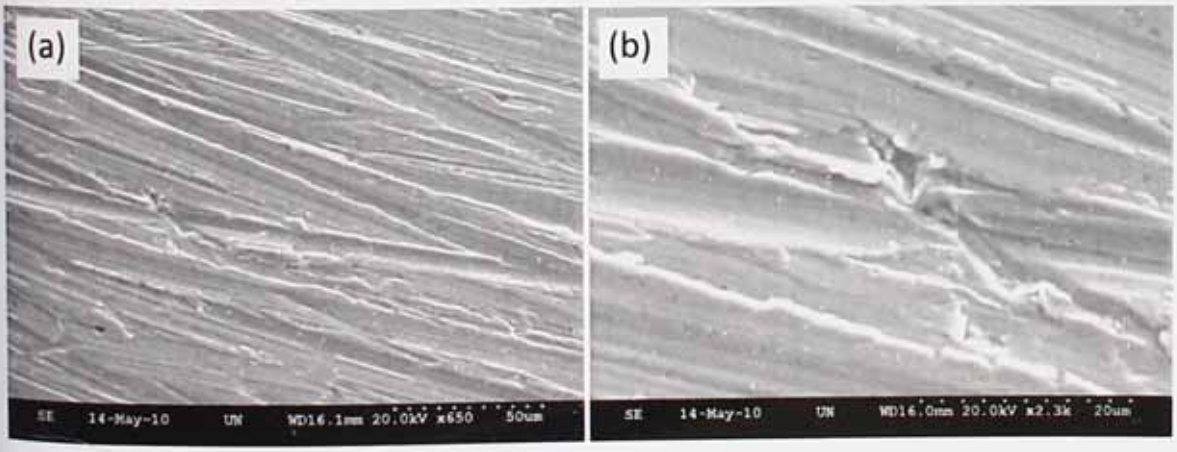

Figure 4.6 SEM micrograph of abraded steel at (a) 650 and (b) 2,300 magnifications with accelerating voltage of 20kV.

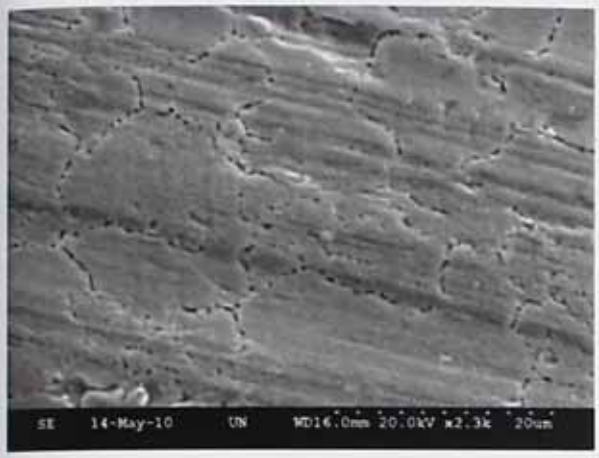

Figure 4.7 SEM micrograph of acid etched steel with 2.3k magnification and accelerating voltage of 20kV.

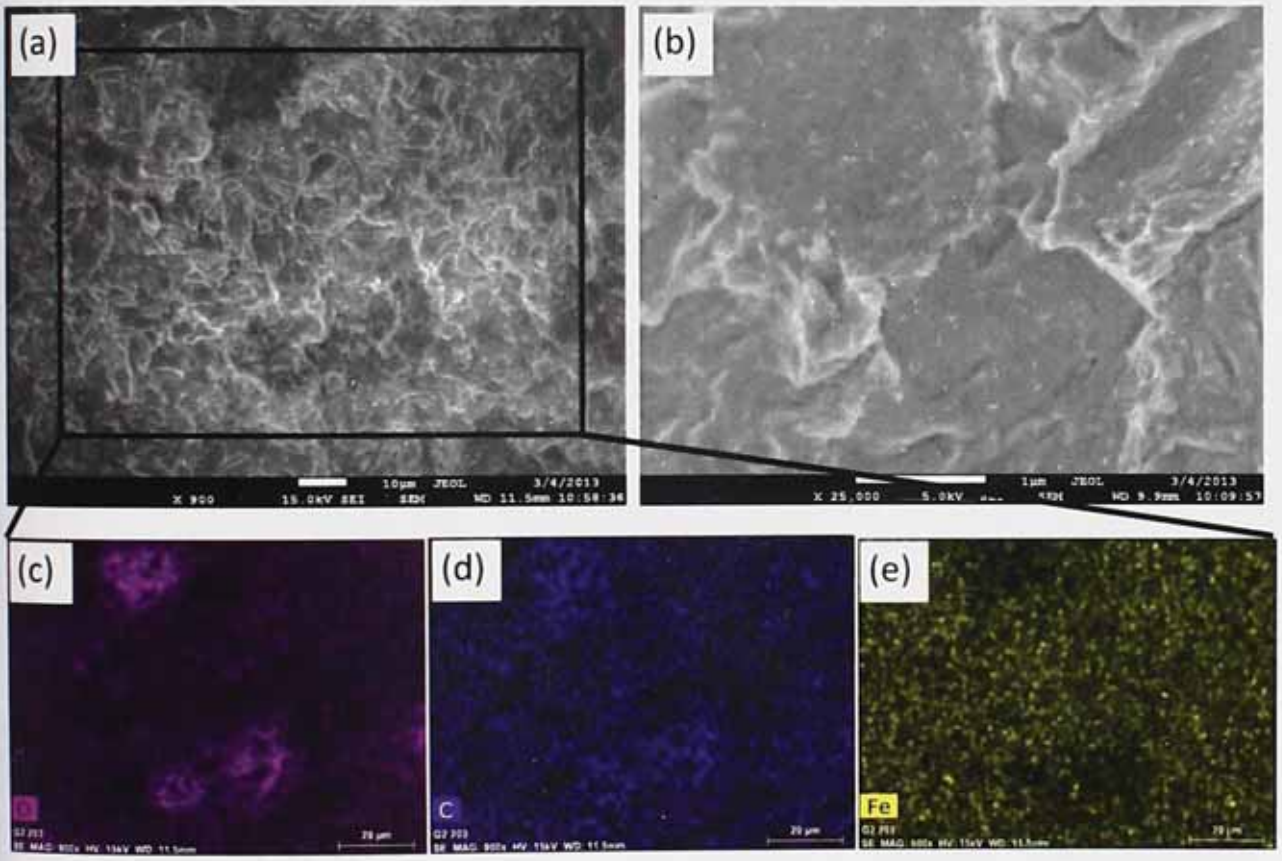

Figure 4.8 SEM micrograph of UHP hydroblasted steel at (a) 900 and (b) 25,000 magnifications (accelerating voltage 20kV) and EDXS elemental mapping for (c) oxygen, (d) carbon and (e) Fe.

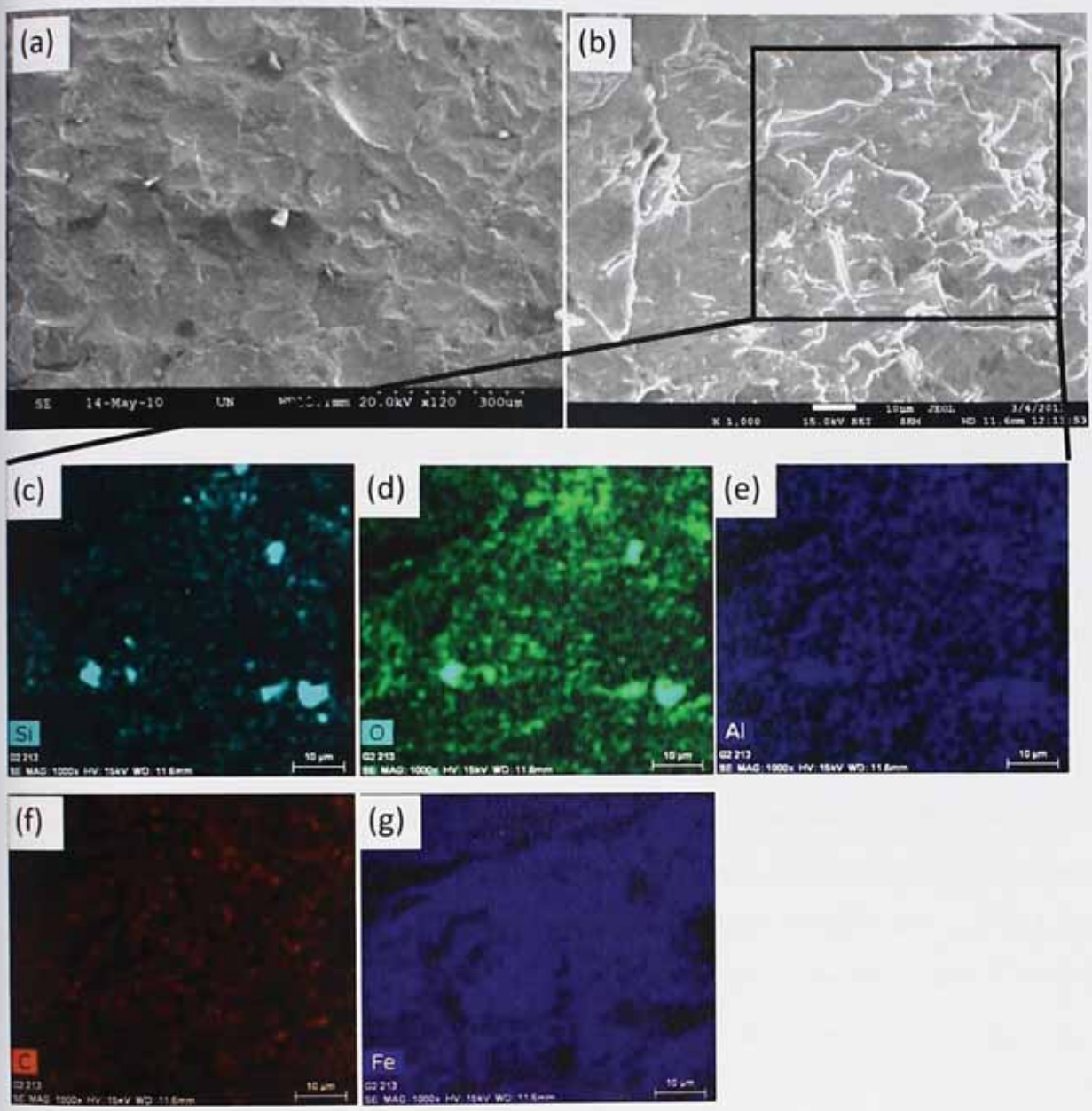

Figure 4.9 SEM micrograph of wet abrasive blasted steel at (a) 120 and (b) 1000 magnifications (accelerating voltage 20kV) and EDXS elemental mapping for (c) silicon, (d) oxygen, (e) aluminium, (f) carbon and (g) Fe.

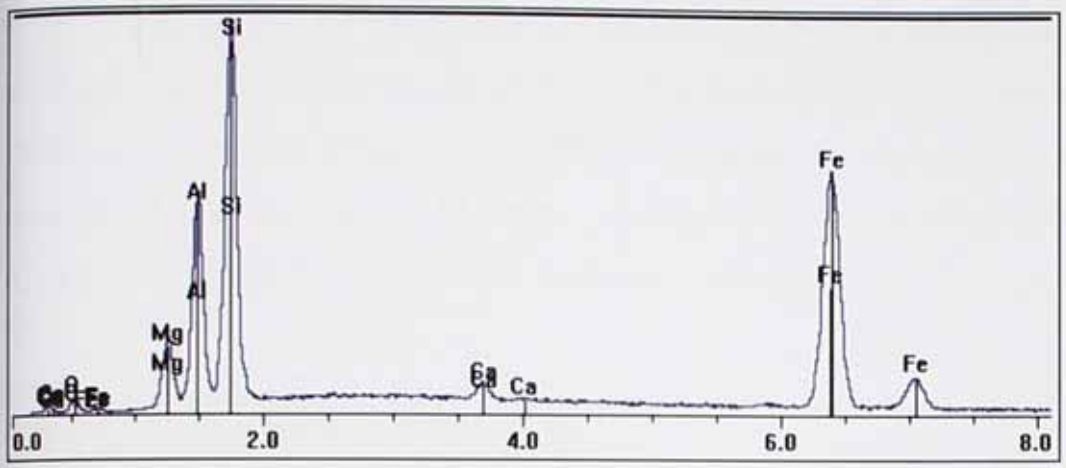

Figure 4.10 Single point elemental analysis of an embedded particles on the surface of wet abrasive blasted steel by EDX Spectroscopy. The particle was differentiated earlier in EDXS elemental mapping as a spot with relatively higher percentage of Si, O and Al.

4.3.2 Surface morphology

Profilometry experiments showed Sz[1] of 62µm and 119µm for the hydroblasted and wet abrasive blasted surfaces, respectively, indicating a very coarse surface produced by wet abrasive-blasting, twice as much as the surface roughness produced by hydro-blasting. Other surface preparation methods produced relatively smooth surfaces with S_z in the range of 3-5 µm. The R_a[2] was not significantly altered by acid etching compared to the as-received Q-panel, however abrasion slightly flattened the surface resulting in a submicron R_a as illustrated in Figure 4.12. Figures 4.11-4.15 demonstrate the optical profilometry results provided with a colour scale, red representing the peaks and blue representing the valleys. The abrasion, as shown in Figure 4.12, has removed the large irregularities while it creates more low height irregularities. Figure 4.13, shows that acid attacks the surface uniformly during the etching process resulting in a surface profile very similar to that of the as-received Q-panel. Despite the visual presence of the etched grain boundaries, they could not be detected in the roughness map.

The true areas of the surfaces with 1.7*2.3 mm (3.91 mm^2) of apparent area are given in Figure 4.16. The slightly higher surface area of plain Q-panel corresponds to the

[1] Sz is the Ten Point Height over the complete 3D surface and represents the average difference between the 5 highest peaks and 5 lowest valleys

[2] R_a is the average roughness calculated over the entire measured array as the arithmetic average of the distance between the roughness profile and its mean, imaginary, line.

irregularities resulted by cold-rolling processing of steel, illustrated in Figure 4.5. Acid etching and abrasion have not altered the surface area significantly. Hydroblasting with 40K Psi has increased the surface area by about 27% while the wet abrasive blasting further increased the surface area by 2.45 times. The increased surface area can potentially provide a larger interface for the subsequent organic coating to adhere to.

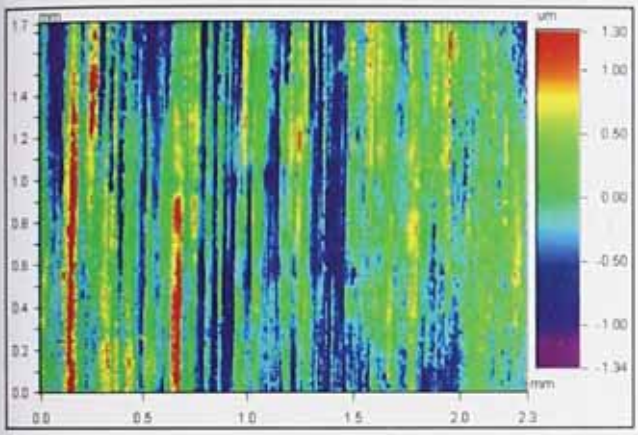

Figure 4.11 Surface profile of degreased steel within 1.7x2.3 mm area acquired by optical profilometry at 2.73X magnification with 3.63 µm sampling step.

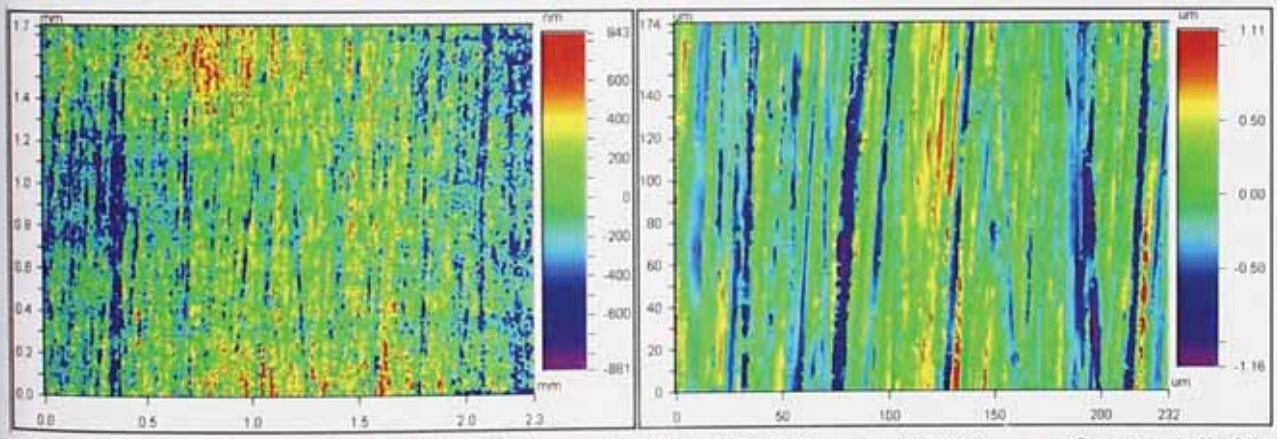

Figure 4.12 Surface profile of abraded steel within 1.7x2.3 mm (2.73X magnification) (left) 174x232 µm (27.3X magnification) areas (right) acquired by optical profilometry with 3.63 µm sampling step.

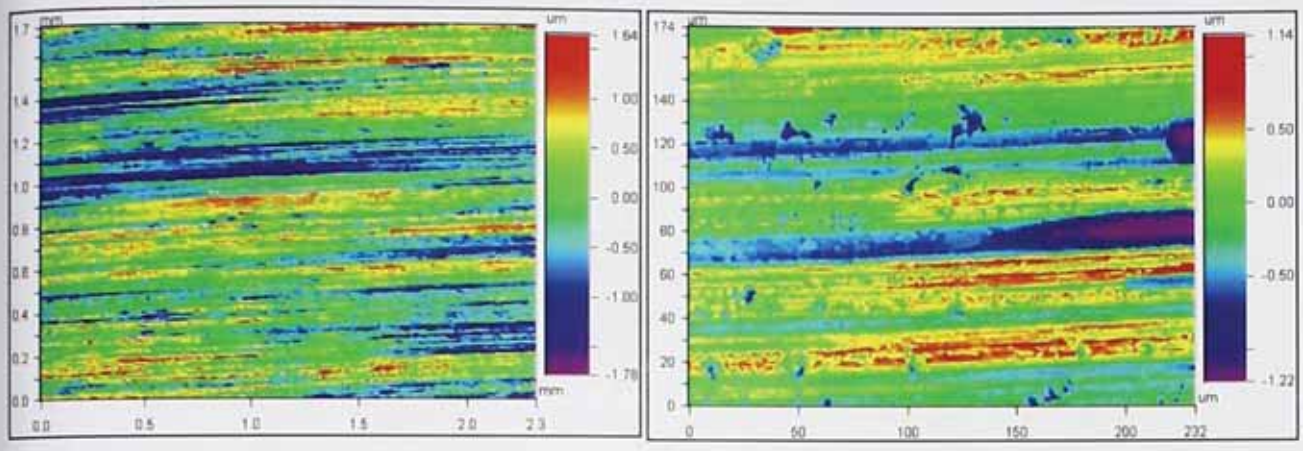

Figure 4.13 Surface profile of acid etched steel within 1.7x2.3 mm (2.73X magnification) (left) 174x232 µm (27.3 magnification) areas (right) acquired by optical profilometry with 3.63 µm sampling step.

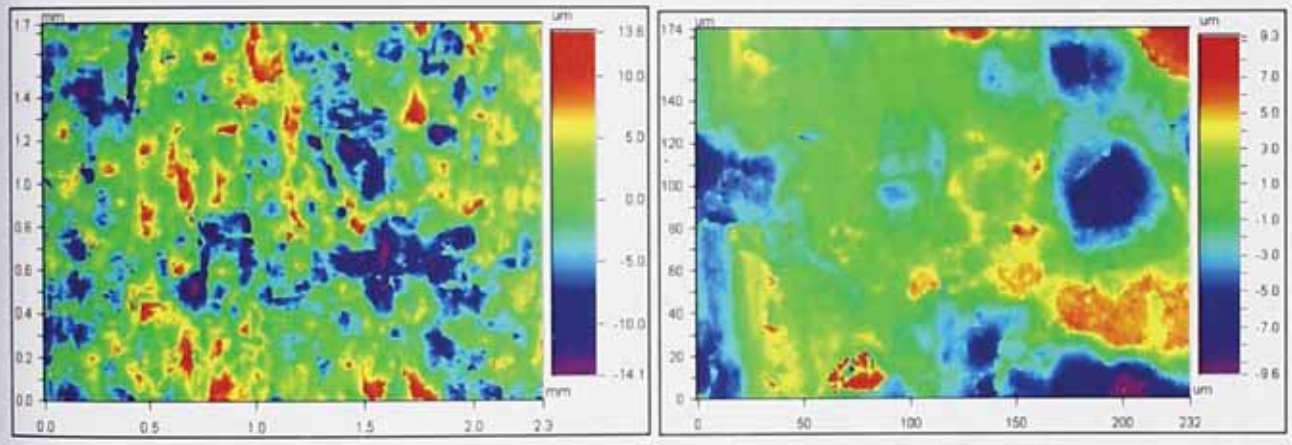

Figure 4.14 Surface profile of hydro-blasted steel within 1.7x2.3 mm (2.73X magnification) (left) 174x232 µm (27.3 magnification) areas (right) acquired by optical profilometry with 3.63 µm sampling step.

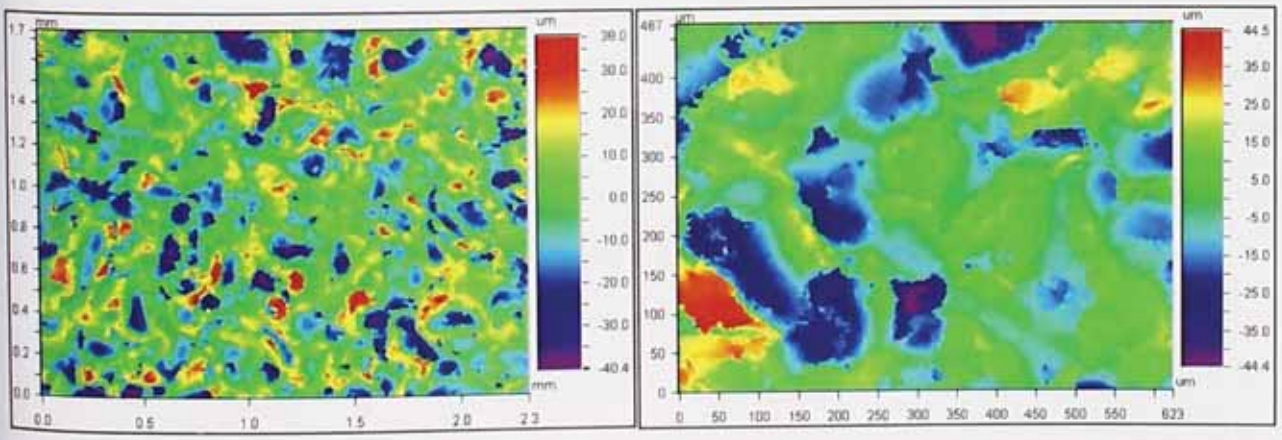

Figure 4.15 Surface profile of wet abrasive blasted steel within 1.7x2.3 mm (2.73X magnification) (left) 467x623 µm (10.1X magnification) areas (right) acquired by optical profilometry with 3.63 µm sampling step.

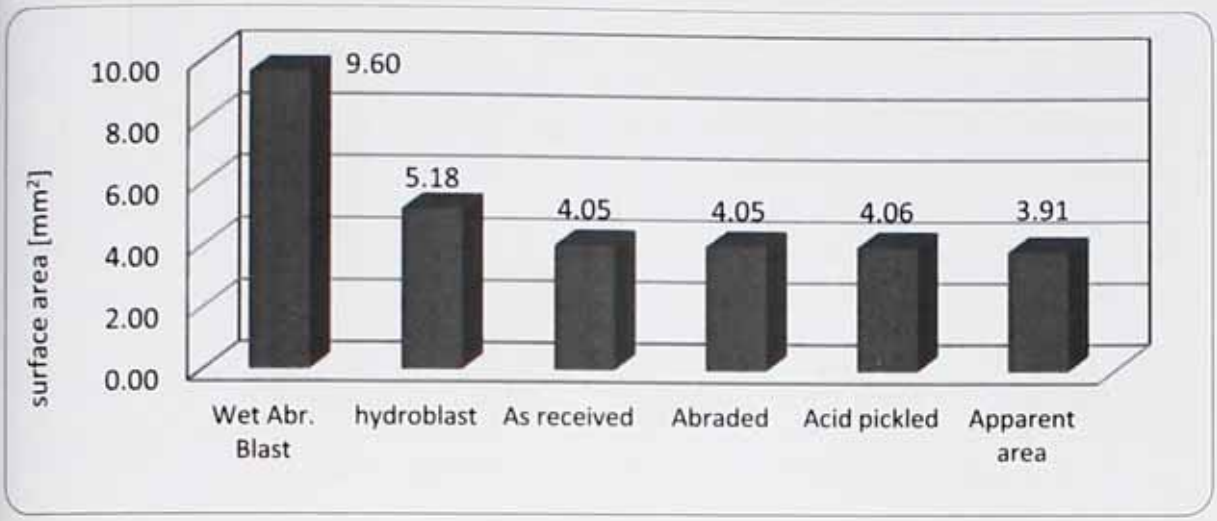

Figure 4.16 Actual surface area produced by applying different surface preparation methods on 3.91 mm^2 area of steel.

4.3.3 Missing volume

Figure 4.17 shows the amount of liquid required to submerge the surface profile to its highest peak in mm^3 (or in other words the missing volume). Abrasion with 180 grit emery has decreased the missing volume indicating that this level of abrasion flattens the surface to some extent. This is due to the removal of the large irregularities from the surface of cold-rolled steel resulting in a somewhat flatter surface. Etching by acid has slightly increased the missing volume. The hydroblasting has remarkably increased the missing volume by more than an order of magnitude, $2.90*10^{-2}$ mm^3 (3.29E-2 - 0.387E-3), compared to the plain Q-panel. The wet abrasive blasting dramatically increased the missing volume to $7.56*10^{-2}$ mm^3 compared to the plain Q panel. Therefore, to submerge and cover the surface profile to its highest peak and avoid flash rusting, for hydroblasted surface an extra 7.4 cm^3/m^2 and for an abrasive blasted surfaces an extra 18.7 cm^3/m^2 amount of paint is required. For example, if the targeted thickness of coating was 100µm, this represents 7.4% and 18.7 % extra paint respectively (calculated for 100% solid paint).

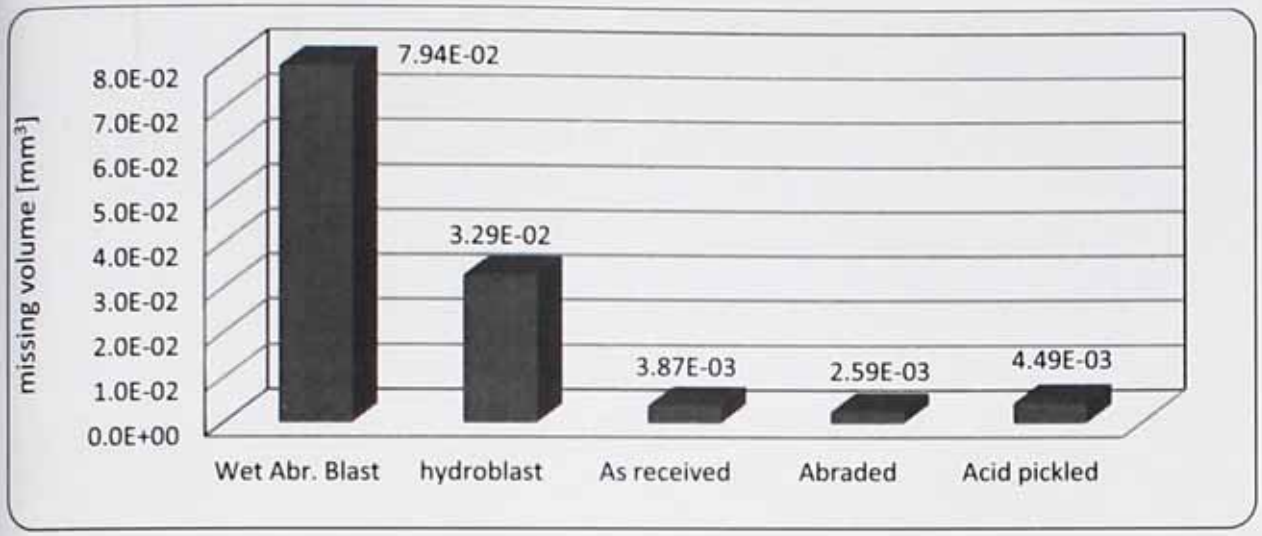

Figure 4.17 The volume of the liquid required to submerge the surface profiles produced by different preparation methods.

4.3.4 Surface free energy

Figure 4.18 (a-d) illustrates the results of contact angle measurement for the surfaces of subject of this study, degreased Q-panel, abraded, acid etched, hydro-blasted and abrasive blasted steel. The lowest contact angle was observed on the surface chemically etched by HCl indicating its very high free surface energy and excellent wettability. Significantly higher contact angle on degreased surface with similar surface profile to the acid etched surface reveals the effectiveness of acid etching in chemical activation of the steel surface. Surface abrasion also reduced the contact angle compared to the as-received Q-panel. Hydroblasted and abrasive blasted surfaces show the largest contact angle indicating their hydrophobicity. By definition, surfaces with contact angle of larger than 90^{o} are considered hydrophobic.

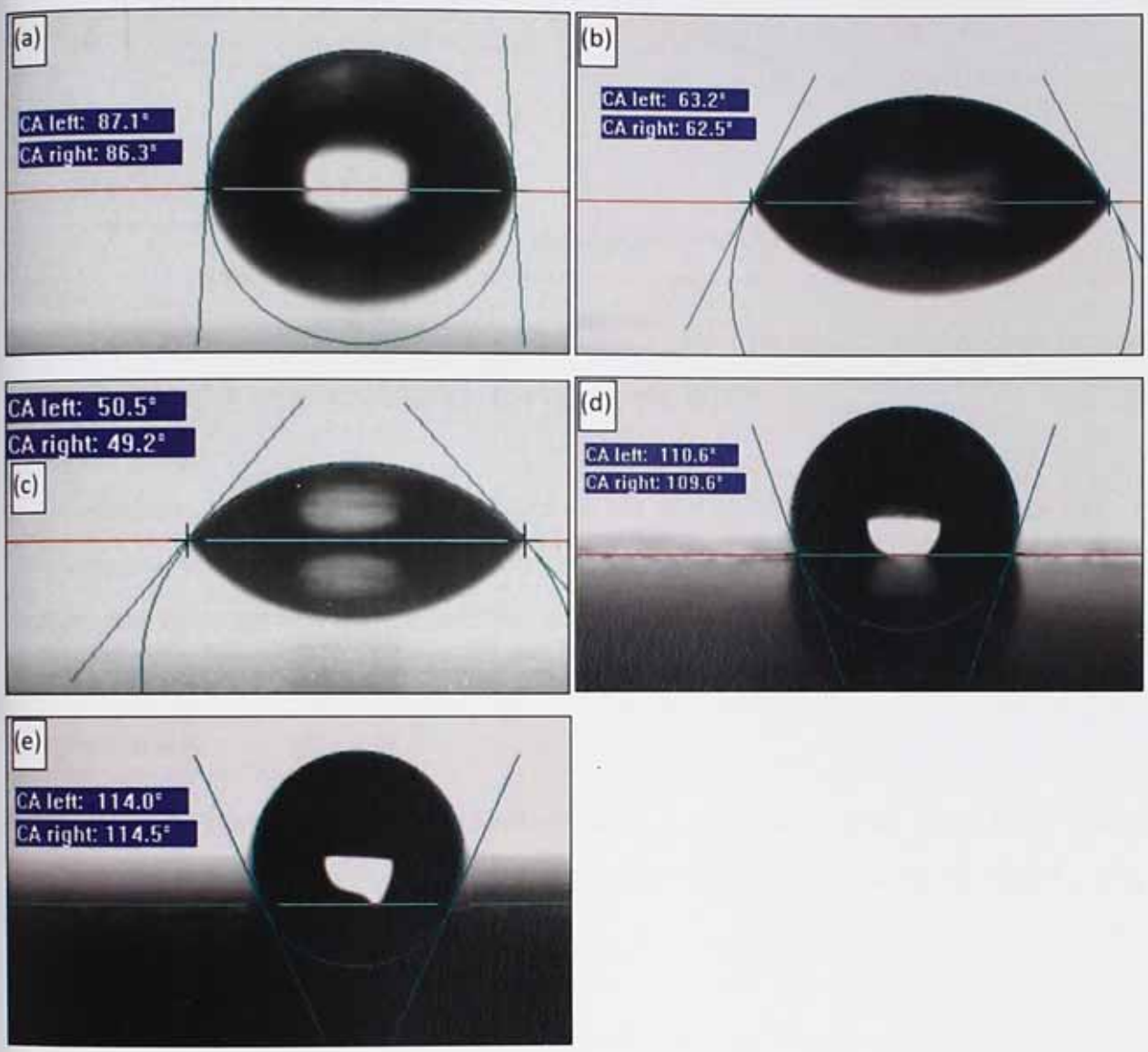

Figure 4.18 Contact angle measured on (a) degreased Q-panel, (b) abraded by 360 grit emery, (c) acid etched with 20% HCl for 100 Sec, (d) hydro-blasted and (e) abrasive blasted steel surface.

Apart from the surface free energy, the contact angle also depends on the surface roughness. It has been shown that wettability of steel surface improves by roughening the surface and varies slightly by the type of steel [30]. However, certain surface profiles may increase the contact angle by so-called the lotus effect [31] as shown in Figure 4.19.

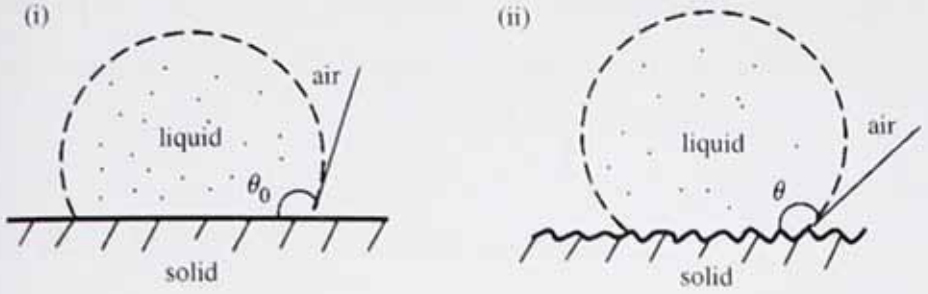

Figure 4.19 Schematic of a liquid droplet in contact with (i) a smooth solid surface (contact angle, θ_o) and (ii) a rough solid surface (contact angle, θ)[32].

To examine the effect of oxide structure on surface free energy it is necessary to calculate the corrected contact angle for smooth surfaces. For a rough solid surface with typical size of roughness details smaller than the size of the droplet as shown in Figure 4.19(ii), without air pockets, the contact angle is given by:

$$\cos\theta = R_f \cos\theta_o \qquad \text{(Eq. 4.2)}$$

where θ is the contact angle for the rough surface; θ_o is the contact angle for a smooth surface; and R_f is a roughness factor defined as the ratio of the solid–liquid area A_{SL} to its projection on a flat plane, A_F,

$$R_F = \frac{A_{SL}}{A_F} \qquad \text{(Eq. 4.3)}$$

Surface roughness was not considered a significant factor in varying the contact angle between degreased, abraded and acid etched surfaces since they all possess very similar A_{SL}/A_F values. From the Figure 4.16 R_F for hydro-blasted and abrasive blasted surfaces calculates 1.31 and 2.45. Thereby, the corrected contact angles of hydro-blasted and abrasive blasted surfaces are 105° and 99.5°, respectively. This implies that hydroblasting produces the most hydrophobic oxide layer with the lowest surface energy followed by the abrasive blasting. Contact angle measurement ranks the surface preparation methods in terms of surface free energy in the following order

Acid etch > abrasion > degreasing > abrasive blasting > hydroblasting

The very high surface energy produced by acid etching indicates that the oxide layer is an inconsistent film that leaves parts of the surface, chemically cleaner (oxide free) and very active [26]. The presence of oxide on the bare metal surface can significantly increase the

contact angle [33]. Takeda and Fukawa [34] found that contact angle is highly dependent on the presence and density of OH groups when measured for metal oxide surfaces.

4.3.5 Bulk electrochemical properties

OCP was measured during the first few hours of contact with 0.001 M NaCl. As shown in the Figure 4.20, in all 5 cases the potential dropped steadily down to more negative potentials suggesting a relatively quick breakdown of the air formed oxide layer and a growing anodic area. Decreasing OCP is a typical characteristic of porous oxide/hydroxide layer that only slows the rate of corrosion, but does not protect metal from further corrosion [35]. The fall in potential was too fast to be due to reducing oxygen concentration in the solution. Also the surface was open to air and thus oxygen was readily replenished. The hydroblasted and acid etched treatments show the largest potential drop (~ 0.45 V) indicating a reasonable conversion of cathodic area to anodic. The equation 4.4, Barnartt [36], explains how the change in anodic/cathodic area alters the corrosion potential.

$$f_a \neq 0 \text{ or } 1 : E_{corr} = E_{0.5} - \left[\frac{1}{b_a} + \frac{1}{|b_c|}\right] \log \frac{f_a}{f_c} \quad \text{(Eq. 4.4)}$$

where f_a and f_c are the fractions of anodic and cathodic area respectively so that $f_a + f_c = 1$, b_a and b_c are the anodic and cathodic slopes and $E_{0.5}$ represents the corrosion potential when anodic and cathodic area are equal ($f_a = f_c = 0.5$). The mechanism by which the potential drop may be explained relates to the faster movement of Fe(II) compared to OH^-. Due to the high solubility of $FeCl_2$ and OH^- they can move through the electrolyte and form the $Fe(OH)_2$ which is the initial form of solid corrosion product. As a result of higher mobility of Fe(II) to hydroxyl ions the ferrous hydroxide, $Fe(OH)_2$, usually precipitates at cathodic sites. Consequently the anodic area expands due to the build up of corrosion deposits on cathodic area which impedes the access to oxygen in those areas. The lower oxygen concentration shifts the potential towards negative direction (Nernst equation) which converts the cathodic site to anodic. This so-called "differential aeration" mechanism may be enhanced by presence of the hard-to-access sites on deep profiled (coarse) steel surfaces. The initially noble potential of hydro- and wet abrasive blasted surfaces is associated with the dense oxide layer formed as a result of the preparation method. In contrast, the noble potential of the acid-etched sample is believed to be a result of relatively

homogeneous surface after removal of grain boundaries which leaves an electrochemically more homogeneous surface.

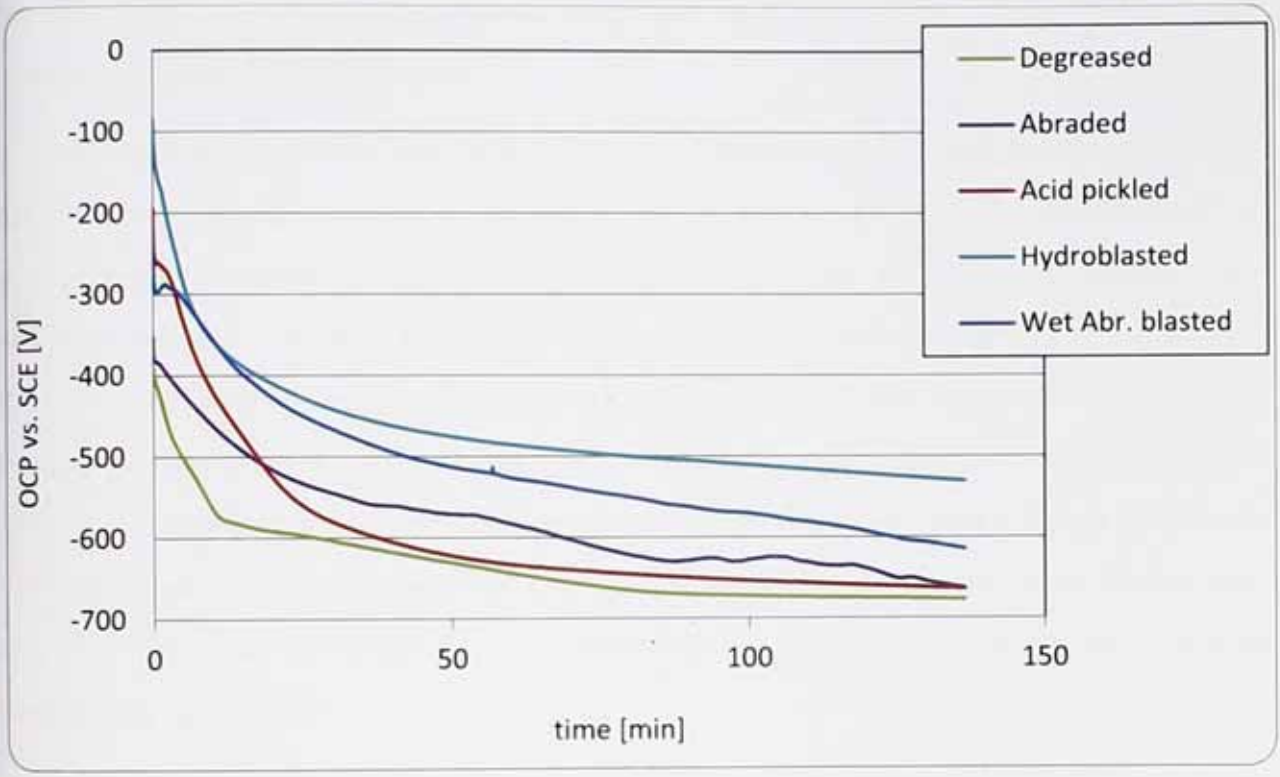

Figure 4.20 Open circuit potential (OCP) of the bare surfaces during the first 100 minutes of contact with 0.001 M NaCl.

Figure 4.21 compares the corrosion current density for different surfaces as measured by potentiodynamic polarization technique in 1 mM NaCl. In all cases the corrosion current increases in the early stages of contact with solution. This can be due to the process of establishment of anodic dissolution sites as described earlier in discussion of the OCP result. Further immersion in aqueous media results in the hydration and thickening of the pre-existing oxide that forms a porous layer and somewhat slows down the corrosion by diffusion polarization. This later stage can be clearly seen for degreased, abraded and acid etched surfaces resulting in a continued decrease in voltage. It takes significantly longer time until corrosion rate starts to drop for hydroblasted surface and for the abrasive blasted surface the corrosion rate continues to increase for the whole duration of measurement. This can be due to the higher stability of the pre-existing oxide film that delays the chloride induced break down and reformation of hydrated oxide film. A stable pre-existing oxide can

potentially act as galvanic cathode and accelerate the corrosion process. The reduction process of oxygen is believed to be the usual rate determining step in most forms of corrosion of bare steel. Therefore an efficient and stable cathode will significantly increase the corrosion rate. Also increased surface roughness and surface area provide larger number of anodic nucleation sites.

To further investigate the rate determining step of corrosion for these bare steel surfaces the changes of anodic and cathodic slopes, β_a and β_c, are plotted as a function of immersion time as shown in Figures 4.22 and 4.23, respectively. Relevance of β_a and β_c to the corrosion rate is described in appendix A. From comparison between corrosion current and β_a and β_c, it appears that β_a leads the changes in corrosion rate of hydro- and abrasive blasted surface. In other words the anodic process is the rate determining step in the corrosion of these two surfaces. This result further confirms the hypothesis of oxide film being a better cathode in the case of hydro- and abrasive blasted surfaces that obviate the cathodic polarization. Also this is in line with the assumption of larger number of anodes on these two surfaces provided by the increased roughness.

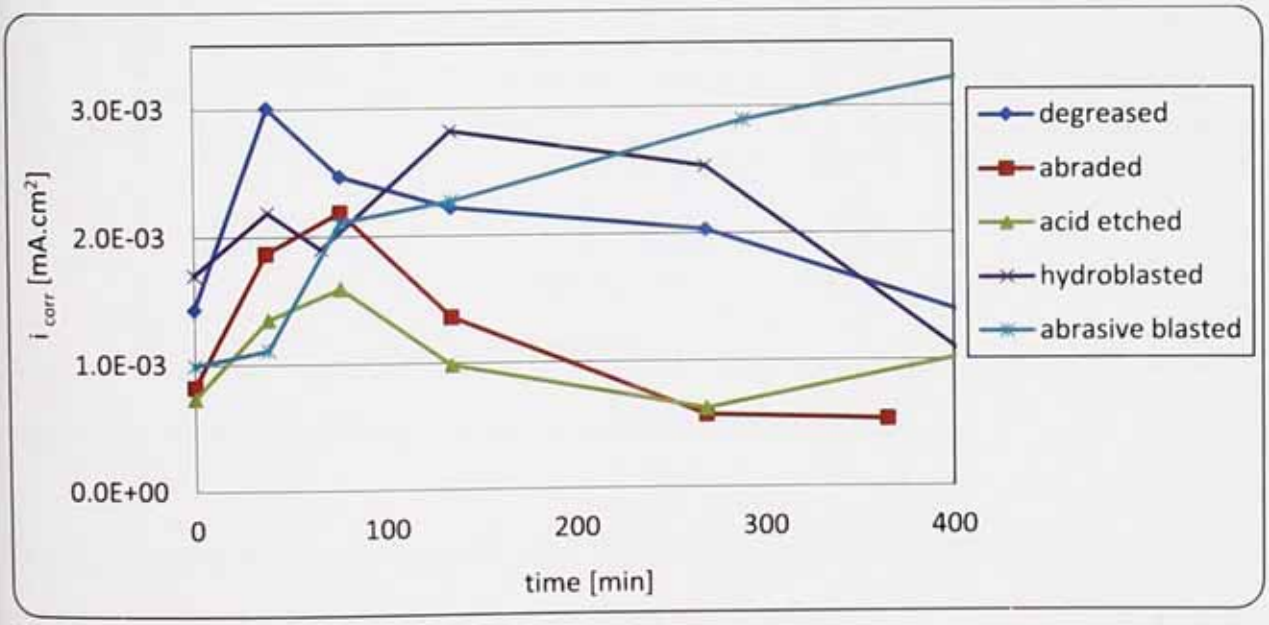

Figure 4.21 Corrosion current density measured by potentiodynamic polarization technique.

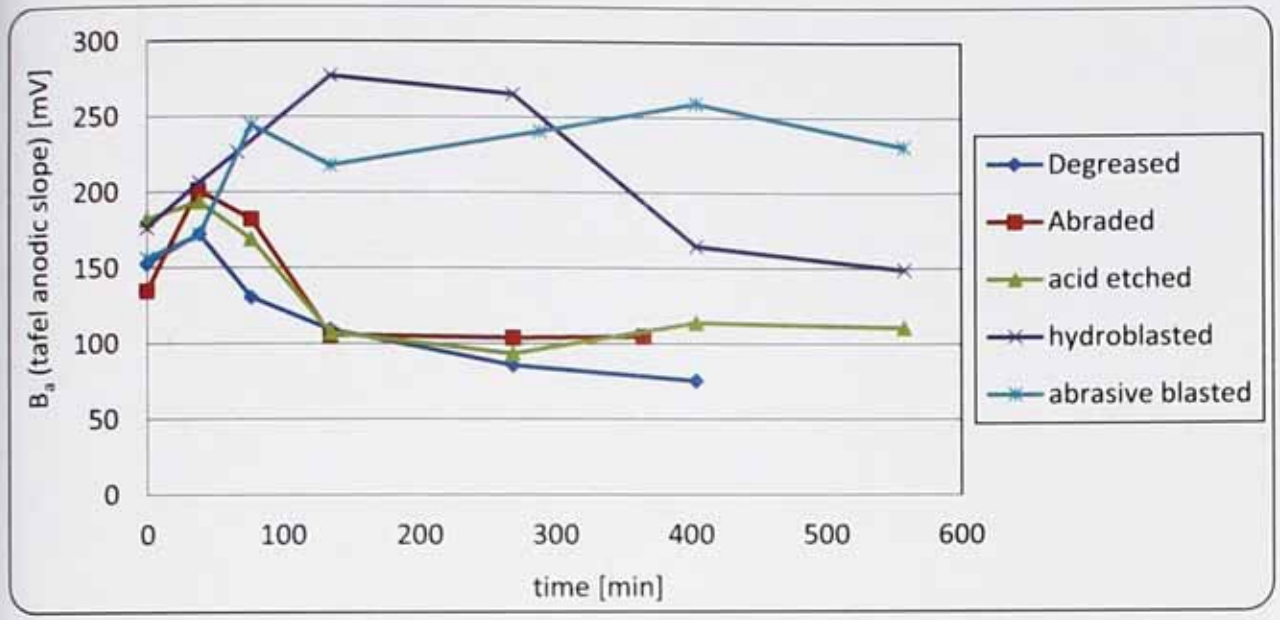

Figure 4.22 Tafel anodic slope, β_a, extracted from Evans diagram.

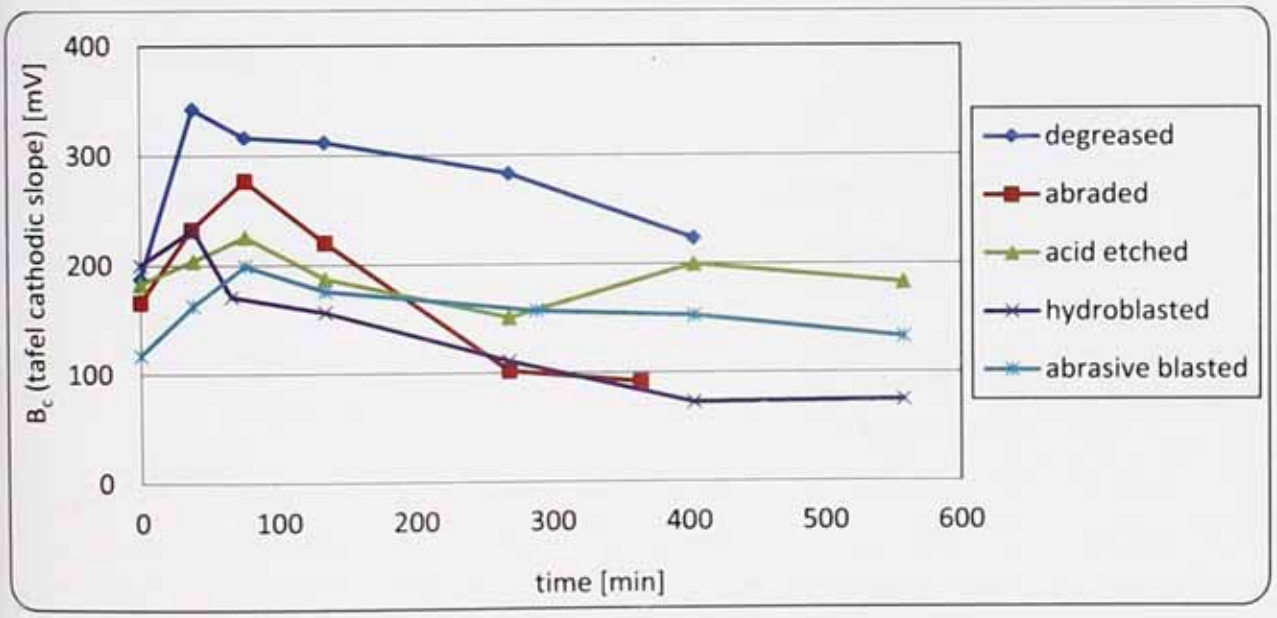

Figure 4.23 Tafel cathodic slope, β_c, extracted from Evans diagram.

The results from an EIS examination after 2 hr contact with 1mM NaCl solution is shown in Figure 4.24. Table 1 provides the electrical double layer capacitance, C_{dl}, and charge transfer resistance, R_{ct}, extracted from EIS results after 2hr immersion. C_{dl} expresses the relationship between the double layer dielectric constants, ε_r, surface area, A, double layer thickness, d via the equation 4.5:

$$C_{dl} = \frac{\varepsilon_o \varepsilon_r A}{d} \qquad \text{(Eq. 4.5)}$$

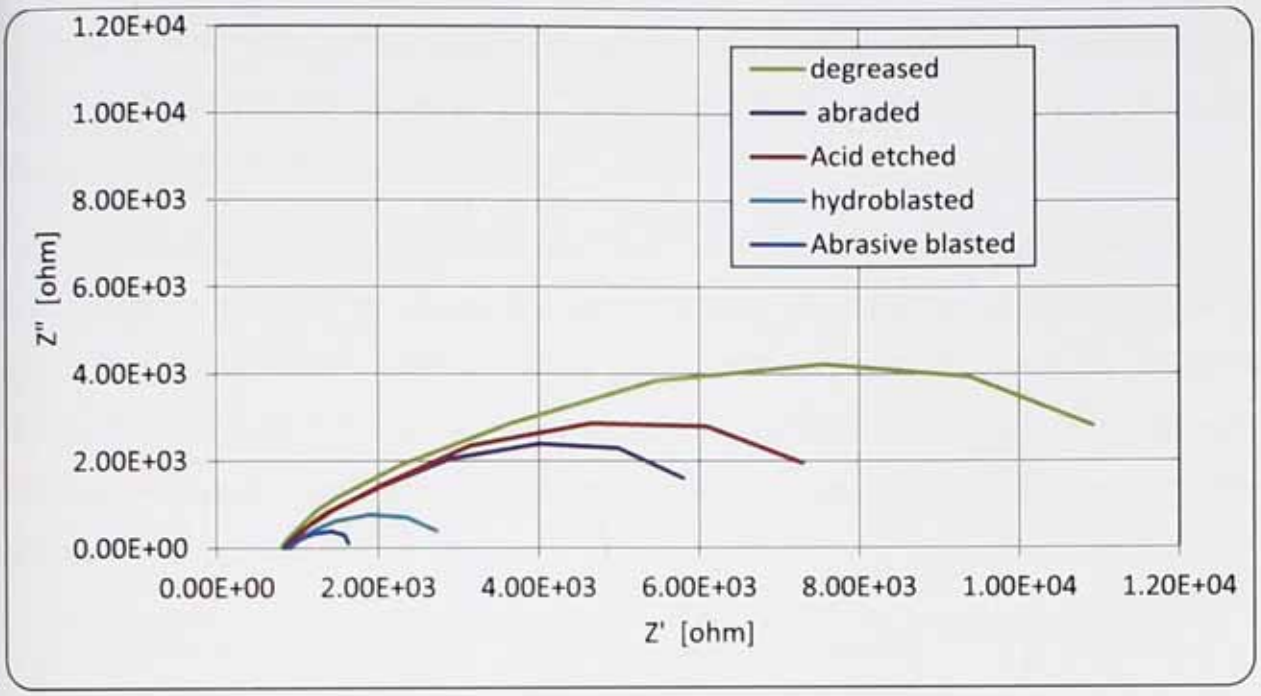

Figure 4.24 Nyquist plots after 2 hr contact with 0.001mM NaCl showing the effect of different preparations.

Table 4.1 R_{ct} and C_{dl} after 2 hrs contact with 0.001mM NaCl for different surface preparations (extracted from EIS results given in Figure 4.24 using Randles equivalent electrical circuit).

	degreased	abraded	acid etched	hydro-blasted	abrasive blasted
R_{ct} [$\Omega.cm^2$]	9143	4737	5988	1683	739.1
C_{dl} [$F.cm^2$]	1.248E-4	2.531E-4	1.617E-4	1.539E-3	2.929E-3

The immediate implication of the table 1 is that the charge transfer is much easier on hydro- and abrasive blasted surfaces than on the degreased, abraded and acid etched surfaces. Although the rougher surface of hydro- and abrasive blasted steel provide larger surface area that independently results in smaller R_{ct} and larger C_{dl}, but differences are far larger than could be caused by only the larger surface area. As suggested earlier, the oxide layer on these two surfaces makes a good cathode which facilitates the charge transfer process and reduction reaction. The larger C_{dl} of hydro- and abrasive blasted samples can be explained by their higher anodic activity. It was concluded from OCP results that a larger

fraction of hydro- and abrasive blasted surfaces are anodes compared to the other three surfaces. In other words larger fraction of surface is covered by corrosion product which is a highly dielectric material. Consequently, general capacitive behaviour of surfaces increases which is indicated by larger C_{dl}.

Resistive/capacitive behaviour of hydro- and abrasive blasted surfaces was further investigated by studying the C_{dl} and R_{ct} components of EIS result as a function of time. In both cases, capacitance initially increases and then consistently decreases as shown in Figures 4.25 and 4.26. The initial rise of capacitance is attributed to the build up of corrosion deposits and hydration of the pre-existing oxide film that forms a layer with higher dielectric constant.

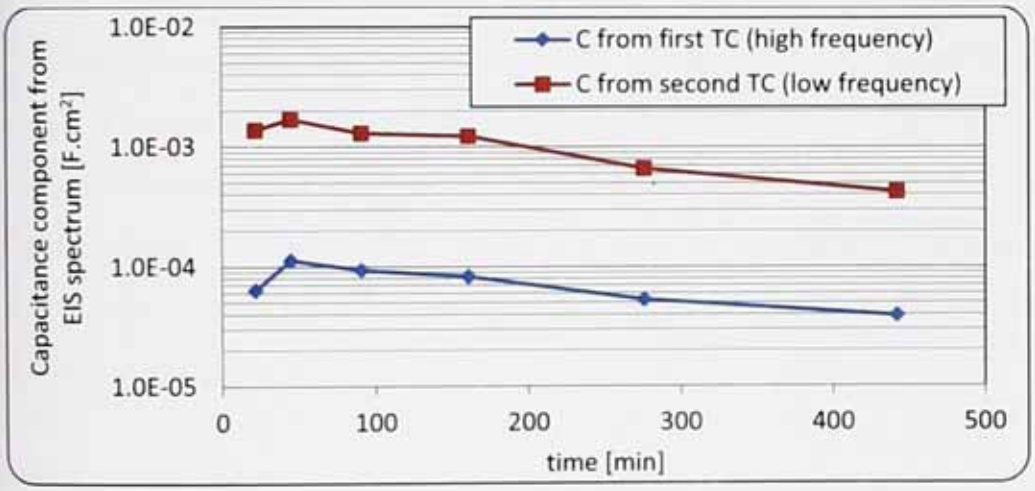

Figure 4.25 Capacitance component from EIS spectrum of Hydro-blasted steel in 1mM NaCl.

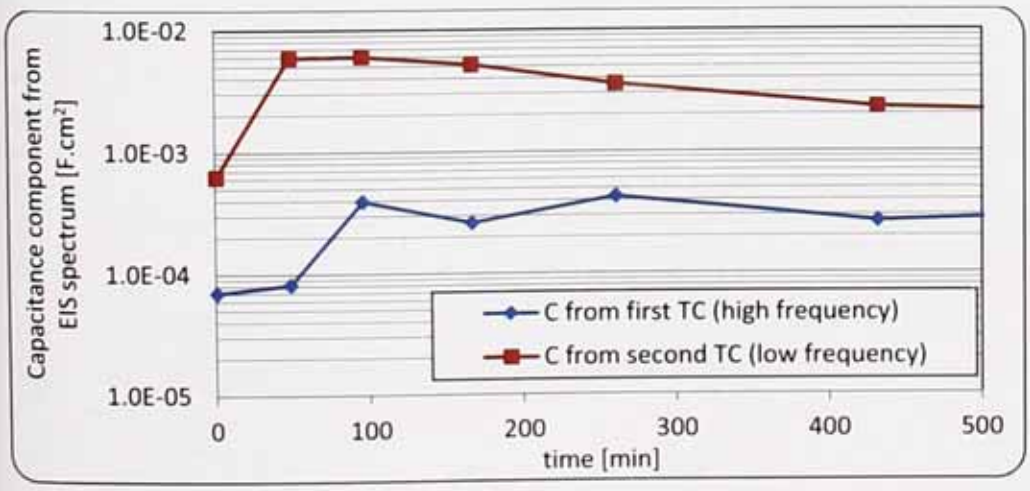

Figure 4.26 Capacitance component from EIS spectrum of abrasive blasted steel in 1mM NaCl.

The more interesting observation was variation of charge transfer and mass transfer resistances at high and low frequency regions, respectively, for hydro- and abrasive blasted surface, Figures 4.27 and 4.28. The low frequency range represents the mass transfer phenomena or diffusion resistance. Both Figures indicate an initial drop and then rise of diffusion resistance. The initial drop is attributed to the initial break down of the pre-existing oxide which facilitates the access to surface and reduces the diffusion resistance. This is followed by build-up of corrosion deposit on the surface which forms a porous oxide film and impedes the diffusion. From the high frequency range the charge transfer phenomena can be studied. Figure 4.27 shows an initial drop and then slight rise of charge transfer resistance for hydroblasted surface. This is connected with the formation of relatively dense and adherent oxide that limits the access of electrolyte to metal in the long term. In contrast, a significant decrease of charge transfer resistance is observed for abrasive blasted surface indicating that the aqueous formed oxide layer affords less protection than the pre-existing oxide. The new oxide does not adhere to the metal surface as good as the pre-existing oxide resulting in a larger area exposed to electrolyte as the new oxide replaces the pre-existing one.

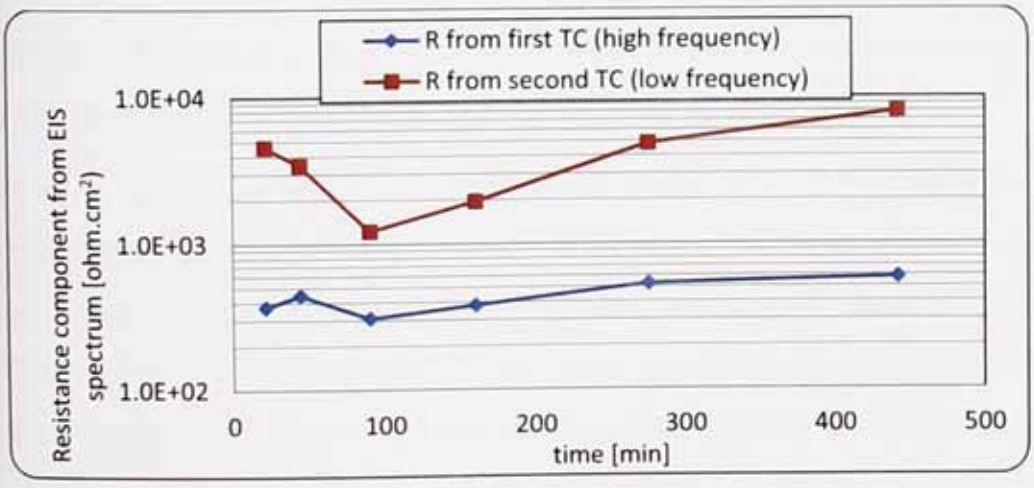

Figure 4.27 Resistance component from EIS spectrum of Hydro-blasted steel in 1mM NaCl.

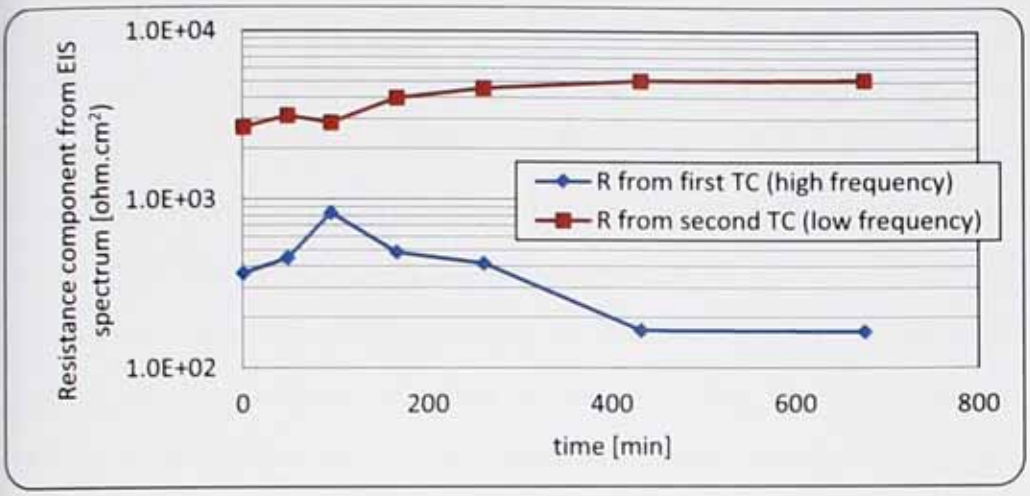

Figure 4.28 Resistance component from EIS spectrum of abrasive blasted steel in 1mM NaCl.

4.3.6 Local electrochemical mapping

Figures 4.29 – 4.33 illustrate the electrochemical activity and the map of local current density 5 min and 2 hr after contact with 0.001 M NaCl. The areas with red colour represent the anodic sites. The least anodic activity is observed on the as-received sample where no chemical or mechanical preparation was applied other than degreasing. The most active sample was the wet abrasive blasted surface which had the largest surface profile. It appears that the number of initial anodic sites plays a key role in the long term anodic/cathodic activity and it varies by the surface preparation method. Surfaces with coarse surface profile present a larger active area. This is due to the larger number of defects and irregularities that increase the chance of anode formation.

In all cases the surface has became more anodic after 2 hr contact with electrolyte in comparison with 5 min immersion. This is a result of precipitation of the corrosion product on the surface that limits the access to oxygen. As suggested earlier by OCP results (Figure 4.20), these local areas turn into anodic sites resulting in a generally more noble potential. The number of initial anodic sites plays a key role in the long term anodic/cathodic activity and it varies by the surface preparation method. Comparison between different surface treatments reveals that the surface roughness has a significant effect on the number of initial anodic sites. According to the profilometry results the surface roughness can be ranked in following order:

abrasive blast > hydroblasted >> degreased = acid etched > abraded

In the case of hydro- and abrasive blasted surfaces the anodic activity seems to follow the surface geometry and the roughness profile. Also a relatively large number of anodes are observed on the abraded surface. This can be due to the larger number of anode nucleation sites compared to the degreased surface as shown earlier by profilometry results (Figure 4.12), even though the irregularities produced by abrasion have slightly lower depth. Comparison between anodic activity of degreased, acid etched and abraded surfaces, suggest that apart from the effect of surface profile, the type and structure of the pre-existing oxide film also play an important role in determining electrochemical activity. It was shown earlier (section 4.3.3) that the oxide film on the acid etched surface has much higher surface free energy than that of the degreased surface. This could explain the higher anodic activity of acid etched surface despite their similar surface profile.

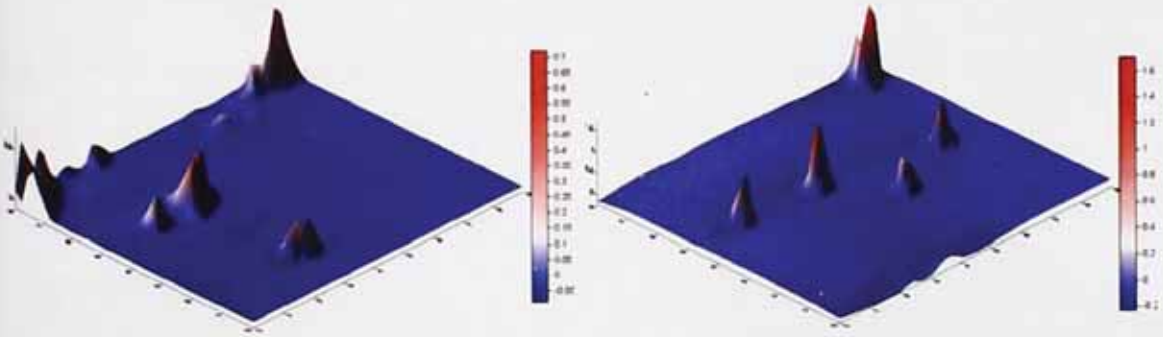

Figure 4.29 local current density maps of degreased sample after 5 min (left) and 2 hrs (right) contact with 0.001 M NaCl.

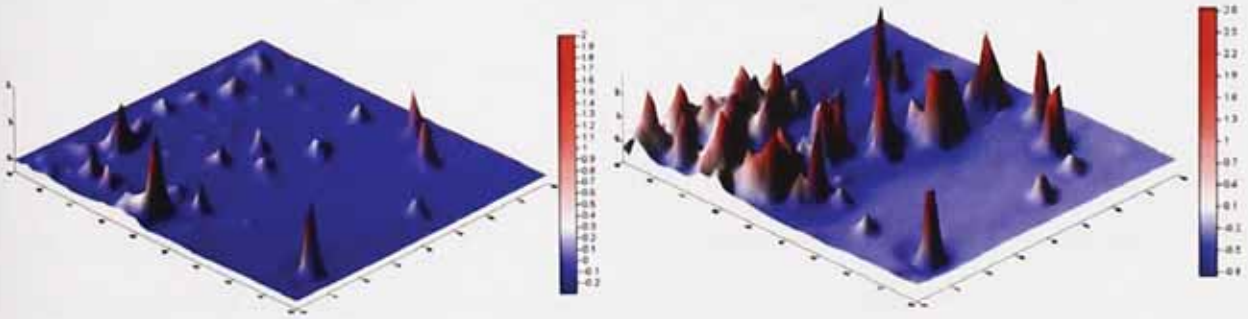

Figure 4.30 local current density maps of abraded sample after 5 min (left) and 2 hrs (right) contact with 0.001 M NaCl.

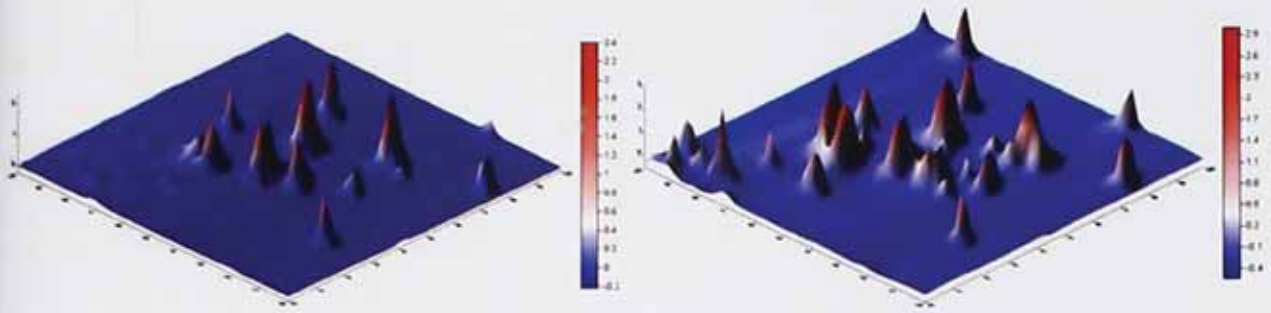

Figure 4.31 local current density maps of acid-etched sample after 5 min (left) and 2 hrs (right) contact with 0.001 M NaCl.

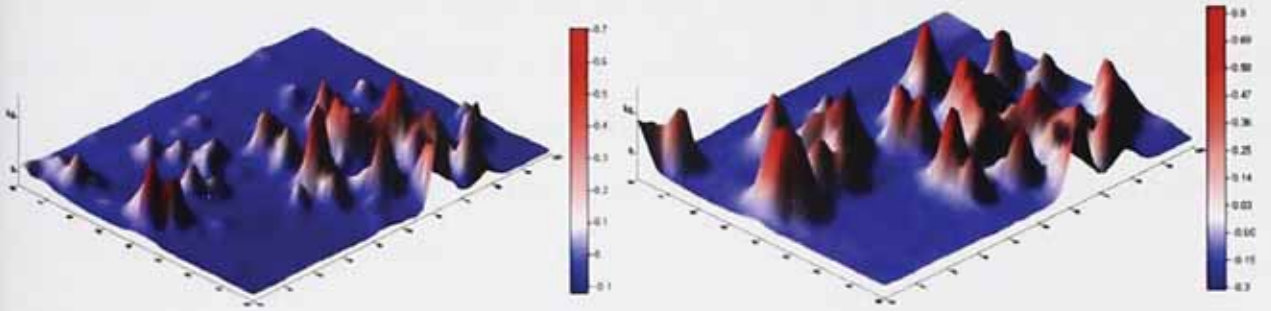

Figure 4.32 local current density maps of hydroblasted sample after 5 min (left) and 2 hrs (right) contact with 0.001 M NaCl.

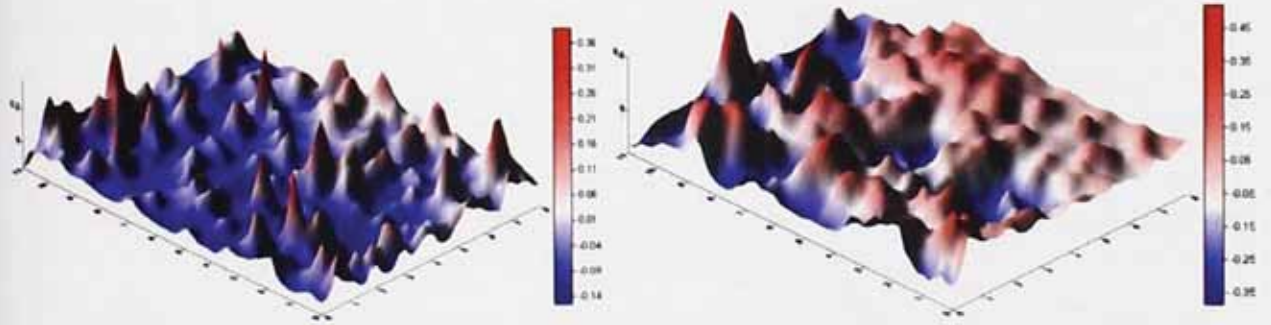

Figure 4.33 local current density maps of abrasive blasted sample after 5 min (left) and 2 hrs (right) contact with 0.001 M NaCl.

The importance of anodic/cathodic activity of metal surface is more pronounced by comparing the SVET results with bulk corrosion measurements. SVET results confirmed that there is an inverse relationship between the charge transfer resistance and anodic activity of surface as suggested earlier from bulk electrochemical measurements. The SVET results also imply that current density at individual anodes is inversely proportional to the surface free energy. The largest local current density was detected on the acid etched and the abraded surface with higher surface free energy (section 4.3.3) while the local current density was lowest on hydro- and abrasive blasted surfaces with lowest surface free energy.

4.4 Results and discussion. Part 2

Effect of surface preparation on corrosion resistance of organically coated steel

4.4.1 Electrochemical examination

The DC resistance was used as a general indication of corrosion protection afforded by the coating. This was regularly measured for both the alkyd paint (Figure 4.34) and alkyd varnish (Figure 4.35) coatings in 0.5 M NaCl solution at ambient temperature. The highest resistance, with both coating systems, was obtained with the hydroblasting surface preparation while the most remarkable deterioration in resistance was observed on the abraded and wet abrasive blasted surfaces.

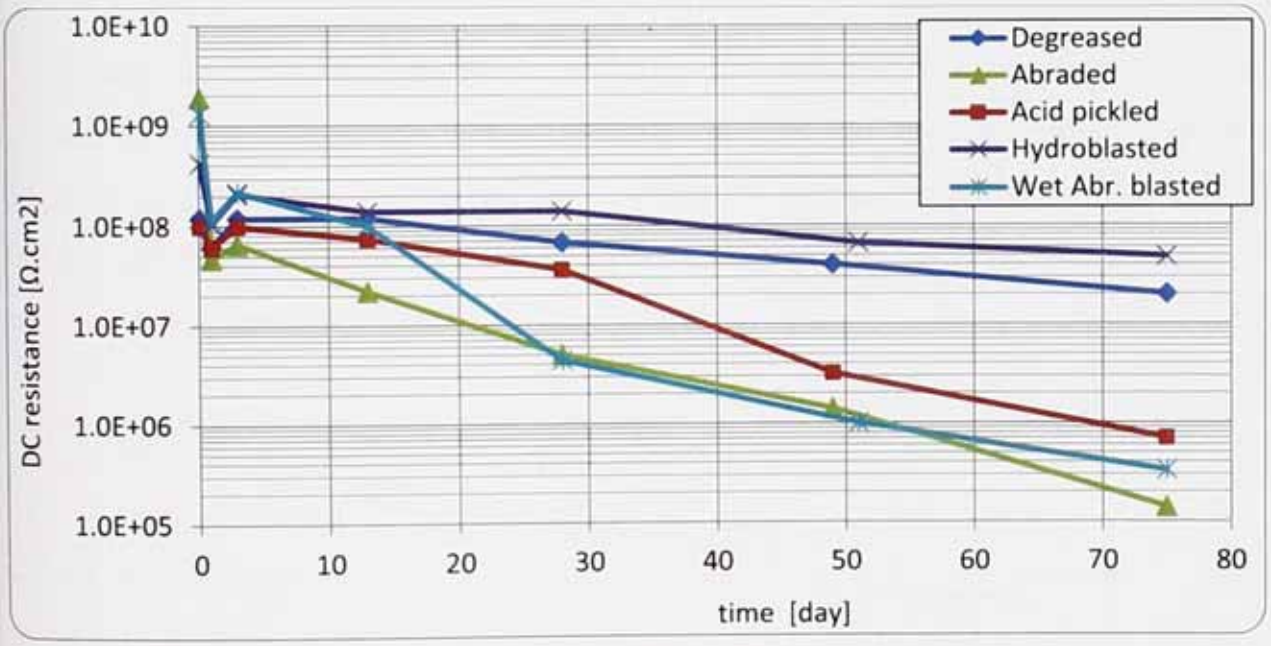

Figure 4.34 DC resistance of alkyd paint on differently prepared steel surfaces during 75 days immersion in 0.5 M NaCl.

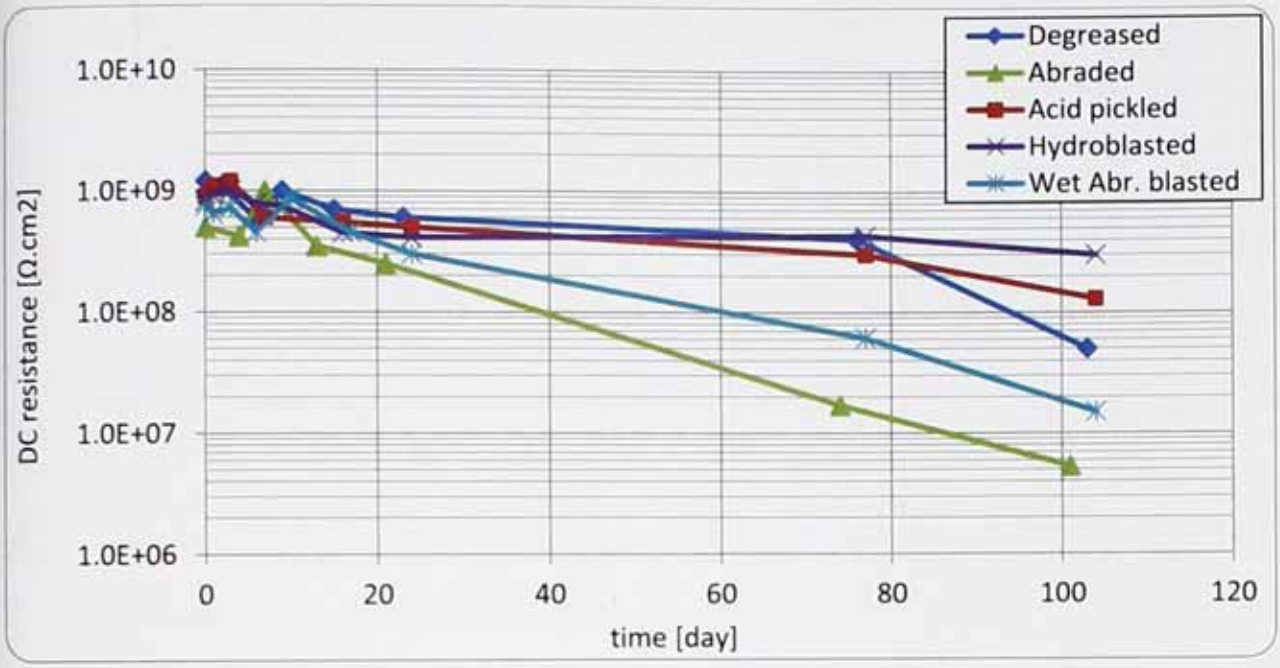

Figure 4.35 DC resistance of alkyd varnish on differently prepared steel surfaces during 104 days immersion in 0.5 M NaCl.

As-received, hydro- and abrasive blasted surfaces were further studied with water-borne polyurethane (WB PU), solvent based polyurethance (PU) and epoxy-polyamide coatings. Samples were placed in oven at 40°C to accelerate the experiment. Results, as shown in Figures 4.36-4.38, reveal the poor performance of abrasive blasted surface which is in-line with the earlier results obtained from alkyd systems.

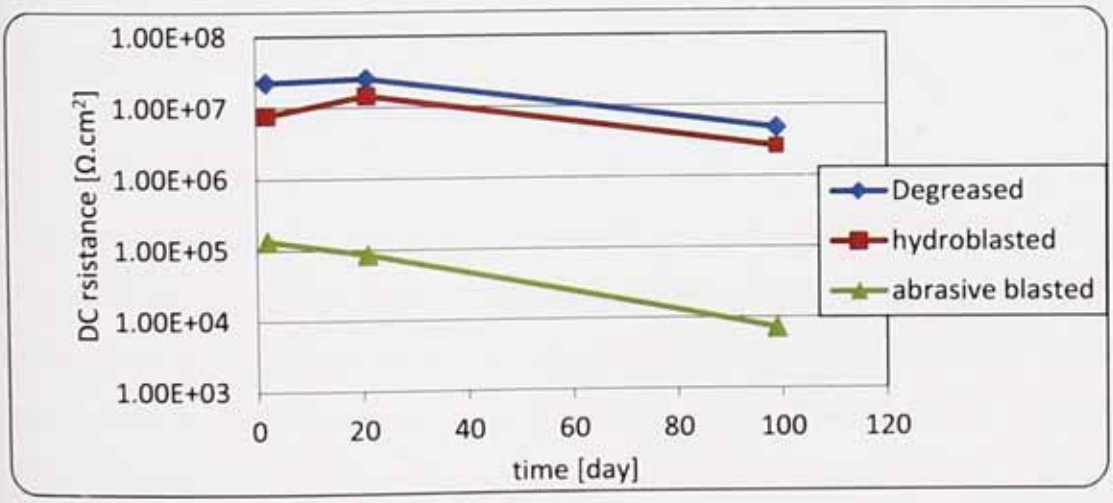

Figure 4.36 DC resistance of water-borne polyurethane on differently prepared steel surfaces during 99 days immersion in 0.5M NaCl at 40°C.

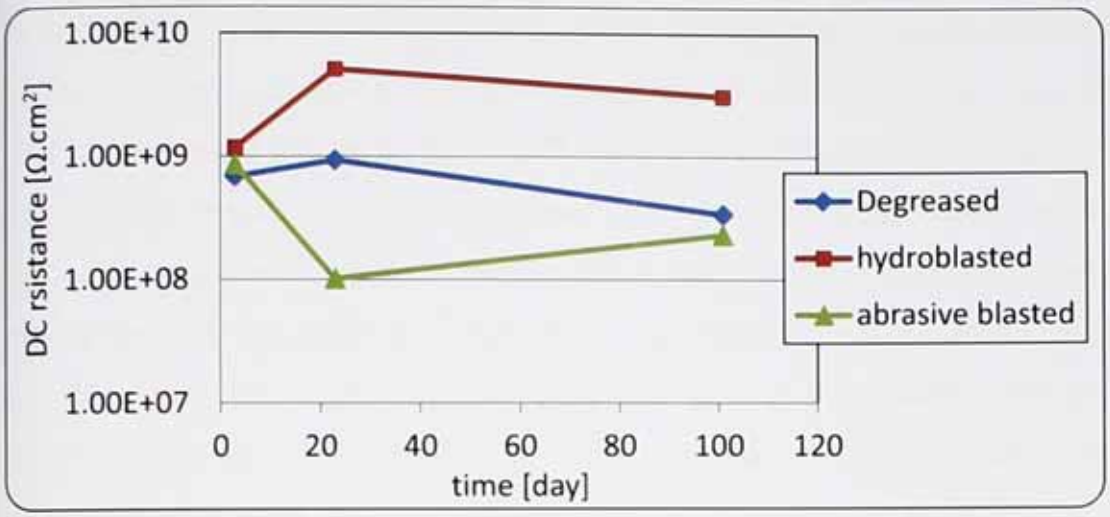

Figure 4.37 DC resistance of solvent based polyurethane on differently prepared steel surfaces during 101 days immersion in 0.5M NaCl at 40°C.

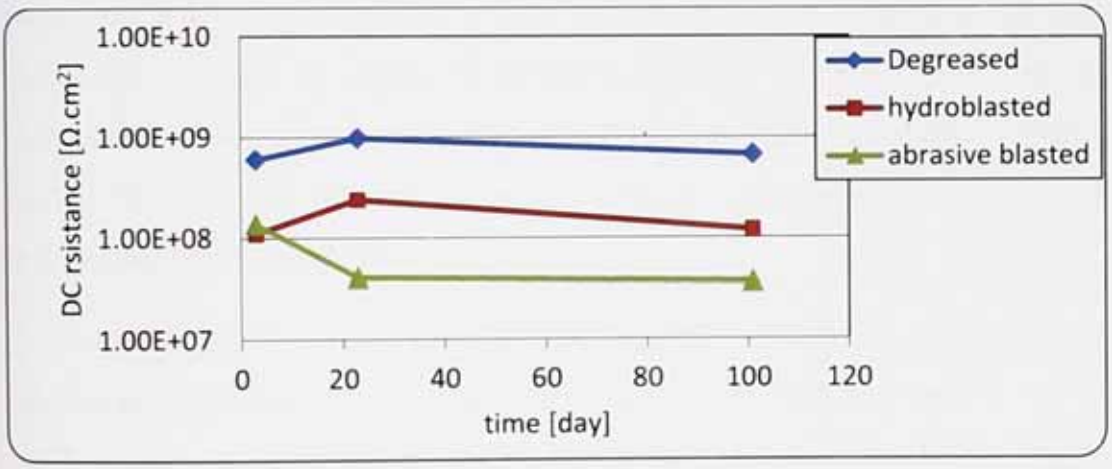

Figure 4.38 DC resistance of epoxy-polyamide on differently prepared steel surfaces during 101 days immersion in 0.5M NaCl at 40°C.

The fluctuations observed during the first 10-15 days of immersion of alkyd systems (Figures 4.34 and 4.35) are probably due to the pore plugging process [37]. In the early stages of immersion the aqueous pathways are not opened up enough yet to transport the solid corrosion product away. Soluble anodic reaction products, mostly Fe^{2+}, while travelling through ionic pathways may meet oxygen and turn into insoluble oxide forms, Fe^{3+}. Consequently the ionic resistance increases temporarily until pathways expand further and micro-capillaries open up again.

After 24 hrs the DC resistance has dropped down by about 1.5 orders of magnitude on the abrasive blasted and abraded surfaces coated with alkyd paint. It should be noted that

both abraded and wet abrasive blasted surfaces had high level of anodic activity as observed by SVET (Figures 4.30 and 4.33) with large number of anode nucleation sites. This suggests that surface activation is beneficial for making stronger electrostatic bonds with polar groups of polymeric coating and high level of corrosion protection before water molecules reach the substrate. However, in the long term highly active surface may provide a stronger driving force for the other polar substance, e.g. water molecules, to adsorb on the metal surface [38]. This result suggests that the surface preparation without producing appropriate surface morphology and oxide characteristics will be detrimental for the protection afforded by an organic coating.

Severe surface contamination after abrasive blasting as demonstrated in Figures 4.9a-4.9e and 4.10 and porous structure of oxide as indicated by EIS results (Figure 4.28) are suggested as the main reasons for poor performance of coating on abrasive blasted steel. Also large variation of coating thickness due to the surface profile may contribute to formation of differential aeration corrosion cells as a result of resistance variation across the coating [39,40]. This provides additional driving force for under-film corrosion and the subsequent coating degradation.

After 75 days DC resistance has dropped by about 4 orders of magnitude on the abrasive blasted and abraded surfaces coated with alkyd paint. This was despite the fact that both systems offered the highest protection at the early stages of test. In the long term, coating disbondment occurs and the wet interface spreads beneath the coating. This is mainly due to the hydrolysis of polymer bonds and/or dissolution of pre-existed oxide film on the metal. Consequently a larger fraction of the substrate will be exposed to electrolyte which drastically reduces DC resistance and the protection level.

As-received and hydroblasted surfaces provided highest level of protection with both alkyd systems. These observations are consistent with earlier findings of Mills and Schaefer [12]. Despite the high anodic activity of hydro-blasted steel (SVET results, Figure 4.32), it affords consistently high level of protection when coated by either paint or varnish alkyd systems. This can be explained by the passivity of the pre-existing oxide film. The relatively noble behaviour of hydroblasted surface was previously illustrated by OCP measurements. Also EIS studies (Figure 4.27) suggested formation of a dense and adherent oxide resulted by aqueous corrosion. It is believed that the hydroblasting produces a relatively stable oxide

film capable of making effective bonds with the alkyd coating to afford consistent corrosion protection. Also it should be noted that both hydroblasted and as-received surfaces had relatively low surface free energy indicating the chemical passivity as measured by contact angle test (section 4.3.3). Hydrophilic/hydrophobic properties of oxide layer to a large extent determine the structural changes of the coating/substrate interface after ingress of water [41]. Therefore the expansion of wet interface is minimized which results in the long term better performance of as-received and hydroblasted surfaces.

Studies with water-borne and solvent base polyurethane and epoxy-polyamine coatings further confirm the above findings. In the cases of solvent base PU and epoxy-polyamine coatings, an initially high resistance of abrasive blasted sample is followed by decreased resistance in the long term. As explained earlier, the good performance in the early stages is due to the strong interfacial bonding in the absence of water. Subsequently, after the ingress of water, surface contaminations and weak oxide film promote the corrosion process in the long term. This is more pronounced in the case of water-borne PU coating where high hydrophilicity of coating warrants extensive access of water to substrate. Thereby micro corrosion cells are formed even after 2 days resulting in very poor performance of coating on abrasive blasted steel.

In general these results agree with the work conducted previously on alkyd and vinyl painted surfaces [12]. This is also in agreement with a previous study revealing increased susceptibility to corrosion of organically protected metals with more active surface, e.g. more deterioration of coating on aluminum substrate compared to steel substrate [42]. Higher ionic resistance was also observed for an alkyd coating when applied to a platinum substrate compared to the same coating when it was applied to steel substrate suggesting that the degree of activity of the substrate assists the delamination and increases the likelihood of corrosion [43].

4.4.2 Adhesion

As part of the studies to elucidate the effect of surface preparation on protection afforded by organic coating, adhesion was examined. The aim was to determine whether the anti-corrosive performance is dominated by the coating barrier properties or by the interfacial adhesion quality. Wet adhesion results as function of time of contact for alkyd

paint and alkyd varnish coated samples are given in Figures 4.39 and 4.40 respectively. The results for the hydroblasted and the wet abrasive blasted samples are much higher, with hydroblasted giving higher wet adhesion than the abrasive blasted. The results also show that there is not much difference between the wet adhesion of the as-received, acid etched and abraded samples. Throughout the experiment they were all several orders lower than the highly profiled hydro- and abrasive blasted surfaces.

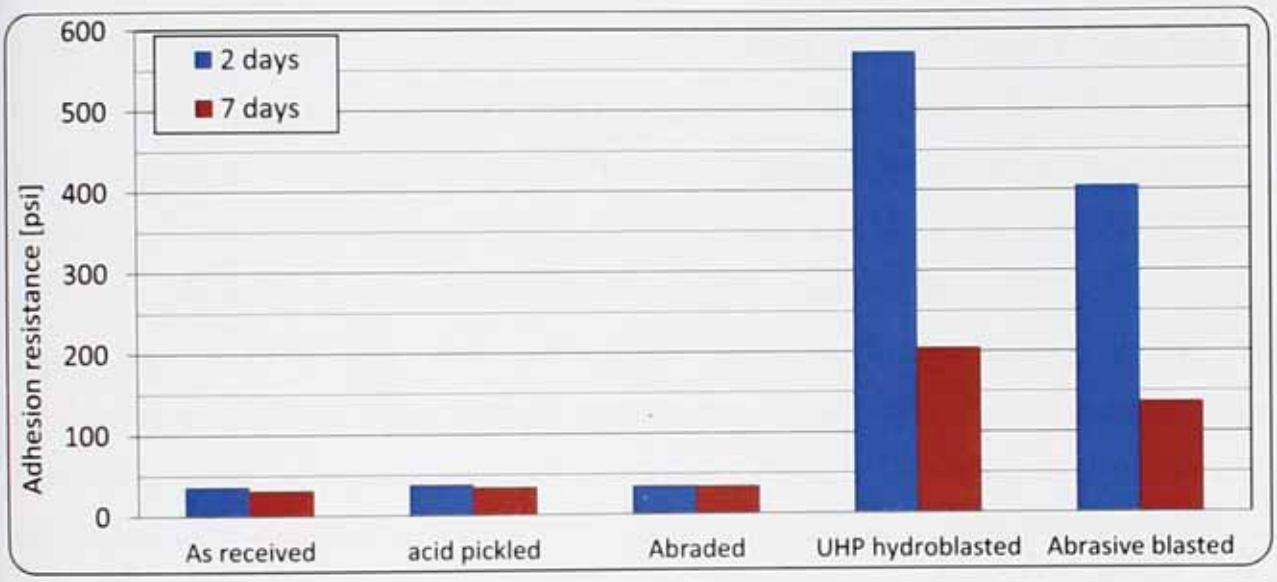

Figure 4.39 Wet adhesion of alkyd paint on differently prepared steel surfaces after 2 and 7 days in 0.5 M NaCl.

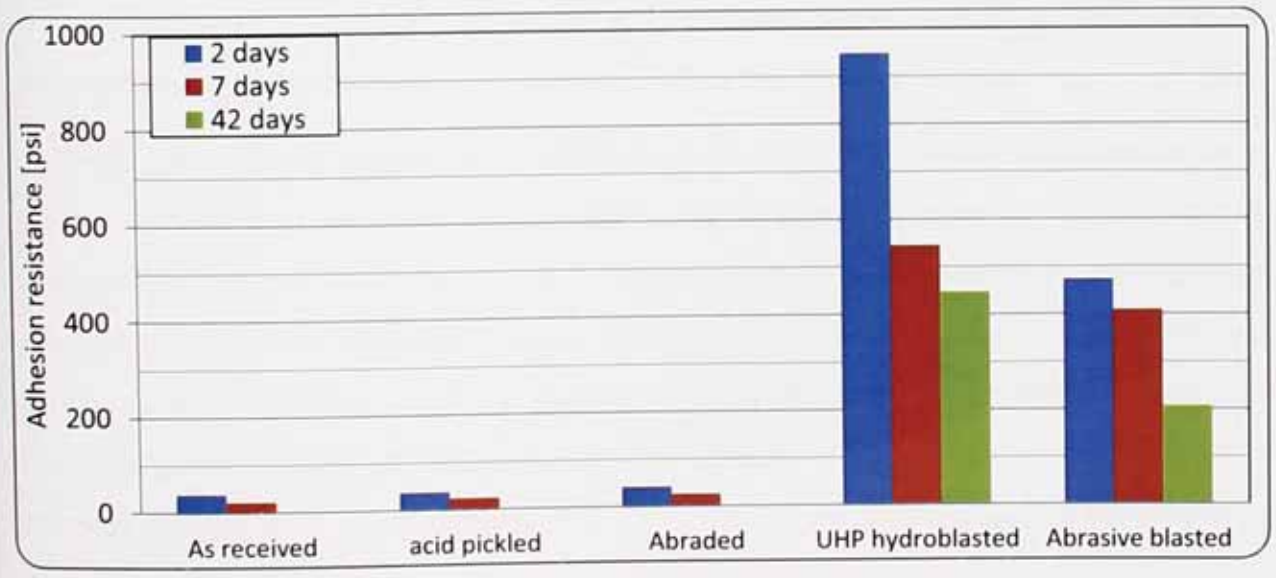

Figure 4.40 Wet adhesion of alkyd varnish on differently prepared steel surfaces after 2 and 7 days in 0.5 M NaCl.

The immediate implication of adhesion results is the key role of surface profile on adhesion regardless of the protection level. An increase of available surface area for adhesion or more mechanical interlocking sites for the coating to adhere would explain superior adhesion to highly profiled surfaces. All samples show a drop between two days and seven days as a result of wet interface spreading underneath the paint film. They continue to show a reduction in adhesion up to 42 days with the higher adhesion of the hydroblasted samples compared with the wet abrasive blasted being maintained.

Dry adhesion measurement (data not presented here) revealed similar performance of hydro- and abrasive blasted surfaces both taking the form of cohesive failure of the coating. Wet adhesion measurement on the hydro- and abrasive blasted preparations shows a reasonably higher level of adhesion on hydroblasted steel with both coating systems. This is due to the higher surface free energy of wet abrasive blasted surface which adsorbs more water and expands the wet surface at interface. It has been shown that hydrophilic/hydrophobic properties of oxide layer are directly reflected by differences of the polymer/substrate adhesion forces and will be maintained during the subsequent stages of immersion [41]. Abrasive blasting increases the surface area remarkably by 2.37 times (Figure 4.16) thus provides larger interface and improves the adhesion despite localized coating degradation and corrosion. Hydroblasting also increases the roughness and surface area by about 27% hence promotes the adhesion through the mechanical interlocking. However in the long term electrochemical stability seems to be more effective resulting in better adhesion on hydroblasted surface compare to the abrasive blasted.

This is believed that detachments initially take place at locally lower resistance areas of paint so-called "D" type areas with Direct relationship between the diffusion and ionic strength. Since these detachments take place at relatively small regions of coating/metal interface, the general adhesion level is significantly higher on abrasive blasted surface compared to the smooth surfaces, degreased, abraded and acid etched. However the corrosion protection was probably more greatly influenced by local detachments. Work in the next chapter looks at the concept of D areas, their origin and distribution on a range of organic coatings.

4.4.3 Further discussion on the adhesion results with respect to the surface profile

If the varying heights along a profile of a (rough) surface are considered as a distribution, it is possible to gauge whether a profile is skewed towards broad peaks and spike-like valleys, or towards broad valleys and spike-like peaks. The parameter used to give this information is skewness or S_{SK}. It has been shown that negatively skewed profile may prevent the perfect wetting of substrate by paint and result in poor bonding between the surface irregularities and the paint [26]. Figure 4.41 shows a very simple schematic of how positively and negatively skewed surfaces may impact the wetting and resultant bonding. Liquid paint on a negatively skewed surface would not flow into the sharp valleys as much as it flows into broad valleys. Average skewness of surface profiles as measured by optical profilometry were: as-received 0.34, abraded -0.17, acid etched -0.23, Hydro-blasted -0.37 and abrasive blasted -0.57 with the as-received specimen being the only positively skewed surface. Abrasive blasted was the most negatively skewed profile followed by the hydroblasted surface. However with the very large irregularities on blasted surfaces it is highly unlikely that paint does not penetrate inside the grooves to wet the substrate. Also very similar dry adhesion result (data not presented here) on as-received, abraded and acid etched surfaces suggests that liquid paint has established the maximum interface with all surfaces regardless of their skewness. This conclusion is very important since it proves that differences in wet adhesion are originated from spreading the wet interface underneath the paint and electrochemical phenomena and not due to the lack initial bonding between coating and substrate. However, the insignificance of dry adhesion on anti-corrosive properties of organic coating has been shown elsewhere [44–46] and therefore dry adhesion was not considered a criterion of ranking the protectiveness of coatings.

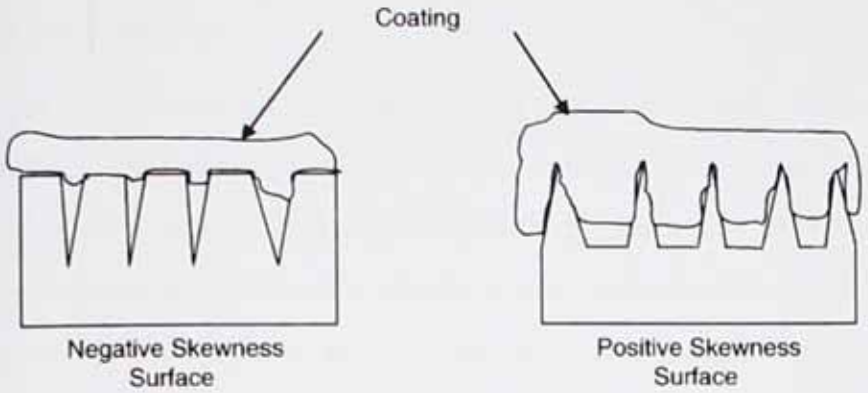

Figure 4.41 Simplistic schematic showing possible splat interaction with negative and positive skewness value surfaces [26]

Contrary to traditional beliefs, this result implies that the overall adhesion strength may play a minor role on the anti-corrosive performance of organic coating. It is believed that a certain level of adhesion is required to eliminate the short circuit between anodic and cathodic regions underneath the coating, but as long as this condition is fulfilled, ionic resistance controls the corrosion rate.

4.5 Summary

This study shows that activation of the surface by means of a surface preparation method could be detrimental to protection afforded by an organic coating, when it does not produce an appropriate oxide film which can withstand breakdown underneath the paint layer. Bare metal surface characterization provides valuable insight into the effect of surface profile, surface free energy and electrochemical properties of pre-existing oxide on the performance of organic coating.

UHP hydroblasting has shown great promise as a modern environmentally friendly replacement for the traditional wet abrasive (garnet) blasting surface preparation method. The reduced surface profile produced by UHP hydroblasting will save a significant amount of the paint required to fill in the surface irregularities when compared with the coarse surface finish obtained by the wet abrasive blasting. It also improves the anti-corrosive properties of organic coating in the long term by producing a contaminant free surface and a densely packed oxide layer capable of making effective bonding with the paint system.

Results of this study have shown that also the level of wet adhesion may not be a reliable criterion for the corrosion protection in some cases. Corrosion may proceed through the small regions of relatively lower ionic resistance causing local detachments while the overall adhesion maintains an acceptable level. It is believed that the absolute value of adhesion beyond the minimum requirement for elimination of the short circuit (between anodic and cathodic sites underneath the coating) is of little importance in determining the anti-corrosion performance of an organic coating.

It is believed that upon the exposure of painted steel to water, spreading the wet interface as a result of ingress of water initially weakens the interfacial bonding even in the absence of corrosion. Subsequently micro galvanic cells establish underneath the paint initiating the oxidation/reduction process. Here ionic resistance of the paint film will decide whether the corrosion can make any further progress or it should stop.

Publications

- D.J. Mills and S.S. Jamali, Effect of different surface preparations prior to painting on the corrosion behaviour and surface activity of mild steel. European Corrosion Conference (EUROCORR) 2010: From Space Heights to Earth's Depths, Moscow, Russia, 13-17 September 2010. Frankfurt, Germany: Dechema. Proc. Published by Curran Associates, Inc. Page 3373

- S.S. Jamali, D.J. Mills, S. Mabbutt, P. Picton, Effect of surface preparation on protective efficiency of organic coatings, European Corrosion Congress (EUROCORR) 2011: Developing Solutions for the Global Challenge, Stockholm, Sweden, 04-08 September 2011. Stockholm, Sweden: Dechema. Proc. Published by Curran Associates, Inc. page 2744

- S.S. Jamali, D.J. Mills, Steel surface preparation prior to painting and its impact on performance of organic coating, *submitted to Progress in Organic Coatings, under review.*

References

[1] G.L. Higgins, R.S. Hullcoop, S. Turgoose, W. Bullough, Volume 4: Management and Control of Corrosion, in: T.J.A. Richardson (Ed.), Shreir's Corrosion, Elsevier Ltd, London, 2010: pp. 2483–2493.

[2] L. Jayson, P.E. Helsel, Surface preparation : A primer, Journal of Architectural Coatings. (2008) 72–75.

[3] C.F. Dong, H.B. Xue, X.G. Li, H.B. Qi, Y.F. Cheng, Electrochemical corrosion behavior of hot-rolled steel under oxide scale in chloride solution, Electrochimica Acta. 54 (2009) 4223–4228.

[4] R. Naderi, M.M. Attar, M.. Moayed, EIS examination of mill scale on mild steel with polyester–epoxy powder coating, Progress in Organic Coatings. 50 (2004) 162–165.

[5] K.B. Tator, J.D. Trim, K.E. Buffington, S.R. Calhoun, Influence of surface preparation upon performance of protective coatings in atmospheric environments, in: Corrosion, Anahelm, Cal, USA, 1983: pp. 27–32.

[6] W. Funke, The role of adhesion in corrosion protection by organic coatings, J. Oil Col. Chem. Assoc. 68 (1985) 229–232.

[7] C.H. Hare, Corrosion control of steel by organic coatings, in: R.W. Revie (Ed.), Uhlig's Corrosion Handbook, Third, John Wiley & Sons, Inc, Hoboken, NJ, USA, 2011: pp. 1023–1039.

[8] C.G. Munger, L.D. Vincent, Corrosion Prevention by Protective Coatings, 2nd ed., NACE International, Houston, TX, 1999.

[9] P.R. Sere, A.R. Armas, C.I. Elsners, A.R. Di Sarli, The surface condition effect on adhesion and corrosion resistance of carbon steel/chlorinated rubber/artificial sea water system, Corrosion Science. 38 (1996) 853–866.

[10] A. Momber, S. Koller, H. Dittmers, Effects of surface preparation methods on adhesion of organic coatings to steel substrates, Journal of Protective Coatings and Linings. (2004) 44–50.

[11] D.M. Santágata, P.R. Seré, C.I. Elsner, A.R. Di Sarli, Evaluation of the surface treatment effect on the corrosion performance of paint coated carbon steel, Progress in Organic Coatings. 33 (1998) 44–54.

[12] D.J. Mills, K. Schaefer, Use of electrochemical methods to examine different surface preparation methods for organic coatings on steel, Progress in Organic Coatings. 69 (2010) 193–198.

[13] L. Cáceres, T. Vargas, L. Herrera, Influence of pitting and iron oxide formation during corrosion of carbon steel in unbuffered NaCl solutions, Corrosion Science. 51 (2009) 971–978.

[14] Y.F. Cheng, M. Wilmott, J.L. Luo, The role of chloride ions in pitting of carbon steel studied by the statistical analysis of electrochemical noise, Applied Surface Science. 152 (1999) 161–168.

[15] F. Atmani, M. Olivier, C. Buess-herman, Electrochemical behavior of mild steel in chloride environment : influence of surface preparation with and without corrosion inhibitor, in: EuroCorr, Nice, France, 2009: pp. 1–8.

[16] Y. Ma, Y. Li, F. Wang, Corrosion of low carbon steel in atmospheric environments of different chloride content, Corrosion Science. 51 (2009) 997–1006.

[17] X. Tang, Y.F. Cheng, Localized dissolution electrochemistry at surface irregularities of pipeline steel, Applied Surface Science. 254 (2008) 5199–5205.

[18] M. Morcillo, J.M. Bastidas, J. Simancas, J.C. Galvan, The effect of the abrasive work mix on paint performance over blasted steel, Anti-corrosion Methods and Materials. 36 (1993) 4–8.

[19] F. Atmani, D. Lahem, M. Poelman, M. Olivier, Mild steel corrosion in chloride environment: effect of surface preparation and influence of inorganic inhibitors, Corrosion Engineering, Science and Technology. 48 (2012) 9–18.

[20] D. Greenfield, J.D. Scantlebury, The protective action of organic coatings on steel: a review, The Journal of Corrosion Science and Engineering. 3 (2000) paper 5.

[21] J.E.O. Mayne, The problem of painting rusty steel, Journal of Applied Chemistry. 9 (1959) 673–680.

[22] D. de la Fuente, J. Simancas, M. Morcillo, Effect of variable amounts of rust at the steel/paint interface on the behaviour of anticorrosive paint systems, Progress in Organic Coatings. 46 (2003) 241–249.

[23] L.F. Vesga, E. Vera, J.H. Panqueva, Use of the electrochemical impedance spectroscopy to evaluate the performance of a primer applied under different surface preparation methods, Progress in Organic Coatings. 39 (2000) 61–65.

[24] C.. Elsner, E. Cavalcanti, O. Ferraz, a. . Di Sarli, Evaluation of the surface treatment effect on the anticorrosive performance of paint systems on steel, Progress in Organic Coatings. 48 (2003) 50–62.

[25] J. Knapp, T. Taylor, Waterjet roughened surface analysis and bond strength, Surface and Coatings Technology. 86-87 (1996) 22–27.

[26] K. Patel, C. Doyle, D. Yonekura, B. James, Effect of surface roughness parameters on thermally sprayed PEEK coatings, Surface and Coatings Technology. 204 (2010) 3567–3572.

[27] D.N. French, National Board Classic Series: Grain boundaries, National Board Bulletin. (1991) 1–3.

[28] M. Phaniraj, D. Kim, Y. Cho, Effect of grain boundary characteristics on the oxidation behavior of ferritic stainless steel, Corrosion Science. 53 (2011) 4124–4130.

[29] C.L. Briant, S.K. Banerji, Intergranular failure in steel: the role of grain-boundary composition, International Metals Review. 23 (1978) 164–199.

[30] X. Jia, Wettability of rough polymer, metal and oxide surfaces as well as of composite surfaces, Journal of Adhesion Science and Technology. 22 (2008) 1893–1905.

[31] B. Bhushan, M. Nosonovsky, Y. Jung, Lotus effect: roughness-induced superhydrophobic surfaces, in: B. Bhushan (Ed.), Nanotribology and Nanomechanics, Springer B, 2008: pp. 995–1072.

[32] B. Bhushan, Y. Jung, K. Koch, Micro-, nano-and hierarchical structures for superhydrophobicity, self-cleaning and low adhesion, Philosophical Transactions of the Royal Society A. 367 (2009) 1631–1672.

[33] W. Zisman, Relation of the equilibrium contact angle to liquid and solid constitution, Advances in Chemistry Series. 43 (1964) 1–51.

[34] S. Takeda, M. Fukawa, Role of surface OH groups in surface chemical properties of metal oxide films, Materials Science and Engineering: B. 119 (2005) 265–267.

[35] S.W. Tait, An introduction to electrochemical corrosion testing for practicing engineering and scientists, Pair o Docs publications, Racine, Wisconsin, 1994.

[36] S. Barnartt, Electrochemical nature of corrosion, in: R. Baboian (Ed.), Electrochemial Techniques for Corrosion Engineering, NACE International, Houston, TX, 1986: pp. 1–11.

[37] F. Zou, D. Thierry, Localized electrochemical impedance spectroscopy for studying the degradation of organic coatings, Electrochimica Acta. 42 (1997) 3293–3301.

[38] W. Funke, Mechanism of protecting metals by organic coatings against corrosion, in: R.A. Dickie, F.L. Floyd (Eds.), Polymeric Material for Corrosion Control, American Chemical Society, 1986: pp. 222–228.

[39] D.. Worsley, D. Williams, J.S.. Ling, Mechanistic changes in cut-edge corrosion induced by variation of organic coating porosity, Corrosion Science. 43 (2001) 2335–2348.

[40] H.N. McMurray, S.M. Powell, D.A. Worsley, Mechanistic changes in cut edge corrosion induced by variation of inhibitor pigmentation in organically coated galvanised steel, British Corrosion Journal. 36 (2001) 42–48.

[41] J. Wielant, R. Posner, R. Hausbrand, G. Grundmeier, H. Terryn, Cathodic delamination of polyurethane films on oxide covered steel – combined adhesion and interface electrochemical studies, Corrosion Science. 51 (2009) 1664–1670.

[42] D.J. Mills, S.J. Mabbutt, G.P. Bierwagen, Y. Pae, S. Berg, The effect of the substrate on the electrochemical response of protective coatings, in: 13th International Corrosion Congress Proceedings: Towards Corrosion Prevention, Melbourne, 1996: p. paper no. 432.

[43] J.E.O. Mayne, D.J. Mills, The effect of the substrate on the electrical resistance of polymer films, Journal of Oil and Colour Chemists Association. 58 (1975) 155–159.

[44] R.A. Dickie, F.L. Floyd, Polymeric materials for corrosion control: An overview, in: R.A. Dickie, F.L. Floyd (Eds.), Polymeric Material for Corrosion Control, American Chemical Society, Washington, DC, 1986: pp. 1–16.

[45] D. Roy, G.P. Simon, M. Forsyth, Blends of maleic-anhydride-grafted polyethylene with polyethylene for improved cathodic disbondment performance, Polymer International. 50 (2001) 1115–1123.

[46] P. Walker, The effect of water on the adhesion of surface coatings, Official Digest J. Paint Technology. 37 (1965) 1561–1592.

Chapter 5

A physico-mechanical and electrochemical study of organic coatings

5.1 Introduction

The second part of chapter 4 showed the impact of metal surface preparation when protected by an organic coating. These results showed that different surface finishes caused different levels of protectivity. The physical and chemical characteristics of metal were discussed and theories were proposed in attempt to explain the connection between the state of substrate and protective efficiency of organic coating. To understand the anti corrosion behaviour of an organically coated metal, it is also essential to study the physical and chemical changes in the coating independently and identify how its performance can be improved. Therefore, it was felt necessary to study the fundamental structure of the organic coatings, particularly the ionic conduction and the heterogeneity of coating in this respect which manifests itself in what are known as D and I areas. The main objective of this chapter is to try to understand the factor(s) that cause coating heterogeneity (D type behaviour) so they can be eliminated in practice to enhance the protection afforded by organic coatings. Also an effort has been made to develop a predictive model for distribution of D areas across coatings with the intention to predict number of D areas in a large surface based on D to I ratio of coating measured using small lab size specimens. Although the main body of work in this chapter is on the properties of detached organic coatings, in some cases results from coated samples are also given to highlight the relevance of properties of detached coatings to the protection afforded by the organic coatings.

5.2 Background on the heterogeneous nature of coating films

A study conducted over 100 years ago by Walker and Lewis showed how discontinuity in a protective lacquer can lead to highly localized corrosion and early failure of the food storage cans[1]. They reported severe corrosion damage of tin cans coated with copal-linseed oil varnish six to eight weeks after they were packed with strawberries resulting in a leak. The corrosion started from crimped joints and quickly spread under the varnish. They found that when the oil lacquer was baked sufficiently long at 250°C the corrosion disappears. Therefore they concluded that the oil varnish is porous in nature and allows the penetration of electrolyte towards the metal substrate. It was also pointed out that the varnish was applied to uncut tin sheets hence the coating could have been damaged in the

process of making the cans which later became where the corrosion started. While the defects mentioned in Walker and Lewis work were rather of macro defect type, around 5 decades later a series of systematic studies at Cambridge University in the laboratory of Dr J. E. O. Mayne (1960-1980) revealed an unusual aspect of intact organic coatings. Organic coatings were found to be electrochemically inhomogeneous in nature with two distinct conduction mechanisms for ions, moreover which conduction mechanism was operative had a major influence on the corrosion protection afforded by the coating. In the first mechanism the resistance of the film was *Inversely* proportional to that of solution, resulting in higher resistance at higher solution concentration. Coatings with such behaviour were so-called "I" or inverse type coatings. The second mode of through-film transport that was identified was named "D" or *direct* type conduction where the film's resistance follows that of the solution. Figure 5.1 illustrates the typical resistance exhibited by D and I type films as exposed to different concentration of salt solution. It was suggested that the water activity plays the key role in ionic conduction through I type coatings whilst the ionic strength controls the transport through D type coatings where the size of conduction pathway is remarkably bigger [2,3]. Further studies [4]revealed that under-film corrosion initially occurs at D type areas and then spreads across the interface.

In the interest of improving the protection properties of organic coatings, it is important to identify the phenomena that originate D type areas and try to eliminate them. A series of studies investigated the effect of electrolyte [3], thickness [5], temperature [6], pigmentation [7] and solvent [8] on D/I type ratio of paint film. A review on these classic studies, written by Greenfield and Scantlebury, can be found in reference [9]. The bulk of these works was conducted by measuring DC resistance on several pieces of 1 cm^2 of detached film to statistically determine the fraction of D or I type behaving paint film. One conclusion from this was that the D type area only occupies a small fraction of a 1 cm^2 area of film (e.g. $^1/_{100^{th}}$ to $^1/_{1000^{th}}$) but this area has a remarkably higher permeability thus dominates the protective properties of the coating.

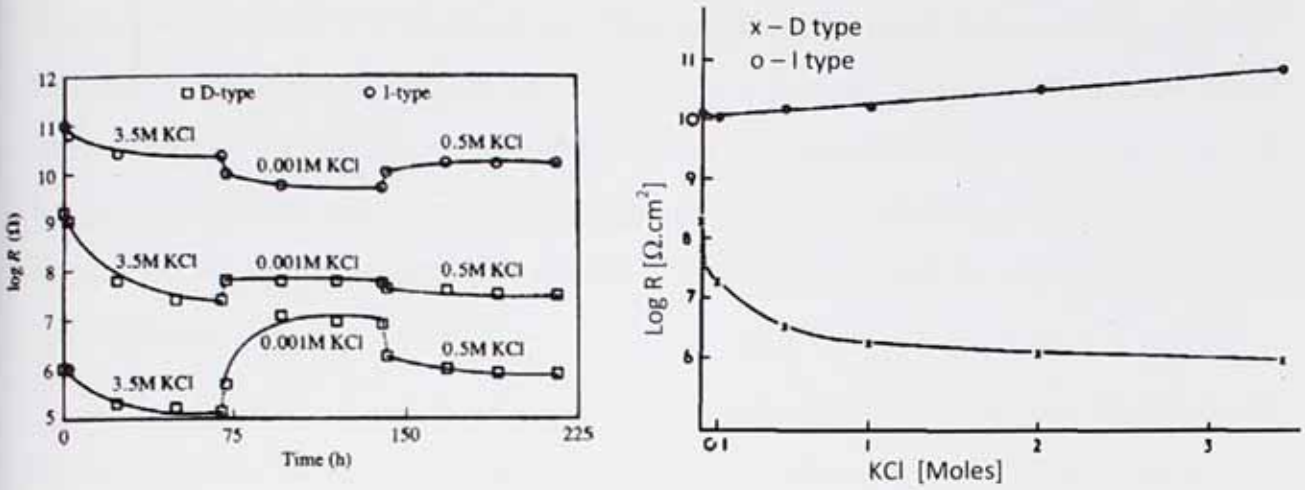

Figure 5.1 Effect of KCl concentration on the DC resistance of D and I type alkyd varnish. Dependence of coating resistance to solution concentration is shown as the direct relationship between ionic strength and coating conductivity for D type coatings and inverse relationship for I types (figure reproduced from Ref.[4]).

As mentioned earlier, most of the early studies on inhomogeneity of the resistance on organic coatings were conducted using 1 cm^2 area of film that suggested, in the case of D type behaviour, highly permeable area occupying small fraction of film. To further study the distribution of resistance within a D type coating, a wire beam electrode (WBE) is used in this study. A wire beam electrode, first introduced by Tan [10], is a multi-piece electrode constructed with an array of metal wires embedded into an insulating material. The surface of each individual electrode serves as a small metal substrate. The principle of this type of electrode is based on subdividing a continuous area of a metal surface into many small parts and measuring the electrochemical properties of each part by means of individual isolated connections. WBE has been successfully utilized for studying inhomogeneity and localized corrosion at surfaces such as steel [11,12], aluminium [13] and a range of organic coatings [14–18]. Tan [16,17] studied the effect of prolonged exposure to salt water on electrical homogeneity of organic coatings using a WBE. His results suggested a homogeneous electrochemical behaviour across the surface of each individual wire while the large statistical distribution of resistance revealed the presence of heterogeneity from wire to wire across the whole surface of the multi-electrode. More recent work by Wu et al. [15] utilized a wire-beam electrode with 121 independent steel arrays to investigate the influence of thickness on homogeneity of paint when coated on a steel surface. Their results

revealed the significance of thickness on the homogeneity of paint and its ionic conduction. They also confirmed the early results of Mills and Mayne [5] in regards to the higher homogeneity of a double coat system compared to a single coat with the same overall thickness. This latter work particularly suggests that either artefacts arising from solvent evaporation and/or insufficiently crosslinked polymeric areas could be potential origins of D type behaviour.

Traditionally most thermoplastic polymers are considered semi-crystalline materials with varying crystalline fraction. The crystalline phase is considered the impermeable phase while the amorphous phase is the more permeable phase with relatively loose structure. It has been shown that thin films of thermoplastic polymers with high degree of crystallinity such as a bi-oriented polypropylene film can be made to exhibit 100% I type behaviour with a uniformly very high resistance across the film [5]. The small crystalline regions may even immobilize the surrounding amorphous phase and as a result significantly reduce permeation rate [19]. It has been suggested that addition of lamellar nano clay has similar effect and improves the barrier properties by immobilization of the polymer chain-segment [20,21]. However, all of the coatings used in this study are cross-linking, thermoset, polymers and therefore they do not contain crystalline phase. Factors affecting ionic permeability in such polymers will be investigated in the following sections.

5.3 Experimental

5.3.1 Materials

The alkyd varnish was based on a short oil soya based alkyd resin with 40% v/v solid content. The solvent was Xylene. The alkyd paint was based on the same resin, pigmented with calcium diphosphate (also known as calcium pyrophosphate with the chemical structure of $Ca_2O_7P_2$). Both alkyd varnish and alkyd paint were supplied by Pronto industrial paints Ltd, Derbyshire, UK.

A typical soya bean oil is composed of linoleic (54%), linolenic (5%), oleic (30%), palmitic (9%), stearic (4%) and arachic (1%) acids that are esterified with polyols (e.g. glycerol) and polyacids (e.g. phthalic anhydride or maleic anhydride) to form alkyd (alcohol-acid) polymer.

The resulting polymer contains C=C bonds owing to the unsaturated fatty acids; linoleic, linolenic and oleic acids. The polymer is crosslinked through its C=C bonds in the air by an oxidative radical co-polymerisation.

Solvent base and waterborne polyurethane (PU) coatings were acrylic polyol (OH functional) resins crosslinked with polyisocyanate. The solvent based acrylic was SETALUX 1196 XX-60 polyol with 60%v/v solid content and Xylene as solvent. Waterborne acrylic was SETAQUA 6515 which was a polyol emulsion in DI water/butylglycol/solvesso 100 (85.8/7.6/6.6). Both poly-acrylic resins were supplied by Nuplex Resins, Nuplex, Netherlands. Both poly-acrylic resins were crosslinked with Tolonate HDT-LV2 which was a solvent free, low viscosity aliphatic polyisocyanate based on Hexamethylene Diisocyanate trimer (HDI homopolymer) supplied by Perstorp, France. Stoichiometric mixing ratio of 1:1 of NCO:OH was used for solvent base PU. Due to the NCO-H_2O reaction in aqueous media, mixing ratio of 1.25:1 (excessive polyisocyanate) was used for waterborne PU to compensate for NCO-water reaction.

Solvent base, waterborne and solvent free epoxy paints were supplied by AkzoNobel International paints, Newcastle, UK, with 63%v/v, 52%v/v and 100% solid contents, respectively.

The nano particles used in this study was BYK-LP-X 21390 which was a pre-dispersed nano silica (SiO_2) with 50%wt solid content in TMPTA (trimethylolpropane triacrylate), 20 nm particle size and acrylic surface treatment. The nano particles were supplied by BYK, Wesel, Germany, and were incorporated by 2.5 wt% in the alkyd varnish.

5.3.2 Sample preparation

A set of alkyd coatings were prepared using the alkyd varnish to study the effect of curing temperature, thickness and nano-additive on electrochemical inhomogeneity. A range of thickness was obtained using a number of spreader bars.

All coatings were prepared at Room Temperature (RT), i.e. 18-22°C, unless otherwise stated.

The alkyd varnish with 85±5 µm film thickness was also cured at 60°C to examine the effect of curing temperature.

To examine the effect of structural change and partial polymerisation the liquid alkyd varnish was incubated at 60°C for 10 days before it was used to prepare the detached film.

Triple layer alkyd varnish was prepared through a layer by layer procedure with the overall film thickness of 85±5 µm. Second and third layers were applied after the former layer was fully cured.

In order to obtain the detached film, the liquid paint was applied on a non-stick PTFE (Polytetrafluoroethylene) sheet (for alkyd coatings) or Polypropylene sheet (for epoxy and PU coatings) using the spreader bar and carefully delaminated after it was fully dried. The coating thickness was then measured by a Defelsko PosiTest DFT thickness gauge.

5.3.3 Wire beam multi-electrode construction

98 steel wires with 1.5 mm diameter were embedded in an acrylic mould to form a square array (figure 5.2 left). The cross-section was carefully cut and polished using 240 grit emery to obtain a flat surface while each steel wire was left protruding at least 2 cm from the other side of the mould for further electrical connection and measurement. With 98 steel wires, each with 7.06 mm^2 area, embedded in a 4×4.5cm (18 cm^2) area, the wires cross-section composed about 7 cm^2 of the whole area. The coatings were then applied using a spreader bar. The coatings were also applied with the same thickness to a steel panel for thickness measurement. The DC resistance of each coated wire was measured in 0.5 M NaCl solution using a 610C solid state Keithley electrometer against a calomel electrode (figure 5.2 right). The multi-electrode was in solution for 24 hours before the DC measurement. All measurements were made at RT, 18-22°C.

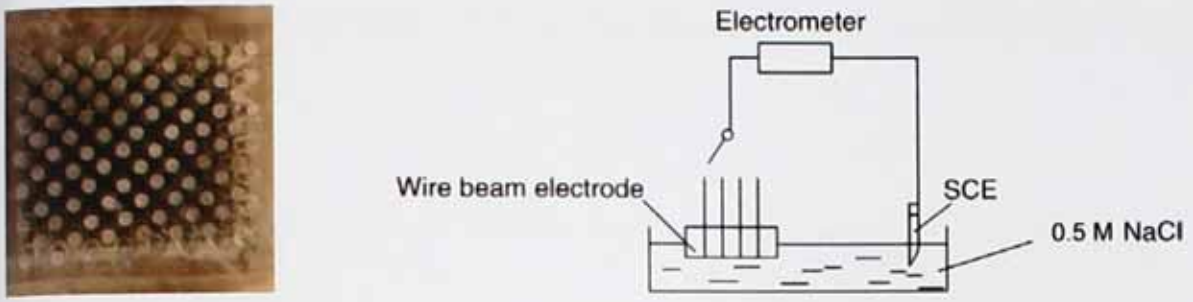

Figure 5.2 Optical image of the WBE surface with 98 steel wires (left) and the set-up used for measuring DC resistance of individual wires using an Electrometer and saturated calomel electrode (SCE) (right).

A distribution map of resistance was produced for each coating using Microsoft Excel 2007 program. Values of individual wires were entered into a data sheet and the missing values (corresponded to the gap between wires) were estimated by averaging from the surrounding measured values. Subsequently the 13×15 matrix of values was plotted with a "3-D surface" format and the image was also rotated to show the top view.

5.3.4 D/I type measurement protocol

The D/I ratio was determined by measuring DC resistance of 3.1 cm^2 detached coatings using a 610C solid state Keithley electrometer. Detached films were cut into approx. 4cm^2 squares (figure 5.3-left) and mounted in U shape glass cells (figure 5.3–middle) where the DC resistance could be measured in a two electrode arrangement across the coating using two calomel electrodes (figure 5.3 right). The DC resistance was measured with 0.001M KCl and 3.5M KCl solutions to identify the conduction type of each piece. If the resistance was lower in the 3.5M solution than that in 0.001M solution it was classified as a D type. If resistance was higher in the 3.5M solution than that in the 0.001M solution it was classified as I type. Coatings were in contact with each solution for at least 2 hrs before the measurements was made. All measurements were performed at room temperature, 18-22°C. Consequently the D/I type ratio was statistically calculated over 20 samples. Different size of specimen used in this study (3.1 cm^2) makes direct comparison with Mayne results difficult. The 3.1 cm^2 specimen used in this study will result in higher D to I ratio due to higher chance of inclusion

of a D area in each specimen when compared with Mayne method which used 1 cm^2 specimens.

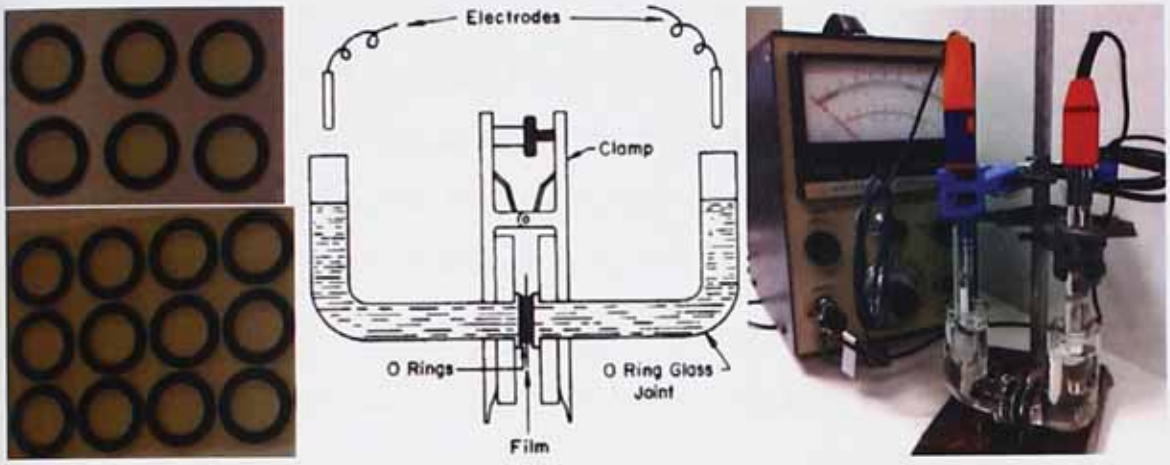

Figure 5.3 Experimental set-up for detached film measurements [22].

5.3.5 Other experimental methods for electrochemical, physico-mechanical and chemical characterization

- EIS was performed using an automated ACM GillAC potentiostat/galvanostat/FRA within 10kHz-10mHz range with the ac amplitude of 10mV rms around OCP. SCE was used as reference electrode and Pt electrodes were used as counter and working electrodes. A standard 3 electrode configuration was used with one Pt electrode in each side of U cell and SCE in the same side with the WE. EIS measurements were performed in 0.001M, 0.5M and 5M NaCl solutions at RT.

- ENM was performed using single cell configuration described in chapter 3. SCE was used as reference electrode and a steel bar was used as working electrode to measure potential and current noise across the coating with the SCE in one side of U cell and steel bar in the other side. ENM was performed in 5M NaCl solution at RT.

- FTIR-ATR was performed using SHIMADZU FTIR-8400S spectrophotometer with a Smiths Detection DuraSampl*IR* II ATR attachment in transmission mode within 750-3950 cm^{-1} wavelength range. 1ml of liquid resin was used as samples to fully cover the diamond crystal detector. Background spectrum was collected from the overhead sample holder and

subtracted automatically from the sample spectrum. Three samples from each resin were measured to ensure the repeatability of spectrum.

- Differential scanning calorimetry (DSC) measurements were performed using DSC facility provided at the Intitute for Creative Leather Technologies (ICLT), University of Northampton, UK, with a METTLER TOLEDO DSC 821 at 5 °C heating rate with the range of -10°C to 150°C under N_2 atmosphere. Standard 40 µL crucible aluminium pans were used and the weight of samples was 8-12 mg. Samples were cut from fully cured detached films. All data presented here are normalized in regard to the weight of samples.

- Dynamical thermo-mechanical analysis (DMTA) experiments were performed by a DMA Tritec 2000, Triton-technology at 5 °C/min heating rate, 1 Hz oscillation under 1 N force and 20 µm displacement. Storage and loss modulus were measured within the temperature range of 20 to 120°C. Specimens were rectangular detached films with a fixed length of 11 mm and approximate width of 8 mm fixed to a single cantilever with tension mode. Tg was determined at the maximum of the α transition peak of the tanδ.

5.4 Practical aspects of D/I type behaviour

5.4.1 Relevance of D/I behaviour to the protective properties of coating on steel

Previous studies [4,23] revealed that D type areas are the locations at which the corrosion of metal starts under organic coating. It has been also pointed out that I type coatings may change to D type over long period of exposure to electrolyte due to high ion exchange capacity of coating. In practice when coating is attached to an electrochemically active substrate, e.g. steel, other functions such as under-film contamination or osmosis can gradually cause coating degradation and change the I type behaviour to D type. A long term experiment was hence designed to look at resistance inhibition of alkyd varnish and its relationship with D/I type behaviour.

Figure 5.4 shows the change of DC resistance for four similarly prepared alkyd varnish coatings on steel with 70±5 µm thickness and 4.15cm^2 of exposed area. DC resistance was measured over 5 month in 0.5 M NaCl solution and D/I type behaviour of coated specimens

was examined using 0.001 M and saturated NaCl solutions after 1 and 24 days. Out of 4 samples, 3 samples retained high resistance over the period of measurement. An unusual observation was the high resistance of sample 1 in the long term despite its D type behaviour and relatively low resistance after one day. One probable explanation for the unexpected behaviour of sample 1 could be the pore plugging mechanism. Since the alkyd structure is normally negatively charged with carboxylic acid groups, it may confine the diffusion of chloride ions which results in a permanent settlement of insoluble oxides in ionic pathways. However, this is in contrast with previous findings indicating D areas to have non-selective permeability (unlike I type areas). An alternative explanation was proposed by Heyes [24]. He observed that once the paint causes passivation of the metal, the system adopts I type conduction characteristics even though the detached coatings that he studied were 100% D type. The coatings he studied contained inhibitive pigments capable of passivating steel while the coatings studied here were alkyd varnish with no pigmentation. However, increased pH beneath the high resistance varnish after initial electrochemical process may establishes passivation of steel even in the absence of inhibitive pigments. This was confirmed by noble potential of all 4 samples in the early stages of immersion.

After one month the early I type behaviour of sample 3 was changed to D type behaviour when checked with 0.001M and 3.5M KCl solutions. This so-called "slow change" occurs as a result of high pH generated by corrosion and partial hydrolysis of polymer network. The important observation was that at the time of measurement the resistance of sample 3 was no different from the rest of samples. Thereafter sample 3 underwent a significant decrease of resistance. This observation highlights the significance of coating degradation in "slow change" process and also reveals the potential of D/I type identification method as a predictive method.

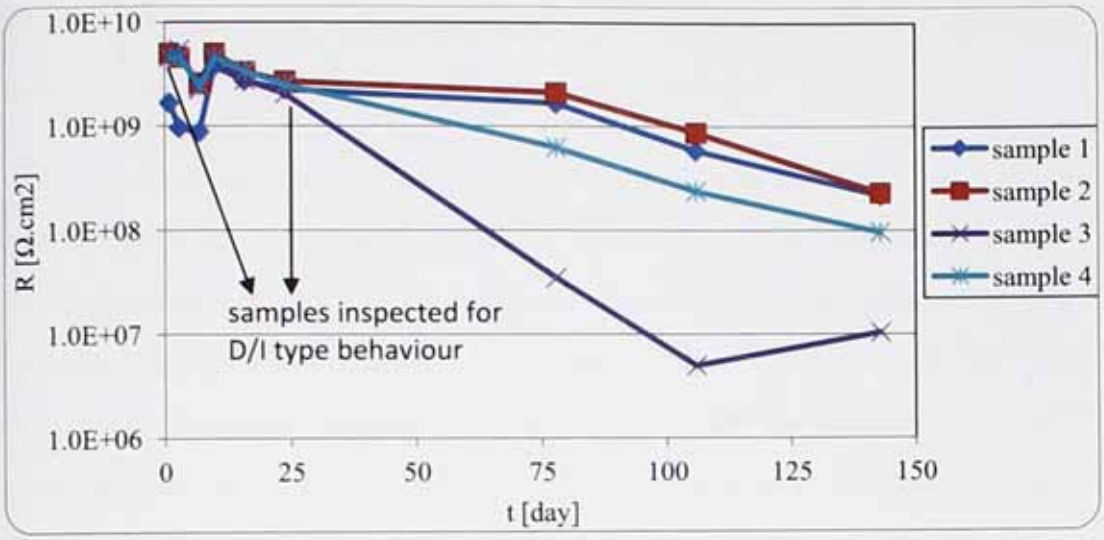

Figure 5.4 DC resistance of 4 similarly prepared samples of alkyd varnish on steel with 70±5 μm thickness.

5.4.2 Identifying D/I type behaviour using electrochemical noise method (ENM)

Measuring DC Resistance has been the major method of identifying D/I type behaviour. It provides a relatively quick and reproducible measurement. However, limitations of DC method, as discussed in chapter 3, make it hard to use in the field. Here electrochemical noise measurement with single cell arrangement is implemented to check if the technique is capable of recognizing D/I behaviour of detached coatings. Figure 5.5 shows the results of individual potential and current noise measurement and noise resistance obtained from these two values for 7 samples. Highly concentrated salt solution (5M NaCl) was used in order to pronounce the effect of conduction mechanism on resistance and maximize detection power of ENM. D/I type behaviour of samples were previously defined using DC method. Results show significantly higher level of potential noise through I type coatings while the level of current noise is hardly different from D type films (except the very low resistance sample no. 2). The important implication of this experiment is that the ionic conduction is mostly triggered by a potential gradient. This potential gradient is supplied by the small external potential applied by electrometer in DC method of measurement. In case of coated metal the inherent electrolytic potential of metal substrate provides this potential

gradient. However due to the absence of this driving force in ENM it is hard to discriminate between the current flow through I and D type coatings.

In absence of ZRA during potential noise measurement the potential gradient is established across the coating which is reflected by large difference of level of potential noise measured for I and D type coating. Thereby, it is also reflected by the R_n which can identify the different resistance of D and I type coatings. Note the ZRA is in action throughout the whole measurement when other ENM configurations, i.e. salt bridge, single substrate and NOCS, are used. Further work is required to examine the capability of other ENM configurations for D/I type identification.

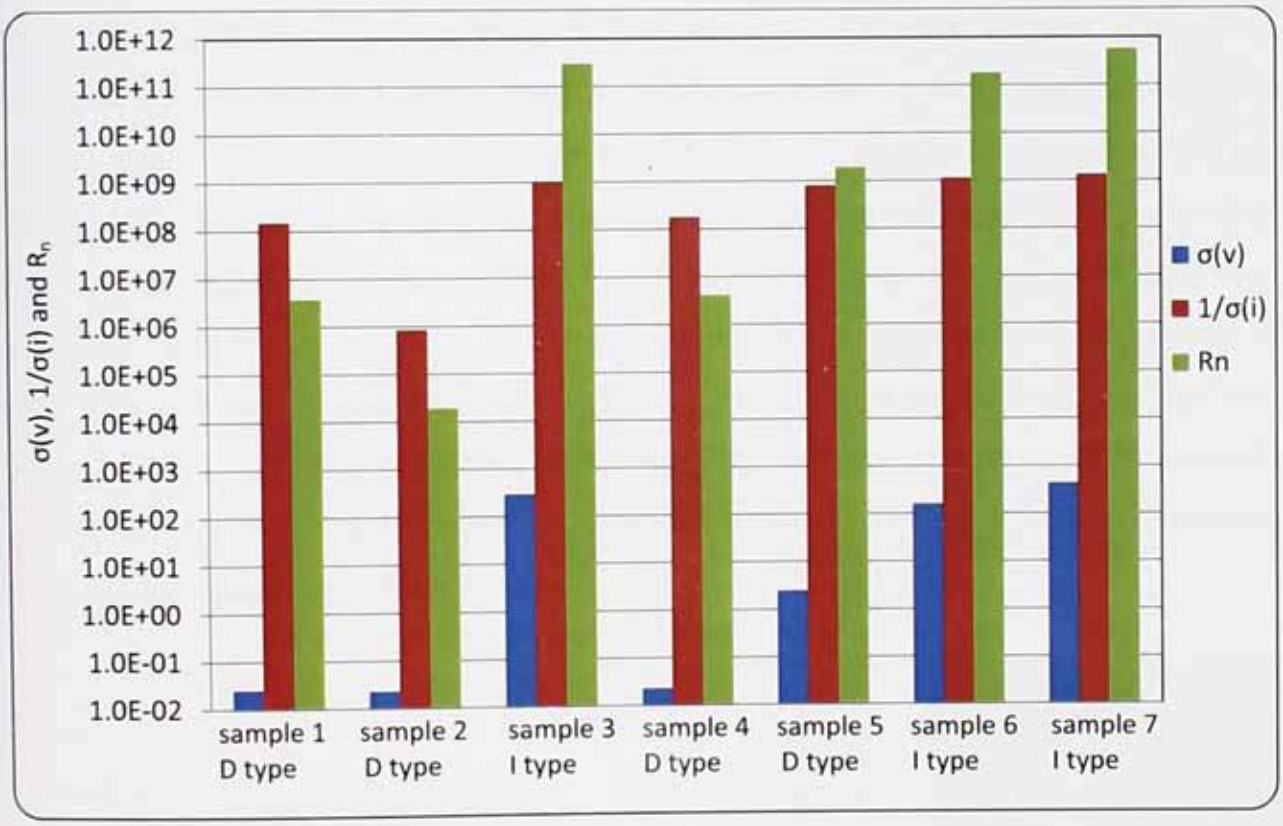

Figure 5.5 σ(v), σ(I) and R_n measured in 5M NaCl solution for a set of alkyd varnish detached films with different ionic conduction (D or I type) mechanisms revealing the capability of ENM for identifying D and I type behaviour.

5.6 Factors affecting D/I ratio

5.6.1 Thickness

Figure 5.6 and 5.7 show the distribution map of DC resistance across alkyd films with 18 µm and 32 µm thickness. The immediate implication of multi-electrode results is that the electrochemical heterogeneity is an inherent characteristic of polymer film which is more pronounced as the film thickness decreases. It is therefore reasonable to assume that permeable or D areas are very small areas with remarkably different conduction properties as also stated elsewhere [9]. The number of spots with low resistance (1E5 – 1E7) has been significantly decreased from 20 to 6 by increasing the thickness from 18 µm and 32 µm. Resistance values have been converted to represent the resistance of each wire on $\Omega.cm^2$ basis. Different shades of each colour (e.g. dark green to light green) appears to be an art effect used by MS Excel and may not represent a differentiation of values. Five categories of colours (cyan, purple, green, red and dark blue) have been assigned to represent different classes of DC resistance from high to low. The statistical analysis (results not presented) showed that increasing the film thickness also narrowed down the distribution of resistance values. In other words, increasing thickness improved the electrochemical homogeneity of alkyd film. It should be noted that the resistance measured by a multi-electrode may not directly indicate D or I type behaviour. It has been shown previously that coating may exhibit up to two orders of magnitude higher resistance when the coating is adhered to metal substrate compared to the detached film.

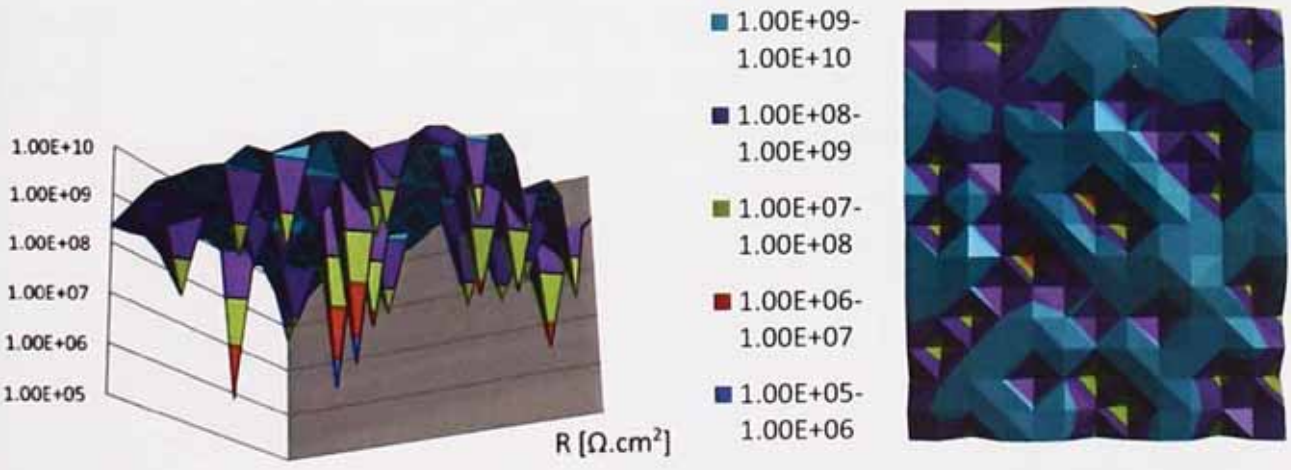

Figure 5.6 DC resistance map acquired by WBE from alkyd coating on steel with 18 µm of film thickness after 24 hours immersion in 0.5M NaCl.

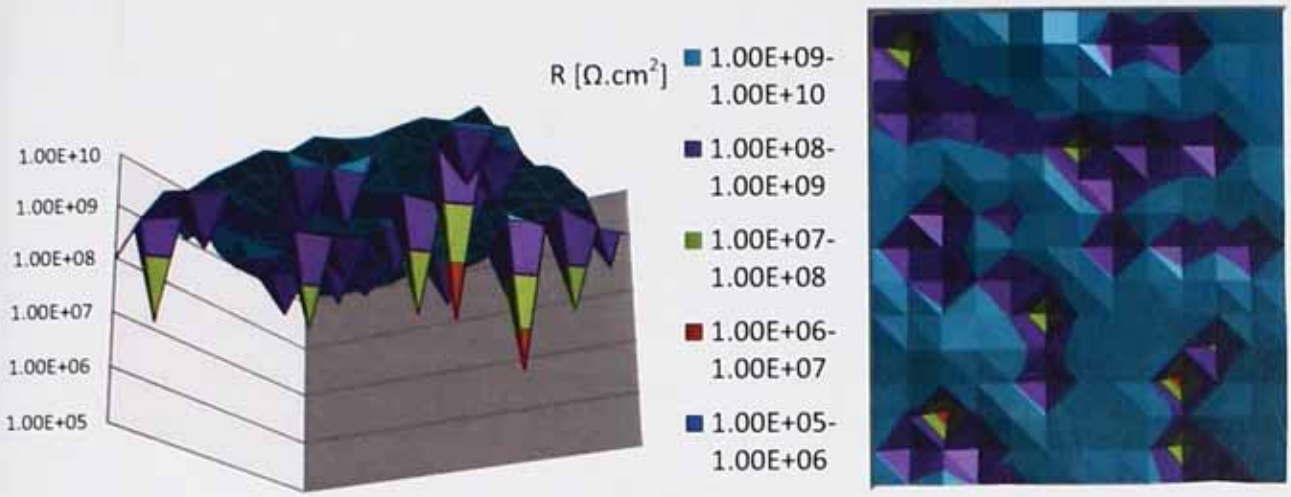

Figure 5.7 DC resistance map acquired by WBE from alkyd coating on steel with 32 μm of film thickness after 24 hours immersion in 0.5M NaCl.

Figure 5.8 shows the distribution of resistance for 89 alkyd varnish specimens of different thicknesses in 0.001M and 5 M NaCl solution regardless of D or I type characteristics. Larger range of distribution in 5 M NaCl is a result of different ionic activity in D and I type films in strong solutions while similar water absorption makes it harder to differentiate D and I type films in dilute solution. Figure 5.9 shows the same data (presented in fig. 5.8) divided by type of film and solution concentration. Figures 5.9b and 5.9d show a general increase of resistance of D type films in both solutions as a function of coating thickness along the line L. This can be explained by the longer conduction pathway in thicker coatings which dominates the resistance of D type films. Distribution along the line W is attributed to the different number and sizes of D areas within samples as also shown elsewhere [25]. I type resistance appears to be independent of coating thickness however it has been reported in the past that resistance of both I type and D type films increase by increasing the thickness [5].

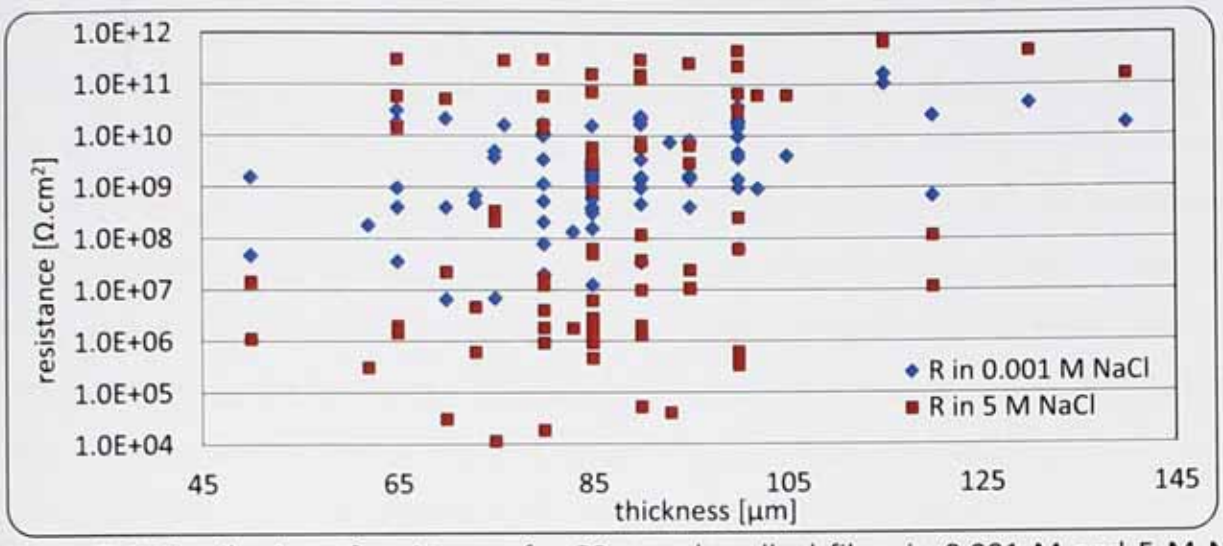

Figure 5.8 Distribution of resistance for 89 samples alkyd films in 0.001 M and 5 M NaCl solution.

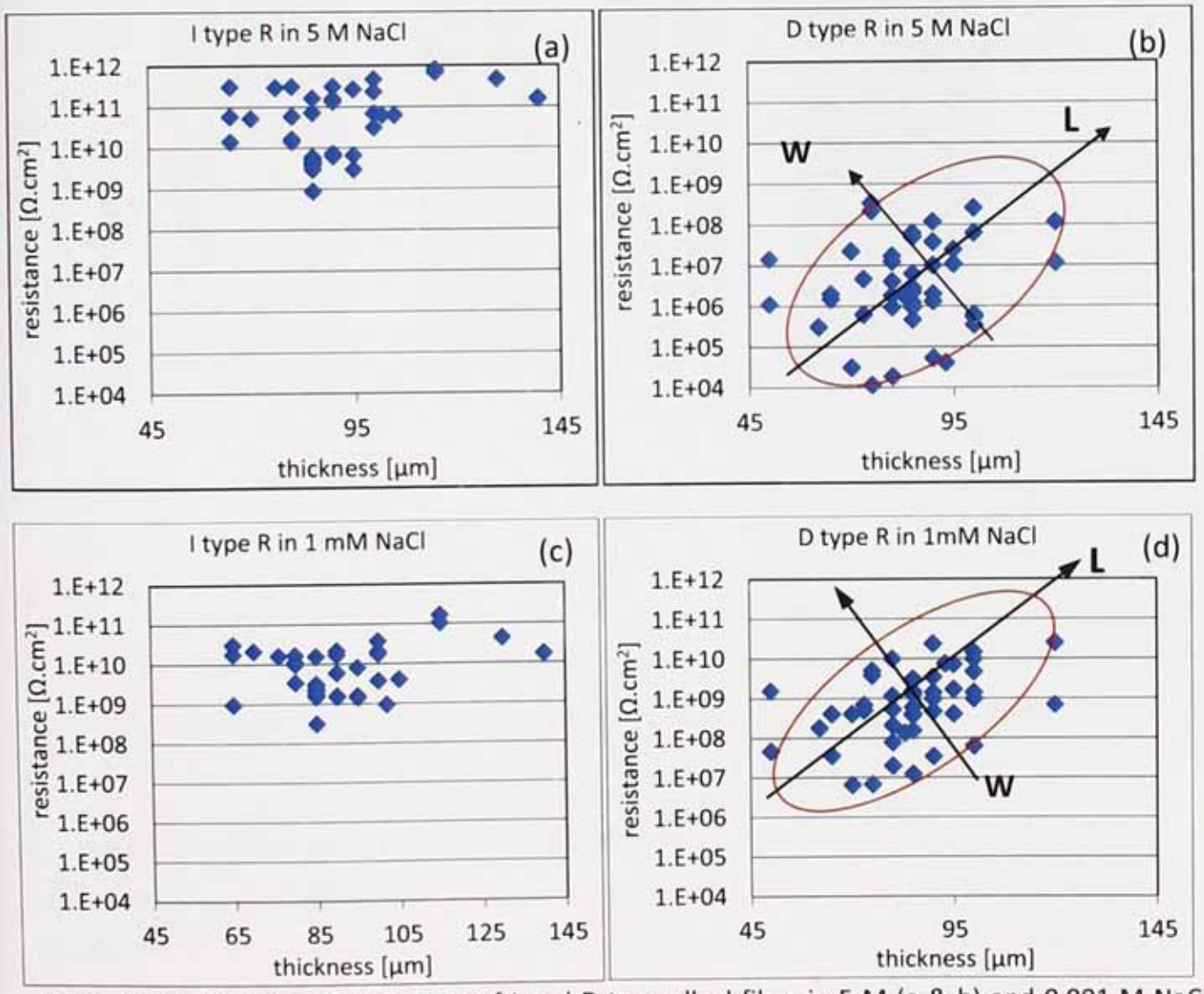

Figure 5.9 Distribution of resistance of I and D type alkyd films in 5 M (a & b) and 0.001 M NaCl (c & d) solutions.

Figure 5.10 shows the effect of thickness on D/I type ratio of alkyd varnish, waterborne PU, solvent base epoxy/polyamide paint and solvent free epoxy/polyamide paint coatings based on 3.1cm^2 areas. Increasing the thickness, as expected, increases the homogeneity and I type behaviour. The presence of a highly conducting continuous aqueous pathway is the essential requirement for D type behaviour. Thickening the polymer layer can potentially block or interrupt the conduction by impermeable polymeric regions (e.g. regions of higher cross linking density). This is however insignificant for highly hydrophilic waterborne PU where ionic conduction is particularly assisted by extensive water uptake.

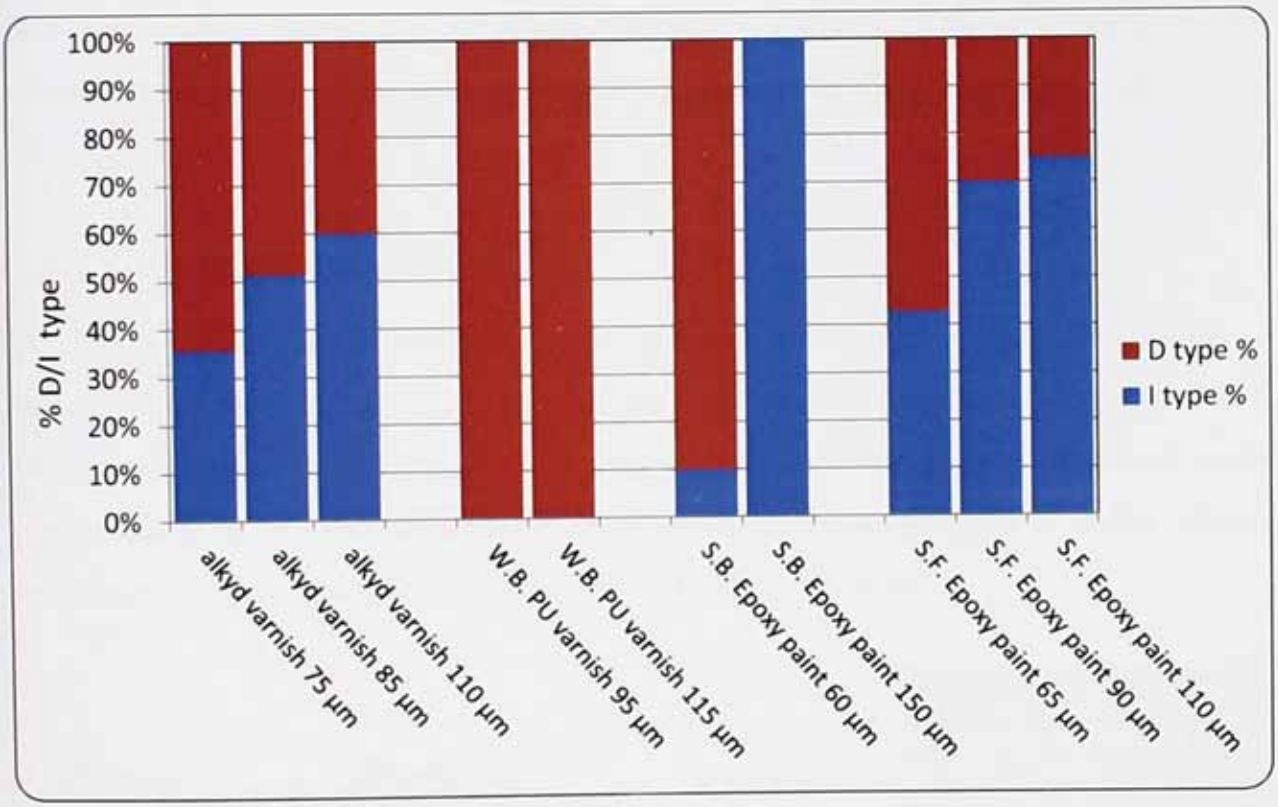

Figure 5.10 Effect of thickness on the D/I type behaviour of alkyd varnish, waterborne PU, solvent base epoxy/polyamide paint and solvent free epoxy/polyamide paint coatings.

Alkyd varnish films were kept immersed for two weeks to see if any films changed from I type to D type. Although a slight decrease was observed in some cases, no I type to D type change was observed. D type resistances dropped significantly after two weeks immersion which is in-line with the earlier results [5]. This could be as a result of formation of water clusters in the long term in D type film [26]. Earlier works however showed instability of

some I type alkyd films in the long term exposure to strong chloride solution. This was attributed to the high ion exchange capacity of the alkyds common at the time. Chemical characterization of the alkyd varnish used in this study showed very high conversion ratio of polymer evidenced by negligible OH peak at 3350-3550 cm^{-1} range of FTIR spectrum. This implies the presence of a very small ratio of carboxylic groups in the chemical structure of resin thus a low ion exchange capacity. The ion exchange process in the case of alkyd results in replacing the –H from carboxylic functional group by cations such as Na^{+}. This process in the long term leads to drastic increase of ionic content within the coating and decrease of resistance. The negligible OH peak in FTIR spectrum indicates the absence of carboxylic groups and low ion exchange capacity of alkyd resin resulting in the stability of I type films over time. It also confirms the hypothesis advanced in the past for explaining the instability of some I type films in strong solution in the long term due to the ion exchange process.

5.6.2 Curing temperature

Figure 5.11 illustrates the resistance map of alkyd film with 32 µm film thickness which was force cured at 60°C for 24 hr. In comparison with figure 5.7, force drying of the alkyd at 60 °C has significantly decreased the number of low resistance spots compared to the sample cured at RT. Also statistical analysis shows a significant increase of the average resistance over the whole 98 wires as a result of force drying at 60°C.

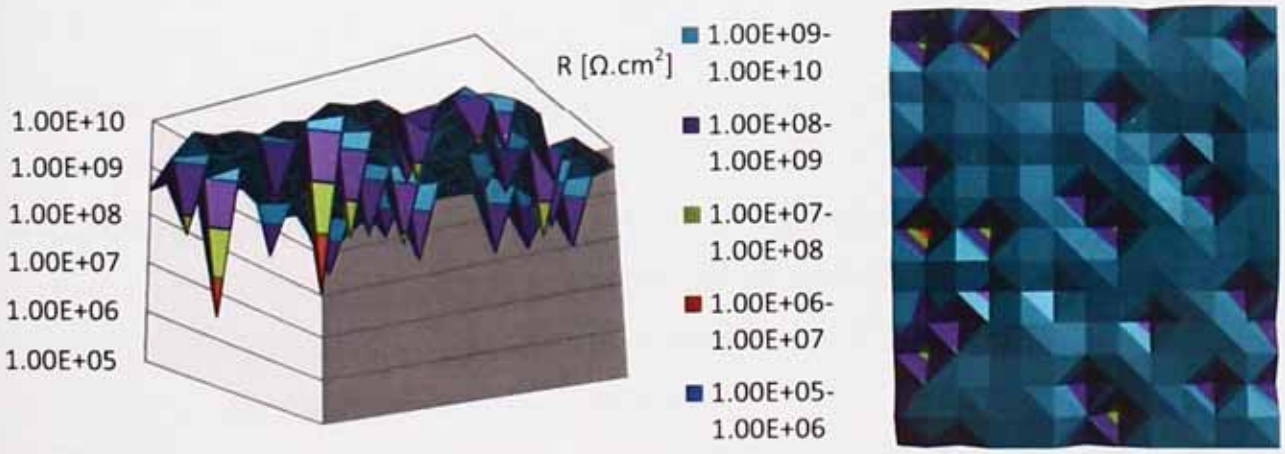

Figure 5.11 DC resistance map acquired by WBE from force cured alkyd coating at 60°C for 24 hr with 32 µm of film thickness after 24 hrs immersion in 0.5M NaCl.

Figure 5.12 shows the D/I type ratio of alkyd coating when cured at RT and 60°C. The significantly lower D/I ratio of alkyd when cured at elevated temperature can be explained by two mechanisms. First explanation is based on enhanced crosslinking as a result of higher temperature and higher yield of oxidative co-polymerisation reactions. It can also be a result of more efficient solvent evaporation at higher temperatures. Solvent pockets when entrapped inside the film may produce hollows and permeable areas. At higher temperatures, increased molecular motions increases the intermolecular space (or free volume) therefore the solvent can be removed more efficiently while the coating is not completely set.

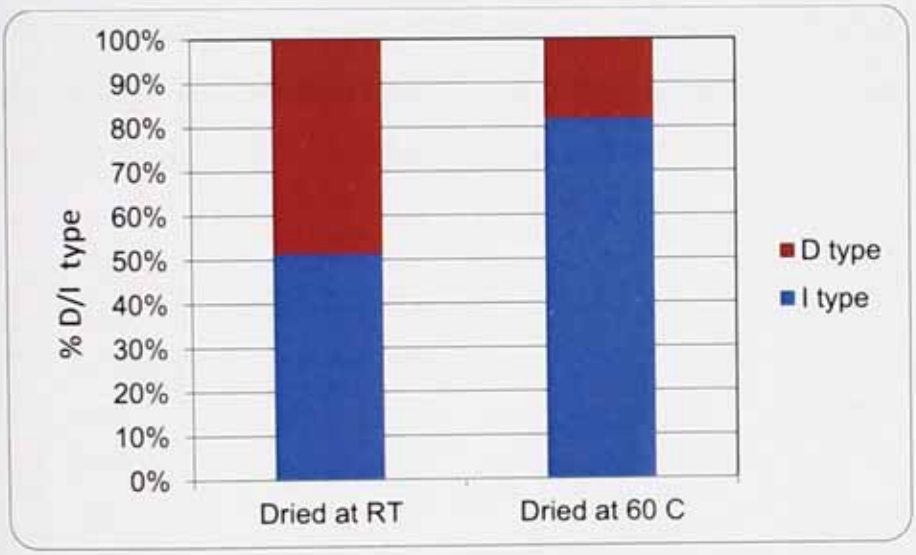

Figure 5.12 D/I type ratio of alkyd films cured at RT and 60 °C with 85±5 µm film thickness.

Thermal analysis results, shown in figure 5.13, reveal a significantly higher residual post-cure exothermic peak for the alkyd coating that was cured at RT compared with one cured at 60°C. This result confirms that there are a larger number of unreacted functional groups when the alkyd is cured at lower temperature and helps to explain the enhanced I type behaviour of the coating which was cured in the oven. Figure 5.14 shows DSC results of wet alkyd films in which larger endothermic peak under 100°C is associated with the water removal from the film. DSC pans were pierced to let the moisture out. Result shows significantly higher water absorption by the RT dried coating compared to the force dried coating. Although the C=C or unreacted alkyd functional groups are no different from C-C

groups in terms of hydrophilicity, the free space in absence of cross-linked polymers provides larger space for water accumulation.

It should be noted that the presence of larger number of unreacted groups does not have a significant effect on the measured glass transition temperature, T_g. This also has no significant effect on the storage modulus of alkyd as measured by DMTA. Figure 5.15 shows similar storage modulus for the wet alkyd coatings cured at RT and 60°C. Generally the lower storage modulus of wet films compared to dry film can be attributed to the presence of water in the film and its plasticizing effect. This plasticizing effect was shown clearer in figure 5.16 as the first (and smaller) peak of tan δ in the range of 20 to 25°C. This peak, which was not observed for the dry film sample, is associated with the plasticization effect of water within the polymeric structure which facilitates movement of polymeric chains and softens the film [27,28]. The DMTA technique did not show adequate sensitivity to differentiate the structural change of alkyd films cured at different temperatures.

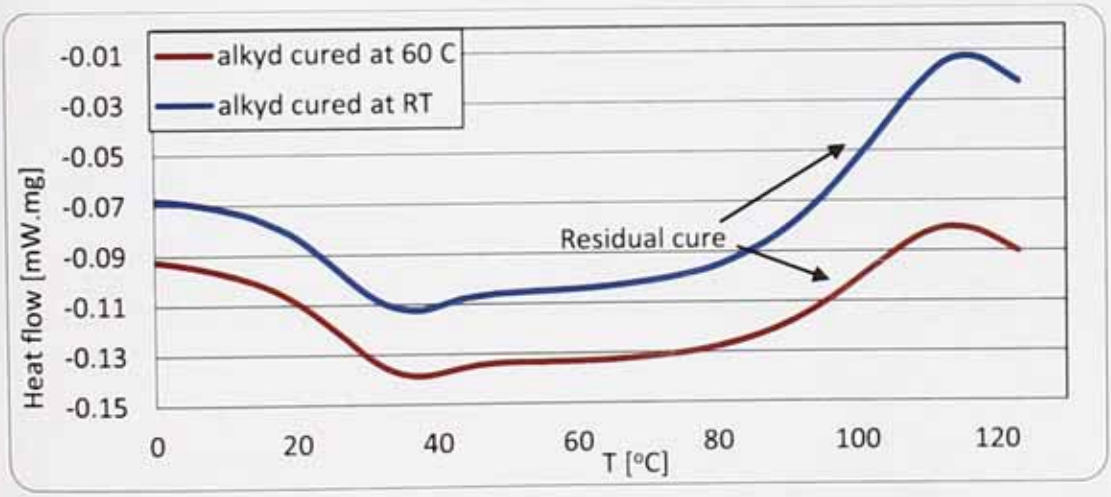

Figure 5.13 DSC thermograms of the alkyd coating cured at room temperature and at 60°C.

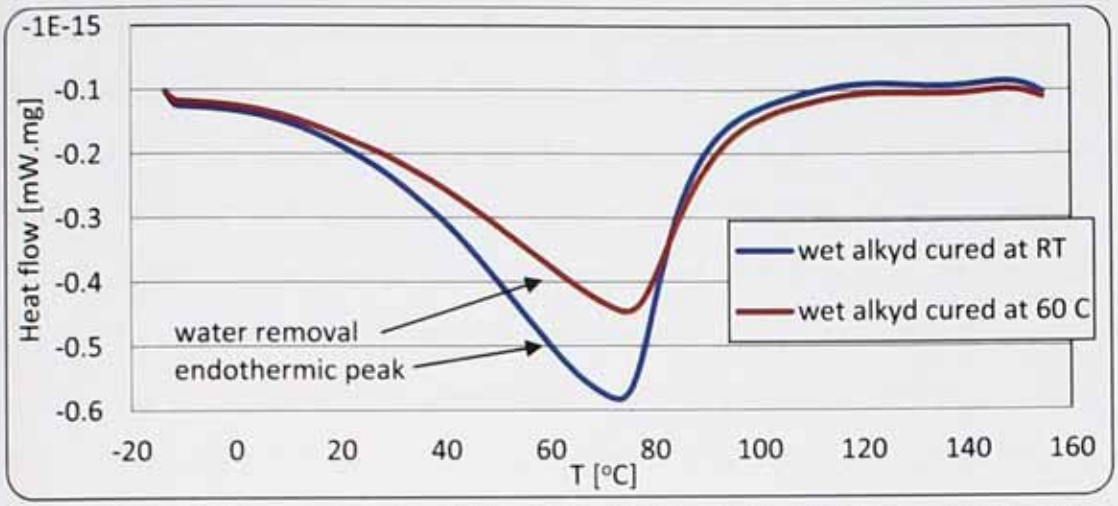

Figure 5.14 DSC thermograms of the wet alkyd coating cured at room temperature and at 60°C.

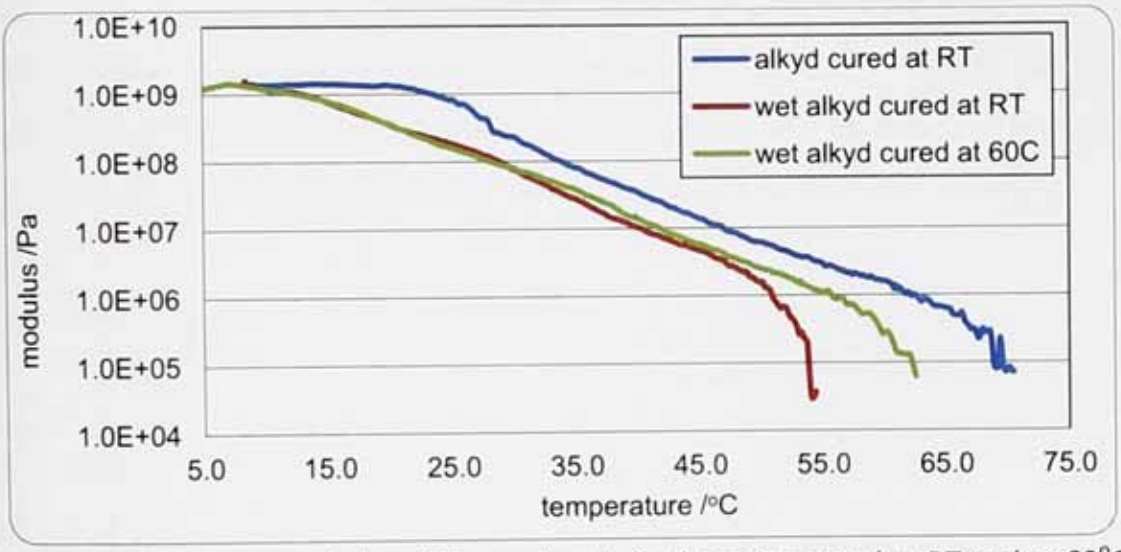

Figure 5.15 Storage modulus of dry and wet alkyd coating cured at RT and at 60°C measured by DMTA.

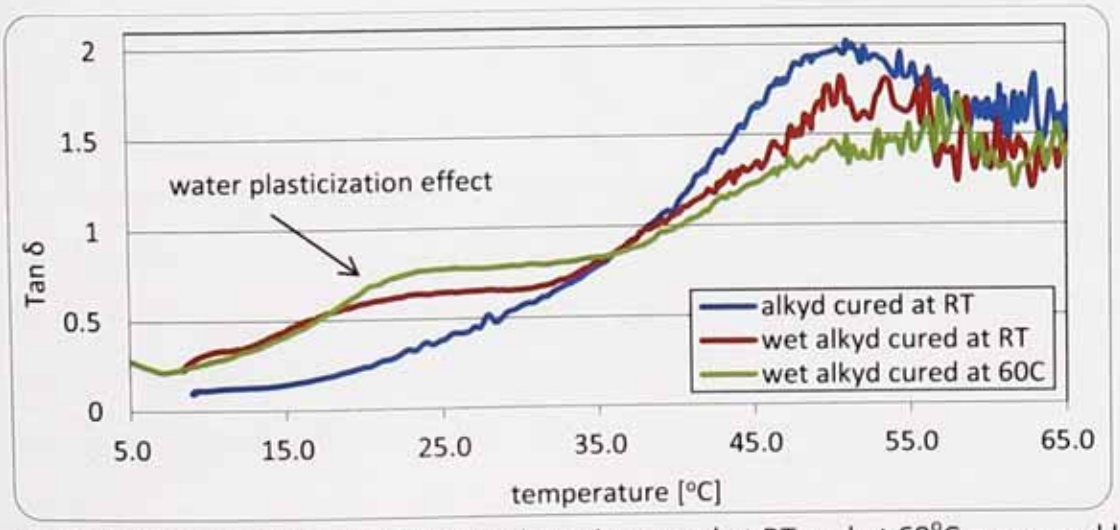

Figure 5.16 Tan δ of dry and wet alkyd coating cured at RT and at 60°C measured by DMTA.

More recently, the beneficial effect of extended curing time on lowering the porosity of polyester coating and its permeability was shown by Worsley *et al.* [29]. Post annealing of thermoset or crosslinked coatings has been shown to make no significant difference to the homogeneity or D/I type ratio of coatings [5]. However a more recent study on a thermoplastic polycarbonate coating showed that post annealing can reduce the size and the number of pores and increase the homogeneity [30]. The effect of temperature of cure was further studied using polyurethane varnish cured at 20°C, 70°C and 110°C. Steel Q-panel was coated with 100±2 µm PU and immersed in 0.5M NaCl for 42 days. Results, as shown in figure 5.17, revealed that elevated curing temperature up to 110 °C can improve DC resistance of coatings by about two orders of magnitude that remained consistent for the duration of experiment. The improved performance of coating is attributed to higher crosslinking density and uniformity of chemical structure as revealed by thermo-mechanical characterization (data not presented). Increase of Tg and crosslinking of organic coatings as a result of force drying at higher temperature is discussed in detail in ref. [31].

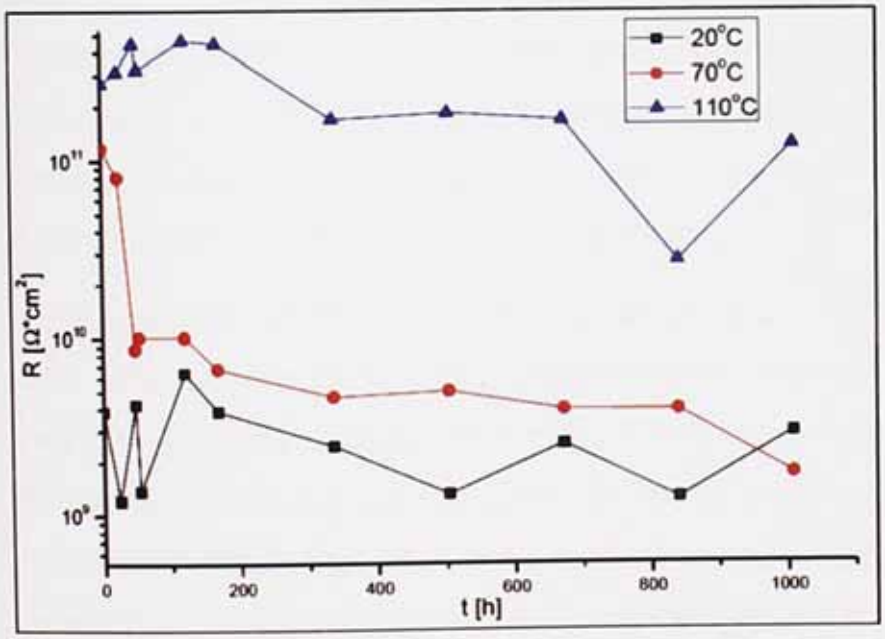

Figure 5.17 Effect of curing temperature on DC resistance of steel Q-panel coated by polyurethane varnish with 100±2 µm thickness immersed in 0.5 M NaCl solution showing the beneficial effect of curing at elevated temperature (reproduced from ref. [32]).

5.6.3Effect of solvent

100% solid epoxies are normally made by using reactive diluents as viscosity modifiers [33]. These reactive diluents are epoxidised molecules that participate in crosslinking reactions of epoxy and become a part of polymeric network. They are mainly used in the paint industry to meet the increasingly strict environmental regulations that push manufacturers towards low VOC paints. Reactive diluents may also be used to impart properties such as flexibility and impact resistance. From the permeability point of view, solvents have always been suspected to play a part in making "escape ways" during the drying process which will later turn into highly permeable areas or D areas [8]. Therefore, the inhomogeneity of 100% solid paints are particularly interesting to study since the volatile matter has been eliminated from the paint formulation and it cannot contribute to D area formation.

Another interesting group of paints (in terms of the solvent used in the paint formulation) are waterborne coatings. Waterborne paints also gained attraction in the paint industry because of their low VOC characteristics but they are also interesting because of their homogeneous chemical structure. Waterborne resins are pre-polymerized polymer micelles with relatively narrow and uniform molecular weight distribution. Final coating forms as a result of evaporation of water and co-solvent followed by inter-diffusion (coalescence) of polymer micelles and poly-functional curing agent.

Here the effect of solvent is studied by comparing a solvent free epoxy/polyamine paint (65±5 µm), a waterborne epoxy/polyamine paint (110±10 µm) and a solvent based epoxy/polyamine paint (60±5 µm) and also a solvent base and waterborne PU varnish with 65±5 µm and 85±5 µm thickness respectively. Result of D/I ratio is shown in figure 5.18. The immediate implication of result is the very poor performance (100% D type behaviour) of waterborne coatings. The solvent base PU varnish performed reasonably well (25% D type) while the solvent base epoxy paint was 90% D type. The solvent free epoxy paint stood in between with 57% D type behaviour.

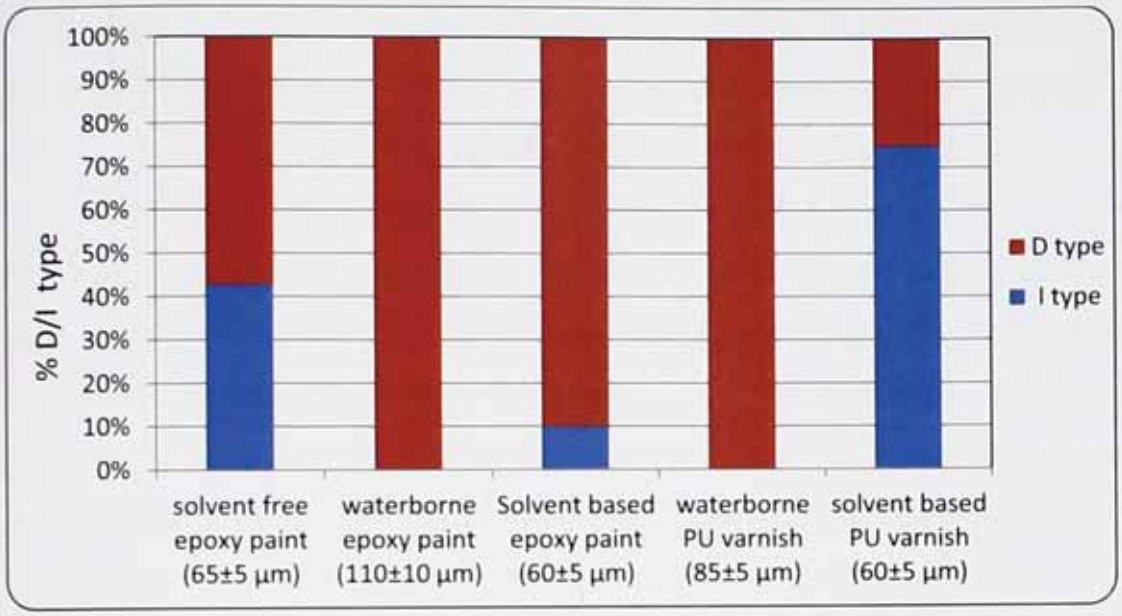

Figure 5.18 D/I type ratio of epoxy/polyamine paint and polyurethane varnish coatings.

There are in essence three main ways of achieving water dispersible resins such as waterborne epoxy and PU including: (1) preparation of an emulsion in water by either dispersing a fully formed resin or polymerising comonomers in an aqueous phase, (2) preparation of an acid rich resin and neutralization with a base hence the resin can be dispersed in water, (3) preparation of a base rich resin and neutralization with an acid [34]. In all cases, the hydrophobicity of coating increases due to the presence of surface active agents (emulsifiers) in the film or a highly ionic structure of resin. The remarkably higher water absorption of waterborne epoxy paint is also confirmed by thermal analysis results shown in Figure 5.19. Similar result was also achieved for PU varnishes (data not presented). The water-uptake induces increases of the polymer permittivity and molecular mobility due to the plasticizing effect [35]. The latter increases also the permittivity of polymer by dipolar relaxation. The highly hydrophilic resin in both cases of waterborne epoxy paint and waterborne PU varnish is believed to be the reason of their 100% D type behaviour. Earlier study by Mayne and Mills [4] also showed 100% D type behaviour of waterborne styrene-butyl acrylate paint with a very uniform resistance behaviour. The unsatisfactory level of protection afforded by waterborne epoxy paint on steel was also stated by the manufacturer (AKZO Nobel, International paints) which could be a result of D type characteristic of the coating.

Mayne [8] in his last contribution to this field, published in 1989, compared a solvent free epoxy/polyamine varnish (75-80 μm) with a solvent based epoxy/polyamine varnish (~98 μm). His results showed 100% I type behaviour of solvent free epoxy which was attributed to the absence of interference of solvent with the curing process thus achieving a highly homogeneous structure. It is believed that a small amount of solvent remains in the coating for a relatively long time after the chemical crosslinking process is completed. Solvent may impact the structural inhomogeneity in two ways. The first is by introducing a spatial hindrance between reacting functional groups during the crosslinking process that results in a lower crosslinking density. The second way that solvent affects inhomogeneity is through it late removal from the paint layer which leaves behind solvent "escape ways". By elimination of solvent from the paint system such detrimental effects are theoretically obviated resulting in an improved I type behaviour. It should be noted again that all works at the Mayne group were performed using 1 cm^2 specimens while here 3.1 cm^2 specimens are used and therefore a direct comparison between these results and Mayne's results is incorrect. However the one case of exception is the 100% I type behaviour at which the size of specimen makes no difference (further detail is given in section 5.9). Compared to the earlier results of Mayne indicating 100% I type behaviour of solvent free epoxy varnish, pigmentation seems to have negatively influenced the homogeneity of solvent free epoxy paint that is studied here. This could be as a result of void formation or poor interfacial interaction between pigment and resin [36]. It should be noted that all epoxy paints used in this study were recommended by manufacturer as primer or as intermediate layer in a multi-layer coating system. Such layers are usually pigmented to near CPVC and therefore they are particularly susceptible to void formation. Unfortunately due to the confidentiality of ingredients and formulation of the industrial epoxy paint system no further information on chemical structure could be obtained and so no further comment on chemical compatibility of the pigment and resin can be made here.

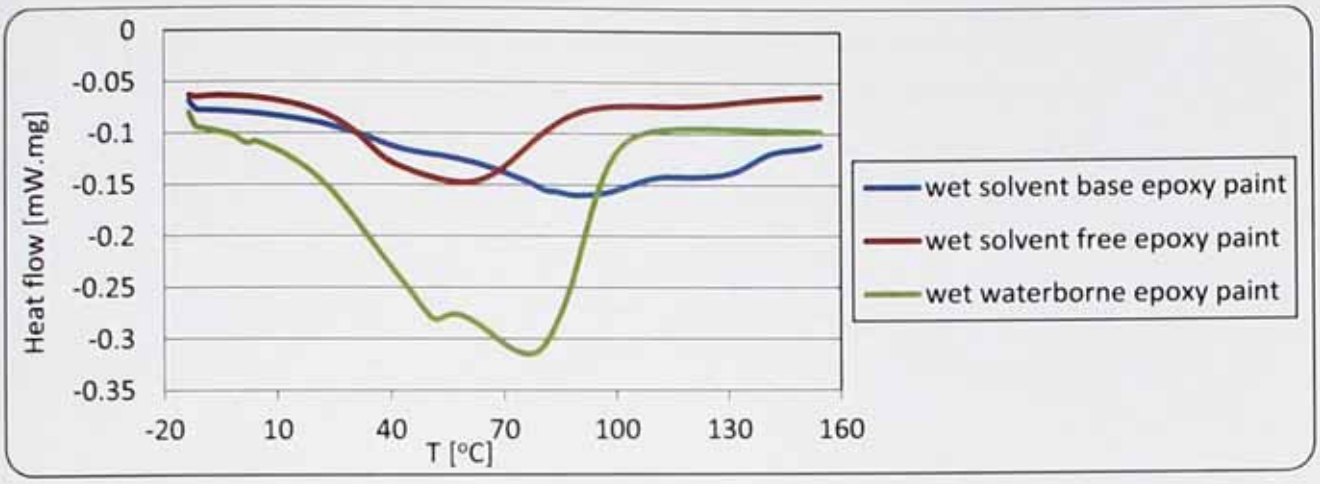

Figure 5.19 DCS thermograms of wet solvent base, waterborne and solvent free epoxy paints.

Figures 5.20 and 5.21 show tan δ and storage modulus of wet films of solvent base, waterborne and solvent free epoxy paints. The water plasticization effect is observed on both solvent based and waterborne epoxies while the solvent free epoxy does not show such effect. Also an interesting observation is that the Tg of solvent free epoxy is lower than Tg of solvent base and waterborne epoxies in water despite its better performance. The relationship between Tg and polymer permittivity has been addressed elsewhere [37,38]. It appears that as long as the Tg of coating is higher than ambient temperature the permittivity is no longer influenced by thermal properties. Figure 5.22 shows the specific volume of a typical amorphous polymer as a function of temperature. The free volume of an amorphous material is the volume not occupied by the molecules making up the material. As temperature increases above Tg, the specific volume increases. There is no additional matter, hence the same molecules are occupying more space as a result of increased molecular motions. Below the Tg, temperature has no influence on the free volume of polymer. The significant increase of free volume is also the reason for increased permittivity and ionic conduction above Tg. A recent study by Li *et al.* also showed that the polarity of resin dominates the equilibrium water content while the free volume is the main factor for diffusion coefficient and activation energy of water sorption [39].

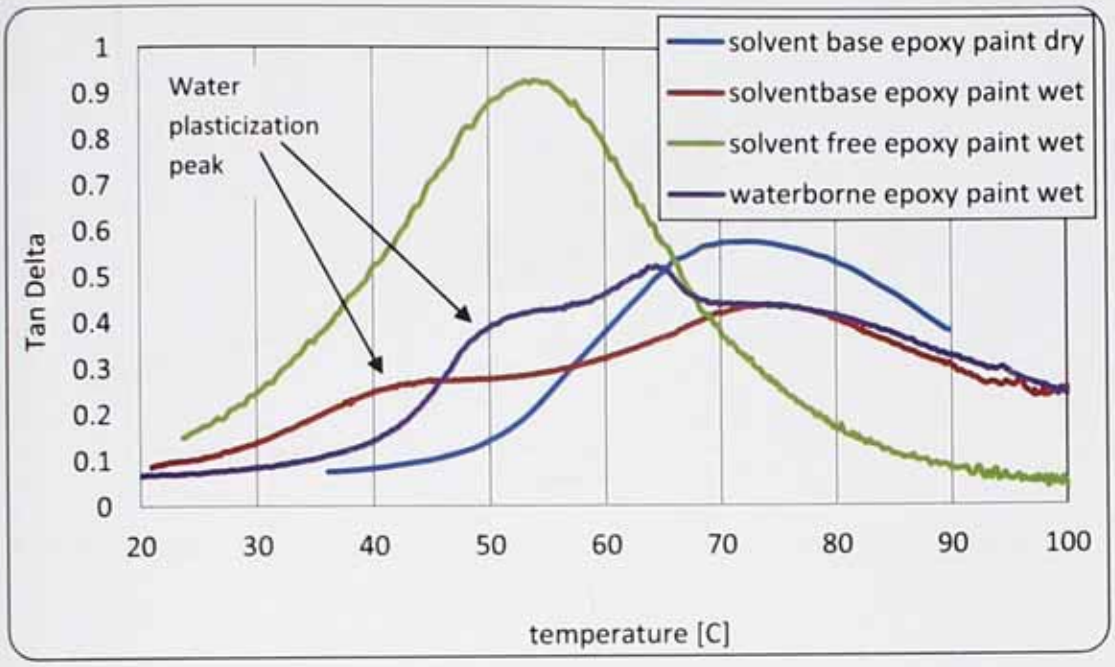

Figure 5.22 Tan δ of solvent base, waterborne and solvent free epoxy paints after being soaked in DI water for 24 hrs. DMTA was performed at 5 oC/min heating rate, 1 Hz oscillation under 1 N force and 20 µm displacement.

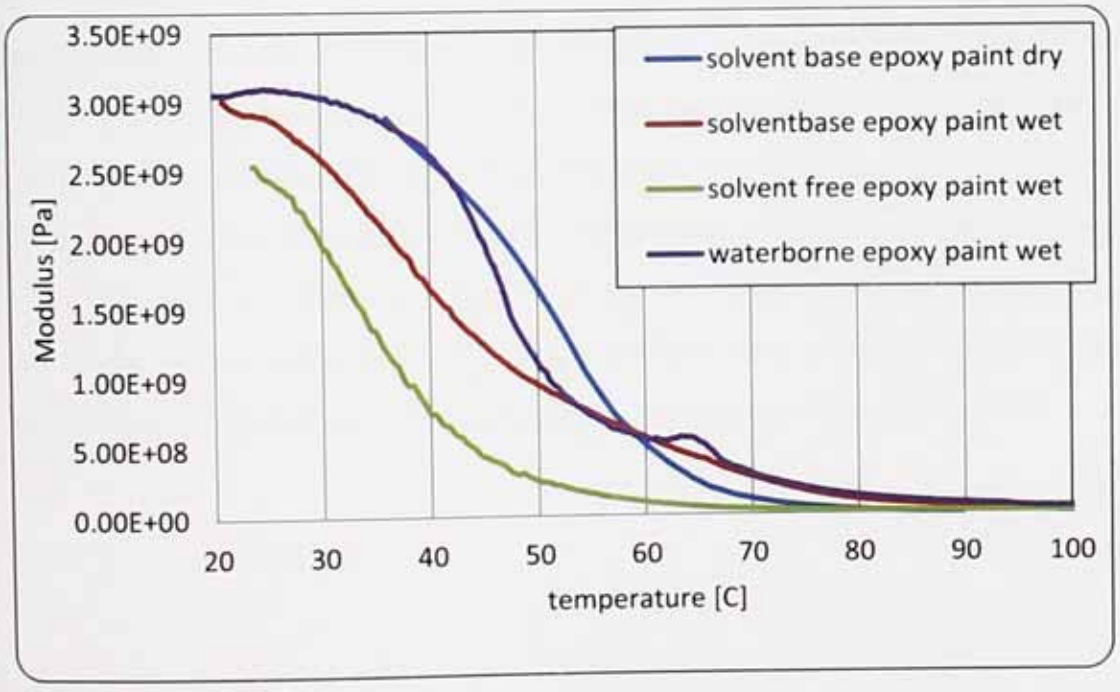

Figure 5.23 Storage modulus of solvent base, waterborne and solvent free epoxy paints after being soaked in DI water for 24 hrs. DMTA was performed at 5 oC/min heating rate, 1 Hz oscillation under 1 N force and 20 µm displacement.

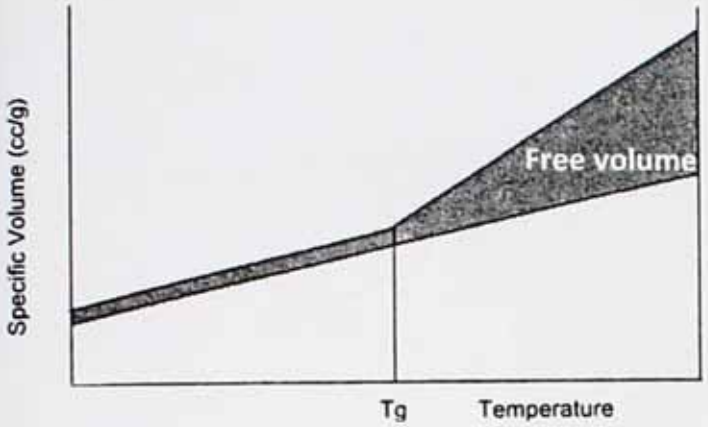

Figure 5.22 relationship between polymer specific and free volume with temperature [40].

The resistance inhomogeneity of waterborne polyurethane varnish on steel was further studied using the wire-beam multi-electrode. The thickness of coating was 45 µm and it was immersed in 0.5 M NaCl solution for 24 hr before the measurement was made. Results showed a relatively homogeneous low resistance across the electrode surface with around 82% of resistances in the range of 1×10^{8} - 2×10^{8} $\Omega.cm^{2}$. The results are also in-line with an earlier study on waterborne acrylic and vinylidene coatings [41]. Compared to solvent based coatings a generally lower resistance with less variation of value among nominally identical samples was reported. This work involved examining large areas of coating on steel panel with DC technique and ENM. A localised breakdown of coating was also suspected in which case the SRET technique was suggested for local examination in the further works. The multi-electrode result presented in figure 5.23 provides evidence for local breakdown of a low resistance waterborne coating as well as locating the breakdown areas.

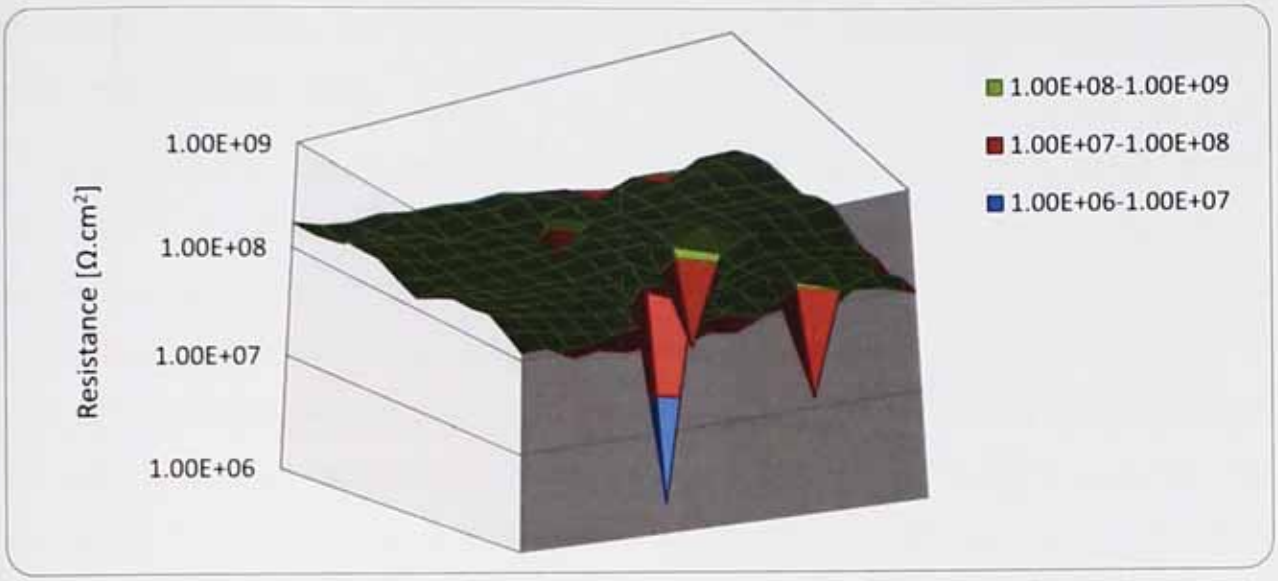

Figure 5.23 DC resistance map acquired by WBE coated by waterborne polyurethane varnish showing distribution of resistance on steel substrate. The film thickness was 45µm and the measurement was made after 24 hrs in 5M NaCl.

5.6.4Effect of solid particles

Effect of addition of nano-silica and pigmentation with zinc phosphate on alkyd resin on D/I type behaviour is shown in figure 5.12. Coatings thickness was 85±5 µm. No reasonable change was observed due to addition of nano particles. It may be that the relatively lower density of nano particles compared to the alkyd has resulted in accumulation/flotation of these particles on the surface and minimal effect on the bulk properties. Improved barrier properties and corrosion resistance of alkyd [42], epoxy [21], polyurethane [43] and a model semi-crystaline thermoplastic polymer film [20] has been reported elsewhere. The key factors of effectiveness of nano particles seem to be the perfection of dispersion [44] and appropriate bonding between nano particles and polymer [45]. Further studies on the effect of addition of nano-silica were conducted using a polyurethane varnish. Earlier results published in reference [32], showed that incompatibility or flocculation of nano silica can negatively influence the protective properties of polyurethane coating. Incompatibility of nano particle could be due to their inappropriate surface treatment, i.e. functional groups on nano particle do not interact with functional groups of polymer, resulting in the phase separation. Silica nano particle are often added into clear coats to improve the mechanical and optical properties such as scratch resistance, mar resistance and UV resistance. Results

presented here shown that such nano particles impart no deleterious effect of protective properties of alkyd coating.

Pigmentation by calcium phosphate has improved the I type behaviour by about 8%. It is suggested that good interfacial bonding between pigment and resin have reinforced the network thus improved the barrier properties. It has been shown that a poor pigment/polymer interface or presence of porous pigment flocculation due to poor dispersion can cause inhomogeneity [36,46]. This result is also in line with early findings of Scantlebury [47] that showed an increased homogeneity of alkyd due to pigmentation with iron oxide. An interesting observation was that unlike alkyd varnish majority of I type alkyd paints changed to D type after 2 weeks immersion in concentrated KCl solution. This is believed to be due to the hydrophobic groups incorporated by calcium diphosphate pigment. It has been shown that even slightly soluble pigments have a remarkable effect of resistance properties of coating [24]. It is also useful to mention the generally lower resistance of alkyd paint on steel, section 4.4.1 figures 4.34 and 4.35, compared to alkyd varnish in the long term. It seems that a critical parameter for an anti-corrosive organic coating with barrier mechanism is not just the I type behaviour in the short term but also retention of such behaviour in the long term.

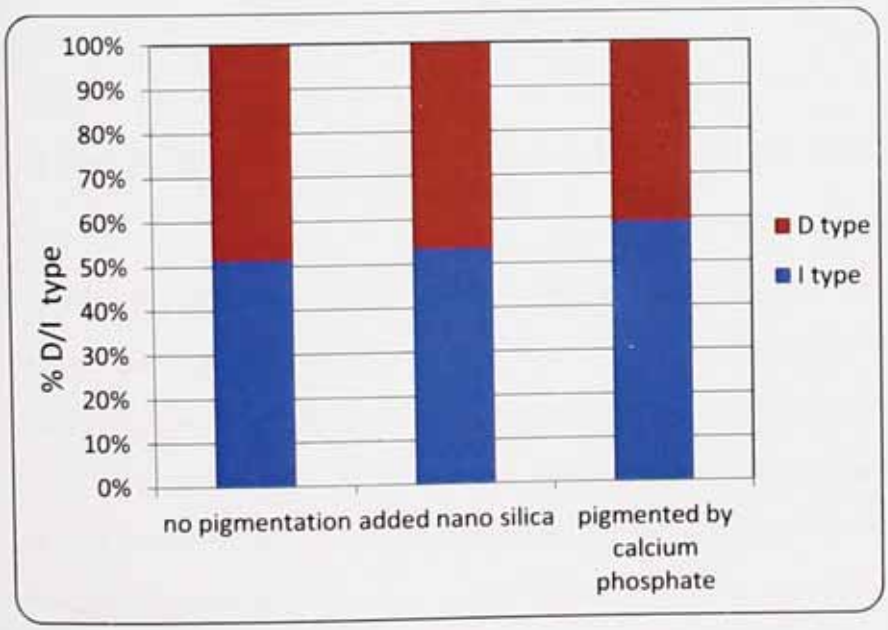

Figure 5.24 Effect of solid particles on D/I type ratio of 85±5 µm alkyd films.

5.6.5Effect of multi-layers

Figure 5.25 shows triple coat alkyd (85±5 µm) exhibiting 100% I type behaviour compared with 50% I type behaviour of a single coat alkyd with the same overall thickness. Note that the triple layer was composed of three coats each about 30 µm. The superior homogeneity of multi-coat system can be due to better solvent removal (similar to the effect of curing temperature) when the layers are applied as a number of thin films. Also it can be a result of D areas being very small and hence most likely they will be overlaid by I type areas present in the subsequent layers. Similar explanation was proposed by Wu *et al.* [15] for better performance of double layer phenolic resin compared to that of the single layer.

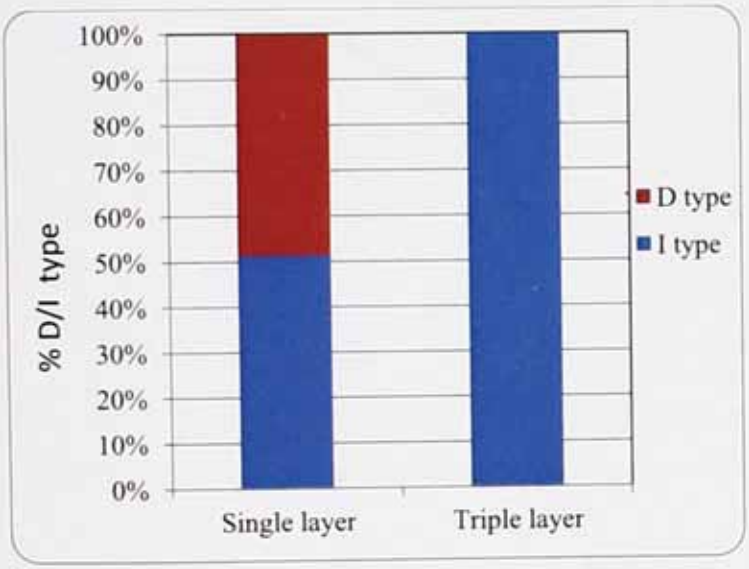

Figure 5.25 Effect of multi-coat application on D/I type behaviour of 85±5 µm alkyd

Solvent retention (also called solvent entrapment) can significantly change the permeability of coating. When the solvent is lost first from the top of alkyd film, a high viscosity, low free volume layer forms at the top of the film through oxidative crosslinking while substantial amount of solvent is still present in the lower levels of the film [40]. It should be noted that most organic coatings are engineered in such a way that Tg of dried coating is higher than the end use temperature. This is mainly because the barrier properties of organic coatings deteriorate as temperature rises above their Tg [48]. The entrapped solvent evaporates through the crosslinked top layer in the long term leaving solvent escape ways. Solvent entrapment results in pinhole formation and macro defects in the worst

scenario if the coating is too thick or if the diluent evaporates too quickly. To avoid this in practice a critical thickness is usually determined by the paint manufacturer. Multi-layer application with thin individual layers reduces the chance of solvent entrapment thus enhances the barrier properties of coating. Multi-layer application may also increase the crosslinking density by providing more accessible oxygen to each individual layer for oxidative drying. However, DSC results for wet and dry alkyd films, figure 5.26, and DMTA examination (data not presented) showed no reasonable difference between single and multi-layer alkyd films hence ruled out the higher crosslinking density hypothesis.

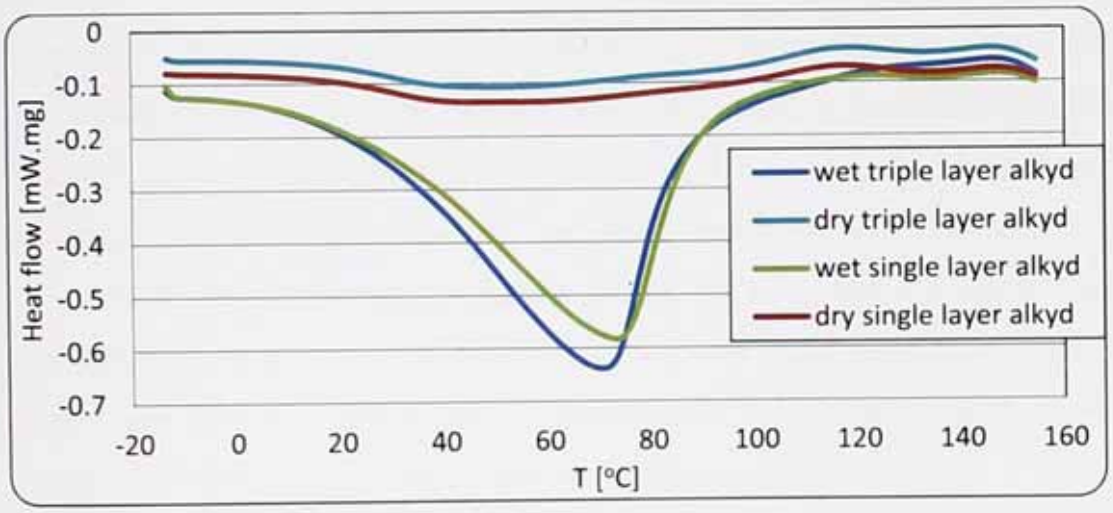

Figure 5.26 DSC thermograms of wet and dry films of single and triple layer alkyd varnishes.

5.6.6 Effect of partially non-functional polymer

One theory of "what D areas consist of" is that they are agglomerates of low functionality polymers that result in locally poor crosslinking in the final coating. A previous unpublished study involved separation of high and low molecular weight alkyd using centrifuge followed by film preparation and D/I ratio measurement. It was shown that the film prepared from low molecular alkyd contains fewer D areas. This was attributed to presence of clumps of non-functional (or *dead*) polymers in the higher molecular weight alkyd. However it could equally be due to the higher crosslinking density of low molecular weight alkyd film. The lower molecular weight fraction of a typical alkyd resin is mainly composed of esters of unsaturated fatty acids with polyols [49] and it is well known that lower molecular weight of

functional resins produce higher crosslinking density. Both hypotheses stand on crosslinking deficiency as the main cause of D area formation.

In this study a comparison was made between detached films of alkyd from freshly opened container and the same material which was incubated at 60 °C for 10 days. Figure 5.27 compares the FTIR-ATR spectrum of a fresh alkyd and the same alkyd resin after incubation. The intensity of spectrums are normalised in regards to the base line and control peaks of $-CH_3$ and $-CH_2$ for the purpose of comparison.

The absence of a strong peak of OH group at 3350-3550 cm^{-1} range indicates a good degree of condensation polymerisation of alkyd that has successfully reduced number of carboxylic acid groups in esterification reaction. The lower number of carboxylic groups has a beneficial effect on reducing the ionic exchange capacity of resin which has been discussed in detail earlier in section 5.61. Asymmetric stretching peak of $-CH_3$ at 2920 cm^{-1}, symmetric stretching peak of $-CH_2$ at 2854 cm^{-1} and bending peak of $-CH_2$ at 1450 cm^{-1}, as well as, a strong C=O carbonyl stretching around 1728 cm^{-1} are all typical of an alkyd. Also present are the C-H bending, C-O and C-C stretching fingerprint peaks at 1261 cm^{-1} (likely due to the esters) and 1118 cm^{-1}. The important peak at 1068 cm^{-1} corresponds to unsaturated (C=C) bonds that play the key role in oxidative curing of an alkyd [50]. It is evident from the spectrum that incubation has reduced the number of potentially active (C=C) groups of alkyd, thereby lower crosslinking density is anticipated from the incubated alkyd.

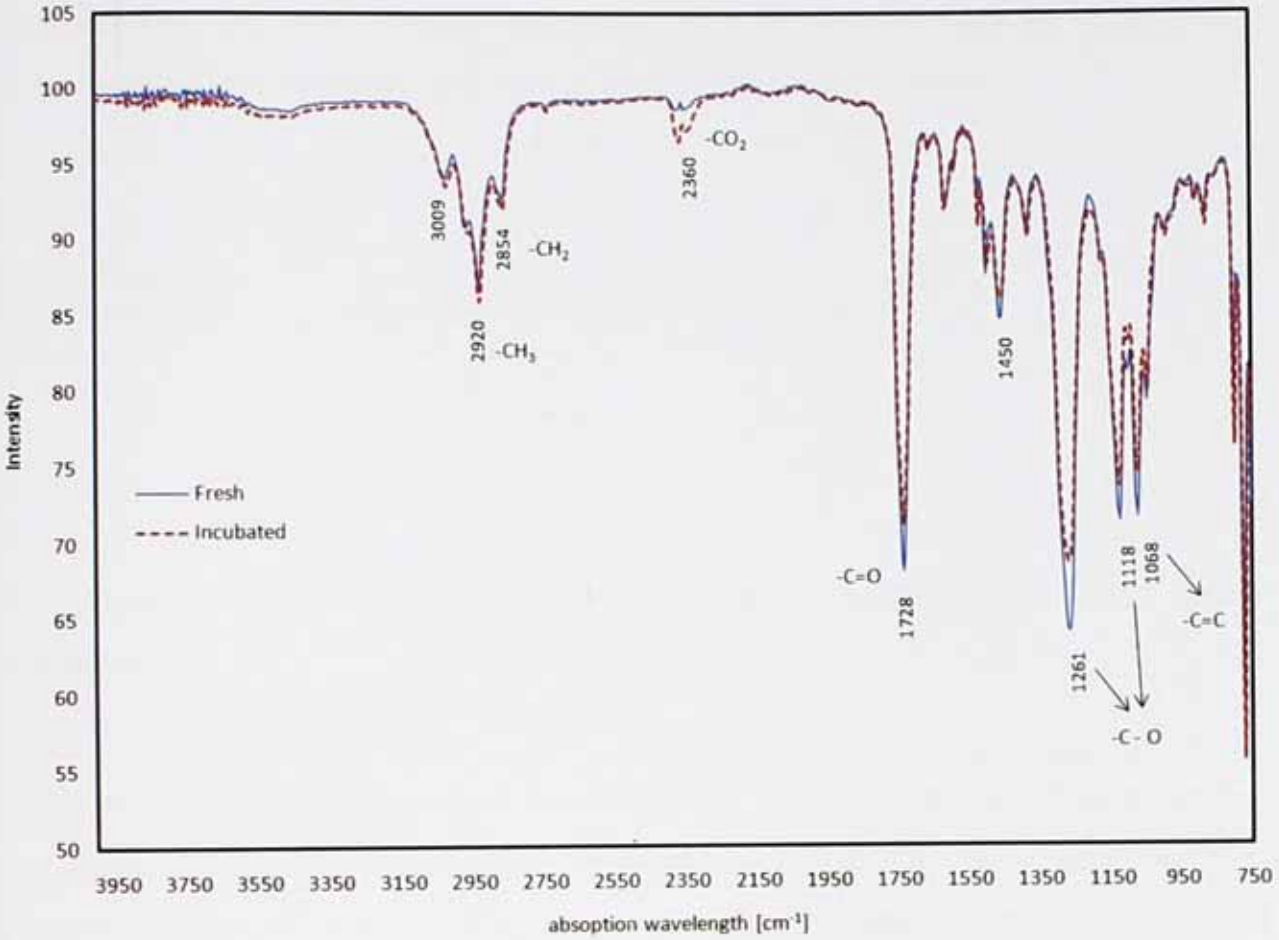

Figure 5.27 FTIR-ATR spectrum of the fresh alkyd resin with the incubated at 60°C for 10 days.

A number of mechanisms can potentially produce the initial radical for grafting co-polymerisation shown in the figure 5.28. Metal catalysts used for preparation of alkyd resin in condensation polymerisation remain in the resin after packaging. These metal catalysts, such as Co^{3+}, might participate in a hydrogen abstraction reaction (equations 5.1 and 5.2) and produce a radical at high temperatures [51,52].

$$Co^{3+} + RH \rightarrow Co^{2+} + R\circ + H^{+} \quad (5.1)$$

$$R - CH = CH - R + Co^{3+} \rightarrow R - {}^{\circ}CH - CH^{+} - R + Co^{2+} \quad (5.2)$$

Alternatively the condensation reaction between the residues of carboxylic acid groups and $-CH_3$ groups on alkyd backbone may produce the initial radical for grafting co-

polymerisation. All these reactions are negligible at ambient temperature so that alkyd remains stable and reactive for long time in the can at room temperature.

Figure 5.28 Grafting mechanism for addition through the double bond of alkyd (radical polymerisation) [53].

Figure 5.15 shows the increased percentage of D type from 64% to 78% as a result of incubation. This significant increase of D type behaviour is due to the reduced number of reactive C=C groups as shown by FTIR spectroscopy. The non-functional parts of resin do not participate in oxidative curing hence produce deficiently crosslinked regions with higher permeability to ions.

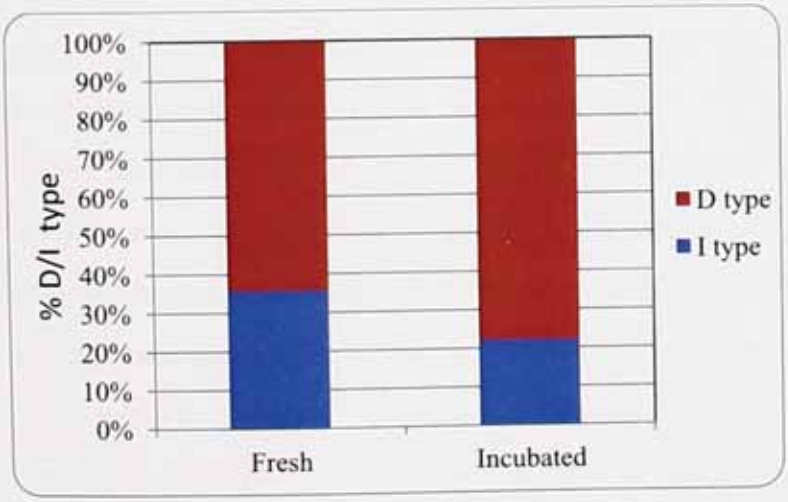

Figure 5.29 Effect of incubation of D/I type behavior of a 75µm alkyd film.

It should be noted that the incubation method used in this study for alkyd resin is widely used in paint industry as artificial aging to predict the shelf-life of paints. Changes in physico-

mechanical properties of liquid paint after long-term storage on shelf are correlated with the changes after short-term incubation. Therefore similar increase of D type behaviour is anticipated for an aged alkyd resin (e.g. shelved for a year). The effect of material aging was also studied by Moongkhamklang and Taylor [25] for epoxy/polyamide coatings. They studied the effect of age of raw material on the number chloride clusters within epoxy film. Their results also showed larger number and size of chloride clusters in the filmed produced by old material.

5.7 Water absorption

Water absorption is a key feature in determining the conduction mechanism of organic coatings. As mentioned earlier, it is believed that ionic conduction is controlled by water activity at I type areas in the absence of continuous aqueous pathways while at D type areas ionic activity dominates the conduction mechanism. This is because of higher water absorption at D areas that is caused by structural inconsistency such as local lack of crosslinking or inclusion of hydrophobic chemical groups.

The water absorption by alkyd films of different ionic conductions (i.e. D and I types) behaviour was studied using the capacitive component extracted from EIS measurement. Capacitive component is frequently used, in Brasher-kingsbury equation [54], to calculate water absorbed by a polymer film in a given electrolyte. Rise of dielectric constant of polymer film in electrolyte is attributed to the absorbed water which has a remarkably higher dielectric constant, i.e. 80, compared to that of a typical polymer, which is 4-8. Here capacitive component is directly used as an indication of water absorption. Table 5.1 shows the resistance, capacitance and relative change of capacitance for alkyd films in different concentrations of NaCl solutions. The capacitance method, used by Brasher-Kingsbury [54] or by Sykes in the corrected equation [55], assumes the water absorption a uniform process. The similarity of the value of water absorption suggests that D areas are fairly small regions of the coating, with no major influence on overall water absorption.

Table 5.1 Capacitance values of a set of alkyd varnish detached films with bimodal (D or I type) behaviour at different salt concentration, all having 85±5 µm film thickness.

		5 M NaCl		0.5 M NaCl			0.001 M NaCl		
Order	Type	R (ohm.cm^2)	C (F/cm^2)	R (ohm.cm^2)	C (F/cm^2)	$C_{0.5M}/C_{5M}$	R (ohm.cm^2)	C (F/cm^2)	$C_{0.001M}/C_{5M}$
1	D	1.80E+06	6.73E-11	8.84E+06	7.69E-11	1.14	1.03E+08	8.35E-11	1.24
2	D	1.48E+07	7.54E-11	3.31E+08	8.51E-11	1.13	6.88E+08	9.39E-11	1.25
3	I	1.27E+09	3.01E-11	1.25E+09	3.60E-11	1.20	8.66E+08	3.69E-11	1.23
4	D	2.68E+06	4.89E-11	1.69E+07	5.81E-11	1.19	3.75E+08	6.48E-11	1.32
5	D	3.48E+07	4.55E-11	1.45E+08	5.49E-11	1.21	7.13E+08	5.86E-11	1.29
6	I	1.17E+09	4.66E-11	9.07E+08	5.46E-11	1.17	8.06E+08	5.62E-11	1.20
7	I	1.37E+09	4.29E-11	1.03E+09	4.78E-11	1.12	9.49E+08	5.08E-11	1.19

5.8 Statistical model for distribution of D type areas

Despite the comprehensive systematic studies performed by Mayne group in Cambridge, limited work was done in the area of theoretical modelling of D areas distribution. It has been suggested that D type areas obey the Poisson model of distribution. The wisdom received from the previous works [5] also showed that D ratios measured based on groups of 20 samples follows Gaussian distribution, e.g. D ratios are not exactly the same when measured for different groups of samples but they are distributed around a mean value with Gaussian or Normal distribution.

The critical assumption here is that D areas are very small fraction of the film. It has been estimated that D type areas occupy a very small fraction, i.e. $10^{-3} - 10^{-4}$, of a 1cm^2 film, while the conduction could be 10^7-10^8 easier than in I areas [5]. Miskovic *et al.* estimated the radius of the pores in the range of 3 to 7.2 µm by statistical analysis of microscopy and spectroscopy results [56]. More recently Moongkhamklang and Taylor [25,57] developed a fluorescence microscopy technique using a chloride specific chromophore to image the areas at which chloride is clustered. Their results showed chloride clusters within areas of 10 µm sizes or less. A recent EDX mapping study of epoxy coating by Eltai *et al.* [58] showed sodium accumulation sites within different sizes up to 40 µm. The very small size of D areas also explains the similarity of resistance of D type and I type films at low concentration of salt and also insignificance of D areas on macroscopic properties, e.g. water-uptake, mechanical properties.

To develop a statistical model for D areas distribution, several random distributions of D areas in a 2-D plane with varying number of D areas were generated using "homogeneous Poisson point pattern distribution" tool of "R" statistical programming software. Figure 5.30 shows six examples of such data generations for a certain case of 20 D areas distributed in a 10x10 area with 2x2 sampling size. D to I ratios for these examples are 64%, 56%, 48%, 44%, 60% and 56%. It is apparent that choosing a smaller sample size, e.g. 1x1, would result in a lower D to I ratio for a given number of D areas. To obtain a repeatable mean value a large number of these examples, i.e. 1000, were generated and the average D to I ratio was calculated using Monte Carlo simulation model. D to I ratio was defined as fraction of squares containing one or more D areas. Using Monte Carlo simulation model and a very large number of data generation for each given number of D areas and mesh size resulted in virtually zero error for each D ratio calculation.

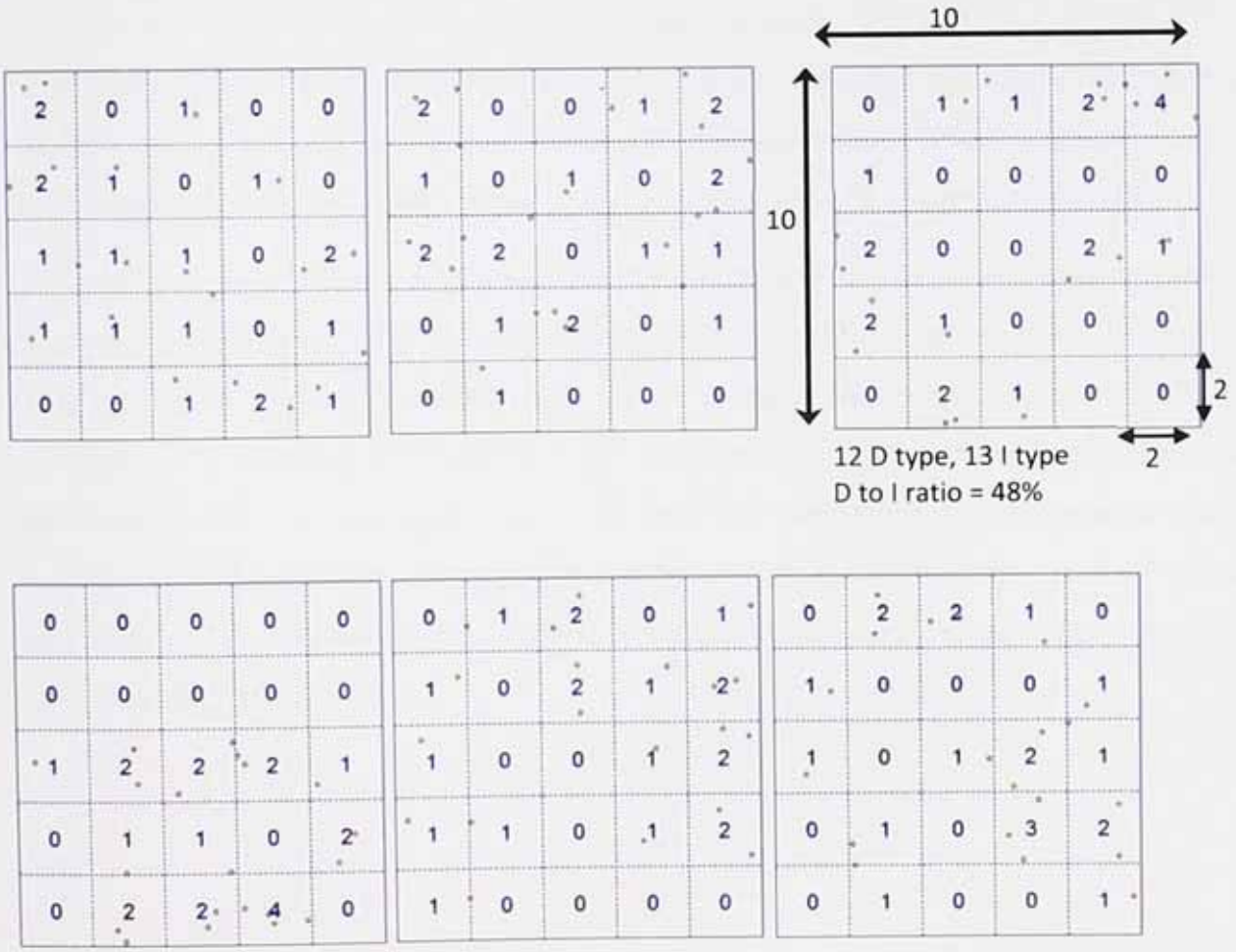

Figure 5.30 Six random distributions of 20 D areas in a 2-D plane generated using "Poisson point pattern". Numbers in each square represent the number of D areas.

Resulting D to I ratios for a given number of D areas and mesh (sample) size had a normal or Gaussian distribution around a mean value. The mean value was taken as the average D to I ratio and used in subsequent modelling.

The above process was repeated for varying number of D areas distributed in a 100x100 area with varying mesh size. Note, using the dimensionless window size brings about the possibility of applying the model to different size of samples, e.g. 10×10 m^2,10×10 dm^2, 10×10 cm^2 etc. Figures 5.31 and 5.32 plot the number of D areas against D to I ratio for different samples sizes. Figure 5.32 is basically magnified version of figure 5.31 for up to 200 D areas. The first important use of these plots is that the number of D areas can be estimated in a large surface based on the D to I ratio measured in the lab. For example about 65 D areas are *expected* on a 100 cm^2 coating when D to I ratio is 50% based on 1 cm^2 samples. The D to I ratio can be measured on a relatively few number of samples, e.g. 20 samples, and the result is generalized for a large surface. This is due to an important assumption of the random distribution of D area that is a true assumption here. Therefore a smaller group of samples, e.g. 20, would be a true representative of the large group. The significance of D areas has been defined earlier as potential spots of corrosion initiation.

Figures 5.31 and 5.32 are also useful for converting the D ratio results obtained using different size of samples. For example all early studies in Mayne group were conducted using 1cm^2 sample size while in this study 3.1 cm^2 samples were used. Therefore a 50% D ratio measured in Mayne group (using 1 cm^2 specimens) is equal to 88% D ratio if it was measured using 3.1 cm^2 specimens. Such coating is also expected to contain approximately 65 D areas within a 10×10 cm coating. It should be noted that all converted values extracted from these plots are statistical "expected values" and the actual value may differ due to the random distribution of D areas.

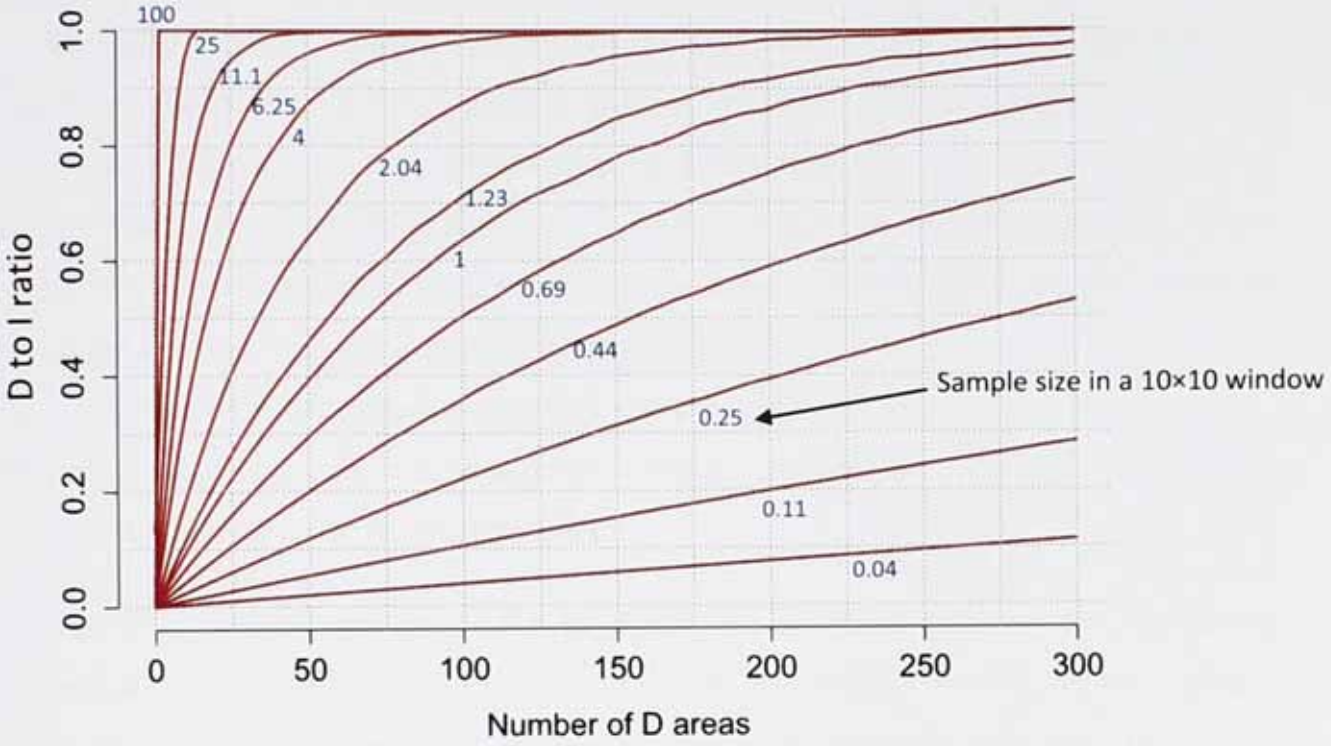

Figure 5.31 Statistical predictive plots for number of D areas, up to 300 D area, in a 10x10 area of coating based on the D to I ratio and the sample size.

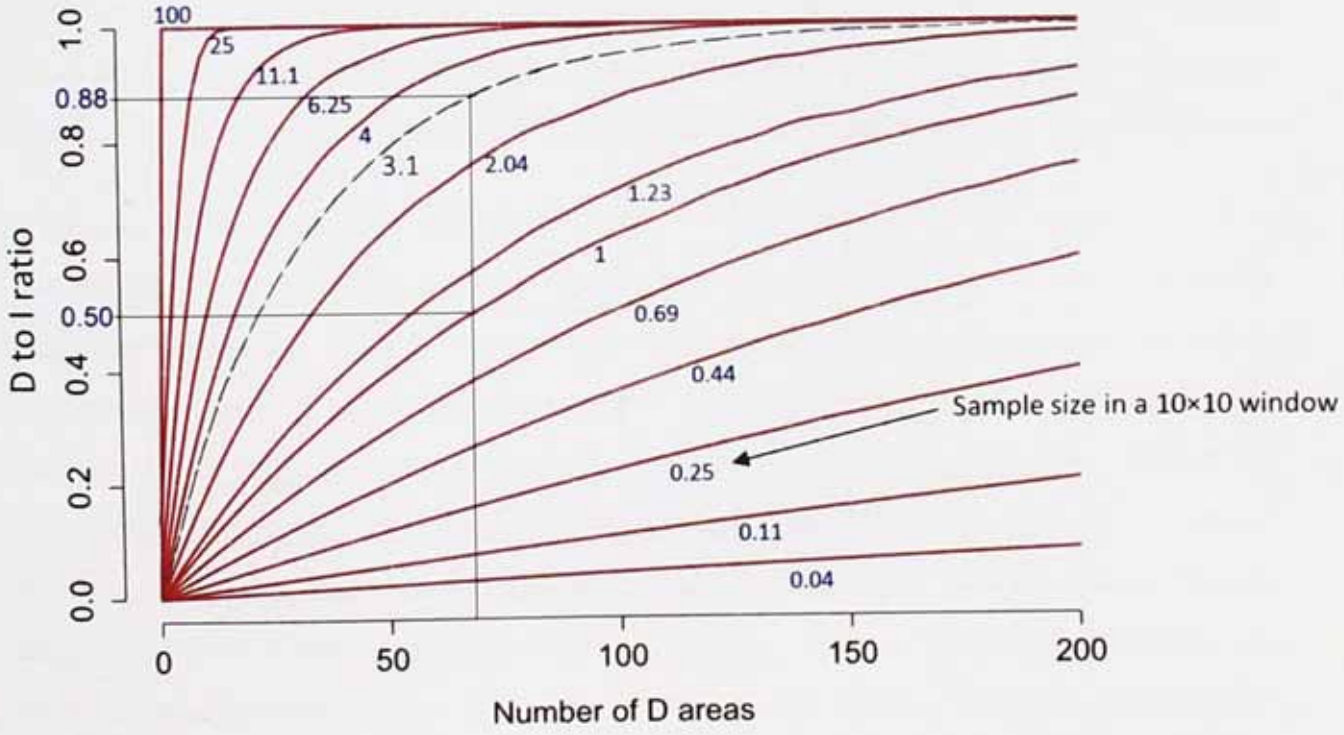

Figure 5.32 Statistical predictive plots for number of D areas, up to 200 D area, in a 10x10 area of coating based on the D to I ratio and the sample size.

5.9 Summary

The early findings in Mayne's group (and the experiments here) strongly suggested that water absorption is remarkably higher at D areas therefore conduction in D type areas is a function of salt concentration independent of water activity. In fact, factors that attract water inside coating can potentially form D areas. The first big question is whether D type areas form due to the chemical or physical discontinuity. Three hypotheses were advanced from the early works as causes of D areas including:

- congregates of low molecular weight material in polymer film
- weakening the crosslinking as solvent escapes in certain areas
- presence of innate material in the resin

The sole chemical variables, such as partly non-functional polymer and hydrophilic functional groups (waterborne coatings), and sole physical parameters, such as coating thickness and multiple layers of coating, studied here suggested that both factors are significant. In the absence of both chemical and physical interaction, e.g. incorporation of a non-reactant nano silica, no significant change in D/I ratio was observed. Several theories of origins of inhomogeneity in organic coatings have been discussed. The experimental results presented here confirmed earlier hypothesis and the significance of the solvent escape ways, the dead or non-functional polymer parts and inherently hydrophilic functional groups as the mechanisms playing a part in formation of locally permeable areas or D type coatings.

In case of the improved homogeneity achieved by elevated curing temperature it is believed that more effective removal of solvent and enhanced crosslinking synergistically improved the coating. The DSC results indicated that the enhancement in resistance and in homogeneity brought about by force drying is associated with a higher yield of oxidative reactions and improved crosslinking at elevated temperature. However, since this improvement is most significant at small D type sites, the bulk physico-mechanical techniques (DSC & DMTA) could not detect the significance on the bulk physico-mechanical properties such as glass transition temperature, T_g. Previous findings [5] showed that annealing of alkyd coating after it has been dried does not make a significant change in D/I type ratio. This is due to the insignificant change that temperature makes on an immobilised network with crosslinked structure. It has been shown that annealing can improve the

homogeneity of thermoplastic coatings with significant reduction in the size and the number of pores [30].

Crosslinking deficiency of polymers such as epoxy and PU seem to have a synergistic effect on coating permittivity and inhomogeneity by providing larger space between non-linked polymer chains and by providing larger number of unreacted hydrophilic groups such as –NH, -OH, -NCO. This study also showed that waterborne coatings are intrinsically hydrophilic and may not afford anti-corrosion protection by barrier mechanism. The surface active agents used for emulsification and/or high ionic content of resin remarkably increase the water uptake and results in 100% D type coatings. The D/I ratio results and resistance distribution map of waterborne coatings presented here are also consistent with earlier work [4] on styrene-butyl acrylate emulsion paint that revealed 100% D type behaviour with very uniform resistance behaviour. The result presented in the previous chapter, section 4.4.1 figure 4.36, revealed a poor level of protection afforded by the waterborne PU varnish.

In case of most functional polymers, e.g. epoxy, PU, it is hard to separate the effect of crosslinking from the hydrophilicity of unreacted functional groups. For instance in case of epoxy resin, unreacted amine/amide groups cause more water to be absorbed while the lack crosslinking provides space for the absorbed water. Alkyd is particularly interesting since the unreacted, C=C, groups are not significantly different from C-C groups in terms of hydrophilicity, so that the effect of crosslinking can be investigated independently from the hydrophilic nature of polymer/functional groups. It has been also postulated from this study that highly hydrophilic polymers, such as waterborne coatings, are 100% D type.

The effect of presence of –COOH groups in alkyd is more pronounced in the long term. Ideally a fully polymerized alkyd resin should not contain any COOH groups as COOH groups (of fatty acid) are supposed to react with OH groups of polyols in an esterification reaction to yield a high molecular weight alkyd polymer. However in practice no polymerisation reached 100% yield and therefore COOH groups are remains of imperfect polymerisation. Although COOH groups do not participate in oxidative drying of alkyd film, they increase ion exchange capacity of coating which in the long term may result in the increased water uptake and change of I type films to D types. Similar process (turning I types to D types) may be triggered by pigmentation as observed in this study.

Multi-electrode results showed that increasing the thickness of an alkyd film increases both the resistance and the homogeneity of the film. The multi-electrode also detected the changes in homogeneity and average resistance due to the force drying at 60°C. Similar results was achieved by measuring the D/I type ratio of detached pieces of coating which were about 4 times thicker and of 45 times larger surface area. It is therefore concluded that the Multi-electrode array method is a powerful way of finding out relatively quickly about important variables such as composition, drying conditions, thickness on the resistance and homogeneity of coatings.

The model suggested in figure 5.33 explains the synergistic effect of crosslinking density and solvent entrapment in a typical crosslinking polymer structure. A well crosslinked polymer is shown in figure 5.33a. If the major crosslinking occurs before the solvent is removed from the coating (figure 5.33b), the spatial hindrance caused by solvent molecules results in lower crosslink density in the locations of solvent entrapment (figure 5.33c). As the solvent evaporates in the later stages of drying, it leaves behind nano cavities. The permittivity of the resultant film is significantly higher within these cavities. As these cavities connect, they form a continuous easy pathway for ions (figure 5.34a) where relatively large volume of water can be accommodated, thus the ionic activity of solution defines the electrical resistance (characteristic of D type areas). By increasing the film thickness there will be higher chance of interruption of pathway by an insulating phase resulting in lower permittivity thus I type behaviour (figure 5.34b).

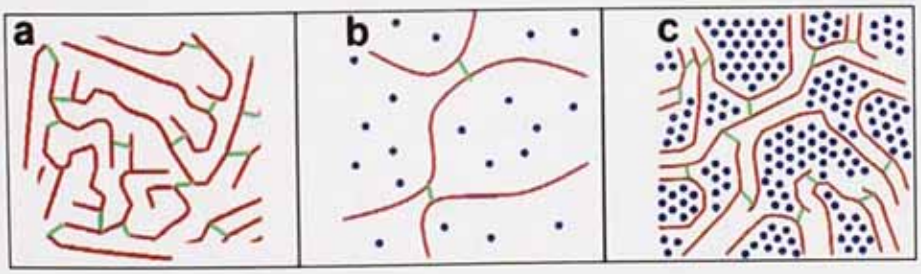

Figure 5.33 Schematic model of a crosslinking polymer with (a) an ideal network (b and C) the lack of crosslinking as a result of solvent entrapment.

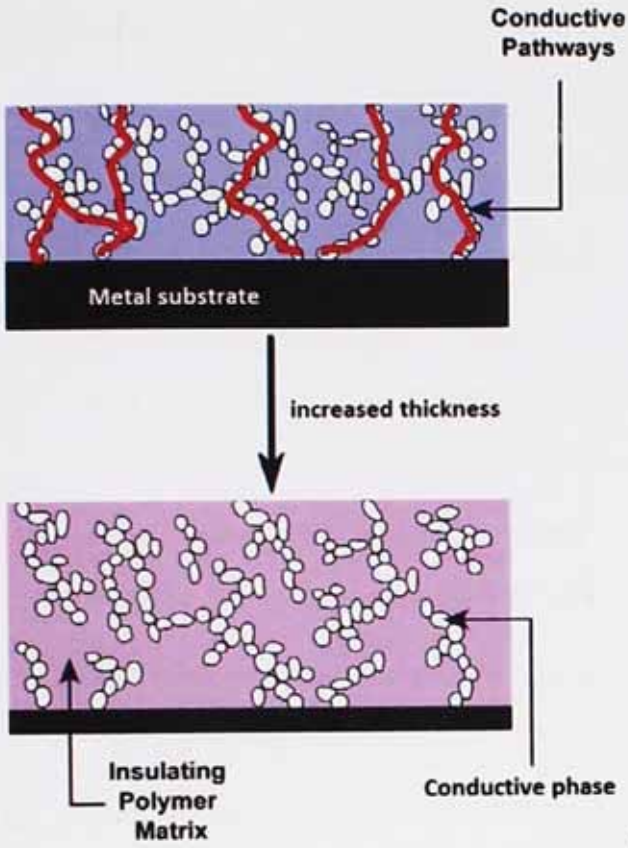

Figure 5.34 Formation of continuous ionic pathways by adjoining the molecular size cavities (a) and interruption of continuous pathways by increasing the film thickness (b).

Publications

- S.S. Jamali, D.J. Mills, Inhomogeneity of organic coatings and its effect on protection, in: N. Birbilis (Ed.), Corrosion and Protection, ACA, Melbourne, November 2012, paper no. 150.

- D.J. Mills, S.S. Jamali, Use of wire-beam multi-electrode to examine coating heterogeneity and thus assist in understanding how it arises and can be improved, EUROCORR 2012, Istanbul, Turkey, September 2012 , paper no. 1299.

- D.J. Mills, S.S. Jamali, K. Paprocka, Investigation into the effect of nano-silica on the protective properties of polyurethane coatings, Surface & Coatings Technology. 209 (2012) 137–142.

References

[1] W.H. Walker, W.K. Lewis, Paint and varnish coatings as accelerators in the corrosion of metals, Industrial and Engineering Chemistry. (1909) 754–758.

[2] M.D. Buller, The effect of pigmentation on conduction in polymer films, PhD thesis, University of Cambridge, 1976.

[3] E.M. Kinsella, J.E.O. Mayne, Ionic conduction in polymer films I. influence of electrolyte on resistance, British Polymer Journal. 1 (1969) 173–176.

[4] J.E.O. Mayne, D.J. Mills, The effect of the substrate on the electrical resistance of polymer films, Journal of Oil and Colour Chemists Association. 58 (1975) 155–159.

[5] D.J. Mills, The function of basic pigments in protection by organic coatings, PhD thesis, Dept. of Materials Science and Metallurgy, University of Cambridge, 1973.

[6] E.M. Kinsella, J.E.O. Mayne, J.D. Scantlebury, Ionic conduction in polymer films III. influence of temperature on water absorption, British Polymer Journal. 3 (1971) 41–43.

[7] J.E.O. Mayne, J.D. Scantlebury, Ionic conduction in polymer films IV. the effect of pigmentation with iron oxide, British Corrosion Journal. 3 (1971) 237–239.

[8] J.E.O. Mayne, The crosslinking and adhesion to mild steel of epoxypolyamine films, in: J.D. Scantlebury, M.W. Kendig (Eds.), Advance in Corrosion Protection by Organic Coatings III, Electrochemical society, Cambridge, UK, 1989: pp. 1–7.

[9] D. Greenfield, J.D. Scantlebury, The protective action of organic coatings on steel: a review, The Journal of Corrosion Science and Engineering. 3 (2000) paper 5.

[10] Y.J. Tan, Monitoring localised corrosion processes and estimating localized corrosion rates using a wire beam electrode, Corrosion. 54 (1998) 403–413.

[11] Y.-J. Tan, S. Bailey, B. Kinsella, Mapping non-uniform corrosion using the wire beam electrode method. I. Multi-phase carbon dioxide corrosion, Corrosion Science. 43 (2001) 1905–1918.

[12] Y.-J. Tan, S. Bailey, B. Kinsella, Mapping non-uniform corrosion using the wire beam electrode method. III. Water-line corrosion, Corrosion Science. 43 (2001) 1931–1937.

[13] D. Battocchi, J. He, G.P. Bierwagen, D.E. Tallman, Emulation and study of the corrosion behavior of Al alloy 2024-T3 using a wire beam electrode (WBE) in conjunction with scanning vibrating electrode technique (SVET), Corrosion Science. 47 (2005) 1165–1176.

[14] Z. Qingdong, Potential variation of a temporarily protective oil coating before its degradation, Corrosion Science. 43 (2001) 317–324.

[15] C.-I. Wu, X. Zhou, Y. Tan, A study on the electrochemical inhomogeneity of organic coatings, Progress in Organic Coatings. 25 (1995) 379–389.

[16] Y.J. Tan, The effects of inhomogeneity in organic coatings on electrochemical measurements using a wire beam electrode: Part I, Progress in Organic Coatings. 19 (1991) 89–94.

[17] Y.J. Tan, The effects of inhomogeneity in organic coatings on electrochemical measurements using a wire beam electrode, Part II, Progress in Organic Coatings. 19 (1991) 257–263.

[18] Z. Qiungdong, Measuring corrosion beneath organic coatings using wire beam electrodes, in: L. Yang (Ed.), Techniques for Corrosion Monitoring, Woodhead Publishing Ltd, USA, 2012.

[19] Z. Mogri, D. Paul, Gas sorption and transport in side-chain crystalline and molten poly (octadecyl acrylate), Polymer. 42 (2001) 2531–2542.

[20] B. Xu, Q. Zheng, Y. Song, Y. Shangguan, Calculating barrier properties of polymer/clay nanocomposites: Effects of clay layers, Polymer. 47 (2006) 2904–2910.

[21] D. Greenfield, F. Clegg, Enhancement of Barrier Properties in Organic Coatings using Nanocomposites, Journal of Corrosion Science and Engineering. 8 (2004) paper no. 8.

[22] M.L. White, D.J. Mills, H.J. Leidheiser, Resistance measurements of organic coatings as a means for evaluating corrosion protection in acid solutions, in: M.W. Kendig, H.J. Leidheiser (Eds.), Corrosion Protection by Organic Coatings, Electrochemical society, San Diego, Calif., 1986: pp. 208–216.

[23] D.J. Mills, J.E.O. Mayne, The inhomogeneous nature of polymer films and its effect on resistance inhibition, in: H.J. Leidheiser (Ed.), Corrosion Control by Organic Coatings, NACE International, Bethelehem, PA, USA, 1981: pp. 12–17.

[24] P.J. Heyes, The effect of pigment polymer interaction on protection by organic coatings, PhD thesis, Downing College, University of Cambridge, 1977.

[25] P. Moongkhamklang, S.. Taylor, The delineation of ionic pathways in organic coatings using a molecular probe technique, Progress in Organic Coatings. 46 (2003) 259–265.

[26] B.R. Hinderliter, S.G. Croll, D.E. Tallman, Q. Su, G.P. Bierwagen, Interpretation of EIS data from accelerated exposure of coated metals based on modeling of coating physical properties, Electrochimica Acta. 51 (2006) 4505–4515.

[27] G.P. Bierwagen, K. Allahar, B. Hinderliter, A.M.P. Simões, D.E. Tallman, S.G. Croll, Ionic liquid enhanced electrochemical characterization of organic coatings, Progress in Organic Coatings. 63 (2008) 250–259.

[28] G.P. Bierwagen, The physical chemistry of organic coatings revisited—viewing coatings as a materials scientist, Journal of Coatings Technology and Research. 5 (2008) 133–155.

[29] D.. Worsley, D. Williams, J.S.. Ling, Mechanistic changes in cut-edge corrosion induced by variation of organic coating porosity, Corrosion Science. 43 (2001) 2335–2348.

[30] G.S. Sekhon, S. Kumar, C. Kaur, N.K. Verma, S.K. Chakarvarti, Effect of thermal annealing on pore density, pore size and pore homogeneity of polycarbonate NTFs, Radiation Measurements. 43 (2008) 1357–1359.

[31] W. Schlesing, M. Buhk, M. Osterhold, Dynamic mechanical analysis in coatings industry, Progress in Organic Coatings. 49 (2004) 197–208.

[32] D.J. Mills, S.S. Jamali, K. Paprocka, Investigation into the effect of nano-silica on the protective properties of polyurethane coatings, Surface & Coatings Technology. 209 (2012) 137–142.

[33] P.K.T. Oldering, The chemistry of epoxy resins, in: P. Oldering (Ed.), Waterborne and Solvent Based Epoxies and Their End User Applications, John Wiley & Sons, Inc, London, 1996: pp. 11–57.

[34] P. Oldering, Chemistry of modified epoxy resins, in: P. Oldering (Ed.), Waterborne and Solvent Based Epoxies and Their End User Applications, John Wiley & Sons, Inc, London, 1996: pp. 126–131.

[35] S. Duval, Y. Camberlin, M. Glotin, M. Keddam, F. Ropital, H. Takenouti, Influence of the thermal transition on the evaluation on water-uptake in surface polymer film by EIS method, in: F. Mansfeld, F. Huet, O.R. Mattos (Eds.), New Trends in Electrochemical Impedance Spectroscopy (EIS) and Electrochemical Noise Analysis (ENA), The Electrochemical Society, Pennington, USA, 2001: pp. 50–59.

[36] R.S. Fishman, D.A. Kurtze, G.P. Bierwagen, Pigment inhomogeneity and void formation in organic coatings, Progress in Organic Coatings. 21 (1993) 387–403.

[37] C.H. Hare, Free volume, Journal of Protective Coatings & Linings. (1996) 67–80.

[38] C.H. Hare, Water Permeability in unpigmented films, Journal of Protective Coatings and Linings. (1997) 67–86.

[39] L. Li, Y. Yu, Q. Wu, G. Zhan, S. Li, Effect of chemical structure on the water sorption of amine-cured epoxy resins, Corrosion Science. 51 (2009) 3000–3006.

[40] N. Tuck, General considerations on paint formulation, in: Waterborne and Solvent Based Alkyds and Their End User Applications, John Wiley & Sons, Inc, London, 2000: pp. 85–102.

[41] D.J. Mills, S.J. Mabbutt, Inhomogeneities in organic coatings. a look at their importance to protection and at ways of detecting them, in: I. Sekine, M.W. Kendig, D. Scantlebury, D.J. Mills (Eds.), Advances in Corrosion Protection by Organic Coatings III, Electrochemical society, Noda, Japan, 1997: pp. 89–100.

[42] S.K. Dhoke, T.J. Mangal Sinha, a. S. Khanna, Effect of nano-Al_2O_3 particles on the corrosion behavior of alkyd based waterborne coatings, Journal of Coatings Technology and Research. 6 (2008) 353–368.

[43] J.-M. Yeh, C.-T. Yao, C.-F. Hsieh, L.-H. Lin, P.-L. Chen, J.-C. Wu, et al., Preparation, characterization and electrochemical corrosion studies on environmentally friendly waterborne polyurethane/Na^+-MMT clay nanocomposite coatings, European Polymer Journal. 44 (2008) 3046–3056.

[44] J.-J. Chen, C.-F. Zhu, H.-T. Deng, Z.-N. Qin, Y.-Q. Bai, Preparation and characterization of the waterborne polyurethane modified with nanosilica, Journal of Polymer Research. 16 (2008) 375–380.

[45] J. Yang, Z. Zhang, A. Schlarb, K. Friedrich, On the characterization of tensile creep resistance of polyamide 66 nanocomposites. Part II: Modeling and prediction of long-term performance, Polymer. 47 (2006) 6745–6758.

[46] C.H. Hare, The effects of pigment dispersion and flocculation on coatings, Journal of Protective Coatings & Linings. (2001) 69–94.

[47] J.D. Scantlebury, The mechanism of conduction in pigmented polymer membranes, PhD thesis, Downing College, University of Cambridge, 1969.

[48] G.P. Bierwagen, C.S. Jeffcoate, J. Li, S. Balbyshev, D.E. Tallman, D.J. Mills, The use of electrochemical noise methods (ENM) to study thick, high impedance coatings, Progress in Organic Coatings. 29 (1996) 21–29.

[49] N. Tuck, Polymerisation process in polyesters and alkyds, in: Waterborne and Solvent Based Alkyds and Their End User Applications, John Wiley & Sons, Inc, London, 2000: pp. 9–17.

[50] R. Ploeger, D. Scalarone, O. Chiantore, The characterization of commercial artists' alkyd paints, Journal of Cultural Heritage. 9 (2008) 412–419.

[51] Z.O. Oyman, Towards environmentally friendly catalysts for alkyd coatings, PhD thesis, Technical University of Eindhoven, 2005.

[52] G. Ye, F. Courtecuisse, X. Allonas, C. Ley, C. Croutxe-Barghorn, P. Raja, et al., Photoassisted oxypolymerization of alkyd resins: Kinetics and mechanisms, Progress in Organic Coatings. 73 (2012) 366–373.

[53] L. Hudda, J.J.G. Tsavalas, F.J. Schork, Simulation studies on the origin of the limiting conversion phenomenon in hybrid miniemulsion polymerization, Polymer. 46 (2005) 993–1001.

[54] D. Brasher, A. Kingsbury, Electrical measurements in the study of immersed paint coatings on metal. I. Comparison between capacitance and gravimetric methods of estimating water-uptake, Journal of Applied Chemistry. 4 (1954) 62–72.

[55] J.M. Sykes, A variant of the Brasher–Kingsbury equation, Corrosion Science. 46 (2004) 515–517.

[56] V.B. Miskovic-stankovic, D.M. Drazic, M.J. Teodorovic, Electrolyte penetration through epoxy coatings electrodeposited on steel, Corrosion Science. 37 (1995) 241–252.

[57] P. Moongkhamklang, S. Taylor, The delineation of ionic pathways in epoxy coatings using molecular probes, in: V. Agarwala (Ed.), Tri-service Corrosion Conference, Las Vegas, Nevada, 2003: p. paper no. AM025715.

[58] E.O. Eltai, J.D. Scantlebury, E.V. Koroleva, The effects of different ionic migration on the performance of intact unpigmented epoxy coated mild steel under cathodic protection, Progress in Organic Coatings. 75 (2012) 79–85.

Chapter 6

Conclusion and future works

The major findings of this study are reviewed in the first part of this chapter. This study was particularly concerned about the connection between theoretical and practical aspects of the research into organic protective coatings. In all three major areas of work attempts have been made to derive practical conclusions from the theoretical knowledge that was acquired. In the second part of the chapter suggestions are made for the future work.

6.1 Major remarks

In the first part of this thesis (chapter 3) work was described in which further steps were taken towards development of ENM method to become more practically applicable for assessing anti-corrosive coatings on-site. A new way of noise measurement that involved only one working electrode was introduced as single cell (S.C.) configuration. Unlike the previous ENM configurations that required recording both current and potential data at the same time, a sequential potential-current data collection was used. The repeatability and accuracy of the R_n measured with this configuration was tested and compared with the results of other electrochemical techniques, i.e. DC resistance and EIS. Single cell measurement showed a great promise as a practical in-situ testing method with a high level of conformance with other standard techniques. It is anticipated that this will find applications particularly where preparing two isolated working electrode is difficult, or characterization of one particular area is required. Necessary considerations for measuring electrochemical noise on a single working electrodes were defined as steadiness of system and the used of an appropriate reference electrode with low impedance and stable potential (i.e. low level of potential noise).

It was found that ENM configurations that involve two or more electrodes are particularly sensitive to asymmetry of electrodes and may give an erroneous result if the limitations of reference electrodes and individual components of noise (i.e. potential and current) are not considered. Asymmetry of electrodes is a common situation in the real field application as most organic coatings exhibit inhomogeneous resistance properties. It appears that in asymmetric measurements the level of potential noise is controlled by the

low resistance sample while the high resistance sample controls the current flow and hence the level of current noise.

Practical reference electrodes in the form of carbon, platinum and copper sheets were investigated as noise counter electrodes for in-situ application in section 3.5. Platinum was the most stable electrode while the carbon showed highest level of instability. However, all three electrodes showed adequate reliance for field measurement. Sampling rate was also investigated with an intention to determine the fastest yet reliable sampling rate to minimize the time needed for a noise measurement. It was found that very rapid data collection, e.g. at 5 or 10 Hz rate, results in invalid noise resistance that was calculated on coated samples. Also shortening the length of data set intensifies this error. Also the equilibrium time was studied for a range of thick anti-corrosive coatings. Results suggested the necessity of repetitive measurements on un-exposed coatings until a steady result is obtained.

The second part of the work (chapter 4) looked at the effect of surface preparation of steel and its impact on the anti-corrosion performance of organic coatings. The earlier work of Schaefer and Mills on the electrochemical studies of the effect of surface preparation on the performance of anti-corrosive coatings was continued with five surface preparation methods and 5 different types of coating. The results presented in this thesis confirmed the earlier findings and revealed superior performance of organic coatings on hydro-blasted steel compared to that of the wet abrasive blasted substrate. Steel surface characterization revealed the presence of contaminants on the wet abrasive blasted steel as a result of preparation method. The poor performance of wet abrasive blasting was attributed to the presence of contaminants and the less protective nature of the oxide layer. The formation of differential aeration galvanic cells as a result of the very large surface profile may also play a part.

In contrast to the wet abrasive blasted steel, the hydroblasted steel was found to have a contaminant-free surface with about half the roughness of the wet abrasive blasted surface.

Also electrochemical characterizations showed a more noble potential of hydroblasted surface and a relatively dense and adherent aqueous formed oxide film (section 4.3). In addition, to the better anti-corrosive performance of organic coatings on hydroblasted surface, it showed great promise as an environmentally friendly preparation technique with no pollutant residues left from the preparation method. The smoother surface produced by hydroblasting method also decreased the surface porosity, and hence the amount of paint required to fill the porosity, by approximately 150% compared to wet abrasive blasting. Despite the smoother surface of hydroblasted surface it maintained a higher level of wet adhesion compared to the abrasive blasted surface.

Adhesion testing (section 4.2.2) revealed that surface roughness has a major influence on the adhesion level measured by mechanical adhesion tester, pull-off method. Both wet abrasive and hydro- blasting methods produced excellent adhesion level before immersion and in the earlier stages of immersion compared to relatively smooth surfaces prepared by degreasing, acid pickling and abrasion. The adhesion level dropped significantly as immersion time increased which is due to the propagation of the wet interface underneath the coating. In addition to the major influence of surface roughness on adhesion level, it is suggested that the surface free energy plays an important role by attracting water molecules towards the interface. Results showed that surface activation by means of acid pickling or abrasion without producing an appropriate surface profile or a stable oxide layer can significantly decrease the performance of organic coating. However, the adhesion level on these surfaces was too low and could not be differentiated by means of mechanical adhesion tester.

Comparing the resistance and adhesion testing results with visual assessment of the steel samples coated with different coatings revealed that adhesion testing is not sensitive enough to pick up the initiation of under-film corrosion. This is attributed to the corrosion starting under very small areas of coating at which the coating is highly permeable to ions. Electrochemical tests, such as DC resistance, ENM and EIS, are more sensitive to the lowest resistance in the electrical circuit. However, mechanical adhesion testing measures the

average of mechanical work required to pull-off a relatively large area of the coating and so it is insensitive to the small local detachments. This is a very important concept which is most often neglected when adhesion results alone are used to call a coating, a "good" or "poor" anti-corrosion coating. It is suggested that both electrochemical and mechanical testings are used to evaluate the protective performance of organic coatings.

A third area of the work (chapter 5) looked in more detail at the local resistance properties of the organic coating itself. This confirmed the above assumption of permeable areas of coatings being locally very small areas and that the resistance behaviour was bimodal (D and I type areas). It was further confirmed that examining the conduction mechanism of organic coatings may be used as a predictive tool for its protective performance in the long term. Also it was shown that the new configuration of ENM, single electrode developed here, can be used as a practical way of detecting the D or I type behaviour. Bulk analytical methods such as DMTA, DSC and measuring water absorption were unable to differentiate between the D and I type coatings due to the small size of D areas. However, the physico-mechanical analyses were found useful in understanding the structural changes of coatings and relate these changes to the conduction mechanism of coatings.

It was found that several structural and environmental factors play a part in formation of D areas (section 5.6). Excessive presence of non-functional polymer parts in the resinous phase of paint facilitates the formation of these continuous permeable pathways. It is likely that these "dead" parts of polymer are attracted to each other, possibly due to similar surface tension, and form agglomerates which later form D areas. Overlaying several thin layers of coating instead of a single thick layer dramatically improves the homogeneity of coating. It is believed that, in multi-layered coatings, large I type areas in each layer are superimposed on small D areas of the other layers resulting in insulated D areas. This hypothesis is also in line with the results obtained from different thicknesses of a single coat. Although increasing thickness improves the homogeneity, it does not entirely eliminate the D areas. Improvement is due to the increase of the $(\frac{coating\ thickness}{size\ of\ D\ areas})$ ratio and

the fact that there is a lesser chance of formation of a continuous pathway as the coating thickness increases. However, in practice, it is much more cost effective to apply several thin layers of coating instead of a very thick coating to effectively eliminate D areas.

Solvent escape ways were found an important mechanism of formation of D type areas. In the first stage of solvent evaporation from a film, the evaporation rate depends on the vapour pressure at the temperature, the ratio of surface area to volume and the rate of airflow over the surface. As the solvent evaporates, viscosity increases, Tg increases and the rate of loss of solvent becomes dependent on how rapidly solvent molecules can diffuse through to the surface of the film. As solvent loss continues, Tg increases, free volume decreases further, and solvent loss slows. If the film is formed at 25°C from a solution of a polymer that, when solvent free, has a Tg greater than 25°C, the film retains considerable solvent even though it is a hard "dry" film. Solvent slowly leaves the coating but, it has been shown experimentally elsewhere, 2-3% of solvent may remain in the coating after several years at ambient temperature. Curing the coating at an elevated temperature above the Tg of the solvent free polymer will facilitate effective removal of solvent resulting in increased homogeneity and enhanced anti-corrosion properties of organic coatings. In the case of crosslinking or thermoset coatings, elevated curing temperature also improves the coating homogeneity by increasing the crosslinking density of the polymer.

In case of waterborne coatings, the inherent hydrophobicity of resinous phase results in extensive water absorption and 100% D type behaviour. Multi-electrode measurements showed a homogeneously distributed resistance with very uniform D type conduction. Results of attached coatings on steel substrate revealed very poor protective performance of waterborne coatings. Further studies on the effect of solvent revealed that the type of solvent may also alter the inhomogeneity of coating. Studies were conducted using MEK and toluene as the sole solvent for the alkyd varnish. Compatibility level of solvent with polymeric phase and evaporation rate of solvent may each have an effect on the chemical homogeneity and thus the conduction mechanism of coating.

Environmental factors such as exposure period and temperature may also change the conduction mechanism. Pigmentation of alkyd with calcium diphosphate improved the homogeneity of coating in the short term but most I type pigmented coatings will change to D type in the long term. It was suggested that inorganic pigments attract water which in the long term results in water clusters and formation of D type pathways. The significance of the retention of I type behaviour in the long term was pronounced by lower performance of pigmented alkyd on steel compared to the un-pigmented alkyd varnish. Further work on environmental factors involved examining the conduction mechanism of solvent based PU varnish at different temperatures. It was observed that the electrical resistance of coating decreases as temperature increases with a distinct thermal transition point corresponding to glass transition temperature (Tg) of the immersed coatings. The ingress of water was demonstrated by DMA results as the plasticisation effect on the coating film.

Recent findings of Sykes have elucidated that the substrate polarization plays an equally important role in protection of metal by organic coatings. This has been also reflected in the previous studies of Mills that showed remarkably larger resistance of coating on inert substrates compared to the same coating on an active substrate. The resistance decreases with increasing the electrochemical activity of substrate. It appears that there is a cooperative effect of coating homogeneity with substrate electrochemical stability that leads to a more efficient protection. In contrast a heterogeneous (highly D type) coating may not be able to polarize the substrate sufficiently to become passive. Consequently the depolarized substrate in areas of high permeability may not survive for long.

6.2 Future works

Despite the usefulness of ENM for studying different properties of organic coatings it has not received the attention it deserves. The very few groups who have worked on developing this technique for coatings are Prof. Bierwagen group at North Dakota State University (mainly on new applications of technique), Prof. Mansfield at University of Southern California (mainly on data analysis) and Dr. Mills group at University of Northampton (mainly on new data acquisition protocols). There are plenty of unexplored

avenues of ENM such as development of more accurate and stable reference electrodes and development of an implantable electrode for long term monitoring of anti-corrosive coatings. The new generation of mobile and accurate ZRA/potentiometers provide endless opportunities for the field applications of ENM with the variety of data acquisition configurations that are already developed in the lab. Major developments are particularly required in regards to the effective isolation of the noise measuring device and data collection signal in order to become less affected by environmental electrical and electromagnetic noises. New electronic communication methods such as Bluetooth and other wireless communication protocols show great potential for providing an effective and isolated way of communication between the samples, data logger and the computer. Electrical noise data can be translated into coded signals, transmitted unaffected over a long distance and de-coded into a computer where the data is analysed.

UHP hydroblasting is a relatively new method of surface preparation in the industry and yet many contractors are hesitant to use it in the large scale. The superior performance of UHP hydroblasting over the more traditional abrasive blasting method brings a great promise for replacing the polluting traditional method with this new and environmentally friendly method. Future works in this field should focus more on the field applications of these preparation methods and their performance in the long term. Cathodic disbondment is a test method that examines the resistance of coating against detachment while under cathodic protection. The method is widely used to evaluate anti-corrosive coating particularly used in the field of transportation pipelines and on-shore corrosion protection. The test method is also known to involve the adhesion properties at interface and permeability of coating at the same time. Given the promising results of UHP hydroblasting method, future studies may involve the use of cathodic disbondment test method to further predict the performance of coating in the field using different surface preparation methods.

The author's earlier experience with bituminous coatings showed an exceptionally low level of water absorption and excellent retention of high resistance for coatings based on coal tar pitch. Despite the fact that these substances have been listed as environmental hazard, they are still used as modifier of epoxy coatings (i.e. coal tar epoxy) to lower their

water absorption. The interesting point here is that bituminous materials are thermoplastic and they typically decrease the crosslinking density of epoxy systems, but they improve the protective properties of coating. Considering the influence of both low crosslinking density and hydrophobicity on formation of D areas, it is of major interest to study how D/I ratio changes by addition of hydrophobic materials into crosslinking coatings. A large number of literatures in the last few decades have reported improvement of anti-corrosion properties of organic coatings by making them more hydrophobic. However, the local resistance distribution and conduction mechanism in form of D/I type has been rarely investigated for such systems. Hence it is unclear whether the improvement in protective properties is due to the enhanced of the I type characteristics or it is a result of the decreased hydro-sensitivity of coating/metal interface. Further studies in this area may be conducted on addition of hydrophobic agents, such as hydrophobic silanes or polyolefin waxes, into epoxy or PU coatings and studying their performance as a detached film and coating on metal substrate.

Recent studies by the author with scanning electrochemical microscope (SECM) on the electrochemical heterogeneity of poly (lactic-co-glycolic acid or PLGA) coatings on magnesium substrate showed heterogeneous permeation of hydrogen through the PLGA coating. H_2 permeation sites were the location of corrosion of the magnesium substrate after 2 days immersion in simulated biological electrolyte. Heterogeneous accumulation of ions, e.g. chloride and sodium, has been shown elsewhere using elemental mapping tools of analytical microscopes such as Raman or SEM. However, there has been limited success in using electrochemical scanning techniques, such as SVET, SKP or LEIS, to characterise D areas mainly due to insufficient resolution and low sensitivity. Very high sensitivity of modern SECMs, i.e. up to 10^{-12} amp, and submicron resolution makes it an ideal tool for future studies on inhomogeneity of coatings. Ion-selective modes of scan may be used to examine the perm-selectivity of coatings at D areas and investigate their significance on the protection afforded by the organic coating.

As a result of increasingly strict environmental regulations, solvent free coating systems such as waterborne and solvent free coatings have been the main subject of research and

development, particularly in the commercial sector. Although conventional waterborne coatings showed a rather poor performance in this study, more advanced generation of waterborne paints, such as electro-deposition paints (also known as e-coat), have been the subject of study in the past and showed exceptionally good performance (100% I type behaviour). The secret may lie in the colloidal dispersed system which does not contain surface active agents (e.g. emulsifiers) but uses very small size of polymer micelle to obtain a stable colloidal system. The controllable application method of these paints produces highly uniform films which together with the elimination of hydrophobic agents results in a very high performance waterborne coatings. Future works may involve further studies of e-coats with an intention to reveal their secret and incorporate their concept into conventional waterborne paints. Hybrid powder coatings are also an interesting class of solvent-less coatings that are applied on the substrate using the same concept employed in the application of e-coats (i.e. adsorption of charged particles on the metal substrate with opposite charge). Lack of solvent, high crosslinking density and a very uniform film could potentially produce a highly homogeneous (I type) coating. However, the electrochemical inhomogeneity of these coatings has rarely been investigated and may be considered as future studies in this field. Also powder coatings have been traditionally regarded as coatings with relatively poor adhesion on metal. So studies in this field may further elucidate the role of adhesion and conduction mechanism on the protective properties of organic coatings.

Further statistical studies of D areas may involve 3D-modeling of D areas in order to estimate the size of inter-molecular spaces by which their connections make a contentious pathway. The Poisson connectivity model in a 3D space may be used in combination with actual laboratory data of D ratios for different thicknesses of coating. Increasing thickness would reduce the chance of *connectivity* hence the model can be adjusted/trained to fit the known information of D ratio/thickness and predict the size of D areas. Also an important future work may include developing a theoretical basis to define a minimum thickness of coating at which, with 99% confidence, no D area will be expected for a very large surface based on D ratio measured in the lab. A "reliability factor" should be defined to add to the minimum thickness at which 100% I type behaviour is observed.

Appendix A

Relationship between polarization resistance and the corrosion rate

Many researchers have experimentally observed that the applied current (i_{app}) was approximately linearly related to applied potential within a few millivolts of polarization from E_{corr}. So the slope of the i_{app}-E curve at the corrosion potential within ±5 to ±10 mV defines the polarization resistance as shown in 4.6.

$$R_P(ohm/cm^2) = \left[\frac{\Delta E}{\Delta i_{app}}\right]_{(E-E_{corr})\to 0} \quad \text{(Eq. 4.6)}$$

Stern-Geary 4.7 simplifies the relation between i_{app} and R_P using the proportionality constant *B*.

$$i_{corr} = \frac{B}{R_P} \quad \text{(Eq. 4.7)}$$

In which the i_{corr} is the corrosion current, R_P is polarization resistance and *B* defines as

$$B = \frac{1}{2.3}\left(\frac{\beta_a \beta_c}{\beta_a + \beta_c}\right) \quad \text{(Eq. 4.8)}$$

With a known and constant *B* over the time, corrosion rate can be always determined by measuring the R_P via LPR method.

Anodic and cathodic Tafel constants are determined by the kinetic controlling phenomena like charge transfer resistance and electrolyte diffusion resistance. Corrosion product precipitation and the dissolved ions in the electrolyte due to the corrosion reactions are the factors that can change the chemical composition of electrical double layer and the electrolyte and consequently the kinetic controlling phenomena. So as the corrosion proceeds anodic and cathodic Tafel constants may alter and change the proportionality constant *B*.